THE HYDROLOGIC REGIME AT SUB-ARCTIC AND ARCTIC

WATERSHEDS: PRESENT AND PROJECTED

By

Anna K. Liljedahl

RECOMMENDED: _____

_____

_____

_____

_____

_____
Advisory Committee Chair

_____
Chair, Department of Civil and
Environmental Engineering

APPROVED: _____
Dean, College of Engineering and Mines

_____
Dean of the Graduate School

_____
Date

THE HYDROLOGIC REGIME AT SUB-ARCTIC AND ARCTIC WATERSHEDS: PRESENT AND PROJECTED

A

DISSERTATION

Presented to the Faculty

of the University of Alaska Fairbanks

in Partial Fulfillment of the Requirements

for the Degree of

DOCTOR OF PHILOSOPHY

By

Anna K. Liljedahl

Fairbanks, Alaska

May 2011

Abstract

The wetlands in the Arctic Coastal Plain, Northern Alaska, support a multitude of wildlife and natural resources that depend upon the abundance of water. Observations and climate model simulations show that surface air temperature over the Alaskan arctic coast has risen in recent history. Thus a growing need exists to assess how the hydrology of these arctic wetlands will respond to the warming climate. A synthesis study was conducted combining the analysis of an extensive field campaign, which includes direct measurements of all components of the water balance, with a physically-based hydrologic model forced by downscaled climate projections.

Currently, these wetlands exist despite a desert-like annual precipitation and a negative net summer water balance. Although evapotranspiration is the major pathway of water loss, there are multiple non-linear controls that moderate the evapotranspiration rates. At the primary study site within the Barrow Environmental Observatory, shallow ponding of snowmelt water occurs for nearly a month at the vegetated drained thaw lake basin. Modeling studies revealed that the duration and depth of the ponding are only replicated faithfully if the rims of low-centered polygons are represented. Simple model experiments suggest that the polygon type (low- or high-centered) controls watershed-scale runoff, evapotranspiration, and near-surface soil moisture. High-centered polygons increase runoff, while reducing near-surface soil moisture and evapotranspiration.

Soil drying was not projected by the end-of-the century but differential ground subsidence could potentially dominate the direct effects of climate warming resulting in a drying of the Arctic Coastal Plain wetlands. A drier surface would increase the susceptibility to fire, which currently is a major part of the Alaskan sub-arctic but not the arctic landscape. High quality pre- and postfire data were

collected in the same location in central Seward Peninsula, uniquely documenting short-term soil warming and wettening following a severe tundra fire.

Overall, this research concludes that arctic and sub-arctic watershed-scale hydrology is affected by changes in climate, surface cover, and microtopographic structures. It is therefore crucial to merge hydrology, permafrost, vegetation, and geomorphology models and measurements at the appropriate scales to further refine the response of the Arctic Coastal Plain wetlands to climate warming.

Table of Contents

Page

Signature Page i

Cover Page ii

Abstract iii

Table of Contents v

List of Figures x

List of Tables xii

Acknowledgements xiii

CHAPTER 1 1

1.1 General Introduction 1

1.2 Literature Review 5

1.3 Figures 17

1.4 Tables 18

1.5 References 19

CHAPTER 2: PHYSICAL SHORT-TERM CHANGES AFTER A TUSSOCK TUNDRA FIRE, SEWARD PENINSULA, ALASKA 37

Abstract 37

2.1 Introduction 38

2.2 Site Description 39

2.3 Methods 41

2.4 Results 45

2.4.1 Weather 45

2.4.2 Soil Temperature, Soil Moisture, and Active Layer Thickness 45

2.4.2.1 Soil Thermal Regime 45

2.4.2.2 Soil Moisture 47

2.4.2.3 Active Layer Thickness 47

2.4.3 Surface Observations 48

Page

2.4.3.1 Albedo 48
2.4.3.2 Radiation Efficiency and the Richardson Number 48
2.5 Discussion....49
2.5.1 Soil Thermal and Moisture Regime 49
2.5.2 Boundary Layer and Radiation Efficiency 51
2.6 Conclusions 53
2.7 Acknowledgments 53
2.8 Figures 54
2.9 Tables 63
2.10 References 67
CHAPTER 3: PROCESSES CONTROLLING EVAPO-TRANSPIRATION AT AN ARCTIC COASTAL WETLAND....73
Abstract....73
3.1 Introduction 74
3.2 Background....75
3.3 Site Description 77
3.4 Methods 79
3.4.1 Measurements....79
3.4.2 Eddy Covariance Calculations 80
3.4.3 Soil Moisture Analysis 81
3.4.4 Analysis of Resistances and Equilibrium Evaporation 81
3.5 Results 84
3.5.1 Site Conditions 84
3.5.2 Surface Energy Exchange....86
3.6 Discussion....88
3.7 Future Projections....91
3.8 Conclusion....91

Page

3.9 Acknowledgements 92
3.10 Figures 93
3.11 Tables 99
3.12 References 103
CHAPTER 4: THE ROLE OF LOW- AND HIGH-CENTERED POLYGONS IN ARCTIC WETLAND WATER BALANCE 112
Abstract 112
4.1 Introduction 113
4.2 Background 115
4.3 Site Description 117
4.4 Methods 118
4.4.1 Schematic DEMs 118
4.4.2 Hydrologic Model 118
4.4.3 Field Measurements 120
4.5 Results 122
4.5.1 Field Measurements 122
4.5.2 Modeling Analysis 123
4.6 Discussion 124
4.6.1 Surface and Soil Water Storage 124
4.6.2 Lateral Flow 125
4.6.3 Vertical Fluxes 127
4.6.4 Future Directions 128
4.7 Conclusion 128
4.8 Acknowledgements 129
4.9 Figures 130
4.10 Tables 137
4.11 References 139

Page

CHAPTER 5: WATER BALANCE OF AN ARCTIC COASTAL WETLAND, BARROW, ALASKA 148

Abstract 148

5.1 Introduction 149

5.2 Background 150

5.2.1 Wetlands 150

5.2.2 Landscape Features 150

5.2.3 Hydrology 151

5.3 Site Description 152

5.4 Methods 154

5.4.1 Measurements 154

5.4.2 Data Quality Control and Analysis 156

5.4.3 Hydrologic Modeling 157

5.4.3.1 Model Description 157

5.4.3.2 Digital Elevation Model 159

5.4.3.3 Variables and Parameter Settings 160

5.4.3.4 Calibration and Validation 161

5.5 Results 163

5.5.1 Measurements 2006-2009 163

5.5.2 Validation of Hydrology Simulations 2006-2009 164

5.5.3 Simulated Water Balance 1999-2009 165

5.6 Discussion 167

5.6.1 Measurements 167

5.6.2 Modeling 169

5.7 Conclusion 173

5.8 Acknowledgements 174

5.9 Figures 175

Page

5.10 Tables 187
5.12 Appendix 195
5.11 References 198
CHAPTER 6: WATER BALANCE OF AN ARCTIC COASTAL WETLAND, BARROW, ALASKA: END-OF-21ST CENTURY PROJECTIONS 207
Abstract 207
6.1 Introduction 208
6.2 Background 208
6.3 Site Description 211
6.4 Methods 212
6.4.1 Regional Climate Downscaling 212
6.4.2 Hydrologic Modeling 214
6.5 Results 216
6.5.1 Climate 216
6.5.2 Hydrology 217
6.6 Discussion 218
6.7 Conclusion 221
6.8 Acknowledgements 222
6.9 Figures 223
6.10 Tables 225
6.11 References 228
CHAPTER 7 238
7.1 General Discussion 238
7.2 General Conclusions 241
7.3 References 243

List of Figures

Page

Figure 1.1: Map of Alaska. 17
Figure 2.1: Location of Kougarok....54
Figure 2.2: Annual area burned at Seward Peninsula 55
Figure 2.3: K2 station....56
Figure 2.4: Multi spectral principal component analysis 57
Figure 2.5: K2 soil moisture sensors....58
Figure 2.6: Mean annual and September ground temperatures....59
Figure 2.7: Mean daily air, surface, and ground temperatures....60
Figure 2.8: Mean daily unfrozen soil moisture 61
Figure 2.9: Observed mean CALM grid active layer depths 62
Figure 3.1: The Central Marsh (CM) and the Biocomplexity Experiment....93
Figure 3.2: The soil water status 94
Figure 3.3: The measured rate of evapotranspiration....95
Figure 3.4: The relationship of hourly vapor pressure deficit....96
Figure 3.5: Mean midday values of bulk surface resistance 97
Figure 3.6: Meteorological conditions 98
Figure 4.1: Distribution of polygon mires....130
Figure 4.2: Schematic representation of the development of ice wedges 131
Figure 4.3: The schematic digital elevation model 132
Figure 4.4: Aerial photo of the vegetated drained thaw lake basin.....133
Figure 4.5: Measured water levels 134
Figure 4.6: Measured near-surface (10 cm depth) liquid soil water content ...135
Figure 4.7: Simulated water table 136
Figure 5.1: The extremely low-gradient watershed 175
Figure 5.2: Photo including ~90% of the entire watershed.....176
Figure 5.3: Measured (yr 2007) and modeled leaf area index 177

Page

Figure 5.4a: Hydrological model simulations 2006 178
Figure 5.4b: Hydrological model simulations 2007 179
Figure 5.4c: Hydrological model simulations 2008 180
Figure 5.4d: Hydrological model simulations 2009 181
Figure 5.5: Measured ablation curve 182
Figure 5.6: Simulations of water tables 183
Figure 5.7: Interannual variation of net summer water balance 184
Figure 5.8: Summer net P-ET 185
Figure 5.9: The partitioning of the accumulated snow 186
Figure 6.1: The extremely low-gradient watershed. 223
Figure 6.2: Present and projected hydrology. 224

List of Tables

Page

Table 1.1: Summary of bioclimate. 18
Table 2.1: Site descriptions of meteorological stations K1, K2 and K3. 63
Table 2.2: Soil classification scheme 64
Table 2.3: Instrumentation used 65
Table 2.4: Summary table of observations. 66
Table 3.1: Meteorological conditions 99
Table 3.2: Differences in energy balance partitioning 100
Table 3.3: Average midday energy partitioning. 101
Table 3.4: Average midday energy partitioning. 102
Table 4.1: The simulated water balance components 138
Table 5.1: Measurements (x) of meteorology. 187
Table 5.2: Soil parameters 188
Table 5.3: Model parameters 189
Table 5.4: Measured quantities. 190
Table 5.5: Calibrated model parameters 191
Table 5.6: Statistical evaluation of the simulated evapotranspiration 192
Table 5.7: Simulated water balance 193
Table 5.8: Simulated evapotranspiration 194
Table 6.1: A comparison between present and projected. 225
Table 6.2: Hydrological simulations yr 2091-2097 226
Table 6.3: A comparison of simulated mean hydrological fluxes 227

Acknowledgements

Receiving a PhD degree is a team work. I am sharing this dissertation with family, friends, and colleagues across the world who generously offered their precious time and energy. I am forever thankful to you all.

I want to send my special appreciation to a certain group of people. My foremost acknowledgement goes to Larry Hinzman. Thank you, Larry, for accepting to be my advisor, for providing me with numerous opportunities to grow into my doctor shoes (which always seems to out-grow me), and for guiding me through the meandering path towards becoming a research scientist. A big thank you also goes to my committee members Terry Chapin, John Fox, Doug Kane, Sveta Stuefer and Kenji Yoshikawa for providing thoughtful advice and challenging questions.

Thank you Jeff Benowitz for your patience, love, and wise words throughout my graduate studies in Fairbanks, both on and off the university play field. Let‘s have carrot cake again one of these days.

CHAPTER 1

1.1 General Introduction

Although the Earth‘s climatic conditions have continuously fluctuated on geological time scales [*Zachos et al.*, 2001], the recent climate warming, which is amplified at high latitudes [*Polyakov et al*., 2002; *ACIA* 2005; *Serreze and Francis*, 2006], is affecting the people of the North [*Fox*, 2002; *Hinzman et al.*, 2005]. In environments underlain by permafrost, which has a first order affect on hydrologic processes [*Woo*, 1986; *Kane et al.,* 1989; *Hinzman et al.,* 1996], altered thermal fluxes can have profound effects on the abiotic and biotic systems once the threshold of permanently frozen to thawed ground is passed [*Francis et al.*, 2009]. To reduce the uncertainty facing the communities and ecosystems in the Arctic and sub-Arctic, one needs to first understand the hydrologic system at the scale of importance to the issue. This involves analyses of both ground based data collection and model development, validation, and future predictions.

The coupling between the fire and hydrologic regimes within the Arctic and Sub-Arctic ecosystems is particularly intertwined due to the presence of ice-rich permafrost. Fires are an integral component of the sub-Arctic ecosystems [*Chapin et al*., 2006], while wildfires currently are rare in arctic landscapes [*Jones et al*., 2009]. Even though permafrost in arctic regions is expected to remain stable until the end of the 21st century [*Marchenko et al*., 2008], the introduction of increased fire frequency could occur sooner and have profound effects on hydrology, ecology, and permafrost regimes.

Fires are projected to increase in frequency and severity [*Overpeck et al*., 1990; *Flannigan et al*., 2001]. In fact, fire disturbance have increased in recent decades [*Kasischke and Turetsky*, 2006], but have historically been extremely rare in the Arctic such as the North Slope of Alaska [*Racine and Jandt*, 2008] while tundra fires are quite abundant in the sub-arctic tundra of the Seward Peninsula

[*Liljedahl et al.*, 2007]. Nonetheless, during the unusually low precipitation summer of 2007 over 100,000 ha burned near the Anaktuvik River, North Slope, Alaska [*Racine and Randt*, 2008; *Jones et al*., 2009]. One may argue that such events are triggered by dry near-surface soils and could become more prevalent in a warmer arctic.

P-PET (summer precipitation - potential evapotranspiration) is commonly used as a proxy for soil moisture conditions. Although P-PET is projected to become even more negative in Alaskan tundra environments [*O'Brien and Loya*, 2009] and P-PET has shown similar trends during recent decades [*Oechel et al.*, 2000], changes in P-PET may not necessarily correlate linearly with trends in near-surface soil moisture. This is due to inaccurate precipitation measurements [*Black*, 1954; *Benson,* 1969*; Groisman and Legates*, 1994; *Goodison et al*., 1998] and multiple controls on arctic wetland evapotranspiration. In order to project the susceptibility of the arctic landscape to fire, it is therefore necessary to assess the actual fluxes and their controls.

The effect of warmer air temperatures on the Arctic environment have mainly been explored through micro-scale (~1 m) field ecology experiments [*Chapin et al*., 1995; *Hollister et al*., 2005; *Walker et al*., 2006] or large-scale (>50 km) model simulations [*Anisomov and Nelson*, 1997; *Lawrence et al*., 2008]. Although tightly linked to hydrology, terrestrial field and modeling studies have mainly focused on quantifying carbon and surface albedo changes and feedbacks [*Oechel et al*., 2000; *Christensen and Cox*, 2002; *Chapin et al*., 2005; *Frey and Smith*, 2005] while less attention has been given to hydrologic fluxes and stores. Though recently suggested as a significant positive feedback mechanism in a warming Arctic [*Swann et al.*, 2010], evapotranspiration is still one of the least understood components of the Arctic hydrologic cycle [*Kane et al*., 1989, 1992; *Vörösmarty et al*., 2001; *Woo et al*., 2008]. Evapotranspiration is the major

pathway of water loss from many arctic and sub-arctic watersheds [*Woo*, 1986; *Kane and Yang*, 2004] and thus warrants further study.

The hydrologic, permafrost, and fire regimes are interconnected through the complex interaction between vegetation, soils, and ground ice [*Shur and Jorgenson*, 2007]. Yet all three are rarely dynamically described and linked in physical models constraining future projections. Important knowledge can still be gained by identifying thresholds or disconnections in mass and energy transfer through model sensitivity analyses and validation to field measurements.

The objectives of this research were to: a) quantify post-fire effects on the thermal and hydrologic regimes at a tundra environment near the boundary zone of continuous and discontinuous permafrost; b) assess the water balance, including its controls of an extremely low-gradient watershed at the Arctic Coastal Plain, Northern Alaska, by combining field measurements and physically-based model simulations. I am addressing the following hypotheses:

H1: A severe fire on tussock tundra results in a post-fire warming and wetting of the near-surface soil.

H2: Midday evapotranspiration rates from a vegetated drained thaw lake basin are only energy-limited.

H3: A change from a low- to a high-centered polygon dominated landscape affects overall watershed hydrology by increasing runoff, reducing evapotranspiration and near-surface soil moisture.

H4: The projected increase in end-of-the 21st century air temperature and precipitation will lead to a drying of Arctic Coastal Plain wetlands.

These hypotheses are addressed in the five individual manuscripts and revisited in chapter seven. The first paper (Chapter 2) is entitled –Physical short-term changes after a tussock tundra fire, Seward Peninsula, Alaska". It was published in the Journal of Geophysical Research in 2007 and was, to the author's knowledge, the first article analyzing tundra pre- and postfire data collection and analysis at the same location. The severe burn resulted in wetter and warmer soils and a thawing of the permafrost that lasted at least up to four years after the fire. The third chapter entitled –Processes controlling evapotranspiration in an arctic coastal wetland" focuses on a vegetated drained thaw lake basin near Barrow, Alaska. The multi-summer dataset revealed multiple limitations on the evapotranspiration rates including the maritime air mass, soil moisture, and limited land-atmosphere connectivity during higher air vapor pressure deficits. Further, wet and inundated soils appear to alter the midday surface energy partitioning by favoring the ground heat flux and reducing the energy available to latent and sensible heat flux. Chapter four entitled –The role of low- and high-centered polygons on arctic wetland water balance" is a model experiment combined with field measurements. Drastic differences appear in the hydrologic fluxes and stocks between landscapes dominated by low- or high centered polygons, where high-centered polygons increase runoff, manifest drier soils and reduce evapotranspiration. A water balance paper represents chapter five (–Water balance of an arctic coastal wetland, Barrow, Alaska") with the uniqueness that all components of the water balance were measured simultaneously, including the evapotranspiration. Longer-term water balance (yr 1999-2009) was evaluated by applying a physically-based model WaSiM-ETH. This was the first time WaSiM-ETH was applied and validated to a watershed underlain by permafrost. Sensitivity analyses show that low-centered polygon rims needs to be included in order to successfully simulate the multi-week ponding of the studied watershed. Chapter six (–Water balance of an arctic coastal wetland, Barrow, Alaska: End-of-21st century projections") combine downscaled

projected regional climate with high-resolution hydrologic modeling to project future hydrologic conditions of an Arctic Coastal Plain wetland. The increased evapotranspiration was offset by increased summer precipitation resulting in a slight increase in autumn water tables within the vegetated drained lake basin. However, the projections assume no changes in surface topography, which can occur with a degradation of the ice-rich near surface permafrost. In fact, changes in micro-topography may have a larger affect on the soil water stores than the projected direct effects of climate. Chapter seven is a discussion of the integrated results and synthesis of the thesis as a whole.

1.2 Literature Review

The word ―tundra" is commonly used in reference to landscapes that are above the altitudinal or latitudinal tree line [*Brown et al.*, 1980]. In Alaska the tundra environment includes, but is not limited to the Seward Peninsula and the North Slope. Both regions, which represent a portion of Beringia, include or border the continental divide with the rivers draining either to the Bering or the Chukchi Seas (Seward Peninsula) and the Beaufort or Chukchi Seas (North Slope) (Fig. 1.1).

Beringia cannot be treated as a single homogeneous climatic unit [*Mock et al*. 1998]. The central Seward Peninsula experiences a continental climate and Barrow a maritime summer climate and polar winter. The synoptic climatic controls that govern temperature and precipitation anomalies differ spatially for different locations due to topographic features and coastal-inland contrasts [*Mock et al*., 1998]. The Brooks Range serves as an efficient atmospheric circulation barrier separating the Arctic and Pacific air masses between the Seward Peninsula and Arctic Coastal Plain. This is particularly evident in the precipitation regime with a reduced SWE (115 mm) and summer precipitation (93 mm) in Barrow compared to Kougarok (246 and 102 mm, respectively) [*Hinzman et al*., 2003; *Liljedahl*, this dissertation]. In the summer, the consistent maritime winds ensure cool, moist air

along the Arctic Coastal Plain [*Kozo*, 1982], while the Brooks Range Mountains block any warm air mass formed over the interior of Alaska from moving northward. Therefore, the mean July and annual air temperatures are considerably higher in Kougarok (11.0°C and -2.4°C) than in Barrow (5.4°C and -11.3°C) [*Hinzman et al*., 2003].

Although the two watersheds presented in this thesis lie in somewhat differing climate regimes, they are both underlain by continuous permafrost. The permafrost in Kougarok (65° 27'), central Seward Peninsula, is thin (15-50 m) [*Hinzman et al*., 2003], while the permafrost is several hundred meters thick in Barrow (71° 17') [*Shiklomanov et al*., 2010; *Jorgenson et al*., 2008]. The shallow active layers and continuous permafrost prevent winter baseflow in both areas. However, the two sites differs in summer runoff regimes where flow is nearly absent from small, extremely low-gradient Barrow watersheds [*Dingman et al*., 1980; *Brown et al*., 1968], while it does not completely cease in the Central Seward Peninsula [*Carr*, 2003]. The differences in summer runoff regimes is more likely a site specific detail as low amounts of summer runoff have been observed in Arctic Coastal Plain watersheds such as the Putuligayuk River watershed near Prudhoe Bay [*Kane et al*., 2008] and the Nunavak Creek near Barrow.

Underlain by marine and nonmarine sedimentary rocks [*Moore et al.*, 1997], the North Slope of Alaska consists of three major physiographical provinces: The Brooks Range, the Arctic Foothills, and the Arctic Coastal Plain. The Brooks Range, a collisional orogenic belt [*Moore et al.,* 1997], extends E-W across the width of Alaska with peaks reaching 2700 m (8850 ft) and is correlated with latitudinal and altitudinal tree-line. The extensive variation in topography results in diverse habitats for plants and animals with vegetation ranging from lichen cover at exposed sites to shrub tundra in the valley bottoms. Glaciers exist in central and eastern portions of the Range. Late Quaternary [*Hamilton and Porter*, 1975] and Pleistocene [*Hamilton*, 1978; 1979] glacial advances formed moraines at

the northern portion of the Arctic Foothills. The rolling terrain of the Arctic Foothills is vastly covered by tussock tundra with isolated shrub communities concentrated to wetter valley bottoms and drier meadows on ridge tops. The species richness in vegetation declines when moving towards the coastline. Although the floras are similar, mainly consisting of grasses, sedges and mosses, the Barrow and Prudhoe Bay tundra vegetation is markedly controlled by the differing parent material. For example, *Sphagnum* moss is absent near Prudhoe Bay, which is probably due to the relatively high pH [*Steere*, 1978] caused by the calcareous soils. The soils are acidic in Barrow [*Walker et al*., 2003] since the area is not affected by rivers transporting carbonates from the Brooks Range. Acidic soils are found in Kougarok [*Walker et al*., 2003].

Like the North Slope, the highlands and foothills of central Seward Peninsula were glaciated during both the Wisconsin and Illinoian age [*Hopkins*, 1969], while much of the lowlands experienced loess accumulation [*Pewe*, 1975; *Hopkins et al.,* 1982] that supported an arctic steppe [*Guthrie*, 1982, 1990; *Chapin and Starfield*, 1997]. Massive syngenetic ice wedges formed during the late Pleistocene when the land surface was accreting and today the region experiences active growth of epigenetic ice wedges [*Höfle et al*., 2000].

The Quaternary geology of the Arctic Coastal Plain is similar to that of the eastern and western shores of Bering Sea and the Bering Strait with records of high Cenozoic sea levels that left marine deposits [*Hopkins*, 1973; *Kaufman and Brigham-Grette*, 1993]. The marine sediments at the Arctic Coastal Plain are products of seven to eight marine transgressions ranging in age from 175 kya to 58 kya [see *Hinkel et al.*, 2005]. Shallow oriented lakes occupy 15 to 40 % of the Arctic Coastal Plain and they are also abundant in the Seward Peninsula landscapes [*Sellmann et al.*, 1975; *Livingstone et al.,* 1958]. Although the coverage decreases on older surfaces [*Hinkel et al.*, 2005], vegetated drained thaw lake basins (DTLB) cover about 50 % of the Arctic Coastal Plain [*Hinkel et al*., 2003]. With rich

accumulation of soil organic carbon [*Bockheim et al*., 2004], the DTLB possess the potential to be a significant source of CO_2 or CH_4. The relief of the Arctic Coastal Plain (and the northern Seward Peninsula) is restricted to lakes, DTLBs, river terraces, occasional pingos and, on the micro-scale, patterned ground in the form of low- and high centered polygons. The soils are poorly drained in the Barrow region due to the limited hydraulic gradients and the presence of permafrost.

Approximately 65 % of the Barrow Peninsula is covered by polygonal ground [*Sellman et al*., 1972]. The low- and high centered polygons results in a mosaic of soil moisture and vegetation variations. The extensive microtopographical variations induced by polygonal rims, troughs, high or low centers produce vegetation that changes character every meter or so, mainly alternating between mosses and grasses [*Webber et al.*, 1980]. Similarly, the microtopography results in highly variable spatial distribution of soil moisture, thaw depths, and snow cover [*Dingman et al*., 1980; *Engstrom et al*., 2005].

In the Arctic, the presence of permafrost complicates the soil properties where layers are not necessarily uniform following a chronological time sequence. The soils of northern Alaska characteristically exhibit clods or layers of peaty organic material or organic stain included in the mineral portion [*Drew*, 1957; *Bockheim et al.*, 2001]. Although the theory behind the processes that formed the complex soil horizons may vary in detail, they all include freeze-thaw cycles [*Kellogg and Nygard*, 1951; *Tedrow et al*., 1958; *Drew,* 1957; *Hanson,* 1959]. After the initial soil surveys in the 1950‘s it was evident that strong relationships exist between patterned ground and arctic soils [*Drew and Tedrow*, 1962; *Brown*, 1969]. In the years since then, the arctic soils have been recognized as an important component in the local as well as global ecosystem [*Webber et al.*, 1980; *Walker et al*., 2003; *Shiklomanov and Nelson*, 2002; *Schuur et al*., 2008].

Large pools of organic carbon are contained in the arctic soils and upper permafrost layers [*Post et al*., 1982; *Billings*, 1987; *Tarnocai*, 2006; *Ping et al*.,

2008; *Schuur et al*., 2008]. In a warming climate this carbon is susceptible to decomposition and release [*Oechel and Vourlitis*, 1995; *Schuur et al*., 2008]. Already, increased regional ground heat transfer and changes in soil moisture have resulted in increased efflux of CO_2 of up to 1.2 Gt C y^{-1} in just two arctic vegetation types [*Oechel et al*., 1993]. An increased release in CH_4 has also been observed from arctic wetlands [*Christensen et al*., 2004] and lakes [*Walter et al*., 2006]. The potential of Arctic trace gas fluxes affecting the global system is tremendous [*Oechel et al*., 1993; *Dutta et al*., 2006; *Zimov et al*., 2006].

Approximately 40% of the world's soil carbon is contained in the high latitude systems [*McGuire et al.,* 1995], but less than 1 % of the global biomass is found on the Arctic tundra [*Saugier et al*., 2001]. The Net Primary Production (NPP) is expected to increase as climate warms [*Oechel et al.,* 2000; *Shaver et al.,* 2000], partly due to increased nutrient availability as soils warms [*Chapin et al*., 1995]. Reflected by the climatic gradient between Barrow and Kougarok, the live biomass in Seward Peninsula is nearly twice that of Barrow (Table 1.1) [*Walker et al*., 2003]. Similar trends are seen in the Leaf Area Index as well as the Normalized Vegetation Index (NDVI). If one divides the biomass by the "green days" the resulting ratio is quite similar between Barrow (5.1) and Kougarok (5.8), indicating that the length of the growing season accounts for much of the biomass differences. Similar calculations substituting biomass with NPP come to the same conclusion [see *Chapin et al*., 2002].

Arctic vegetation have changed in the past [*Mann et al*., 2002, *Bigelow et al*., 2003], and major changes are expected in the future under a warming climate [*Chapin et al*., 2000; *McGuire et al*., 2000; *Kaplan et al*., 2003]. In fact, shrubs have expanded on the tundra landscapes, including Seward Peninsula and North Slope, in the last decades [*Silapaswan et al*., 2001; *Sturm et al*., 2001; *Tape et al*., 2006]. The role of shrubs on winter soil mineralization, hydrology, and energy exchange [*Sturm et al*., 2005a, b], snowmelt energy balance [*Pomeroy et al*., 2006;

Bewley et al., 2010], and surface albedo [*Chapin et al*., 2005] has gained attention in the literature, but there are limited analyses on the role of shrubs on the summer mass and heat exchange. Short-term differences between summer tundra surfaces with differing vegetation cover (and in some instances also including a differing slope and aspect) show shrubs increasing the sensible heat flux while latent heat fluxes are similar [*McFadden et al.*, 1998; *Beringer et al*., 2005].

Unique hydrologic challenges are encountered in an environment underlain by permafrost. Continuous permafrost acts as an impermeable hydrologic barrier reducing soil water storage capacity and constraining subsurface flow [*Hinzman et al*., 1991, 1998; *Kane et al*., 1991] and is therefore exerting a major control on runoff and the interaction of surface and sub-permafrost water [*Dingman,* 1970, 1973; *Church,* 1974; *Newbury,* 1974; *Slaughter and Kane,* 1979; *Woo and Steer,* 1982, 1983; *Woo,* 1986; *Kane et al.,* 1989]. When permafrost is completely penetrated by a thawed soil column (open talik) the ground surface may either drain or flood depending on the local hydraulic gradients. For example, in Council, Seward Peninsula, *Yoshikawa and Hinzman* [2003] attributed shrinking ponds to open talik formation. In other places such as the Tanana Flats, the absence of permafrost has resulted in an expanding wetland that is constantly fed by subpermafrost groundwater originating from the Alaska Range [*Racine and Walter*s, 1994].

The differences in hydrologic processes are not solely attributed to the absence or presence of permafrost. The thickness of the active layer, the soil column that experiences seasonal freeze and thaw, and its seasonal development also affects the hydrologic fluxes and stores. The storage capacity of the soils is not static. As the summer season progress the storage capacity increases affecting the runoff response [*McNamara et al*., 1997] and recession rates of runoff events [*Yamazaki et al*., 2006]. Deeper thawing increases subsurface storage that potentially can drain. When vascular vegetation is limited and mosses are abundant,

a deeper thaw can result in limited hydrologic connectivity to the atmosphere as vascular plant roots may access deeper soil water than mosses. Conversely, a saturated and frozen active layer can serve as a buffer during dry summers by offering a continuous supply of water to evapotranspiration as ice melts [*Sugimoto et al*., 2003].

In general, low-gradient hydrology, typical of the Arctic slope, mainly depends upon the vertical fluxes of water through precipitation, evapotranspiration, infiltration, and percolation [*Woo et al*., 2008]. Nonetheless, if snow accumulation is sufficient, the lateral component can constitute a significant portion of the wetland water balance as spring freshet [*Woo*, 1986; *Bowling et al*., 2003]. At this time, a substantial amount of water is released in a short time period generating not just perhaps the only runoff event of the year but also extensive surface ponding and eventual recharge of the previous summer‘s surface and soil water storage deficits [*Rovansek et al*., 1996; *Bowling et al*., 2003; *Woo and Guan*, 2006; *Bowling and Lettenmaier*, 2010]. In general, pre-freeze soil moisture levels are an important regulator of spring runoff in northern regions [*Kane et al*., 1978; *Kane and Stein*, 1984]. Within two weeks of the spring freshet, the surface water becomes less abundant and lateral connectivity becomes more complex if not disconnected [*Bowling et al.,* 2003]. It is only through large inputs if water into the basin (as during snowmelt) that restore the connectivity [*Kane et al.,* 2003].

It is generally agreed upon that reliable precipitation estimates in these environments are difficult to obtain [*Black*, 1954; *Benson,* 1969; *Yang et al*., 1998]. This is due to undercatch by gauges caused by winds and our inability to record trace events, both of which are common to the coastal environment of Barrow. While recorded annual precipitation was 124 mm, *Dingman et al.* [1980] estimated the actual precipitation to be closer to 170 mm by multiplying the observations with a correction factor. That is strikingly similar to the adjustment method presented by *Yang et al.* [1998], which results in a mean annual precipitation of 177 mm.

Correction factors from 1.2 (summer) to 3.8 (winter) have been suggested for Barrow [*Benning and Yang*, 2005]. As many water balance analyses rely on the water budget method, often by solving evapotranspiration as the residual, an erroneous description of the precipitation amount can have profound effects on our understanding of the hydrologic system.

Runoff is the most accurately measured water balance component. While observations of runoff from the coastal plain was limited in the 70‘s [*Dingman et al*., 1980], the present situation is even worse. The only long-term coastal plain station still maintained is the Putuligayuk River near Prudhoe Bay (Water and Environmental Research Center), as the USGS observations initiated in 1973 at Nunavak Cr. near Barrow ceased in 2004. Average annual runoff from the coastal plain averages ~110 mm ranging from 53 to 200 mm with a major portion (61 to 98 %) concentrated to the short time period during snowmelt [*Dingman et al*., 1980; *Kane et al*., 2008]. A major portion (22 %) of the accumulated snow is partitioned into lake storage, temporary ponds, or infiltration into the frozen soils [*Bowling et al*., 2003, *Kane et al*., 2003; *Kane et al*., 2008].

Although not including the snowmelt period, *Brown et al.* [1968] presented the first comprehensive hydrologic analysis of an Arctic Coastal Plain watershed. The Barrow study basin mainly constituted a vegetated drained thaw lake basin. Highlighting the challenge in determining the absolute drainage area due to the subtle relief, they found varying hydrograph response to individual storm events with surface runoff primarily occurring through the intricate network of polygonal troughs and ponds. The lateral connection changed as the summer progressed, resulting in the perhaps the first description of a constantly changing drainage area at Arctic wetlands. In fact, several features unique to the permafrost environment may potentially retard surface drainage and increase surface storage [*Kane et al.,* 2003].

When snowmelt runoff ceases, evapotranspiration is typically the only hydrologic process for removing water from the active layer. Despite being an important, if not major, pathway of water loss [*Rovansek et al*., 1996; *Mendez et al*., 1998; *Bowling et al*., 2003; *Bowling and Lettenmaier*, 2010; *Kane et al*., 2008] across pan-Arctic wetlands, evapotranspiration is the least quantified component in the Arctic hydrologic cycle [*Kane et al*., 1989, 1992; *Vörösmarty et al*., 2001; *Woo et al*., 2008]. Estimates of evapotranspiration vary greatly, even within the same basin, resulting in uncertainties of the other water balance component estimates. The higher estimate of total evapotranspiration (210 mm) was suggested by *Weller and Holmgren* [1974], which exceeds the assumed annual precipitation regime. On the lower end, *Dingman et al*. [1980] estimated annual evapotranspiration to less than a third (60 mm) by subtracting the annual runoff from precipitation. The variation in evapotranspiration estimates is most likely not solely due to differing years and methods but also due to the challenge in accurate measurements, particularly precipitation.

The summer surface energy partitioning at wet arctic sites is usually dominated by latent heat flux [*Roulet and Woo*, 1986; *Rouse et al*., 1992; *Lafleur and Rouse*, 1995; *Harazono et al*., 1998; *McFadden et al*., 1998; *Mendez et al*., 1998; *Kodama et al*., 2007], although a seasonal progression from latent heat to sensible heat coinciding with water table reductions has been shown [*Vourlitis and Oechel*, 1999]. In the compilation by *Eugster et al*. [2000] it is evident that a gradient exists from the coast to the inland tundra resulting in the dominance of sensible and latent heat at the coast and inland, respectively. The phenomenon is related to the drastic air temperature contrasts between the immediate coast and the interior portion of the Alaskan Arctic [*Haugen and Brown*, 1980], with the maritime air mass affecting the surface energy balance up to 135 km inland [*Harazono et al*., 1998]. With evapotranspiration representing a major pathway of water loss from current wetlands, an important question arises: Will climate

warming cause large increases in evapotranspiration rates resulting in widespread drying of high-latitude wetlands? Or, will the maritime location prevent a drying of the arctic coastal wetlands?

In contrast to most non-arctic wetlands, summer ground heat flux is substantial and generally amounts to approximately 10-35% of net radiation [*Vourlitis and Oechel*, 1997; *McFadden et al*., 1998; *Eugster et al*., 2005; *Boike et al*., 2008]. While the thaw depth exerts a strong control on the hydrology, the reverse is also true [*Woo and Xia*, 1996; *Hinzman et al*., 1991]. Heat input to the active layer is dependent on the energy available at the ground surface and the partitioning of that energy. This heat is used to melt ice, and to warm both the active layer and permafrost. Conversely, heat is released when soils are cooling and, in even larger amounts, during ice formation as the phase change of H_2O includes latent heat release. The thermal properties of organic soils in particular, due to their low substrate density, are controlled by the moisture and/or ice condition [*Farouki*, 1981]. A high ice content may result in up to nearly four times the thermal conductivity of the same organic soil in a thawed saturated condition, with the difference being even larger with a dry thawed soil [*Farouki*, 1981; *Romanovsky and Osterkamp*, 1995]. It is therefore possible to find permafrost in regions that have mean annual temperatures above freezing [*Burn and Smith*, 1988; *Shur and Jorgenson*, 2007].

Although the dynamic linkage between the thermal and hydrologic regime is agreed upon, the efforts in incorporating such mechanisms into watershed models have been constrained. Nonetheless, detailed one-dimensional coupled heat and mass transfer models (finite difference or finite element) have been developed but simplifications are commonly made on watershed scale [*Fox*, 1992; *Hinzman et al*., 1998]. For example, when simulating arctic watershed response to climate warming, future near-surface soil moisture conditions assumed similar to present, therefore constraining the ground heat flux [*Kane et al*., 1990; *Hinzman and Kane*,

1992; *Marchenko et al*., 2008]. Conversely, the spatially distributed and semi-distributed hydrology models described by *Zhang et al*. [2000] and *Fox* [1992], respectively, produce spatially variable soil moisture while the representation of thaw depth is based upon cumulative degree-days. Other models have detailed coupling of the subsurface mass and heat fluxes, while the surface physical and physiological processes are crudely represented [*Voss et al.*, 2009; *Ossola and Travis*, 2009]. In any of the cases above, the model structures include rough assumptions, where the energy available at the ground surface and its partitioning remain semi-static in both space and time. It is not until recently that hydrologic and thermal models have begun to fully integrate in two dimensions through the energy balance equation, including lateral advective heat transfer, [*Weisser et al*., 2009; *Marsh et al*., 2009] opening an exciting future for not only the hydrologic science but also for all disciplines related to hydrology.

Fire is an integral component of the sub-arctic ecosystem. As an episodic and returning disturbance, its changes to the surface cover may have both long- and short term effects on the hydrologic system. Severe burns often lead to degraded permafrost [*Czudek,* 1970*; Yoshikawa et al.,* 2002; *Myers-Smith et al.*, 2008] that may return as the vegetation cover is re-established [*Racine et al.*, 2004; *Shur and Jorgenson*, 2007]. Thermokarst processes are often observed in recently burned ice-rich permafrost environments. By altering hydraulic gradients and increasing lateral drainage, thermokarsts may also initiate thermal and mechanical erosion [*Hinzman et al.,* 1997] quickly altering the channel networks and therefore also the ecosystem [*Rouse*, 2000]. Short-term (< 4 yrs) hydrologic post-fire effects on tundra environments include increased surface wetness [*Liljedahl et al*., 2007] and even surface ponding [*Shaver*, 2010]. Interestingly, *Shaver* [2010] reported higher latent heat fluxes (+60 %) at the severely burned tussock tundra site compared to the unburned site in mid- to late summer. In the long-term on the other hand, near-surface soil may become drier due to the formation of open taliks that promote

drainage [*Swanson*, 1996; *Yoshikawa et al*., 2002]. While the effects of fires in permafrost environment are relatively well-documented, the mechanisms behind the sometimes complex responses are underexplored [*Chambers et al*., 2005]. Hydrologic responses to disturbance are often much larger and faster than any direct response to long-term climate changes [*Shur and Jorgenson*, 2007].

1.3 Figures

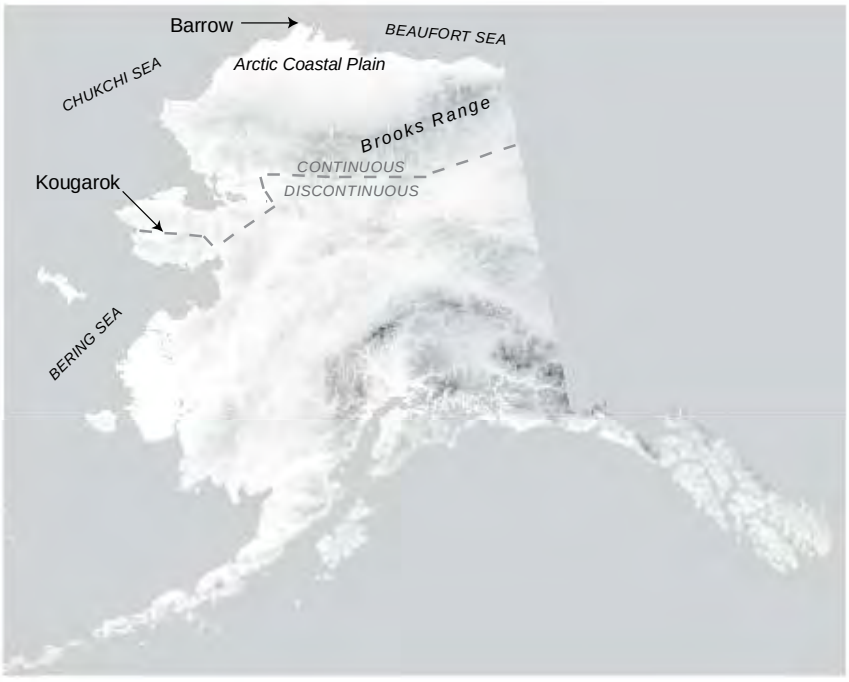

Figure 1.1 Map of Alaska including the study locations and the approximate boarder of the continuous and discontinuous permafrost.

1.4 Tables

Table 1.1 Summary of bioclimate, NDVI, thaw depth, and biomass in Barrow and Kougarok. SWI (Summer Warmth Index) is the sum of the mean monthly temperatures greater than 0 °C (°C months). Green days are the number of days in which the NDVI value is greater than 0.09. The information is obtained from Walker et al. [2003].

	SWI °C months	Thaw depth cm	Max NDVI	Green Days	Biomass g m^{-2}					LAI m^2 m^{-2}
					Total	Lichen	Moss	Shrub	Graminoid	
Barrow	8.84	34	0.418	88	452	103	267	25	25	0.75
Kougarok	32	40	0.482	136	793	18	17	427	326	2.9

1.5 References

Anisimov, O. A., and F. E. Nelson (1997), Permafrost zonation and climate change in the northern hemisphere: Results from transient general circulation models, *Climatic Change 35*, 241–258, 10.1023/A:1005315409698.

Arctic Climate Impact Assessment (ACIA) (2005), *Impacts of a Warming Arctic: Arctic Climate Impact Assessment,* Cambridge Univ. Press, New York, NY.

Benning, J., and D. Yang (2005), Adjustment of daily precipitation data at Barrow and Nome Alaska for 1995–2001, *Arctic, Antarctic, and Alpine Res., 37*(3), 276–283.

Benson , C. S. (1969), The seasonal snow cover of arctic Alaska, *Arctic Institute of North Am. Res. Paper 51*, 47.

Beringer, J., F. S. Chapin, C. C. Thompson, and A. D. McGuire (2005), Energy exchanges along a tundra-forest transition and feedbacks to climate, *Agric. Forest Meteorol. 131*, 143–161.

Bewley, D., R. Essery, J. Pomeroy, and C. Ménard (2010), Measurements and modelling of snowmelt and turbulent heat fluxes over shrub tundra, *Hydrol. Earth System Sci. Disc*., 7(1), 1005–1032.

Bigelow, N. H., L. B. Brubaker, M. E. Edwards, S. E. Harrison, I. C. Prentice, P. M. Anderson, A. A. Andreev, P. J. Bartlein, T. R. Christensen, W. Cramer, J. O. Kaplan, A. V. Lozhkin, N. V. Matveyeva, D. F. Murray, A. D. McGuire, V. Y. Razzhivin, J. C. Ritchie, B. Smith, D. A. Walker, A. D. Igarashi, K. V. Kremenetskii, A. Paur, M. F. J. Pisaric, V. S. Volkova (2003), Climate change and Arctic ecosystems I: Vegetation changes north of 55 °N between the last glacial maximum, mid-Holocene and present, *J. Geophys. Res.,* 108, D19, 8170, doi:10.1029/2002JD002558.

Billings, W. D. (1987), Carbon balance of Alaskan tundra and taiga ecosystems: past, present and future*, Quaternary Sci. Rev., 6*(2), 165–177.

Black, R. F. (1954), Precipitation at Barrow, Alaska, greater than recorded, *Trans. Am. Geophys. Union, 35*, 203–206.

Bockheim, J. G., K. M. Hinkel, and F. E. Nelson, (2001), The soils of the Barrow Region Alaska, *Polar Geogr., 25*(3), 163–181.

Bockheim J. G., K. M. Hinkel, W. R. Eisner, X. Y. Dai, K. M. Peterson (2004), Carbon pools and accumulation rates in an age-series of soils in drained thaw-lake basins, Arctic Alaska. *Soil Sci. Soc. of Am. J., 68*, 697–704.

Boike, J., C. Wile, and A. Abniozva (2008), Climatology and summer energy and water balance of polygonal tundra in the Lena River Delta, Siberia, *J. Geophys. Res., 113*, G03025, doi:10.1029/2007JG000450.

Bowling, L. C., D. L. Kane, R. E. Gieck, L. D. Hinzman, and D. P. Lettenmaier (2003), The role of surface storage in a low-gradient Arctic watershed, *Water Resour. Res., 39*(4), 1087, doi:10.1029/2002WR001466.

Bowling L. C., D. P. Lettenmaier (2010), Modeling the effects of lakes and wetlands on the water balance of arctic environments, *J. of Hydrometeorol., 11*(2), 276–295. doi: 10.1175/2009JHM1084.1

Brown, J. (1969), Tundra soils formed over ice wedges, northern Alaska, *Soil Sci. Soc. Am*. *Proceedings, 31*, 686–691.

Brown, J., P. C. Miller, L. L. Tieszen, F. Bunnell (1980), *An Arctic ecosystem: the coastal tundra at Barrow, Alaska*, Dowden, Hutchinson & Ross Inc., Stroudsburg, PA.

Brown, J. R., S. L. Dingman, and R. I. Lewellen (1968), Hydrology of a drainage basin on the Alaskan Coastal Plain, *Res. Rep. 240*, U. S. Army Cold Regions Res. and Engineering Lab., Hanover, NH.

Burn, C., and C. Smith (1988), Observations of the ‗‗thermal offset'' in near-surface mean annual ground temperatures at several sites near Mayo, Yukon Territory Canada, *Arctic, 41*, 99–104.

Carr, A., (2003), Hydrology comparisons and model simulations of sub-Arctic watersheds containing continuous and discontinuous permafrost, Seward Peninsula, Alaska, M.S. Thesis, University of Alaska, Fairbanks, AK.

Chambers, S. D., J. Beringer, J. T. Randerson, and F. S. Chapin III (2005), Fire effects on net radiation and energy partitioning: Contrasting responses of tundra and boreal forest ecosystems, *J. Geophys. Res. 110*, D09106, doi:10.1029/2004JD005299.

Chapin, F. S., G. R. Shaver, A. E. Giblin, K. J. Nadelhoffer, and J. A. Laundre (1995), Responses of Arctic Tundra to Experimental and Observed Changes in Climate, *Ecology*, *76*(3), 694–711.

Chapin, F. S., and A. M, Starfield (1997), Timelags and novel ecosystems in response to transient climate change in Arctic Alaska, *Climatic Change, 35*, 449–461.

Chapin, F. S. III, A. D. McGuire, J. Randerson, R. Pielke, D. Baldocchi, S. E. Hobbie, N. Roulet, W. Eugster, E. Kasischke, E. B. Rastetter, S. A. Zimov, S. W. Running (2000), Arctic and boreal ecosystems of western North America as components of the climate system, *Global Change Biology, 6*, 211–223.

Chapin, F. S., P. A. Matson, and H. A. Mooney (2002), *Principles of terrestrial ecosystem ecology*, Springer Science, New York, NY.

Chapin, F. S. III, M. Sturm, M. C. Serreze, J. P. McFadden, J. R. Key, A. H. Lloyd, A. D. McGuire, T. S. Rupp, A. H. Lynch, J. P. Schimel, J. Beringer,W. L. Chapman, H. E. Epstein, E. S. Euskirchen, L. D. Hinzman, G. Jia, C.-L. Ping, K. D. Tape, C. D. C. Thompson, D. A. Walker, J. M. Welker **(**2005), Role of land-surface changes in arctic summer warming, *Science, 28* (310/5748), 657–660, doi:10.1126/science.1117368.

Chapin, F. S., M. W. Oswood, K. van Cleve, V. A.Viereck, and D. L. Verbyla (2006), *Alaska's changing boreal forest*, Oxford University Press, New York, NY.

Christensen, T. R., and P. Cox (2002), Response of methane emission from Arctic tundra to climatic change: results from a model simulation, *Tellus, 47*(3), 301–309.

Christensen, T. R., T. Johansson, H. J. Åkerman, M. Mastepanov, N. Malmer, T. Friborg, P. Crill, and B. H. Svensson (2004), Thawing sub-arctic permafrost: Effects on vegetation and methane emissions, *J. Geophys. Res. Lett., 31*, L04501, doi:10.1029/2003GL018680.

Church, M. (1974), Hydrology and permafrost with reference to northern North America, in *Proceedings Workshop Seminar on Permafrost Hydrology*, edited by J. Demers, pp. 7–20, Secretariat, Canadian National Committee, International Hydrological Decade, Environment Canada, Ottawa, Canada.

Czudek, T. (1970), Thermokarst in Siberia and its influence on the development of lowland relief, *Quaternary Res., 1* (1), 103-120, 10.1016/0033-5894(70)90013-X

Dingman, S. L. (1970), Hydrology of the Glenn Creek watershed, Tanana River basin, central Alaska, *Res. Rep. 297*, U.S. Army Cold Regions Res. and Engineering Laboratory, Hanover, NH.

Dingman, S. L. (1973), Effects of permafrost on stream characteristics in the discontinuous permafrost zone of central Alaska, in *Permafrost: North American Contribution to the Second International Conference*, pp. 447–453, National Academy of Sciences, Washington, DC.

Dingman, S. L., R. G. Barry, G. Weller, C. Benson, E. F. LeDrew, and C. W. Goodwin (1980), Climate, snow cover, microclimate, and hydrology, in *An Arctic Eco- system: the Coastal Tundra at Barrow, Alaska*, edited by J. Brown, P. C. Miller, L. L. Tieszen and F. L. Bunnell, pp. 30–56. Dowden, Hutchinson and Ross, Stroudsburg, PA.

Drew, J. V. (1957), *A pedologic study of Arctic Coastal Plain soils near Point Barrow, Alaska*, Ph.D. Thesis, Rutgers Univ., New Brunswick, NJ.

Drew, J. V., and J. C. F. Tedrow (1962), Arctic soil classification and patterned ground, *Arctic, 15*,109–116.

Dutta, K., E. G. Shuur, and S. A. Zimov (2006), Potential carbon release from permafrost soils of Northeastern Siberia, *Global Change Biol., 12*(12), 2336–2351.

Engstrom, R., A. Hope, H. Kwon, D. Stow, and D. Zamolodchikov (2005), Spatial distribution of near surface soil moisture and its relationship to microtopography in the Alaskan Arctic coastal plain, *Nordic Hydrol., 36*(3), 219–234.

Eugster, W., W. Rouse, R. A. Pielke, J. P. McFadden, D. D. Baldocchi, T. G. F. Kittel, F. S. Chapin III, G. E. Liston, P. L. Vidale, E. Vaganov, and S. Chambers (2000), Land-atmosphere energy exchange in Arctic tundra and boreal forest: Available data and feedbacks to climate, *Global Change Biol., 6*, 84–115.

Eugster, W., J. P. McFadden, and F. S. Chapin III (2005), Differences in surface roughness, energy, and CO_2 fluxes in two moist tundra vegetation types, Kuparuk watershed, Alaska, U.S.A., *Arctic, Antarctic, and Alpine Res., 37*(1), 61–67.

Farouki, O. T. (1981), Thermal properties of soils, *Monogr. 81–1*, U. S. Army Cold Regions Res. and Engineering Lab., Hanover, NH.

Flannigan, M., I. Campbell, M. Wotton, C. Carcaillet, P. Richard, and Y.Bergeron (2001), Future fire in Canada‘s boreal forest: paleoecology results and general circulation model – regional climate model simulations, *Can. J. For. Res. 31,* 854–864.

Fox, J. D. (1992), Incorporating freeze-thaw calculations into a water balance model, *Water Resources Res., 28*(9), 2229–2244.

Fox, S. (2002), These are things that are really happening: Inuit perspectives on the evidence and impacts of climate change in Nunavut‘, in *The Earth is Faster Now: Indigenous Observations of Arctic Environmental Change,* edited by I. Krupnik, and D. Jolly, pp. 12–53, Arctic Research Consortium of the United States, Fairbanks, AK.

Francis, J. A., D. M. White, J. J. Cassano, W. J, Gutowski Jr., L. D. Hinzman, M. M. Holland, M. A. Steele, and C. J. Vörösmarty (2009), An arctic hydrologic system in transition: Feedbacks and impacts on terrestrial, marine, and human life, *J. Geophys. Res., 114*, doi:10.1029/2008JG000902.

Frey, K. E., and L. C. Smith (2005), Amplified carbon release from vast West Siberian peatlands by 2100, *Geophys. Res. Lett 32*, L09401, doi:10.1029/2004GL022025.

Goodison, B. E., P. Y. T. Louie, and D. Yang (1998), WMO solid precipitation measurement intercomparison, WMO/TD 872, 212 pp., World Meteorol. Org., Geneva.

Groisman, P. Y., and D. R. Legates (1994), The accuracy of United States precipitation, *Bulletin Am. Meteorol. Soc., 75*(2), 215–227.

Guthrie, R. D. (1982), Mammals of the mammoth-steppe as paleoenvironmental indicators, in *Paleoecology of Beringia*, edited by D. M. Hopkins, J. V. Matthews, C. E. Schweger, and S. B. Young, pp. 307–326., Academic Press, New York, NY.

Guthrie, R. D. (1990), *Frozen fauna of the mammoth steppe: The story of Blue Babe*, Univ. of Chicago Press, Chicago, IL.

Hamilton, T. D. (1978), Surficial geology of the Philip Smith Mountains quadrangle, Alaska, *Map MF-879-A*, scale 1:250,000, U. S. Geol. Surv. Misc. Field Studies, U.S.A.

Hamilton, T. D. (1979), Surficial geologic map of the Chandler Lake quadrangle, Alaska, *Map MF-1121*, scale 1:250,000, U. S. Geol. Surv. Misc. Field Studies, U.S.A.

Hamilton, T. D., and S. C. Porter (1975), Itkillik glaciation in the Brooks Range, northern Alaska, *Quaternary Res*., *5*, 471–497.

Hanson, H. C., 1959, Vegetation and soil profiles in some solifluctuation and mound areas in Alaska, *Ecol*., 31, 606–630.

Harazono, Y., M. Yoshimoto, M. Mano, G. L. Vourlitis, and W. C. Oechel (1998), Characteristics of energy and water budgets over wet sedge and tussock tundra ecosystems at North Slope Alaska, *Hydrol. Process., 12*, 2163–2183.

Haugen, R. K., and J. Brown (1980), Coastal-inland distributions of summer air temperature and precipitation in northern Alaska, *Arctic and Alpine Res., 12*(4), 403–412.

Hinkel K. M., W. R. Eisner, J. G. Bockheim, F. E. Nelson, K. M. Peterson, X. Dai (2003), Spatial extent, age, and carbon stocks in drained thaw lake basins on the Barrow Peninsula, Alaska, *Arctic, Antarctic, and Alpine Res*., *35*, 291–300.

Hinkel, K. M., R. C. Frohn, F. E. Nelson, W. R. Eisner, and R. A. Beck (2005), Morphometric and spatial analysis of thaw lakes and drained lake basins in the western Arctic Coastal Plain, Alaska, *Permafrost Periglacial. Proc., 16*, 327–341.

Hinzman, L. D., D. L. Kane, R. E. Gieck, and K. R. Everett (1991), Hydrological and thermal properties of the active layer in the Alaskan Arctic, *Cold Regions Sci. Technol., 19*, 95–110.

Hinzman, L. D., and D. L., Kane (1992), Potential response of an Arctic watershed during a period of global warming, *J. Geophys. Res., 97*(D3), 2811–2820.

Hinzman, L. D., D. L. Kane, C. S. Benson, and K. R. Everett (1996), Energy balance and hydrological processes in an Arctic watershed, *Ecological Studies*, 131–154.

Hinzman, L. D., D. L. Goering, T. C. Kinney, and S. Li, (1997), Numeric simulation of thermokarst formation during disturbance, in *Disturbance and Recovery in Arctic Lands*, edited by R. M. M. Crawford, pp. 191–211, Kluwer Academic Publishers, Netherlands.

Hinzman, L. D., D. J. Goering, and D. L. Kane (1998), A distributed thermal model for calculating soil temperature profiles and depth of thaw in permafrost regions, *J. Geophys. Res., 103*(22). 28, 975–28,991.

Hinzman, L. D., D. L. Kane, K. Yoshikawa, A. Carr, and M. Fraver (2003), Hydrological variations among watersheds with varying degree of permafrost, in *Proceedings of the Eight International Conference on Permafrost*, edited by Phillips, Springman and Anderson, pp. 407-411, Balkema Publishers, Zurich, Switzerland.

Hinzman, L. D., N. D. Bettez, W. R. Bolton, F. S. Chapin, M B. Durgerov, C. L. Fastie, B. Griffith, R. D. Hollister, A. Hope, H P. Huntington, A. M. Jensen, G. J Jia, T. Jorgenson, D. L. Kane, D. R. Klein, G. Kofinas, A. H. Lynch, A. H Lloyd, A. D. McGuirre, F. E. Nelson, W. C. Oechel, T. E. Osterkamp, C. H. Racine, V. Romanovsky, R. S. Stone, D. A. Stow, M. Sturm, C. R. Tweedie, G. L. Vourlitis, M. D. Walker, D. A. Walker, P. J. Webber, J. M. Welker, K. S. Winker, and K. Yoshikawa, (2005), Evidence and implications of recent climate change in Northern Alaska and other Arctic regions, *Climatic Change, 72*, 251–298. doi:10.1007/s10584-5352-2.

Höfle, C., M. E. Edwards, D. M. Hopkins, and D. M. Mann (2000), The full-glacial environment of the northern Seward Peninsula, *Quaternary Res. 53*, 143–153.

Hollister, R. D., P. J. Webber, and C. E. Tweedie (2005), The response of Alaskan arctic tundra to experimental warming: differences between short- and long-term responses, *Global Change Biol. 11*, 525–536.

Hopkins. D. M. (1969), History of Imuruk Lake, Seward Peninsula, *Alaska, Bull. Geol. Soc. Am. 70*, 103–1046.

Hopkins, D. M. (1973), Sea level history in Beringia during the last 210,000 years. *Quaternary Res.* 3, 520–540.

Hopkins, D. M., J. V. Matthews, C. E. Schweger, and S. B. Young (1982), *Paleoecology of Beringia*, Academic Press New York, New York, NY.

Jones, B. J., C. A. Kolden, R. Jandt, J. T. Abatzoglou, F. Urban, and C. D. Arp (2009), Fire behavior, weather, and burn severity of the 2007 Anaktuvuk River tundra fire, North Slope, Alaska, *Arctic, Antartctic, and Alpine Res., 41*(3), 309–316.

Jorgenson, T., K. Yoshikawa, M. Kanevskiy, Y. Shur, V. Romanovsky, S. Marchenko, G. Grosse, J. Brown, and B. Jones (2008), Permafrost characteristics of Alaska, in *Proceedings of the Ninth International Conference on Permafrost*, Fairbanks, Alaska, edited by D. L. Kane and K. M. Hinkel, Institute of Northern Engineering, University of Alaska Fairbanks. pp. 121–122.

Kane, D. L., J. D. Fox, R. D. Seifert, and G. S. Taylor (1978), Snowmelt infiltration and movement in frozen soils, in *Proceedings of the Third International Permafrost Conference*, pp. 201-206, National Research Council of Canada, Edmonton, Alberta, Canada.

Kane, D. L., and J. Stein (1984), Plot measurements of snowmelt runoff for varying soil conditions, *Geophysica, 20*(2), 123–135.

Kane, D. L., L. D. Hinzman, C. S. Benson, and K. R. Everett (1989), Hydrology of Imnavait Creek, an arctic watershed, *Holarctic Ecology, 12*, 262–269.

Kane, D. L., R. E. Gieck, and L. D. Hinzman (1990), Evapotranspiration from a small Alaskan watershed, *Nordic Hydrol., 21*, 253–272.

Kane, D. L., Hinzman, L. D., Benson, C. S., and Liston, G. E., (1991), Snow hydrology of a headwater Arctic basin 1. Physical measurements and process studies, *Water Resources Res., 27*(6), 1099–1109.

Kane, D. L., L. D. Hinzman, M-K. Woo, and K. R. Everett (1992), Arctic hydrology and climate change, in *Arctic Ecosystem in a Changing Climate*, edited by F. S. Chapin *et al*., pp. 35–57, Academic, San Diego, CA.

Kane D.L., R.E. Gieck, L.C. Bowling (2003), Impacts of surficial permafrost landforms on surface hydrology, in *Proceedings of the Eight International Conference on Permafrost*, edited by Phillips, Springman and Anderson, pp. 507-511, Balkema Publishers, Zurich, Switzerland.

Kane, D. L., and D. Yang (2004), Overview of water balance determinations for high latitude watersheds, in *Northern Research Basins Water Balance*, edited by D. L. Kane and D. Yang, pp. 1-12, IAHS, Oxfordshire, UK.

Kane, D. L., R. E. Gieck, and L. D. Hinzman (2008), Water balance for a low-gradient watershed in Northern Alaska, in *Proceedings Ninth International Conference on Permafrost*, edited by Kane and Hinkel, University of Alaska Press, Fairbanks, AK.

Kasischke, E. S., and M. R. Turetsky (2006), Recent changes in the fire regime across the North American boreal region: Spatial and temporal patterns of burning across Canada and Alaska, *Geophys. Res. Lett., 111*, L09703, doi:10.1029/2006GL025677.

Kaplan, J. O., N. H. Bigelow, P. J. Bartlein, T. R. Christensen, W. Cramer, S. P. Harrison, N. V. Matveyeva, A. D. McGuire, D. F. Murray, I. C. Prentice, V. Y. Razzhivin, B. Smith, D. A. Walker, P. M. Anderson, A. A. Andreev, L. B. Brubaker, M. E. Edwards, L. V. Lozhkin, J. C. Ritchie (2003), Climate change and Arctic ecosystems II: Modeling, paleodatamodel comparisons, and future projections. *J. Geophys. Res., 108,* (D19), 8171, doi:10.1029/2002JD002559.

Kaufman, D. S., and J. Brigham-Grette (1993), Aminostratigraphic correlations and paleotemperature implications, Pliocene-Pleistocene high-sea level deposits, northwestern Alaska, *Quaternary Sci. Rev. 12*, 21–33.

Kellogg, C. E., and I. J. Nygard (1951), The principal soil groups of Alaska, *Agric. Mono. No. 7*, U.S. Department of Agriculture, Washington, DC.

Kodama, Y., N. Sato, H. Yabuki, Y. Ishii, M. Nomura, and T. Ohata (2007), Wind direction dependency of water and energy fluxes and synoptic conditions over a tundra near Tiksi, Siberia, *Hydrol. Proc., 21*, 2028–2037.

Kozo, T. L. (1982), An observational study of sea breezes along the Alaskan Beaufort Sea coast: Part 1, *J. Appl. Meteorol., 21*(7), 891–905.

Lafleur, P. M., and W. R. Rouse (1995), Energy partitioning at tree line forest and tundra sites and its sensitivity to climate change, *Atmos.-Ocean, 33*, 121–133.

Lawrence, D. M., A. G. Slater, R. A. Tomas, M. M. Holland, and C. Deser (2008), Accelerated Arctic land warming and permafrost degradation during rapid sea ice loss, *Geophys. Res. Lett.*, 35, L11506, doi:10.1029/2008GL033985.

Liljedahl, A. K., L. D. Hinzman, R. C. Busey, and K. Yoshikawa (2007), Physical short-term changes after a tussock tundra fire, Seward Peninsula, Alaska, *J. Geophys. Res*., F02S07, doi:10.1029/2006JF000554.

Livingstone, D. A., K. Bryan, R.G. Leahy (1958), Effects of an arctic environment on the origin and development of fresh-water lakes, *Limnology and Oceanography 3*,192–214.

Mann, D. H. , D. M. Peteet, R. E. Reanier, M. L. Kunz (2002), Responses of an arctic landscape to Late glacial and early Holocene climatic changes: the importance of moisture, *Quat. Sci. Rev.,* 21, 997–1021.

Marchenko, S., Romanovsky, V., Tipenko, G. (2008) Numerical modeling of spatial permafrost dynamics in Alaska, in *Proceedings of the Ninth International Conference on Permafrost*, edited by D. L. Kane and K. M. Hinkel, pp. 1125-1130, Univ. of Alaska Fairbanks, Fairbanks, AK.

Marsh, P., S. Endrizzi, W. L. Quinton, R. Thorne, and M. Dall'Amico (2009), Modeling the spatial variability of the depth of ground thaw in a continuous permafrost, arctic tundra landscape, abstract C51A-045 presented at the Am. Geophys. Union Fall Meeting, San Francisco, CA.

McFadden, J. P, F. S. Chapin III, and D. Y. Hollinger (1998), Subgrid-scale variability in the surface energy balance of arctic tundra, *J. Geophys. Res, 103*(D22), 28947–28961.

McGuire, A. D., J. M. Melillo, D. W. Kicklighter, and L. A. Joyce (1995), Equilibrium responses of soil carbon to climate change: Empirical and process-based estimates, *J. Biogeography* 22, 785–796.

McGuire, A. D., J. S. Clein, J. M. Melillo, D. W. Kicklighter, R. A. Meier, C. J. Vörösmarty, M. C. Serreze (2000), Modeling carbon responses of tundra ecosystems to historical and projected climate: sensitivity of pan-Arctic carbon storage to temporal and spatial variation in climate, *Global Ch. Biol., 6*, 141–159.

McNamara, J. P., D. L. Kane, and L. D. Hinzman (1997), Hydrograph separations in an Arctic watershed using mixing model and graphical techniques, *Water Resources Res., 33*(7), 1707–1719.

Mendez, J., L. D. Hinzman, and D. L. Kane (1998), Evapotranspiration from a wetland complex on the Arctic Coastal Plain of Alaska, *Nordic Hydrol., 29*(4/5), 303–330.

Miller, P., W. A. Stoner, and L. L. Tieszen (1976), A model of stand photosynthesis for the wet meadow tundra, Barrow , Alaska, *Ecol*. *57*, 411–430.

Mock, C. J., P. J. Bartlein, and P. M. Anderson (1998), Atmospheric circulation patterns and spatial climatic variations in Beringia, *Int. J. Climatology, 18*(10), 1085–1104.

Moore, T. A., W. K. Wallace, C. G. Mull, K. E. Adams, G. Plafker, and W. J. Nokleberg (1997), Crustal implications of bedrock geology along the Trans-Alaska crustal transect (TACT) in the Brooks Range, Northern Alaska, *J. Geophys. Res., 102*(B9), 20,645–20,684.

Myers-Smith, I. H., Harden, J. W., Wilmking, M., Fuller, C. C., McGuire, A. D., and Chapin III, F. S., 2008, Wetland succession in a permafrost collapse: interactions between fire and thermokarst, *Biogeosciences 5*, 1273–1286, doi:10.5194/bg-5-1273-2008.

Newbury, R. W. (1974), River hydrology in permafrost areas, in *Proceedings Workshop Seminar on Permafrost Hydrology*, edited by J. Demers, pp. 31–37, Secretariat, Canadian National Committee, International Hydrological Decade, Environment Canada, Ottawa, Canada.

Ng, E., and P. C. Miller (1977), Validation of a model of the effects of tundra vegetation on soil temperatures. *Arctic and Alpine Res*., 89–104.

O'Brien, B., and W. Loya (2009), Climate change impacts on water availability in Alaska, *Report*, pp. 4, Scenarios Network for Alaska Planning, Univ. Alaska Fairbanks, Fairbanks, AK.

Oechel, W. C., and G. L. Vourlitis (1995), Effects of global change on carbon storage in cold soils, in *Advances in Soil Science: Soils and Global Change*, edited by R. Lal *et al*., pp. 117-129, Lewis Publishers, Boca Raton, London.

Oechel, W. C, S. J. Hastings, M. Jenkins, G. Riechers, N. Grulke, and G. L. Vourlitis (1993), Recent change of arctic tundra ecosystems from a net carbon sink to a source. *Nature, 361*, 520–526.

Oechel, W. C., G. L. Vourlitis, S. L. Hastings, R. C. Zulueta, L. Hinzman, and D. Kane (2000), Acclimation of ecosystem CO_2 exchange in the Alaskan Arctic in response to decadal climate warming, *Nature 406*, 978–981.

Ossola, I., and B. J. Travis (2009), A model of active layer dynamics, abstract GC51A-0736 presented at the Am. Geophys. Union, San Francisco, C.A.

Overpeck, J. T., D. Rind, and R. Goldberg (1990), Climate-induced changes in forest disturbance and vegetation, *Nature, 343*, 51–53.

Pewe, T. L. (1975), Quarternary geology of Alaska, *Geol. Surv. paper 835*, U.S. Government, Washington, DC.

Ping, C.-L., G. J. Michaelson, M. T. Jorgenson, J. M. Kimble, H. Epstein, V. E. Romanovsky, and D. A. Walker (2008), High stocks of soil organic carbon in the North American Arctic Region, *Nature Geosci.*, doi:10.1038/ngeo284.

Polyakov I. V., G. V. Alekseev, R. V. Bekryaev, U. Bhatt, R. L. Colony, M. A. Johnson, V. P. Karklin, A. P. Makshtas, D. Walsh, and A. V. Yulin (2002), Observationally based assessment of polar amplification of global warming, *Geophys. Res. Lett., 29*, (18), 1878, doi:10.1029/2001GL011111.

Pomeroy J. W., D. S. Bewley, R. L. H. Essery, N. R. Hedstrom, T. Link, R. J. Granger, J. E. Sicart, C. R. Ellis, and J. R. Janowicz (2006), Shrub tundra snowmelt, *Hydrol. Process., 20*(4), 923–941.

Post, W. M., W. R. Emanuel, P. J. Zinke, A. G. Stangenberger (1982), Soil carbon pools and world life zones, *Nature, 298*, 156–159, doi:10.1038/298156a0.

Racine, C. H., and J. C. Walters (1994), Groundwater-discharge fens in the Tanana Lowlands, Interior Alaska, U.S.A., *Arctic and Alpine Research*, *26*(4), 418–426.

Racine, C. H., R. R. Jandt, C. R. Meyers, and J. Dennis (2004), Tundra fire and vegetation change along a hillslope on the Seward Peninsula, Alaska, U.S.A. *Arctic, Antarctic, and Alpine Res., 36*(1), 1–10.

Racine, C. H., and R. R. Jandt (2008), The 2007 ‗‗Anaktuvuk River'' tundra fire on the Arctic Slope of Alaska: A new phenomenon?, in *Ninth International Conference on Permafrost—Extended Abstracts,* edited by D. L Kane, and K. M. Hinkel, pp. 247–248, Institute of Northern Engineering, University of Alaska Fairbanks, Fairbanks, AK.

Romanovsky, V., and T. Osterkamp (1995), Interannual variations of the thermal regime of the active layer and near surface permafrost in northern Alaska, *Permafrost Periglacial Processes*, 6, 313–335.

Roulet, N. T., and M. K. Woo (1986), Wetland and lake evaporation in the low Arctic, *Arctic and Alpine Res., 18*(2), 195–200.

Rouse, W. R. (2000), The energy and water balance of high-latitude wetlands: controls and extrapolation, *Global Change Biol., 6* (Suppl. 1), 59–68.

Rouse, W. R., D. W. Carlson, and E. J. Wieck (1992), Impacts of summer warming on the energy and water balance of wetland tundra, *Climatic Change, 22,* 305-326.

Rovansek, R. J., L. D. Hinzman, D. L. Kane (1996), Hydrology of a tundra wetland complex on the Alaskan Arctic Coastal Plain, U.S.A., *Arctic and Alpine Res., 28*, (3), 311–317.

Saugier, B., J. Roy, and H. A. Mooney (2001), Estimations of global terrestrial productivity: converging towards a single number?, in *Terrestrial Global Productivity*, edited by J. Roy *et al*., pp. 543–557, Academic Press, San Diego, CA.

Schuur, E. G., J. Bockheim, J. P. Canadell, E. Euskirschen, C. B. Field, S. V. Goryachkin, S. Hagemann, P. Kuhry, P. M. Lafleur, H. Lee, G. H. Mazhitova, F. W. Nelson, A. Rinke, V. E. Romanovsky, N. Shiklomanov, C. Tarnocai, S. Venevsky, J. G. Vogel, and S. A. Zimov (2008), Vulnerability of permafrost carbon to climate change; Implications for the global carbon cycle, *Biosci., 58*(8), 701–714.

Sellmann, P., K. L. Carey, C. Keeler, and A. D. Hartwell (1972), Terrain and coastal conditions on the Arctic Alaska Coastal Plain: Arctic environmental data package supplement 1, *Special Report 165*, pp. 72, U. S. Army Cold Regions Res. and Engineering Lab., Hanover, NH.

Sellmann, P. V., L. Brown, R. I. Lewellen , H. L. McKim, and C. J. Merry (1975), The classification and geomorphic implications of thaw lakes on the Arctic Coastal Plain, Alaska, *Res. Report 344*, 20 pp., U. S. Army Cold Regions Research and Engineering Lab., Hanover, NH.

Serreze, M. C., and J. A. Francis (2006), The Arctic amplification debate, *Climatic Change, 76*, 241–264, doi: 10.1007/s10584-005-9017-y.

Shaver, G. R. (2010), Fire and ice: Surprised in a warming Arctic land surface, abstract presented at State of the Arctic Conference, Miami, FL.

Shaver, G. R., J. Canadell, F. S. Chapin III, J. Gurevitch, J. Harte, G. Henry, P. Ineson, S. Jonasson, J. Melillo, L. Pitelka, and L. Rustad (2000), Global warming and terrestrial ecosystems: A conceptual framework for analysis, *BioScience 50*, 871–882.

Shiklomanov N. I., and F. E. Nelson (2002), Active-layer mapping at regional scales: a 13-year spatial time series for the Kuparuk Region, north-central Alaska, *Permafrost Periglac. Process. 13*, 219–230.

Shiklomanov, N. I., D. A. Streletskiy, F. E. Nelson, R. D. Hollister, V. E. Romanovsky, C. E. Tweedie, and J. Brown (2010), Decadal variations of active-layer thickness in moisture-controlled landscapes, Barrow, Alaska, *J. of Geophys. Res.* doi:10.1029/2009JG001248.

Shur, Y. L., and M. T. Jorgenson (2007), Patterns of permafrost formation and degradation in relation to climate and ecosystems, *Permafrost and Periglac. Process., 18*(1), 7–19.

Silapaswan C. S., D. Verbyla, and A. D. McGuire (2001), Land cover change on the Seward Peninsula: The use of remote sensing to evaluate potential influences of climate change on historical vegetation dynamics, *J. of Remote Sensing, 5*, 542–554.

Slaughter, C. W., and D. L. Kane (1979), Hydrologic role of shallow organic soils in cold climate, in *Proceedings Canadian Hydrology Symposium 79 - Cold Climate Hydrology*, pp. 380–389, National Res, Council of Canada, Vancouver, B.C., Canada.

Steere, W. C. (1978), Floristics, phytogeography, and ecology of arctic Alaskan bryophytes, in *Vegetation and Production Ecology of an Alaskan Arctic Tundra*, edited by L. L. Tieszen, pp. 141–167, Springer-Verlag, New York, NY.

Stewart, R. G., and W. R. Rouse (1976), Simple models for calculating evaporation from dry and wet tundra surfaces, *Arctic and Alpine Res. 8*, 263–274.

Stoner, W., P. C. Miller, and W. C. Oechel (1978), Simulation of the effect on the tundra vascular plant canopy on the productivity of four moss species, in *Vegetation and Production Ecology of an Alaskan Arctic Tundra*, edited by L. L. Tieszen, pp. 371–187, Springer-Verlag, New York, NY.

Sturm M., C. Racine, and K. Tape (2001), Increasing shrub abundance in Arctic. *Nature, 411*, 547–548.

Sturm, M., T. Douglas, C. Racine, and G. E. Liston (2005a), Changing snow and shrub conditions affect albedo with global implications, *J. Geophys. Res.*, 110, G01004, doi:10.1029/2005JG000013.

Sturm, M., J., Schimel, G. Michaelson, J. M. Welker, S. F. Oberbauer, G. E. Liston, J. Fahnestock, and V. Romanovsky (2005b), Winter biological processes could help convert arctic tundra to shrub land, *BioScience, 55*(1), 17–26.

Sugimoto, A., D. Naito, N. Yanagisawa, K. Ichiyanagi, N. Kurita, J. Kubota, T. Kotake, T. Ohata, T. C. Maximov, and A. N. Fedorov (2003), Characteristics of soil moisture in permafrost observed in East Siberia taiga with stable isotopes of water, *Hydrol. Process*. *17*, 1073–1092.

Swann, A. L., I. Y. Fung, S. Levis, G. B. Bonan, and S. C. Doney (2010), Changes in Arctic vegetation amplify high-latitude warming through the greenhouse effect, *Proc. Natl. Acad. Sci., 107*(4), 1295–1300.

Swanson, D. K. (1996), Susceptibility of permafrost soils to deep thaw after forest fires in Interior Alaska, U.S.A., and some ecologic implications, *Arct. Alpine Res., 28*(2), 217– 227.

Tape, K., M. Sturm, and C. Racine (2006), The evidence for shrub expansion in Northern Alaska and the Pan-Arctic, *Global Change Biology, 12* (4), 686–702.

Tarnocai, C. (2006), The effects of climate change on carbon in Canadian peatlands, *Global Planetary Change, 53*, 222–232.

Tedrow, J. C. F., J. V. Drew, D. E. Hill, L. A. Douglas (1958), Major genetic soils of the Arctic Slope of Alaska, *J. Soil Sci*., *9*, 33–45.

Vörösmarty, C. J., L. D. Hinzman, B. J. Peterson, D. H. Bromwich, L. C. Hamilton, J. Morison, V. E. Romanovsky, M. Sturm, and R. S. Webb (2001), The hydrologic cycle and its role in Arctic and global environmental change: A rational and strategy for synthesis study, *Report*, 84 pp., Arctic Res. Consortium of the U.S., Fairbanks, AK.

Voss, C. I., J. M. McKenzie, and M. A. Walvoord (2009), Groundwater flow with freeze-thaw in dynamic permafrost systems: Numerical simulation, abstract C53A-04 presented at the Am. Geophys. Union Fall Meeting, San Francisco, CA.

Vourlitis, G. L., and W. C. Oechel (1997), Landscape-scale CO2, H2O vapor and energy flux of moist-wet coastal tundra ecosystems over two growing seasons, *J. Ecol., 85*, 5, 575–590.

Vourlitis, G. L., and W. C. Oechel (1999), Eddy covariance measurement of CO_2 and energy fluxes of Alaskan tussock tundra ecosystem, *Ecol., 80*(2), 686–701.

Walker, D. A., G. J. Jia, H. E. Epstein, M. K. Raynolds, F. S. Chapin III, C. Copass, L. D. Hinzman, J. A. Knudson, H. A. Maier, G. J. Michaelson, F. Nelson, C. L. Ping, V. E. Romanovsky, and N. Shiklomanov (2003), Vegetation-soil-thaw-depth relationships along a low-arctic bioclimatic gradient, Alaska: Synthesis of information from the ATLAS study, *Permafrost and Periglac. Process., 14*, 103–123.

Walker, M. D., C. H. Wahren, R. D. Hollister, G. H. R. Henry, L. E. Ahlquist, J. M. Alatalo, M. S. Bret-Harte, M. P. Calef, T. V. Callaghan, A. B. Carroll, H. E. Epstein, I. S. Jónsdóttir, J. A. Klein, B. Magnússon, U. Molau, S. F. Oberbauer, S. P. Rewa, C. H. Robinson, G. R. Shaver, K. N. Suding, C. C. Thompson, A. Tolvanen, Ø. Totland, P. L. Turner, C. E. Tweedie, P. J. Webber, and P. A. Wookey (2006), Plant community responses to experimental warming across the tundra biome, *Proc. Natl. Acad. Sci., 103*(5), 1342–1346. doi:10.1073/pnas.0503198103.

Walter, K. M., S. A. Zimov, J. P. Chanton, D. Verbyla, and F. S. Chapin III (2006), Methane bubbling from Siberian thaw lakes as a positive feedback to climate warming, *Nature, 443*(7), 71–75.

Webber, P. J., P. C. Miller F. S. Chapin III, and B. H. McCown (1980), The Vegetation: Pattern and Succession, in *An Arctic Ecosystem: the Coastal Tundra at Barrow, Alaska,* edited by J. Brown *et al*., pp. 30–56, Dowden, Hutchinson and Ross Inc., Stroudsburg, PA.

Weisser, D., S. S. Marchenko, C. C. Treat, V. E. Romanovsky, and S. E. Frolking, 2009, Coupled hydrological and thermodynamical modeling of permafrost dynamics: Implications for northern peatlands, abstract C51A-0455 presented at the Am. Geophys. Union, Fall Meeting, San Francisco, CA.

Weller, G., and B. Holmgren (1974), The microclimates of the Arctic tundra, *J. Appl. Meteorol., 13*, 854–862.

Woo, M. K. (1986), Permafrost hydrology in North America, *Atm.-Ocean, 24*(3), 201–234.

Woo, M. K., and P. Steer (1982), Occurrence of surface flow on arctic slopes, southwestern Cornwallis Island, *Can. J. Earth Sci., 19* (12), 2368–2377.

Woo, M. K., and P. Steer (1983), Slope hydrology as influenced by thawing of the active layer, Resolute, N.W.T., *Can. J. Earth Sci., 20* (6), 978–986.

Woo, M. K., and Z. Xia (1996), Effects of hydrology on the thermal conditions of the active layer, *Nordic Hydrol., 27*, 129–142.

Woo, M. K., and X. J. Guan (2006), Hydrological connectivity and seasonal storage change of tundra ponds in polar oasis environment, Canadian High Arctic, *Permafrost Periglac. Process., 17*, 309–323.

Woo, M. K., D. L. Kane, S. K., Carey, and D. Yang (2008), Progress in permafrost hydrology in the new millennium, *Permafrost and Periglacial Proc., 19*, 237–254.

Yamazaki, Y., J. Kubota, T. Ohata, V. Vuglinsky, and T. Mizuyama (2006), Seasonal changes in runoff characteristics on a permafrost watershed in the southern mountainous region of eastern Siberia, *Hydrol. Proc*. *20*, 453–467.

Yang, D., B. E. Goodison, S. Ishida, and C. Benson (1998), Adjustment of daily precipitation data of 10 climate stations in Alaska: Applications of world meteorological organization intercomparison results, *Water Resour. Res., 34*(2), 241–256.

Yoshikawa, K., and L. Hinzman (2003), Shrinking thermokarst ponds and groundwater dynamics in discontinuous permafrost, *Permafrost and Periglacial Proc., 14*(2), 151–160.

Yoshikawa K., W. R. Bolton, V. E. Romanovsky, M. Fukuda, and L. D. Hinzman (2002), Impacts of wildfire on the permafrost in the boreal forests of Interior Alaska, *J. Geophys. Res. 107*, 8148, doi:10.1029/2001JD000438.

Zachos J., M. Pagani, L. Sloan, E. Thomas, K. Billups (2001), Trends, rhythms, and aberrations in global climate 65 Ma to Present, *Science*, *292*(5517), 686–693.

Zhang, Z., D. L. Kane, and L. D. Hinzman (2000), Development and application of a spatially distributed Arctic hydrological and thermal process model (ARHYTHM), *Hydrol. Process., 14*, 1017–1044.

Zimov, S. A., E. A. G. Shuur, and F. S. Chapin III (2006), Permafrost and the global carbon budget, *Science, 312*, 1612–1613.

Zona, D., W. C. Oechel, J. Kochendorfer, K. T. Paw U, A. N. Salyuk, P. C. Olivas, S. F. Oberbauer, and D. Lipson (2009), Methane fluxes during the initiation of a large-scale water able manipulation experiment in the Alaskan Arctic tundra, *Global Biogeochem. Cycles*, *23*, GB2013, doi:10.1029/2009GB003487.

CHAPTER 2
PHYSICAL SHORT-TERM CHANGES AFTER A TUSSOCK TUNDRA FIRE, SEWARD PENINSULA, ALASKA[1]

Abstract

The Kougarok area, situated on the central Seward Peninsula, Alaska, experienced a severe fire in August 2002. This may be the only tundra fire where high-quality prefire (1999–2002) and postfire (2003–2006) active layer and meteorology measurements have been collected in the same locations. After fire, near-surface soil showed increased moisture at the burned tussock site, remaining close to saturation throughout the thawed season 2003–2006. Despite wetter soil after the fire, freezing occurred earlier at the burned tussock site than at the control, indicating the importance of a reduced soil organic layer. Severe combustion of lichen and moss left 15–25 cm high tussocks, resulting in a doubling of the surface roughness coefficient. Average September temperature at the tussock site increased 2.3 ± 0.7°C throughout the 1 m soil profile, doubling the active layer depth, although this is due partly to favorable meteorological conditions. The shrubby control station experienced an average increase of 1.1 ± 0.3°C in the upper 0.5 m of soil (pre- versus postfire mean temperature). A similar annual change was found at the burned tussock site. Cooler weather conditions in 2006 retarded the soil-warming trend, which occurred after 2002. How the thermal and moisture regimes in tundra will be affected after fire is highly influenced by weather, fire severity, vegetation regrowth, prefire vegetation, and ground ice conditions.

[1]Liljedahl, A., L. Hinzman, R. Busey, and K. Yoshikawa (2007), Physical short-term changes after a tussock tundra fire, Seward Peninsula, Alaska, *J. Geophys. Res.*, Vol. 112, F02S07, doi:10.1029/2006JF000554.

2.1 Introduction

The Arctic and sub-Arctic are particularly sensitive to climate change [*Manabe et al*., 1991; *Houghton et al*., 1996; *Watson et al*., 1998]. Increased fire frequency, severity, and area burned are among the anticipated effects of climate warming [*Stocks et al*., 1998; *Rupp et al*., 2000; *Flannigan et al*., 2001; *McCoy and Burn*, 2005]. The historical and potential future extent, effects, and feedbacks of fires in the sub-arctic boreal forest are better known [*Kasischke and Turetsky*, 2006; *Lynch et al*., 2002; *Valeo et al*., 2003] than in arctic regions [*Chambers et al*., 2005; *Racine*, 2004]. Dramatic changes may follow in the Arctic and sub-Arctic, where short-term thawing/freezing processes and longer-term permafrost dynamics shape the ecosystem through plant growth, evapotranspiration, infiltration, runoff, wetland dynamics [*Hinzman et al*., 2003], biogenic gas fluxes to the atmosphere [*Waelbroeck and Monfray*, 1997], and export of carbon and nutrients to rivers and seas [*Vörösmarty et al*., 2001].

In Arctic regions, many physical and biological processes are confined to the active layer, the near-surface layer above permafrost that freezes and thaws each year. Critical microclimatic variables interactively controlling the active layer include surface temperature, snow cover, the nature of the vegetation canopy, soil organic horizon thickness, soil moisture content, and ground ice conditions [*Kane et al*., 1992; *Burn*, 1997; *Hinzman et al*., 2003]. Previous studies have shown that short-term (<10 years) postfire effects on surface characteristics include (1) depletion of the insulating organic layer, increasing the near-surface soil thermal conductivity and heat flow into the ground [*Yoshikawa et al*., 2002]; (2) reduced albedo, increasing the energy absorption; and (3) increased insolation on the ground surface [*Kasischke et al*., 1995] and reduction in the surface-atmosphere coupling [*Chambers et al*., 2005] due to changes in the canopy structure. These fire effects are known to increase the active layer thickness [*Heginbottom*, 1976;

Viereck, 1982; *Mackay*, 1995; *Burn*, 1997]. Continued degradation of permafrost over longer periods can result in drier near-surface soils [*Swanson*, 1996; *Yoshikawa et al*., 2002] due to enhanced drainage capacity. Fire-induced changes can therefore have broad effects hydrological, biological, and morphological systems and land-atmosphere interactions in the Arctic.

This study examines the short-term (4 years) postfire changes on the thermal and moisture regimes of the active layer. Unlike most previous studies, observations were made at fixed locations before and after the fire. Ground and surface temperatures, near-surface soil moisture, freezing and thawing degree-day sums, and seasonal n-factors were observed before and after the fire in 2002 at burned (K2) and control (K3) sites, to determine whether fire-induced effects, weather variations, or both explain postfire changes in the active layer. We also examine prefire and postfire radiation efficiency, albedo, surface roughness at K2, and broader scale (1 km^2) thaw depth observations. Information obtained about ground ice and snow conditions during the study period was limited, restricting the discussion of their contribution to observed changes.

2.2 Site Description

The Kougarok area (also known as Quartz Creek), occupies an area of transition between the continuous and discontinuous permafrost zones [*Brown and Péwé*, 1973] in the central part of the Seward Peninsula, northwestern Alaska (Fig. 2.1). Kougarok (65°250N, 164°380W), approximately 140 km north of Nome, has a continental climate and is locally underlain by thin (15–50 m) continuous permafrost (>90% areal cover). The rolling landscape supports low Arctic tundra dominated by sedge tussock communities, with shrubs in the valley bottoms. The Ruptic-Histic Aquiturbel soils are of eolian origin [*Sturm et al*., 2005], with thickness of a half-meter on the ridges to a few meters in the valleys. Frost boils, circular features resulting from freezing and thawing processes, exist in the area.

The Seward Peninsula has a relatively high fire frequency compared to other tundra regions [*Racine et al*., 1987] but longer return intervals than the boreal forest of Interior Alaska [*Stocks et al*., 2003]. The annual area burned on the Seward Peninsula was episodic during 1954– 2006 (Fig. 2.2), consistent with another study of Alaska [*Kasischke et al*., 2002] but without the trends observed in the boreal regions of Alaska and Canada [*Kasischke and Turetsky*, 2006]. The largest fire year was 1977, both in number of fires larger than 0.02 km^2 (13) and area burned (4700 km^2) (http://agdc.usgs.gov/data/blm/fire/index.html).

The Kougarok area experienced three fires in the last 35 years: 1971, 1997, and 2002. Three meteorological stations (K1, K2, and K3) were installed in the area during 1999 under the Arctic Transitions in the Land-Atmosphere System (ATLAS) program [*Sturm et al*., 2005; http://www.uaf.edu/water/projects/atlas/atlas.htm] (Fig. 2.3, Table 2.1 and 2.2). All three stations are located on land affected by the 1971 fire. The 1997 fire (311 km^2, 22 July to 25 August) burned the location of the meteorological station K1 while the 2002 fire (87 km^2, 4 August to 19 August) destroyed instrumentation at the K2 site. Instrumentation was replaced in October 2002. A principal component analysis of two Landsat images (band 3, 4, and 7) acquired in July 1997 and October 2002 shows the spatial distribution of the 1997 and 2002 burns (Fig. 2.4). On the basis of the fire severity classification system of *Viereck et al*. [1979], the 2002 fire resulted in severe (soil organic material completely or nearly consumed down to mineral soil) to moderate burns (organic layer partially consumed) with a few unburned patches. Approximately 5–7 cm of the 14 cm thick organic soil layer remained after the fire in August 2002, where the K2 thermistors and water content reflectometers were installed (Fig. 2.5). The surface below the long- and short-wave radiation instrument experienced a partial burning, leaving unburned patches. Thermal and mechanical erosion initiated by the 2002 fire were observed 400 m to the east of K2 in the Niagara Creek streambed (Fig. 2.5), resulting in a gully of

>3500 m^3 in volume by September 2006. The erosion exposed ice-rich permafrost and ice wedges, with active thermokarst processes extending several meters away from the bank. The ice wedges probably formed during the Holocene, although the ice-rich permafrost is of older age (V. E. Romanovsky, personal communication, 2006). A Circumpolar Active Layer Monitoring (CALM) grid [*Brown et al*., 2000] was installed in 1999 adjacent to K3 in the Mauze Gulch watershed (Fig. 2.1 and 2.4). The 1 km^2 grid, with nodes at 100 m spacing, extends over the creek and includes both a south- and a north-facing slope. The 2002 fire burned 90 grid nodes, mainly represented by tussock communities. Most of the 31 control nodes (unburned in 2002) were in the moist valley bottom and vegetated by high (<2 m) shrubs. A few unburned sites occupied areas of moss and lichen at the northwest corner of the grid, on a south-facing slope shoulder.

2.3 Methods

Thaw depth observations on the 1 km^2 CALM site were made manually at the 121 nodes locations by inserting a metal probe to the depth of refusal during the end of September or early October. The CALM grid results were divided into two groups, burned and control. Meteorological and soil variables were collected from 1999 through 2006. Temperature, wind speed, precipitation, radiation, and moisture instruments are summarized in Table 2.3. Meteorological measurements were made every minute and averaged into hourly intervals at K1, K2, and K3. Soil temperature and moisture were measured every 5 min and recorded as a 3-hour mean at K2 and K3. Information was stored in a Campbell Scientific CR10X data logger. The depth of each ground sensor was defined as the distance from the surface at the time of observation. Therefore near-surface prefire and postfire data from K2 represent different soil material. Unfrozen soil moisture was estimated from volumetric water content (VWC) observations. Spring peak in VWC was assumed to represent saturated conditions (all micro and macro pore spaces filled

with liquid water) and for winter conditions, organic and mineral soil was set to 8% and 10% saturation, respectively [*Hinzman et al*., 1991].

Thermistors were calibrated each fall following the method described by *Romanovsky and Osterkamp* [1995] using the phase equilibrium temperature between 0°C and 0.1°C during freezing. Mean daily ground temperatures provided information about the beginning of thaw, freeze, freeze-up dates, and the length of thawing and freezing seasons. The beginnings of the thawing and freezing periods were defined by ground surface temperatures remaining consistently above and below 0°C, respectively. The freeze-up date for the 1 m profile represented the day when all temperatures began to decrease sharply after the ‗‗zero curtain'' disappeared [*Romanovsky and Osterkamp*, 1995]. The n-factor, the ratio of the accumulated seasonal ground surface thawing or freezing degree-day sums to the seasonal air freezing and thawing indexes, is a generalized representation of the various climatic and vegetative variables affecting the soil thermal regime. Originally developed for engineering purposes [*Carlson*, 1952], the n-factor has also been used to examine the surface energy balance in natural regimes [*Klene et al*., 2001; *Karunaratne and Burn*, 2004; *Kade et al*., 2006] and for active layer mapping [*Shiklomanov and Nelson*, 2002]. Because of continuous temperature records, the n-factor was approximated using measurements 5 cm below surface (K2) and directly under green vegetation (0 cm) at K3. The K2 n-factor calculations should therefore be seen as a modified parameter similar to that employed by *Kade et al*. [2006]. Owing to the limited number of soil temperature measurements, permafrost table temperatures (T_{ps}) were estimated following *Romanovsky and Osterkamp* [1995, equation (13)] where:

$$\overline{T}_{ps} = \frac{K_t \times I_t - K_f \times I_f}{K_f \times P} \leq 0 \qquad (1)$$

where K_t and K_f are the bulk thawed and frozen thermal conductivities, I_t and I_f are the ground surface thawing and freezing indices (degree-days), and P is the annual period (365 days). Information about active layer depth was interpolated from soil temperature measurements. The thermal offset, the difference between the mean annual permafrost and ground surface temperatures, was also calculated.

End-of-winter snow observations were made in 1999 and 2000 between K2 and the Niagara Creek streambed. Snow depth was obtained by 50 probed measurements along a transect at 1 m intervals. Snow water equivalents were based on five samples using an Adirondack tube. Tussock and shrub tundra were observed separately.

Net all-wave radiation (Q^*) represents the amount of energy available at the surface, described during daytime as:

$$Q^* = K\downarrow - K\uparrow + L\downarrow - L\uparrow \qquad (2)$$

where $K\downarrow$, $K\uparrow$, $L\downarrow$, and $L\uparrow$ represent incident and reflected short-wave radiation, incoming long-wave radiation emitted by the atmosphere, and outgoing long-wave emitted from the surface, respectively [*Oke*, 1987]. A slight negative feedback mechanism is present because a surface with low albedo absorbs energy well, increasing emission of longwave radiation from the surface unless there is rapid heat dissipation [*Oke*, 1987]. An approach used by *Chambers et al*. [2005] was applied to reduce the influence of incoming short-wave radiation differences, energy budget components, and climatic conditions on the net all-wave radiation: (1) the net all-wave radiation was treated in terms of radiation efficiency (R_e), which is net-radiation normalized to incoming short-wave radiation; (2) the period of interest was restricted to local noon ±2 hours; and (3) only data obtained during clear-sky conditions (>500 W m^{-2}) and not directly following rain were included. A

wind speed cooling effect algorithm [*Campbell Scientific Inc*., 1996] was applied to the net-radiation observations, which were made early June to late September.

The height and spacing of the micro-roughness and macro-roughness elements of the surface, i.e., the surface roughness length (z_o) was obtained under neutral conditions, defined as the Richardson number (R_i) lying between –0.01 and 0.01. The R_i relates the relative roles of free and forced convection and is positive for stable and negative during unstable atmospheric conditions [*Oke*, 1987]. Following *Braun* [1985], calculations of R_i and, roughness length (z_o) were based on a wind speed and temperature profile between the surface and 10 m, calculated as:

$$R_i = \frac{g^* z_2^* (T_a - T_{surf})}{u_{z2}^* (T_a + 273.15)} \qquad (3)$$

$$z_0 = \exp \frac{u_{z2} \ln z_1 - u_{z1} \ln z_2}{u_{z2} - u_{z2}} \qquad (4)$$

where z_o is in meters, g is the gravitational constant (m s^{-2}), z is the height of the wind-speed and temperature measurement (m), Ta is air temperature at height z (°C), T_{surf} is the effective surface temperature (°C), and u_{z1} and u_{z2} are wind-speed (m s^{-1}) at heights 1 and 2. Emitted longwave radiation represented effective surface temperature in surface roughness and air stability estimations, assuming an emissivity equal to one.

2.4 Results

2.4.1 Weather

The area experienced a period of warmer weather beginning in 2002. The warmest mean annual air temperature was −3°C (2002 and 2004), while 2001 and 2006 were cooler (−5.5°C) (Table 2.4). Longer thaw seasons were observed at the control site (K3) in the 2002–2006 period than in 2000 and 2001. The warmest year (2004) experienced a thaw season nearly 100 days longer than in 2001. The cooler mean annual temperatures in 2001 and 2006 resulted primarily from lower summer temperatures. Hourly air temperatures in the 2000–2006 period ranged from −40°C to +30°C, with postfire mean daily temperature at K2 and K3 strongly correlated (R^2 0.93, $p < 0.001$). Average rainfall from June through August during the study period was 94 mm, with the largest monthly proportion falling in August. The 2002 and 2006 summers experienced the minimum rainfall amounts (64 mm) and 2005 the maximum (134 mm). With regard to total winter precipitation, early May snow water equivalent was 80 mm and snow depth 0.4 m at Niagara Creek in 1999 and 2000 at the tussock tundra. Shrub tundra showed approximately doubled values. A 0.15–0.3 m thick depth hoar layer was usually found at the bottom of the snowpack at the tussock site.

2.4.2 Soil Temperature, Soil Moisture, and Active Layer Thickness

2.4.2.1 Soil Thermal Regime

Both the burned tussock tundra (K2) and the shrub control site (K3) experienced warmer September and annual ground and surface temperatures after the 2002 burn (Fig. 2.6). The colder weather in 2006 resulted in soil cooling and reduced thermal offsets at K2 and K3, compared to the previous year (Table 2.4). A comparison of 0.3 m (K2) and 0.4 m (K3) mean annual ground temperatures between 2001 and 2006 (2002 excluded) shows a total change of +1.1°C and +1.3°C, respectively. Mean September temperatures at 0.5 m depth in 2000, 2003–2006 show a 2.7°C

(K2) and 1.5°C (K3) increase. The warming in September was generally larger close to the surface than deeper in the 1 m soil profile (+0.9°C at 0.95 m depth, K2), while the annual averages showed the opposite trend at both stations. Annual soil temperatures in the same years were always higher at K3 than at K2, with the upper 0.4 m at K3 above freezing except in 2000. Averaged September soil and surface temperatures were higher at K3 before the fire, while postfire temperatures were higher at K2. Mean daily air, surface, and ground temperatures at K2 and K3 are shown in Figure 2.7. The effect of vegetation on ground temperatures is clearly visible at K3, especially during the winter season. K3 never experienced temperatures colder than −4°C at 0.4 m depth, compared to −16°C at K2 (0.3 m). K2 reached a summer maximum of 2.1°C at 0.3 m before the fire, while the postfire maximum was 8°C in 2004. Similar changes between the summers can be found at K3 station at 0.4 m depth. The cumulative thawing degree-days at the surface can be seen as a measure of the total amount of energy received at the ground surface during the thawed season (Table 2.4). During all 4 years after the fire, K2 has higher cumulative thawing surface degree-days than K3, despite a shorter thaw season as a result of an earlier freezing. The thaw season n-factor shows a higher prefire value at K3 than at K2 (Table 2.4). After the burn, the K2 n-factor was equal to or higher than K3. When averaging all years, the K2 winter/spring n-factor (first day of the year until beginning of thaw) shows a higher value (0.70 ± 0.12) than fall/winter (0.32 ± 0.06). K3 experienced similar partitioning but with lower ratios and relatively higher interannual variation 0.18 ± 0.11 (winter/spring) and 0.08 ± 0.06 (fall/winter). No significant difference was evident between prefire and postfire years at the K3 site. The postfire freeze-up date at K2 occurred in January, except after the warm summer of 2004, which resulted in freeze-up on 11 February 2005. The duration of the freeze-up period ranged between 87 to 130 days, a length similar to the frozen period of 86 to 134 days. Calculated mean annual temperature at the top of the permafrost was −3.7°C

(K2) before the fire and reached −2.1°C in 2004 and 2005, with a cooling in 2006 (-3.4°C). K3 showed similar trends in mean annual temperatures at 1 m depth but under thawing conditions (Table 2.4). Thermal offsets varied around −1°C at K2. The negative offsets were usually larger at K3.

2.4.2.2 Soil Moisture

The fire resulted in relatively wetter near-surface soils. Before the fire and directly following the spring peak saturation, observations of near-surface soil moisture at K2 showed a rapid decrease to 40% saturation of unfrozen water content (Fig. 2.8), which remained relatively stable during the rest of summer. After the fire, the near-surface soil was nearly saturated throughout the thawed season (70–100% saturation). This clear prefire and postfire difference did not occur at the control site (K3). A rapid increase during the beginning of thaw was observed postfire a month earlier at both stations. The decrease in unfrozen moisture content due to soil freezing occurred 19–30 days (K2) and approximately a month (K3) later after the fire than prior 2002.

2.4.2.3 Active Layer Thickness

Active layer depths at control and burned grid nodes, exhibit a similar trend from 2000 to 2002 (Fig. 2.9) with the control 0.11 to 0.16 m deeper than the burned group. The control showed an active layer depth of 0.55, 0.67, and 0.64 m, while the group that later would be affected by fire was measured at 0.44, 0.53, and 0.48 m in 2000, 2001, and 2002, respectively. Fall 2003, 1 year after the burn, resulted in a 0.11 m shallower thaw in the control group compared to 2002, while the burned area active layer depth increased with 0.06 m. The years following the tundra fire were characterized by consecutive deepening of the active layer over the entire CALM grid in 2004–2005 (control 0.68, 0.75 m, burned 0.60, 0.75 m) with a slight reduction after the cooler summer of 2006 (control 0.72 m, burned 0.70 m). The prefire difference (0.11–0.16 m) between mean of the two groups was reduced

drastically after fire to ≤0.02 m, except in 2004 with 0.08 m deeper thaw in the control. Standard deviations indicate larger variability of thaw depths within the control group (≤0.21 m) than in the burned (≤0.15 m). In the shrubby valley, a few control thaw depth observations exceeded the 1.23 m long probe in 2004–2006. In the NW corner of the CALM grid, some control sites had rocks present, complicating thaw depth measurements.

2.4.3 Surface Observations

2.4.3.1 Albedo

Short-wave noontime absorbed insolation at K2 increased slightly after the fire, owing to reduced albedo. Mean albedo from the end of snowmelt to solstice was 16% (2000), 15% (2001) 11% (2004), 13% (2005), and 14% (2006) with standard deviation of ±2 %. From solstice to end of August, the observations were 17% and 16% before fire and 13%, 15%, and 17% in 2004–2006, respectively. A 5-week earlier snowmelt in 2004 compared to 2001 at K2 (Table 2.4) was evident through the drastic reduction in surface albedo. Despite the disappearance of snow cover on Julian day 106 in 2004, the thaw did not start until Julian day 123.

2.4.3.2 Radiation Efficiency and the Richardson Number

At K2, there was no prefire to postfire difference in radiation efficiency, Re, which varied between 0.66 and 0.69 (Table 2.4). More pronounced air instability was found after fire through lower Richardson numbers. The average for June was −0.45 (2000–2001) and −0.75 (2004–2005) and July changed from −0.39 to −0.67. Surface roughness increased after fire, from a June-July average of 0.02 in 2000–2001 to 0.04 m 2004–2005, enhancing turbulent mixing.

2.5 Discussion

2.5.1 Soil Thermal and Moisture Regime

The major factors influencing spatial and temporal changes in the thermal and hydrological regimes are weather, vegetation, fire effects, snow, and ground ice conditions. The effect of fire on the sub-Arctic physical and biological systems is influenced by the presence of permafrost. Ice rich permafrost promotes thermal stability at depth owing to latent-heat effects, while thawing of the ice-rich transition zone (the uppermost permafrost that alternates in status between seasonally frozen ground and permafrost over Sub-decadal to centennial timescales) results in release of water to the active layer [*Shur et al*., 2005]. Unfortunately, information about ground ice conditions was not obtained in this study. The potential response of permafrost to fire, and the dependence of surface conditions on ground ice, will therefore be discussed through observed changes in the active layer.

The increased thaw depths and warmer soils at both burned and control sites after the fire show the dependence on weather. Although the changes in mean annual soil temperature 2001–2006 were very similar in the upper half meter of the soil, the change in September was nearly twice larger at K2 than at K3. Higher vegetation resulting in more efficient snow trapping and winter insulation [*Sturm et al*., 2001] at K3, offset the warming fire effects during summer at K2, on the annual scale.

The postfire soil warming at K2 can be explained by several factors: (1) Approximately 50% of the 14 cm organic layer was destroyed by fire, causing drastic changes in near-surface thermal conductivity. Destruction of the insulating organic layer increased the heat conducted into the ground during summer, resulting in deeper thaw and increased n-factors. (2) Earlier snowmelt and onset of thaw after the fire was confirmed by albedo observations (K2) and ground surface temperatures (K2 and K3). In a period of high incoming short-wave radiation, such

a shift in snowmelt can have a significant effect on the energy available for soil heating and sensible heat flux. To what degree the earlier snowmelt was caused by warmer weather or reduced snow cover cannot be evaluated due to lack of postfire snow observations. (3) Summer albedo decreased after the fire (2004–2006) but not as drastically as observed in a previous study by *Rouse and Mills* [1977], reducing the possible magnitude in soil temperature change. The limited burn and rapid regrowth of the well-developed tussocks resulted in little change in albedo, with the canopy shading moderately to severely burned ground between tussocks. No information on albedo during the first summer following fire existed, a time period that most likely experienced the lowest value. It is possible that a low albedo was an important factor in 2003 due to a) the large postfire difference between K2 and K3 in 2003 September soil temperatures and b) the increase in active layer thickness from the previous year in the burned CALM grid group compared to a decrease in the control group.

A negative correlation should be expected between snow depth and n-factors, with lower ratios in the latter half of the winter as snow depth increases. However, lower n-factors were usually observed during the first half of the winter (beginning of freezing to end of year) than the second half, indicating a strong and efficient dissipation of heat from the ground toward the surface. Unfortunately, there were no postfire observations of snow depth, density, and timing to evaluate the influence of postfire snow, which plays a significant role through its insulating effects [*Sturm et al*., 2001; *Stieglitz et al*., 2003].

The thaw season was longer at K3 than at K2 after the fire (the reverse was true before the burn), through a consistently earlier freezing of K2 near-surface soil. K2 experienced an earlier postfire thaw than K3, which also occurred in 2000. The observations were somewhat different compared to those of *Burn* [1998], who found a longer thaw period after the fire, which was explained by a more effective heat transfer (depletion of surficial organic soil), increased energy absorption

(earlier thaw and reduced albedo), and increased heat capacity (wetter soils). Reduced organic layer and increased soil moisture may be competing mechanisms during freezing of the near-surface soil. At K2, reduced thermal conductivity was the dominant factor over the increased latent heat storage, resulting in relatively earlier freezing at K2 than K3. To what degree K2 was affected by a larger ice volume in the near-surface soils during thaw cannot be determined through these observations. Increased soil moisture favors a higher ice content, which can slow the descent of the thawing front [*Woo*, 1986].

Possible contributors to the moister postfire near-surface include modified soil properties at 10 cm depth, thawing of the upper part of the transition zone, and reduced evapotranspiration. (1) Soil moisture was presented as relative saturation of unfrozen water, which does not describe the absolute change in total volume of water. Before the fire, a porous organic layer represented the soil at 10 cm depth. After the fire, the observations were made in an organic-rich mineral soil, with a relatively larger surface area per volume and different pore shape, resulting in higher water-retaining efficiency. (2) The fire resulted in deepening of the active layer and partial thaw of the ice-rich transition zone. Owing to the enrichment of ice in the transition zone relative to the active layer, a disturbance (fire) may be accompanied by increased moisture throughout the thawed soil profile. (3) The fire combusted vegetation between tussocks, resulting in reduced evapotranspiration capacity. Mosses and lichens will probably require many decades to regenerate [*Racine*, 2004], while the tussocks recovered well within the 4-year post-fire observation period.

2.5.2 Boundary Layer and Radiation Efficiency

The postfire soil warming at K2 caused increased convective heat loss from the surface to the atmosphere during local noon throughout the summer, as shown by the Richardson number (R_i). A 40% and 43% reduction after fire in Ri occurred in

June and July, respectively, resulting in stronger buoyancy forces. This change in Ri indicates an increased partitioning of net radiation into sensible heat, seen at both burned spruce stands and tundra surfaces [*Chambers et al*., 2005]. At local scales, this may have resulted in a warming of unburned areas from adjacent burned areas. With stronger buoyancy forces, a large burn area can produce local to regional circulation patterns [*Vidale et al*., 1997], which include the potential to affect the overall atmospheric heat and water budgets even above the atmospheric boundary layer [*Eugster et al*., 2000].

Postfire June-July surface roughness length (z_0) doubled. Prefire estimates of z_0 (0.02 m) are in agreement with studies made in northern Alaska tussock tundra of 0.02 m [*Hinzman et al*., 1996]. Field observations support a post-fire increase in microscale surface topography, since the fire-affected landscape was composed of 15–25 cm high tussocks separated by predominantly bare soil, owing to an efficient burn between the tussocks. *Chambers et al*. [2005] found a decrease in surface roughness in fire-affected, sedge-dominated tundra.

Radiation efficiency (R_e) was relatively stable throughout the observation period (66–69%), differing from previous studies. Directly after fire, boreal forest have shown a decrease [*Yoshikawa et al*., 2002; *Chambers et al*., 2005; *Liu et al*., 2005], while *Chambers et al*. [2005] found a R_e increase at a tundra regime. The slight decrease in albedo at K2 might have been balanced by increased emitted longwave radiation, which may be partly explained by a higher emissivity of the surface due to wetter conditions and relatively bare ground. Further, the inconsistency in R_e and z_0 compared to the study of *Chambers et al*. [2005] may be due to the different observation times after fire and the vegetation type and recovery. Observed increases in ground temperatures, buoyancy forces, and wetter near-surface soils are all indicators of changed partitioning in the net radiation among sensible, latent, and ground heat fluxes.

2.6 Conclusions

Short-term fire effects at a sub-Arctic tussock tundra area included both increased soil temperatures and near-surface soil moisture, altered energy partitioning through both increased ground heat and sensible heat flux, changes in surface characteristics such as increased roughness length and slightly reduced albedo. The soil warming after the fire was the combined result of weather and the thermal evolution of the system induced by the fire. Reduction in the organic layer was an important mechanism during near-surface freezing in fall, despite the increased latent heat of wetter soil. However, differences in snow cover accumulation may also affect interannual variations in soil freezing rates. The study shows the importance of postfire effects in influencing the physical status of the tundra ecosystem. Continuing long-term observations of the area would better characterize both fire impacts and recovery, as well as give insight to the future of tundra systems under a warming climate when fire frequency may increase.

2.7 Acknowledgments

Financial support for this research was provided through the National Science Foundation, grants OPP-03332964 and OPP-0328686. Any opinions, findings, conclusions, or recommendations expressed are those of the authors and do not necessarily reflect the views of NSF. Mention of specific product names does not constitute endorsement by NSF. Ken Irving, Stefan Kooman, Crane Johnson, Matt Stone, Kristin Susens, Andy Monaghan, Jeremy Kasper, and Robert Bolton provided field assistance. The authors are grateful to Claude Duguay for advice in remote sensing and the Alaska Fire Service for providing information. Associate Editor Fritz Nelson and reviewers C. Burn and C. Racine made many helpful suggestions that improved the paper.

2.8 Figures

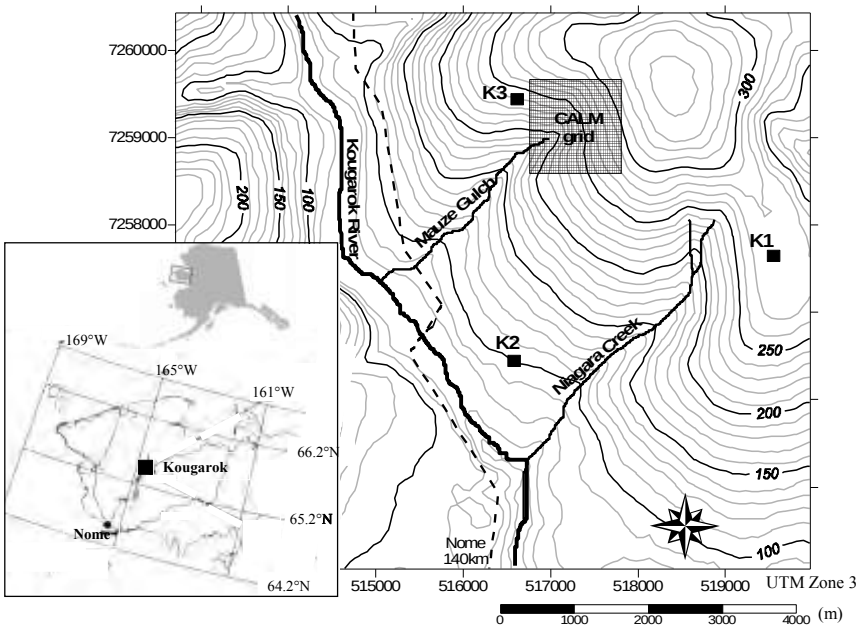

Figure 2.1 Location of Kougarok area (65° 25‘N, 164° 38‘W), central Seward Peninsula, northwestern Alaska. Topographic map showing Mauze Gulch and Niagara Creek watersheds, with the three meteorological stations, K1, K2 and K3, and the Circumpolar Active Layer Monitoring (CALM) grid.

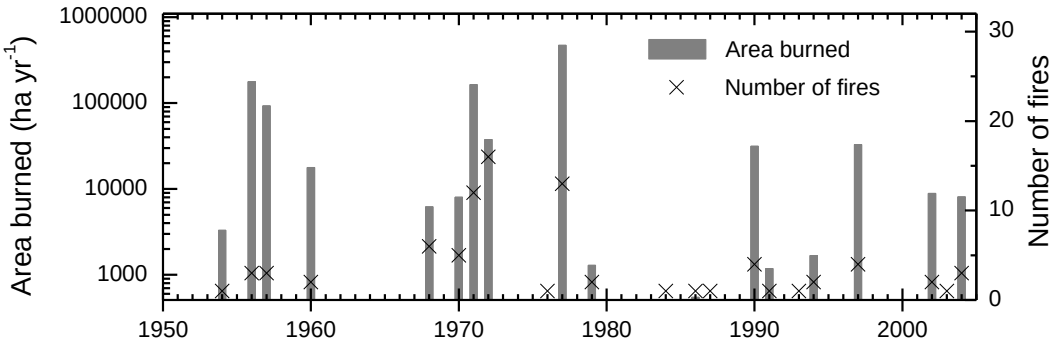

Figure 2.2 Annual area burned at Seward Peninsula 1954 through 2006 based on fires larger than 2 km^2 [http://agdc.usgs.gov/data/blm/fire/index.html]. Although most of Seward Peninsula is represented by open tundra, some spruce forest exists in the east [*Thayer-Snyder,* 2002].

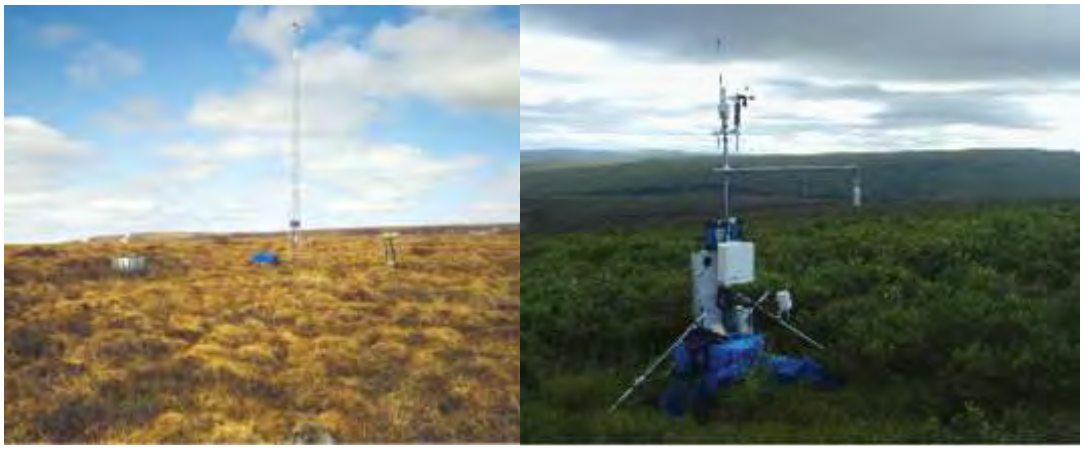

Figure 2.3 K2 station before fire, showing rain gauge, 10 m tower and radiation instruments in June 2001. Right: The 3 m high K3 station summer 2005 with Mauze Gulch watershed in the background.

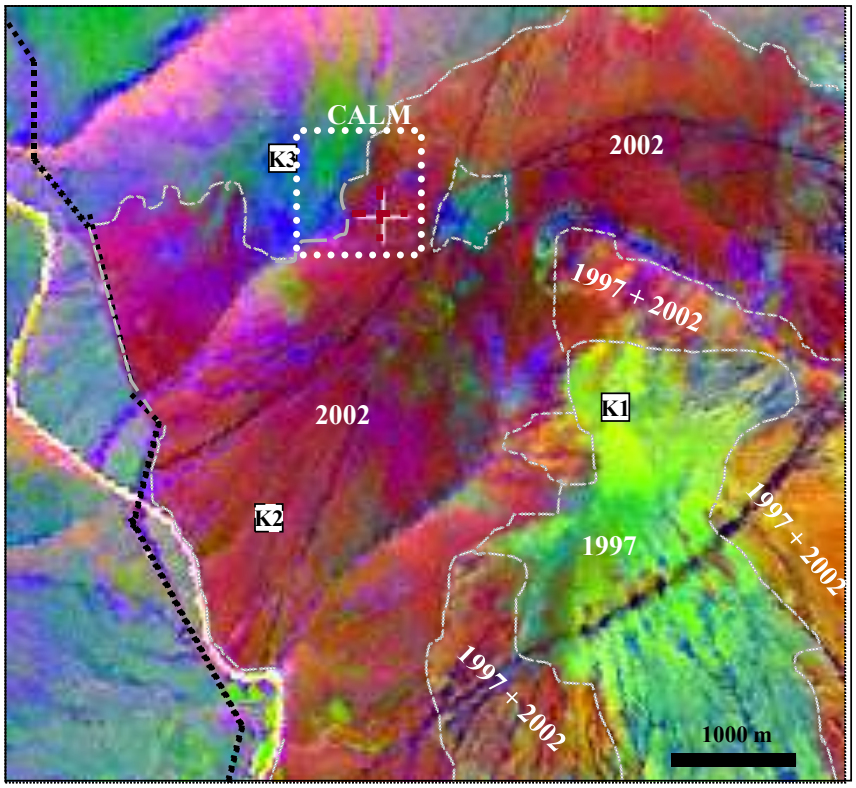

Figure 2.4 Multi spectral principal component analysis (PCA) based on Landsat (band 3, 4 and 7) of two overlaid images acquired in early July 1997 and October 2002. The 1997 and 2002 burns are shown in non-natural colors. Also marked are the year of fire, the three meteorological stations (K1, K2 and K3) and the 1 km^2 CALM grid. Darker lines across the area show ATV and truck trails and the white line (NW to SE) is the Kougarok River.

Figure 2.5 K2 soil moisture sensors were re-installed in October 2002 at 5, 10, 15, 20 and 30 cm depth. The photo shows the fire severity through the reduced organic material between the tussocks. Right: Erosion of Niagara Creek with exposed ice-rich permafrost in September 2003. The gully has become wider and longer since then, reaching 275 m in length by fall 2006. Substantial ground subsidence has occurred along the banks, resulting in more gentle sides. Note that the tussocks survived the fire.

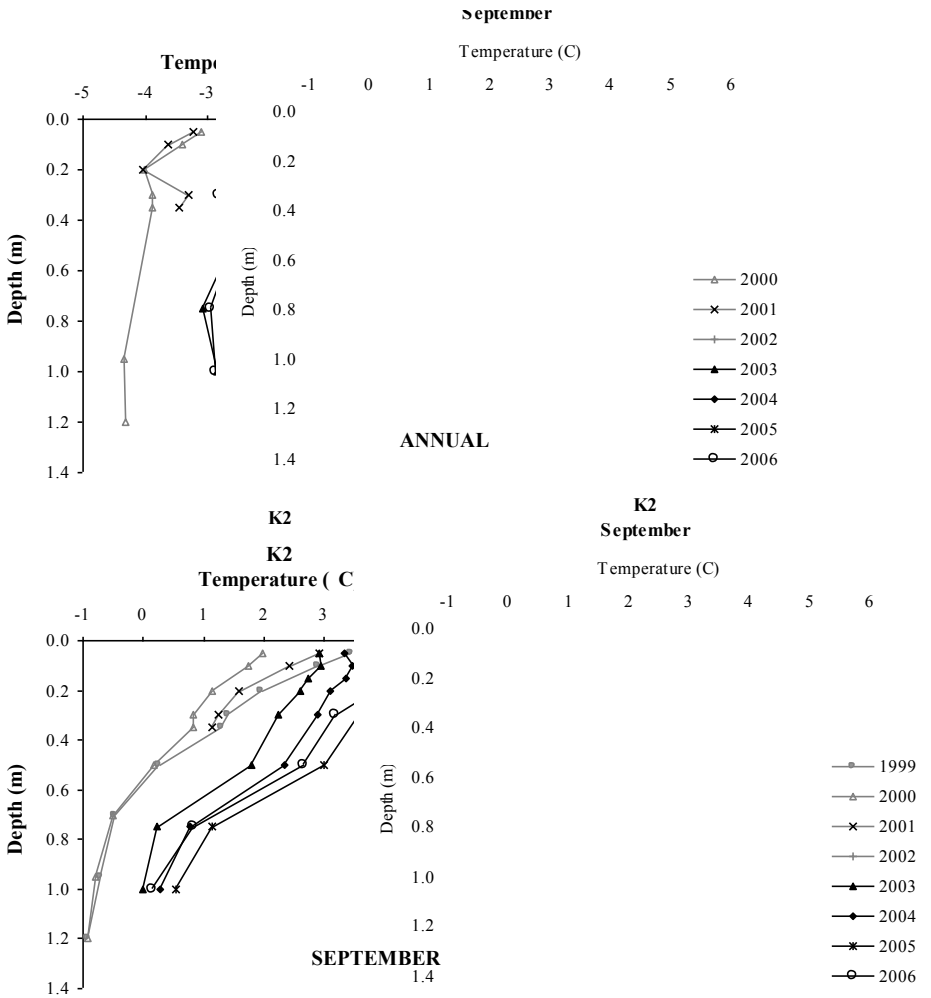

Figure 2.6 Mean annual and September ground temperatures at K2 (burn) and K3 (control) station during years 1999 through 2005 of pre-fire (gray) and post-fire (black) observations. The depth is relative to the surface at the time of observation. Yr 1999 is only included in the mean September temperatures at K2.

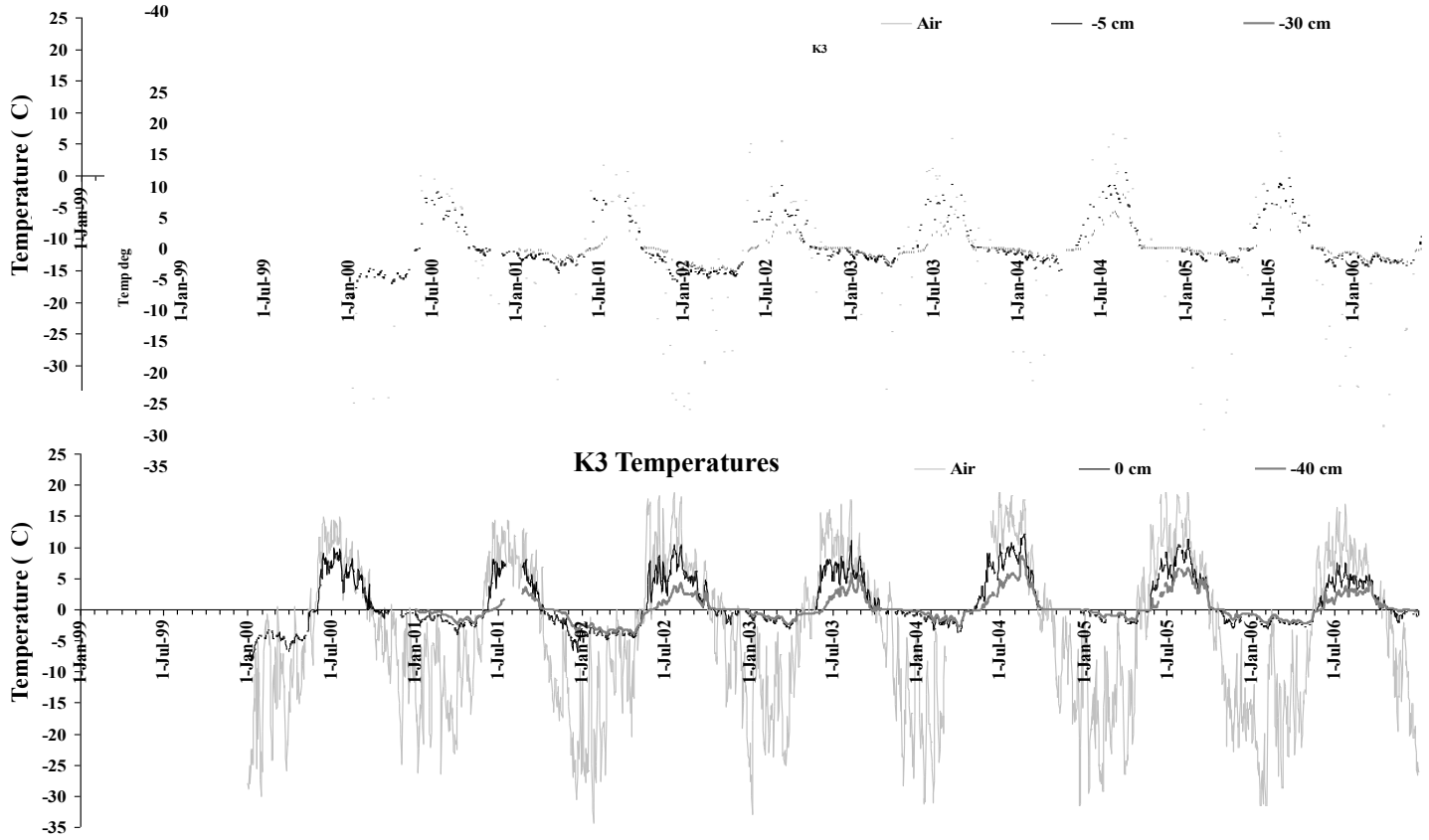

Figure 2.7 Mean daily air, surface, and ground temperatures at K2 (–5 cm and –30 cm) and K3 (0 cm and –40 cm) stations 1999-2006.

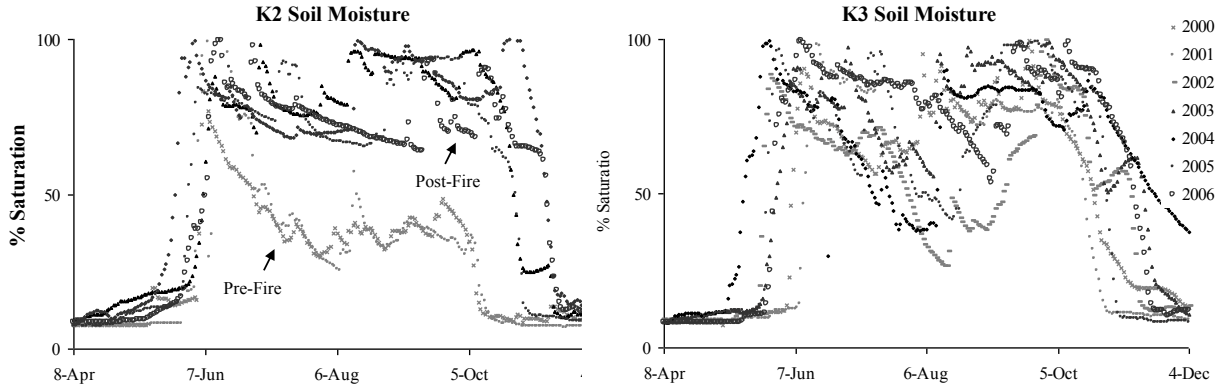

Figure 2.8 Mean daily unfrozen soil moisture presented as percent saturation at K2 (-10 cm) and the control K3 (-5 cm) 2000-2006. Gray and black lines represent observations made before and after 2002.

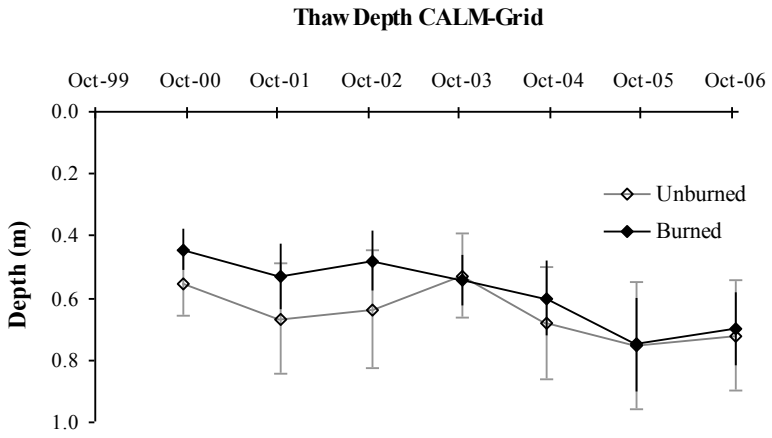

Figure 2.9 Observed mean CALM grid active layer depths acquired in late September or early October 2000-2006 of 21 control sites (gray) and 90 sites that were burned in 2002 (black).

2.9 Tables

Table 2.1 Site descriptions of meteorological stations K1, K2 and K3.

Site description	K1	K2	K3
Latitude	65º 26.42'	65º 25.70'	65º 27.58'
Longitude	164º 34.71'	164º 38.61'	164º 38.29'
Elevation	290 m	110 m	260 m
Aspect	None	SW	S
Slope	Level	3 deg.	6.5 deg.
Landform	Ridge	Broad, alluvial fan	Slope
Vegetation	Moss, lichens	Eriophorum tussocks	Shrub
Parent material	loess	loess	loess
Organic-Mineral interface	-2 cm	-15 cm	- 15 cm
Fires	1971, 1997	1971, 2002	1971
Watershed	Niagara Cr. (6.5 km^2)	no name	Mauze Gulch (4.5 km^2)

Table 2.2 Soil classification scheme of K2 and K3 stations. From *Sturm et al.* [2005] with frozen thermal conductivities by *Hinzman et al*. [1991].

	Horizon	Depth (cm)	< 2 mm Clay	< 2 mm Silt	< 2 mm Sand	> 2 mm	Saturation (% by weight)	Bulk density (g cm^{-3})	Soil class	Thermal conductivity k_thaw (W m^{-1} K^{-1})	Thermal conductivity k_frozen (W m^{-1} K^{-1})
Tussock (K2)	Oi/Oe	0-4					518.3	0.08	Organic	0.695	1
	O/A	4-14					336.8	0.24	Organic	0.695	1
	Bg/Ajj	14+	21.6	57.6	20.8		35.7	1.52	Fine	1.535	2.689
Shrub (K3)	Oi	0-15					724.5	0.05	Organic	0.745	1
	O/A	15-18	64	34.4	1.6		157.8	0.58	Organic	0.695	1
	AB	18-25	16.4	42.4	41.2	13	80	0.94	Fine	0.843	2.919
	BA	25+	21.6	39.6	38.8				Fine	0.843	2.920

Table 2.3 Instrumentation used at the three meteorological stations. K3 station, only 3 m tall, was equipped with soil water content reflectometers of model CS 615.

Meteorological variable	**Instrument**
Air temperature	Vaisala HMP45C
Rainfall	Texas Electronic TR-525M
Pyranometer	Campbell Scientific Eppley PSP
Pyrgeometer	Campbell Scientific Eppley PIR
Net radiation	Radiarion and Energy Balance System REBS Q-7.1 Net Radiometer (1.5 m)
Soil temperature	Alpha thermistors 13A5001-C2
Soil moisture	Campbell Scientific CS615 (pre-fire), CS616 (post-fire)
Wind speed	Met one 014A Anemomenter (1 m) and
	R.M. Young Wind Monitors 05103 (3 m and 10 m)

Table 2.4 Summary table of observations made at K1, K2, and K3 stations with calculated thermal offsets and top of the permafrost annual temperatures.

Variable	Units	Station	1999	2000	2001	2002	2003	2004	2005	2006
Snow water equivalent	m	tuss./shrub	0.08/0.21	0.08/0.24	na	na	na	na	na	na
Snow depth	m	tuss./shrub	0.39/0.73	0.39/0.74	na	na	na	na	na	na
End of snowmelt (albedo <20%)	Julian Day	K2	na	138	150	na	(before 131)	106	125	137
Beginning thaw	Julian Day	K2/K3	na	156/154	152/160	na/141	140/144	123/127	128/145	139/146
Beginning freezing	Julian Day	K2/K3	286	294/280	289/281	na/291	292/316	305/343	277/298	298/310
Duration thawing season (-5cm/0cm)	Days	K2/K3	na	138/126	137/121	na/150	152/172	182/216	149/153	159/164
Freeze-up (-1m)	Julian Day	K2	na	na	na	na	6	15	42	9
Duration freeze-up period (-1m)	Days	K2	na	na	na	na	88	103	97	87
Duration frozen period (-1m)	Days	K2	na	na	na	na	134	108	86	130
n-factor thawed	-	K2/K3	na	0.51/0.71	0.46/na	na/0.61	0.7/0.71	0.74/na	0.84/0.63	0.77/0.55*
n-factor frozen 2nd	-	K2/K3	na	0.84/0.38	0.68/0.17	na/0.30	0.82/0.11	0.68/0.18**	0.49/0.09	0.66/0.13
n-factor frozen 1st	-	K2/K3	0.47	0.31/0.08	0.38/0.19	na/0.07	0.31/0.04	0.21/0.02	0.36/0.10	0.33/0.06
Thawed Air Degree-Days	Deg.-Days	K2/K3	na	919/917	973/893	na/1156	1121/969	1508/na	1218/1193	1108/995
Thawed Surface Degree-Days (-5cm/0cm)	Deg.-Days	K2/K3	na	471/648	447/na	na/707	788/684	1122/767	1019/748	850/543
Freezing Surface Degree-Days 2nd (-5cm/0cm)	Deg.-Days	K2/K3	na	-1455/-638	-1102/-272	na/-473	-1357/-163	-1245/-195	-942/-162	-1457/-279
Freezing Surface Degree-Days 1st (-5cm/0cm)	Deg.-Days	K2/K3	na	-156/-46	-519/-234	na/-39	-253/-30	-146/-7	-395/-100	-260/-42
Freezing Air Degree-Days 2nd	Deg.-Days	K2/K3	na	-1723/-1659	-1618/-1638	na/-1573	-1653/-1502	-1843/na	-1921/-1777	-2207/-2143
Freezing Air Degree-Days 1st	Deg.-Days	K2/K3	na	-495/-600	-1354/-1256	na/-558	-822/-741	-710/-319	-1084/-1032	-797/-765
Rainfall (June-Aug.)	mm	Mean all	na	101	102	64	120	72	134	63
Min air temp.(hourly)	ºC	K1/K2/K3	na	-31/-40/-34	na/-38/-32	na/na/-38	-33/-38/-34	-33/-40/na	-32/-37/-32	-35/-40/-37
Max air temp. (hourly)	ºC	K1/K2/K3	na	21/24/24	19/22/22	na/na/27	24/25/25	27/30/na	26/27/28	24/27/26
Annual mean air temp. (1m)	ºC	K1/K2/K3	na	-3.9/-3.6/-3.7	na/-5.5/-5.6	na/na/-2.7	-3.6/-3.7/-3.5	-3.1/-2.9/na	-5/-4.9/-4.3	-5.5/-5.2/-5.9*
Annual mean surface temp. (-5cm/0cm)	ºC	K2/K3	na	-3.1/-0.1	-3.2/na	na/0.5	-2.3/1.3	-0.8/1.9	-0.9/1.5	-2.4/0.2
Annual mean ground temp. (-30cm/-40cm)	ºC	K2/K3	na	-3.9/-1.3***	-3.3/na	na/-0.5	-2.5/0.2	-1.5/0.9	-1.2/0.9	-2.8/-0.5
September mean ground temp. (-50cm)	ºC	K2/K3	0.3/na	0.2/1'	na/na	na/1.3'	1.8/1.7'	2.3/2.1'	3/3.1'	2.7/2.4'
Annual mean ground temp. (-1m)	ºC	K2	na	-4.4	na	na	-2.8	-2.6	-1.5	-2.9
Annual min ground temp. (-1m)	ºC	K2	na	-11.7	na	na	-11.5	-10.6	-7.5	-9.2
Annual max ground temp. (-1m)	ºC	K2	-0.6	-0.6	na	na	0.1	0.5	0.8	0.3
Min soil temp. (-30cm/-40cm)	ºC	K2/K3	na	-15.9/na	-12/na	na/-4	-16/-2.5	-14.8/-2.8	-10.21/-1.8	-13.5/-3.1
Max soil temp. (-30cm/-40cm)	ºC	K2/K3	na	1.7/na	2.1/na	na/4.5	7.4/6	8.6/9.3	7.8/6.9	4.2/4.8
Radiation Efficiency (June/July)	-	K2	na	0.67/0.66	0.69/0.67	na	na	0.68/0.66	0.69/0.68	na

na = No data available

* Air temp at K3 missing 9/13-10/7, replaced with K2 temperature

** No K3 air temperature in March, April, and May. Replaced with K2 temperature

*** K3 estimated through linear interpolation

1st = Beginning of freezing to end of calendar year

2nd = First day of calendar year to beginning of thaw

2.10 References

Braun, L. N. (1985), Simulation of snowmelt-runoff in lowland and lower alpine regions of Switzerland, *Zuricher Geogr. Schr. 21*, Geogr. Inst. Eidgenossische Technische Hochschule, Zurich, Switzerland.

Brown, J., K. M. Hinkel, and F. E. Nelson (2000), The circumpolar active layer monitoring (CALM) program: Research designs and initial results, *Polar Geogr., 24*(3), 165–258.

Brown, R. J. E., and T. L. Péwé (1973), Distribution of permafrost in North America and its relationship to environment: A review, 1963–1971, paper presented at *North American Contribution, Permafrost Second International Conference*, Natl. Acad. of Sci., Washington, D. C.

Burn, C. R. (1997), The response (1958– 1997) of permafrost and near-surface ground temperatures to forest fire, Takhini River Valley, southern Yukon Territory, *Can. J. Earth Sci., 35*, 184–199.

Burn, C. R. (1998), The active layer, *Permafrost Periglacial Proc., 59*, 411– 416.

Campbell Scientific Inc. (1996), *Instruction Manual Q-7.1 Net Radiometer*, Revision: 5/96, 12 pp., Logan, Utah.

Carlson, H. (1952), Calculation of depth of thaw in frozen ground, in *Frost Action in Soils: A Symposium*, Highway Res. Board Spec. Rep. 2, pp. 192–223, Natl. Res. Council, Washington, D. C.

Chambers, D. S., J. Beringer, T. J. Randerson, and S. F. Chapin III (2005), Fire effects on net-radiation and energy partitioning: Contrasting responses of tundra and boreal forest ecosystems, *J. Geophys. Res., 110*, D09106, doi:10.1029/2004JD005299.

Eugster, W., W. Rouse, R. A. Pielke, J. P. McFadden, D. D. Baldocchi, T. G. F. Kittel, F. S. Chapin III, G. E. Liston, P. L. Vidale, E. Vaganov, and S. Chambers (2000), Land-atmosphere energy exchange in Arctic tundra and boreal forest: Available data and feedbacks to climate, *Global Change Biol., 6*, 84–115.

Flannigan, M., I. Cambell, M. Wotton, P. R. Carcaillet, and Y. Bergeon (2001), Future changes in Canada‘s boreal forest: Paleoecology results and general circulation model – regional climate model simulations, *Can. J. For. Res., 31*, 854–864.

Heginbottom, J. A. (1976), Some effects of a forest fire on the permafrost active layer at Inuvik, N. W. T, *Report 73-16*, 29 pp., Task Force on Northern Oil Dev., Ottawa, Canada.

Hinzman, L. D., D. L. Kane, R. E. Gieck, and K. R. Everett (1991), Hydrologic and thermal properties of the active layer in the Alaskan Arctic, *Cold Regions Sci. Technol., 19*, 95–110.

Hinzman, L. D., D. L. Kane, C. Benson, and K. R. Everett (1996), Energy balance and hydrological processes in an Arctic watershed, in *Ecological Studies: Analysis and Synthesis*, vol. 120, edited by J. F. Reynolds and J. D. Tenhunen, pp. 131– 154, Springer, NY.

Hinzman, L. D., D. L. Kane, and K. Yoshikawa (2003), Soil moisture response to a changing climate in Arctic regions (extended abstract), *Tohoku Geophys. J*., *36*(4), 369–373.

Houghton, J. T., L. G. M. Filho, B. A. Callandar, N. Harris, A. Kattenberg, and K. Maskell (1996), Climate change 1995, in *Contribution of Working Group 1 to the Second Assessment Report of the Intergovernmental Panel on Climate Change*, Cambridge Univ. Press, NY.

Kade, A., V. E. Romanovsky, and D. A. Walker (2006), The n-factor of nonsorted circles along a climate gradient in Arctic Alaska, *Permafrost Periglacial Proc., 17*, 279–289.

Kane, D. L., L. D. Hinzman, M. Woo, and K. R. Everett (1992), Arctic hydrology and climate change, in *Arctic Ecosystem in a Changing Climate*, pp. 35–57, Academic, San Diego, CA.

Karunaratne, K. C., and C. Burn (2004), Relations between air and surface temperature in discontinuous permafrost terrain near Mayo, Yukon Territory, *Can. J. Earth Sci., 41*, 437–1451.

Kasischke, E. S., N. L. Christensen Jr., and B. J. Stocks (1995), Fire global warming, and the carbon balance of boreal forests, *Ecol. Appl., 5*, 437–451.

Kasischke, E. S., D. Williams, and B. Donald (2002), Analysis of the patterns of large fires in the boreal forest region of Alaska, I*nt. J. Wildland Fire, 11*, 14–131.

Kasischke, E. S., and M. R. Turetsky (2006), Recent changes in the fire regime across the North American boreal region: Spatial and temporal patterns of burning across Canada and Alaska, *Geophys. Res. Lett., 111*, L09703, doi:10.1029/2006GL025677.

Klene, A. E., F. E. Nelson, and N. I. Shiklomanov (2001), The n-factor in natural landscapes: Variability of air and soil-surface temperatures, Kuparuk River basin, Alaska, U.S.A., *Arct. Antarct. Alpine Res., 33*(2), 140–148.

Liu, H., J. T. Randerson, J. Lindfors, and S. F. Chapin III (2005), Changes in the surface energy budget after fire in boreal ecosystems of interior Alaska: An annual perspective, *J. Geophys. Res., 110*, D13101, doi:10.1029/2004JD005158.

Lynch, J. A., J. S. Clark, N. H. Bigelow, M. E. Edwards, and B. P. Finney (2002), Geographic and temporal variations in fire history in boreal ecosystems of Alaska, *J. Geophys. Res., 107*, 8152, doi:10.1029/2001JD000332.

Mackay, R. J. (1995), Active layer changes (1968 – 1993) following the forest-tundra fire near Inuvik, N.W.T, Canada, *Arct. Alpine Res., 27*, 323–336.

Manabe, S., R. J. Stouffer, M. J. Spelman, and K. Bryan (1991), Transient responses of a coupled ocean-atmosphere model to gradual changes of atmospheric CO2. part I: Annual mean response, *J. Climate, 4*(8), 785–818.

McCoy, V. M., and C. R. Burn (2005), Potential alteration by climate change of the forest-fire regime in the boreal forest of central Yukon Territory, *Arctic, 58*, 276–285.

Oke, T. R. (1987), Boundary Layer Climates, 2nd ed., 435 pp., Routledge, New York.

Racine, C. H. (2004), Tundra fire effects on soils and three plant communities along a hillslope gradient in the Seward Peninsula, Alaska, *Arctic, 34*(1), 71–84.

Racine, C. H., L. A. Johnson, and L. A. Viereck (1987), Patterns of vegetation recovery after tundra fires in Northwestern Alaska, U.S.A, *Arct. Alpine Res., 19*(4), 461–469.

Romanovsky, V. E., and T. E. Osterkamp (1995), Interannual variations of the thermal regime of the active layer and near-surface permafrost in Northern Alaska, *Permafrost Periglacial Proc., 6*, 313–335.

Rouse, W. R., and P. F. Mills (1977), A classification of fire effects on the microclimate of forests and tundra ecosystems, *Final Rep. R71–19/2*, 21 pp., Minister of Indian and Northern Affairs, Ottawa, Canada.

Rupp, S. T., S. F. Chapin III, and A. M. Starfield (2000), Response of subarctic vegetation to transient climatic change on the Seward Peninsula in north-west Alaska, *Global Change Biol., 6*, 541–555.

Shiklomanov, N. I., and F. E. Nelson (2002), Active layer mapping at regional scales: A 13-year spatial time series for the Kuparuk region, North-Central Alaska, *Permafrost Periglacial Proc., 13*, 219–230.

Shur, Y., K. M. Hinkel, and F. E. Nelson (2005), The transient layer: Implications for geocryology and climate-change science, *Permafrost Periglacial Proc., 16*, 5–17.

Stieglitz, M., S. J. Déry, V. E. Romanovsky, and T. E. Osterkamp (2003), The role of snow cover in the warming of arctic permafrost, *Geophys. Res. Lett., 30*(13), 1721, doi:10.1029/2003GL017337.

Stocks, B. J., M. A. Fosberg, T. J. Lynham, L. Mearns, B. M. Wotton, Q. Yang, J.-Z. Jin, K. Lawrence, G. R. Hartley, J. A. Mason, and D. W. McKenney (1998), Climate change and forest fire potential in Russian and Canadian boreal forests, *Climate Change, 38*, 1–13.

Stocks, B. J., J. A. Matson, J. B. Todd, E. M. Bosch, B. M. Wotton, B. D. Amiro, M. D. Flannigan, K. G. Hirsh, K. A. Logan, D. L. Martell, and W. R. Skinner (2003), Large forest fires in Canada, 1959–1997, *J. Geophys. Res., 107*, 8149, doi:10.1029/2001JD000484.

Sturm, M., J. P. McFadden, G. E. Liston, S. F. Chapin III, and C. H. Racine (2001), Snow-shrub interactions in arctic tundra: A hypothesis with climate implications, *J. Climate, 14*, 336–344.

Sturm, M., J. Beringer, and L. D. Hinzman (2005), Seward Peninsula data and documentation 2 CD-ROM set: Arctic transitions in the land atmosphere system (ATLAS) project, produced by D. Stott, G. Stossmeister, and J. A. Moore, NSF Office of Polar Progr., Boulder, CO.

Swanson, D. K. (1996), Susceptibility of permafrost soils to deep thaw after forest fires in Interior Alaska, U.S.A., and some ecologic implications, *Arct. Alpine Res., 28*(2), 217–227.

Thayer-Snyder, C. R. (2002), ATLAS vegetation studies: Seward Peninsula, Alaska, 2000, ARCCS-ATLAS-AGC data report, Univ. of Alaska, Fairbanks, AK.

Valeo, C., K. Beaty, and R. Hesslein (2003), Influence of forest fires on climate change studies in the central boreal forest of Canada, *J. Hydrol., 280*, 91–104.

Vidale, P. I., R. A. Pielke, L. T. Steyaert, and A. Barr (1997), Case study modeling of turbulent and mesoscale fluxes over the BOREAS region, *J. Geophys. Res., 102*(D24), 29,167–29,188.

Viereck, L. A. (1982), Effects of fire and firelines on active layer thickness and soil temperatures in Interior Alaska, in *Proceedings of the Fourth Canadian Permafrost Conference*, pp. 123– 135, Natl. Res. Council of Can., Calgary, Alberta, Canada.

Viereck, L. A., J. Foote, C. T. Dyrness, K. van Cleve, D. Kane, and R. Seiveret (1979), Preliminary results of experimental fires in the black spruce type of Interior Alaska, *Res. Not. PNW-332*, 27 pp., Pacific Northwest and Range Exp. Station, U. S. Dep. of Agric., Portland, OR.

Vörösmarty, C. J., L. D. Hinzman, B. J. Peterson, D. H. Bromwich, L. C. Hamilton, J. Morison, V. E. Romanovsky, M. Sturm, and R. S. Webb (2001), The hydrologic cycle and its role in Arctic and global environmental change: A rationale and strategy for synthesis study, *Report*, 84 pp., Arct. Res. Consortium of the U.S., Fairbanks, AK.

Waelbroeck, C., and P. Monfray (1997), The impact of permafrost thawing on the carbon dynamics of tundra, *Geophys. Res. Lett., 24*(3), 229–232.

Watson, R. T., M. Zinyowera, and R. H. Moss (1998), *The Regional Impacts of a Climate Change: An Assessment of Vulnerability*, Cambridge University Press, Cambridge, U.K.

Woo, M. K. (1986), Permafrost hydrology in North America, *Atmos. Ocean, 24*, 201– 234.

Yoshikawa, K., W. R. Bolton, V. E. Romanovsky, M. Fukuda, and L. D. Hinzman (2002), Impacts of wildfire on the permafrost in the boreal forests of Interior Alaska, *J. Geophys. Res., 107*, 8148, doi:10.1029/2001JD000438. [printed 108(D1), 2003]

CHAPTER 3
PROCESSES CONTROLLING EVAPOTRANSPIRATION AT AN ARCTIC COASTAL WETLAND

Abstract

We quantify the multi-year patterns and controls on midday arctic coastal wetland evapotranspiration measured with the eddy covariance method at two vegetated drained thaw lake basins near Barrow, Northern Alaska. Near-surface soil moisture and atmospheric vapor pressure deficits have non-linear effects on midday evapotranspiration rates. Vapor pressure deficits near and above 0.3 kPa appear to be an important hydrological threshold, allowing latent heat fluxes to exceed sensible heat fluxes. Although increased atmospheric demand initially favors latent heat fluxes, an increased bulk surface resistance prevents evapotranspiration from reaching its potential rate (Priestley-Taylor α ~1.26) despite wet soils. Dry soils increase the bulk surface resistance (water-limited), while wet soils favor ground heat flux and therefore reduce the energy available to sensible and latent heat fluxes (energy-limited). Thus, midday evapotranspiration is suppressed on both dry and wet soils but through different mechanisms. Ultimately, the various limiting factors reduce midday evapotranspiration under a range of meteorological and hydrologic conditions. The negative feedbacks on the hydrologic system have the potential to moderate interannual variation of total evapotranspiration. The multiple limitations on evapotranspiration, including the prevailing maritime winds and the projected increase in precipitation, will likely prevent extensive future soil drying and hence maintain the presence of coastal wetlands.

3.1 Introduction

The response of arctic wetland hydrology to projected future climate warming is uncertain. Evapotranspiration is the least understood component in the Arctic hydrologic cycle [*Kane et al*., 1989, 1992; *Vörösmarty et al*., 2001; *Woo et al*., 2008]. Regional research varies proposing increased [*Lafleur*, 1993] to unchanged [*Rouse et al*., 1992] future evapotranspiration rates from arctic coastal wetlands. As evapotranspiration is the major pathway of water loss from the flat tundra landscape [*Rovansek et al.*, 1996; *Mendez et al*., 1998; *Bowling et al*., 2003], an increase in evapotranspiration could reduce the extent of Arctic wetlands [*Barnett et al*., 2005]. If soil drying occurs, a region, that for a long time has sequestered carbon, would then shift to a carbon source, causing a positive feedback to global climate warming [*Oechel et al.*, 1998; *Olivas et al.,* 2010].

A vast majority of extremely-low gradient arctic tundra is located within 135 km of the Arctic Ocean [*Walker et al*., 2005; *Minke et al*., 2007]. The summer climate of the arctic coastal zone is controlled by a steady mesoscale phenomenon; a nearly 24-hour sea breeze [*Moritz*, 1977; *Walsh*, 1977; *Kozo*, 1979, 1982] resulting in low diurnal temperature fluctuations and low vapor pressure deficits (VPD). All components of the coastal wetland energy balance, except net radiation, depend on wind direction with cold moist maritime air suppressing evapotranspiration losses [*Rouse et al*., 1987]. One may expect the sea-breeze to continue in a warmer climate, yet the fate of future evapotranspiration rates from coastal wetlands is debated.

Measurement of energy fluxes in arctic environments are challenging due to climatic and logistical constraints. Hence, most field studies are of relatively short duration. There are several field studies of arctic surface energy exchange [see *Eugster et al*., 2000] and arctic water balance [see *Kane and Yang*, 2004] but few studies have conducted multi-year analyses of evapotranspiration measured by the

eddy covariance technique. Here we present results from one of the longest time series of flux measurements available for any arctic ecosystem represented by two vegetated drained thaw lake basins (5 years at one site; 3 years in an adjacent site) on the Arctic Coastal Plain, Northern Alaska. Our analyses confirm earlier work from different locations that relied on Bowen ratio and energy balance techniques. In addition, we show that evapotranspiration from the arctic coastal wetlands experience multiple limitations, which include constrained midday evapotranspiration rates during both wet and dry near-surface conditions. The identified thresholds and multiple controls may be important factors in successfully projecting the future evapotranspiration regime and Arctic ecosystem changes and their global implications.

3.2 Background

Extremely low-relief wetlands represent a significant portion (> 400,000 km^2) of the pan-Arctic landscape [*Walker et al*., 2005] and are unique in that they exist in an environment with a desert-like annual precipitation (~ 250 mm yr^{-1}). The negative summer net water balance, which is limited to the summer precipitation–evapotranspiration (P–E) [*Mendez et al*., 1998] as summer runoff is rare [*Brown et al*., 1968; *Kane et al.*, 2008], is offset by the annual replenishment of water from snowmelt [*Rovansek et al*., 1996]. The abundance of snowmelt water results in extensive surface inundation during the first week following snowmelt [*Bowling et al*., 2003; *Woo et al., 2006*] and spring runoff is not generated until the surface stores are replenished [*Rovansek et al*., 1996; *Bowling and Lettenmaier*, 2010]. Accordingly, evapotranspiration, through P-ET, is not only the major pathway of water loss in summer but it also affects the lateral exports of water.

Evapotranspiration from wet and moist tundra ecosystems of the North Slope of Alaska is estimated to 0.8-4.2 mm day^{-1} resulting in estimated annual totals ranging from 70 to 190 mm [see *Vourlitis and Oechel*, 1997]. A majority is

evaporation from moss and open water (55 to 85%) [see *Engstrom et al*., 2006] even though bryophytes receive only 10-20 % of direct solar radiation during a clear summer day [*Miller and Tieszen*, 1972]. Upward migration of water, attributed to capillary flow, occurs with 0.2 m deep water tables in Sphagnum moss [*Hayward and Clymo*, 1982; *Price et al.*, 2009]. Capillary water flow in moss, and hence moss evaporation, is negligible at water potentials below -0.1 MPa [*Hayward and Clymo*, 1982]. In comparison, stomatal closure in vascular plants due to water stress occurs at soil water potentials of -0.4 MPa (*Arctophila fulva*) to -1.2 MPa (*Carex aquatilis*) [*Stoner and Miller,* 1975; *Johnson and Caldwell,* 1975]. Transpiration is closely related to Leaf Area Index (LAI) as stomatal closure is rare at wet coastal Arctic sites [*Miller and Tieszen*, 1972]. However, the conductance of tundra plants can be reduced by leaf cell water stress induced by vapor pressure gradients ranging from 0.7 to 2 kPa between the leaf and the ambient air [*Johnson and Caldwell,* 1975]. Arctic bryophytes are extremely sensitive to air vapor pressure deficits due to the direct changes in tissue water content [*Oechel and Sveinbjörnsson*, 1978].

The effect of maritime air mass on surface energy partitioning has been observed 135 km inland from the Arctic Coast [*Harazono et al.*, 1998]. Cold moisture-laden air along the coast increases the partitioning of surface energy into sensible heat flux (*H*) due to a) a steep temperature gradient between the ground surface and air, which favors *H,* and b) a nearly saturated air mass that reduces latent heat flux (*LE*) [*Rouse et al*., 1987; *Lafleur and Rouse*, 1988, 1995; *Price,* 1991; *Harazono et al*., 1998; *Boike et al*., 2008]. This explains the finding that, despite the wet soils, evapotranspiration is in general below its potential rate in coastal arctic wetlands [*Rouse et al*., 1987; *Mendez et al*., 1998]. However, it is unclear what values in air vapor pressure deficits result in significant changes to surface energy partitioning and evapotranspiration rates.

Soil moisture may play a major role on tundra surface energy balance partitioning. Coinciding with a seasonal reduction in the water table depth (from surface ponding to 30 cm below the ground surface), a larger portion of the net radiation was partitioned into latent heat in early season (Bowen ratio marginally <1), while sensible heat dominated the late season energy balance at a coastal wet- and moist herbaceous tundra site [*Vourlitis and Oechel,* 1997]. Wet organic soils transfer heat more efficiently than dry soils [*Farouki*, 1981; *Hinzman et al*., 1991], which in theory, would leave less net radiation available to sensible and latent heat fluxes. That evokes the question whether the arctic wetlands display important negative feedback mechanisms on the local hydrological system that constrain evapotranspiration rates not only during dry near-surface conditions but also when wet.

3.3 Site Description

The two sites, hereafter referred to as Central Marsh, CM, (71º19'12.5"N, 156º37'20.211"W, elevation 1 m) and the Biocomplexity Experiment, BE, (71°16'51.17"N 156°35'47.28"W, elevation 4.5 m) are located 4.5 km apart, and both are only few kilometers from the ocean near Barrow, Alaska, on the Arctic Coastal Plain (Fig. 3.1). Mean annual air temperature at Barrow Airport is −12 °C (1977-2009) with a summer (June through August) average of 3.3 °C. A large amount (72 mm) of the annual precipitation (173 mm, 1977-2009) falls during June through August. Fog and drizzle are common during the summer because the area receives a steady cool and moist wind (mean 5 m s^{-1}) off the ocean from east-northeast [*Shulski and Wendler*, 2007]. The BE site is located in the control treatment of a large-scale hydrologic manipulation experiment that began in 2007 (identified as the South site in the work by *Zona et al*. [2009a]).

The BE and CM sites are representative of vegetated drained thaw lake basins that appear to have drained between 50 and 300 years ago [*Hinkel et al*.,

2003]. The sites are poorly drained and are characterized by wet meadow tundra with Typic Aquiturbels soils [*Bockheim et al*., 1999] underlain by 600 m thick permafrost [*Brown and Johnson,* 1965]. Large diameter (~50 m) low-centered polygons are found at the vegetated drained thaw lake basin while high-centered polygons cover the upland areas of the watersheds. Vegetated drained thaw lake basins (DTLB) [*Mackay,* 1963] occupy approximately 26% of the Arctic Coastal Plain [*Hinkel et al*., 2005] and 50% of the Barrow Peninsula north of ~71° latitude [*Hinkel et al*., 2003]. Longer-term (>2 yr) energy balance studies of DTLB are limited, which constrains our understanding of interannual controls of DTLB evapotranspiration rates.

Non-vascular vegetation contributes significantly to biomass and land cover [*Webber,* 1974, 1978; *Oechel and Sveinbjornsson,* 1978; *Rastorfer,* 1978]. Bryophytes represent between 60 and 95% of the overall live biomass in similar wet meadow communities [*Tieszen*, 1978] with much of the variation due to small scale heterogeneity associated with micro-topography [*Tieszen*, 1978; *Hollister and Flaherty*, 2010]. Across the BE drained lake bed, mosses represent most of the live above ground biomass [*Zona et al*., 2009a, 2009b]. Up to 60 % of the ecosystem net day time CO_2 uptake at the end of the growing season at BE is represented by *Sphagnum* [*Zona et al*., 2011].

The sites differ somewhat in vascular plant composition, LAI (green biomass unless otherwise stated) and the amount of standing dead biomass (which is defined as attached or upright dead plant matter). *Arctophila fulva* is the dominant vascular plant species at the CM site where vegetation is also represented by sedges, mosses and lichens. LAI at the CM site reached 1.4 in mid-August 2001 [*Mano, 2003*]. At the BE vegetated drained lake, the vascular plant coverage is represented by *Carex aquatilis*, *Eriophorum spp.* and *Dupontia fisheri* with an average LAI in mid-August 2006 of 0.43, 0.13 and 0.02, respectively [*Zona et al*., 2011]. Sedges at the BE site did not experience water stress in mid-July 2008 [P.

Olivas, unpublished data]. Standing dead leaf biomass in the Barrow area reaches LAI of 1.23 [*Dennis et al*., 1978]. The CM site has a larger abundance of standing dead biomass than the BE site (personal observation). End of growing season plant senescence extends from the end of August to late September [*Myers and Pitelka, 1979*].

The sparseness of live subsurface material at depths greater than 25 cm at Barrow suggests that the cold temperatures near the bottom of the active layer are limiting to vascular root growth [*Dennis and Johnson,* 1970]. Moss may reach thicknesses of 20 cm at wet sites but the bulk of their living biomass is usually within ~1 cm of the soil surface [*Engstrom et al*., 2005]. While the rate of thaw is higher in early summer, the maximum thaw depth (active layer depth) is reached late August/September. The active layer depth at a nearby drained lake basin varied from 19 to 62 cm (mean 36 cm) in 1995-2009 while the mean active layer depth at the BE site was 30 cm (2006), and 26 cm (2007 and 2008) [*Shiklomanov et al*., 2010].

3.4 Methods

3.4.1 Measurements

We analyzed summer measurements for five years at the CM site (1999-2003) and three years at the BE site (2006-2008). Energy flux measurements were made at a 10 Hz sampling interval using an eddy covariance system. The path length of anemometer and gas analyzer sensor at CM was 10 cm and the separation distance between the center of sonic anemometer and open-path IRGA sensors was 16 cm. The three components of wind speed, air temperature and water vapor concentration from the above sensors were recorded on a magneto-optical disc by a digital recorder (Teac, DRM3). At BE, the sensor separation of the Li-7500 and WindMasterPro was 10 cm. The Li-7500 was calibrated every two to four weeks using ultra high purity nitrogen as zero and a dew point generator (Li-610, Li-

COR) that produced an air stream with a known water vapor dew point (typically 7 °C lower than the air temperature in a laboratory). Micrometeorological variables were sampled on a data logger every 5 s (CM) or 10 s (BE) and then averaged every 30 minutes. Additional descriptions of the measurements and data analysis are presented in the work of *Harazono et al*. [2003] and *Zona et al*. [2009a].

Sporadic measurements of the volumetric water content at two locations within the CM drained lake basin were obtained in 2000-2003 by inserting a 7 cm Vitel probe (Hydra soil moisture probe, Vitel Inc.) vertically into the ground. The instrument was calibrated through comparison to multiple oven-dried soil samples [*Engstrom et al*., 2005]. The CM site was often inundated in early summer. Such events are here presented as 100 % VWC to indicate ponding.

Hourly atmospheric air pressure for years 1999-2003 were obtained from the NCDC web archive (http://cdo.ncdc.noaa.gov/cgi-bin/cdo/cdostnsearch.pl) and used in the calculations of the psychrometric constant. Long-term records of daily precipitation and air temperature were retrieved from the National Climatic Data Center (NCDC) web archive for the Barrow Airport (STN 700260, WBAN 27502, www.7.ncdc.noaa.gov/CDO/cdoselect.cmd?datasetabbv=GSOD).The characteristic increase in net radiation defined the start date of the summer in order to evaluate the total summer solar radiation received by the snow-free ground surface.

3.4.2 Eddy Covariance Calculations

We calculated fluxes of heat and momentum in 30 min intervals according to typical covariance calculation procedures. The following corrections were applied (see *Harazono et al*., [2003] and *Zona et al*. [2009a]): the humidity effect on the sonic thermometry [*Kaimal and Gaynor,* 1991], effects of path length and sensor separation on the spectrum for high-frequency flux ranges [*Moore,* 1986], air density effects [*Webb et al*., 1980; *Leuning et al*., 1982], and coordinate rotation [*Tanner and Thurtell,* 1969]. We removed calculated fluxes during rain, fog, and

low wind, which may have caused a bias (i.e. reduced representation of low evapotranspiration rates). Extreme amplitudes in the flux data (greater than three times the average) were removed. At the BE site, fluxes of latent heat, sensible heat and momentum were calculated using the EdiRe program and software (version 1.4.3.1169, Robert Clement, University of Edinburgh). No gap filling was performed when analyzing the bulk parameters and energy flux ratios, which represented half hourly values around solar noon (defined as ± 2 hours from local solar noon ~ 14:00 Alaska Standard Time). Extreme amplitudes in the bulk parameters (greater than six times the average) were removed. For daily evapotranspiration rates, gap filling was performed for missing data (< 2 consecutive hours) using linear interpolation and negative 30 min latent heat fluxes were given a value of zero.

3.4.3 Soil Moisture Analysis

Unfrozen soil moisture as percent saturation was estimated from volumetric water content (VWC) measurements at 10 cm depth at the BE site. The spring peak in soil moisture was assumed to represent saturated conditions (100%, all micro and macro pore spaces filled with liquid water), and during winter, the organic soil was assumed to have 6 % saturation with unfrozen water content [*Hinzman et al*., 1991]. Soil water potential (ψ) was calculated by fitting a curve after *van Genuchten* [1980] to a measured water potential sequence (WP4-T, Decagon Devices) from a surface organic moss layer sampled at the BE site. We adjusted the daily precipitation to account for gage undercatch according to *Yang et al*. [1998].

3.4.4 Analysis of Resistances and Equilibrium Evaporation

We quantified parameters affecting evapotranspiration by applying measured heat fluxes to the Penman-Monteith equation [*Monteith,* 1973] expressed in terms of aerodynamic, r_a, and bulk surface resistance, r_c:

$$LE = \frac{sQ_a + \rho C_p[e_s(T_a) - e_a]/r_a}{s + \gamma[1 + r_c/r_a]} \qquad (1)$$

where s is the slope of the saturation vapor pressure versus air temperature curve, Q_a is available energy (sensible + latent heat) in W m^{-2}, γ is the psychrometric constant (kPa K^{-1}), ρ the air density (kg m^{-3}); C_p is the specific heat capacity of air (kJ kg^{-1} K^{-1}) at constant pressure, e_s the saturation vapor pressure (kPa) at ambient air temperature (K), T_a, and e_a the air vapor pressure (kPa). The aerodynamic resistance, r_a (s m^{-1}), is calculated from Equation (2) following *Monteith* [1973] with an additional term on the right side representing the laminar boundary layer resistance from *Thom* [1975] and *Lafleur and Rouse* [1988]:

$$r_a = \frac{u}{u*^2} + \frac{4}{u*} \qquad (2)$$

where $u*$ is friction velocity (m s^{-1}) obtained by eddy covariance measurements and u is wind speed. From here and onwards, the sum of the aerodynamic and laminar boundary layer resistance in Equation 2 is referred to as aerodynamic resistance (r_a). The aerodynamic resistance is the bulk meteorological descriptor of the role of atmospheric turbulence in evaporation.

The isothermal resistance, r_i, (m s^{-1}) was originally defined by *Monteith* [1965] and is sometimes referred to as the climatological resistance. It is the ratio of water vapor deficit to available energy at the canopy

$$r_i = \frac{\rho \times C_p}{\gamma} \frac{e_s(T_a) - e_a}{Q_a} \qquad (3) \qquad [\textit{Stewart and Thom,}\ 1973]$$

Saturation vapor pressure deficit $\{e_s(T_a) - e_a\}$ is calculated using the relative humidity and air temperature measurements. Shallow ponded water can represent a significant portion (< 50 %) of the net radiation partitioning [*Harazono et al*., 1998], therefore, we defined Q_a as the sum of sensible and latent heat fluxes since no water temperature measurements were obtained. Equations (1), (3) and the Bowen ratio (*H/LE*) can be combined to solve for the bulk surface resistance, r_c (m s^{-1}):

$$r_c = \left(1+\beta\right)\bar{r}_i + \left(\beta\frac{s}{\gamma}-1\right)r_a \qquad (4)$$

The bulk surface resistance characterizes the control of water loss by a vascular plants, non-vascular vegetation, and bare ground where β is the Bowen ratio and s is the slope of the saturation vapor pressure curve versus temperature modified from *Brutstaert* [1982].

The bulk surface resistance approaches zero either because the surface boundary layer becomes saturated and VPD = 0 or if the air travels over an unsaturated surface with constant r_c and the moisture deficit in the air becomes equal to the value if the surface. A r_c close to 0 results in Penman-Monteith Equation [*Monteith*, 1973] collapsing into:

$$LE = \alpha\left(\frac{s}{s+\gamma}\right)Q_a \qquad (5) \qquad [\textit{Priestley and Taylor}, 1972]$$

which is known as the Priestley-Taylor equation. When α equals one, the evapotranspiration is referred to as "equilibrium", which is most commonly

achieved when VPD = 0 (note that equilibrium rates can also be measured over unsaturated surfaces and VPD > 0). The method assumes that the latent heat flux depends only upon the absolute temperature and the available energy. Results from a variety of arctic sites, both wet and dry, indicate that latent heat flux is often above the equilibrium rate [see *Engstrom et al*., 2002], as originally suggested by *Priestley and Taylor* [1972] at a non-water-limited grassland. Larger scale mixing of the planetary boundary layer and the entrainment of drier air from above the mixed layer results in evaporation over saturated surfaces greater than the ~~"~~equilibrium" rate [*McNaughton and Jarvis*, 1983; *DeBruin*, 1983]. *DeBruin* [1983] indicates α is a function of wind speed, surface roughness, and bulk surface resistance.

The McNaughton and Jarvis Ω-factor sets the relative importance of r_c and r_a:

$$\Omega = \left(1 + \frac{s}{s + \gamma}\frac{r_c}{r_a}\right)^{-1} \qquad (6)$$

Also, a vigorous turbulent mixing of the air mass suppress Ω by promoting increased VPD at the surface while Ω approaches unity during limited atmospheric mixing [*McNaughton and Jarvis*, 1983]. However, as long as $r_c >> r_a$, Ω will approach 0. In general, VPD is the main driver of evapotranspiration when Ω *is* low, while net radiation has the dominant control during Ω near 1.

3.5 Results

3.5.1 Site Conditions

During the study period, the mean air temperature (3.2 °C) and precipitation (86 mm) were near the long-term means (3.4 °C and 99 mm, respectively yr 1979-2008) but large interannual variations occurred (Table 3.1). Summer 2007

experienced unusually high air temperatures (5.4 °C) and low precipitation (24 mm). Most of the precipitation in summer 2007 occurred in a single event in mid-August. During the study period, a third of the recorded total daily precipitation events in summer represent trace observations, while 77 % were less than 2 mm day^{-1}. Accumulated winter precipitation ranged from 93 to 158 mm of snow water equivalent (SWE).

The maritime air mass reduced variation in VPD and air temperature. Mean daily VPD was 0.08 kPa with a typical diurnal min and max of 0.02 and 0.17 kPa, respectively. Mean midday VPD was similar amongst all years (0.10-0.12 kPa) although it was slightly higher in summer 2007 (0.17 kPa) (Table 3.1). Maximum VPD recorded was 1.76 kPa. Days exceeding VPD‘s of 0.3 kPa were few (8 to 14 days per summer).

Onshore winds (defined as 1-135 and 225-360 degrees) were dominant with 89 % of the wind directed from the ocean (1999-2008). The diurnal air temperature fluctuated on average 4.5°C. The mean daily maximum temperature was 5.2°C. Air during onshore winds was colder than the ground surface. Offshore winds (from land to sea) typically produced higher VPD‘s and air temperatures than onshore winds, reversing the typical midday temperature gradient between the air and the ground surface (Table 3.2).

The porous organic soils remained close to saturation near the surface throughout the study period with the exception of 2007 (Fig. 3.2). Even though the soils within the vegetated drained lake basins were unusually dry in late summer 2007 (water table dropped below 15 cm depth), the typical extensive ponding of snowmelt water in spring ―re-set” the soil water storage the following year. Water table measurements at the BE basin show a multi-week long ponding period following the snowmelt with ~10 cm of water accumulating above the ground surface (note that the water table measurements were initiated ~ 1 week before the flooding began). In two of the eight summers (2001 and 2008), the drained lake

basins experienced inundation also in late summer, resulting in a total inundation period lasting for at least half of the summer. Unfortunately, no soil water measurements were made in summer 1999 but the near-normal precipitation (82 mm) suggests wet soil conditions.

3.5.2 Surface Energy Exchange

A major portion of the midday surface energy balance was partitioned into sensible heat flux CM: 35 %, BE: 46 %) resulting in a mean midday Bowen ratio above unity at the both sites (CM: 1.40, BE: 1.38) (Table 3.3). Latent heat flux represented 29 % and 36 %, and ground heat flux averaged 16 % and 12 % at CM and BE, respectively. Measured evapotranspiration ranged from 0.2 to 5.7 mm day^{-1} (mean 1.8 mm day^{-1}) and 1.3 to 7.2 mm day^{-1} (mean 4.2 mm day^{-1}) at the CM and BE sites, respectively. Not unusual for tundra and grassland ecosystems [*Zona et al*., 2009b; *Cava et al*., 2008; *Ryu et al*., 2008; *Wilson et al*., 2002], the energy balance closure was high at BE (97 %) although slightly lower at CM (80 %).

The large variation in near-surface soil moisture at the BE site allowed an analysis of its role on the surface energy balance. Approximately 71 % ($P < 0.01$, probability that correlation is zero) of the variance in the Priestley-Taylor α is correlated to the near-surface soil moisture (Fig. 3.3a). Accordingly, bulk surface resistance is higher during dry ($\Psi < -0.13$ MPa) near-surface soil conditions (Table 3.4). Wetter soils also increased the partitioning to ground heat flux from ~5 % during a soil water potential of about –0.15 MPa to ~15 % at saturated conditions (Fig. 3.3b, Table 3.4). However, the partitioning into *G* reached up to 40 % during an individual day in early summer. Late-summer (July 20 through August 12) midday partitioning into *LE* is strikingly similar between dry and wet soils (38 and 35 %, respectively), suggesting a suppression of midday *LE* also under wet near-surface conditions.

Similar to previous studies, the surface energy partitioning depended on wind direction (Table 3.2), i.e. whether the winds are directed towards the ocean (offshore) or land (onshore). Onshore winds favored energy partitioning into sensible heat flux (β 1.37), while the Bowen ratio was slightly below unity during offshore conditions (0.87) at the CM site. Both the partitioning into ground and latent heat increased with offshore winds, while the sensible heat flux portion decreased. No onshore-offshore analysis was performed at the BE site as the two wind directions represents differing landscape features (low-centered polygons high-centered polygons, respectively).

Increased VPD affected the energy balance partitioning and the Priestley-Taylor α (Fig. 3.4). Latent heat fluxes from a wet surface were always larger then sensible heat fluxes (Bowen ratios below unity) if VPDs were above 0.25 (2006), 0.31 (2007), and 0.28 kPa (2008). In comparison, a similar threshold for dry soils ($\Psi < -0.12$ MPa) was at 1.19 kPa (2007). A VPD above these thresholds (wet soils) resulted in a Priestley-Taylor α near one or higher. Bowen ratios and Priestley-Taylor α varied during VPD below 0.3 kPa. When the drained lake basin‘s soil was unusually dry, such in late July through early August 2007, the evapotranspiration remained below the equilibrium rate despite VPD reaching 1.7 kPa. Overall mean midday evapotranspiration was near or slightly below the equilibrium rate (CM 0.94, BE 0.88) (Table 3.3).

High bulk surface resistance (~100 s m^{-1}) often occurred with elevated VPD (~1 kPa) throughout the study period (Fig. 3.5). Excluding summer 2007, which had unusually dry soils, midday events with VPD‘s above 0.3 kPa resulted in a higher mean bulk surface resistance (73 s m^{-1}) than those below 0.3 kPa (39 s m^{-1}). However, high bulk surface resistance also occurred with low VPD such as the gradual increase in bulk surface resistance during summer 2003 and 2007. The increased bulk surface resistance suppresses the evapotranspiration during large atmospheric demand.

Two days in late July 2000 show the cascading effects on meteorological conditions and surface energy balance that are induced by an altered wind direction (Fig. 3.6). The first day represent near-normal meteorological conditions with onshore winds resulting in an equal partitioning of *LE* and *H*. Offshore winds occurred during the following day, which resulted in high VPD (1.3 kPa) and *LE* dominating *H*. The *LE* exceeded *H* when the VPD passed 0.37 kPa (see vertical dashed lines) in the morning. Conversely, *LE* and *H* became equal in the afternoon when the VPD returned to 0.37 kPa. Bulk surface resistance and Priestley-Taylor α responded accordingly with increasing mean midday bulk surface resistance (from 75 to 128 s m^{-1}) and Priestley-Taylor α (from 0.84 to 1.03).

3.6 Discussion

The two Arctic Coastal Plain wetlands experience multiple limitations on current evapotranspiration rates. We concur with previous studies that state the importance of maritime air mass that favor sensible heat (large temperature gradients) and suppressing latent heat flux (low VPD) [*Rouse et al*., 1987; *Lafleur and Rouse*, 1988; *Price,* 1991; *Harazono et al*., 1998]. While the high McNaughton and Jarvis Ω-factor (CM: 0.74, BE: 0.79) suggests that net radiation is the main driver of evapotranspiration rates, we show that near-surface soil moisture conditions and VPD express non-linear effects on midday evapotranspiration. Ultimately, the various suppressing factors reduce the evapotranspiration under a range of meteorological and hydrologic conditions, which has the potential to buffer interannual variation of total evapotranspiration.

The generally low vapor pressure deficits (mean midday 0.12 kPa) play an important role in suppressing the evapotranspiration from the arctic coastal wetlands. A VPD near 0.3 kPa appears to represent a threshold during wet near-surface soils. Above 0.3 kPa, latent heat fluxes always dominated the sensible heat fluxes, and the evapotranspiration rates always remained near or above the

equilibrium rate. Although increased atmospheric demand initially favors *LE*, an increased bulk surface resistance prevents evapotranspiration from reaching its potential rate (α ~1.26). The rate of water movement through moss (capillary forces upwards from the water table) may not be able to keep up with potential evaporation rates and thus the bulk surface resistance is greater during unsaturated near-surface conditions or high atmospheric demands. Our findings agree with earlier plot-scale studies of tundra vascular and non-vascular conductance (inverse of resistance) [*Johnson and Caldwell,* 1975; *Oechel and Sveinbjörnsson*, 1978] where the current surface cover (despite wet soils) is unable to deliver enough moisture when atmospheric demands are high. Hence, the evapotranspiration from the two studied vegetated drained lake is suppressed during both low and high VPD‘s through differing controlling processes.

Despite large interannual variations in mean summer air temperatures, the number of days exceeding a VPD of 0.3 kPa varied only between 8 (2003) and 14 days (2001). In addition, it was the coldest summer (2001) that had the most days above 0.3 kPa although the two warmest summers (1999 and 2007) trailed closely behind (12 and 13 days, respectively). Hence, warmer mean summer air temperatures do not necessarily mean an increased number of days with VPD‘s above 0.3 kPa.

Near-surface soil moisture plays an important role in controlling energy balance in vegetated drained thaw lake basins. A high near-surface soil moisture favor evapotranspiration when analyzing the Priestley-Taylor α and the bulk surface resistance (Fig. 3.3, Table 3.4). However, the linkage between evapotranspiration and soil moisture appears to be more complex as the ratio of latent heat flux to net radiation is similar amongst dry and wet soils (Table 3.4). Simultaneously, the partitioning into ground heat flux is larger during wet soils, which reduces the energy available for midday sensible and latent heat flux. Not unlike the our discussion about the role of VPD on evapotranspiration, we suggest

that midday evapotranspiration is suppressed during both dry and wet soils through differing mechanism that tend to reduce water loss to the atmosphere during a range of soil moisture conditions.

The measurements employed in this study cannot distinguish transpiration from evaporation, but our results can be compared to past findings. Firstly, measured ET rates (1.8 and 4.2 mm day^{-1}) were more than twice as high as the maximum vascular transpiration (0.2 mm day^{-1}) estimated by *Miller and Tieszen* [1972] during peak LAI. Secondly, the measured near-surface soil water potentials never reached thresholds for stomatal closure typical for tundra vascular vegetation presented by *Stoner and Miller* [1975] and *Johnson and Caldwell* [1975]. However, soil water potentials approached the threshold for effective water transport through moss (−0.1 MPa), which coincided with increased canopy resistances (yr 2007). Thirdly, if the vascular vegetation played a dominant role, the observed increase in bulk surface resistance in late summer of 2003 and 2007 is less likely since thresholds for stomata closure related to moisture stress was never reached. Fourthly, as mosses represent the majority of the live biomass [*Zona et al*., 2009a, 2009b], one could argue that they represent a key hydrologic pathway between land and atmospheric systems. And, in fact, boreal mosses are known to act as a heat and moisture ~~r~~rectifier" allowing heat and moisture fluxes to proceed when they are moist and reducing heat and moisture fluxes under hot dry conditions when the uppermost moss surfaces dry [*Oechel and van Cleve*, 1986]. However, a determination of the contribution and amount of transpiration and evaporation on total evapotranspiration would require hydrologic model simulations or isotopic analyses, which are beyond the scope of this study.

Overall, the two vegetated drained thaw lake basins experienced similar distribution in the energy balance partitioning and bulk parameters despite differences in weather amongst the years (Table 3.3). It should be noted that at least a third of the data from the BE site represents the unusually dry summer of 2007,

which may explain the site-to-site difference in Priestley-Taylor α and energy closure. Still, the energy balance components are in the same order. The limited differences between the two sites suggest that our findings are valid for other locations that include coastal vegetated drained thaw lake basins.

3.7 Future Projections

According to global climate model projections for the mid-21st century, air temperature and precipitation will generally increase in the Arctic [*Walsh,* 2008]. While some parts of the land-ocean-atmosphere system are projected to change, we may also hypothesize resilience in some components of the system. For example, future summer air mass conditions at the Arctic Coastal Plain are likely to continue to be dominated by a 24-hour sea breeze. Further, midday evapotranspiration is constrained under both wet and dry soil conditions. The future evapotranspiration rates will therefore likely remain dampened, which is in agreement with *Rouse et al*. [1992] while in contradiction to the hypothesis of *Lafleur* [1993].

However, a lengthening of the thawed season could have a major effect on total heat and mass fluxes, especially with an earlier onset of snowmelt. Over the long term, thawing of permafrost or ice wedges and invasion of a denser canopy and vascular (stomata-controlled) vegetation, could drastically affect the surface energy exchange and the hydrologic cycle. Therefore, it is challenging to predict long-term effects of climate warming on arctic coastal wetland hydrology. To reduce the uncertainty in our projections we hope the research community continues to strive towards supporting longer-term field studies that are integrated with modeling efforts across multiple disciplines and scales.

3.8 Conclusion

Evapotranspiration from low-relief Arctic coastal wetlands experience multiple limitations through complex, non-linear relationships to atmospheric vapor demand and near-surface soil moisture conditions. Midday evapotranspiration is suppressed

during both high and low VPD as well as both wet and dry near-surface soils through different mechanisms. In other words, we have negative feedbacks on the hydrological system that suggests that climate warming will not lead to strong drying of coastal arctic tundra. Assuming no changes in vegetation and microtopography, we propose that the wetness of the arctic coastal wetlands will persist despite a warming climate due to the prevailing maritime winds, increased precipitation, and multiple controls on evapotranspiration.

3.9 Acknowledgements

The contributing authors were R. Engstrom, Y. Harazono, L. D. Hinzman, R. Hollister, W. C. Oechel, C. E. Tweedie, and D. Zona. Thanks to A. Aquierra who provided Figure 3.1, R. Busey for technical assistance, and G. Victorino and S. Villareal for assistance with field work, Barrow Arctic Science Consortium for logistical assistance and Ukpeagvik Iñupiat Corporation for land access to the Barrow Environmental Observatory. Financial support for this research was provided through the National Science Foundation, grants 0652838, 0632263, and 0421588. Any opinions, findings, conclusions, or recommendations expressed are those of the authors and do not necessarily reflect the views of NSF. Mention of specific product names does not constitute endorsement by NSF.

3.10 Figures

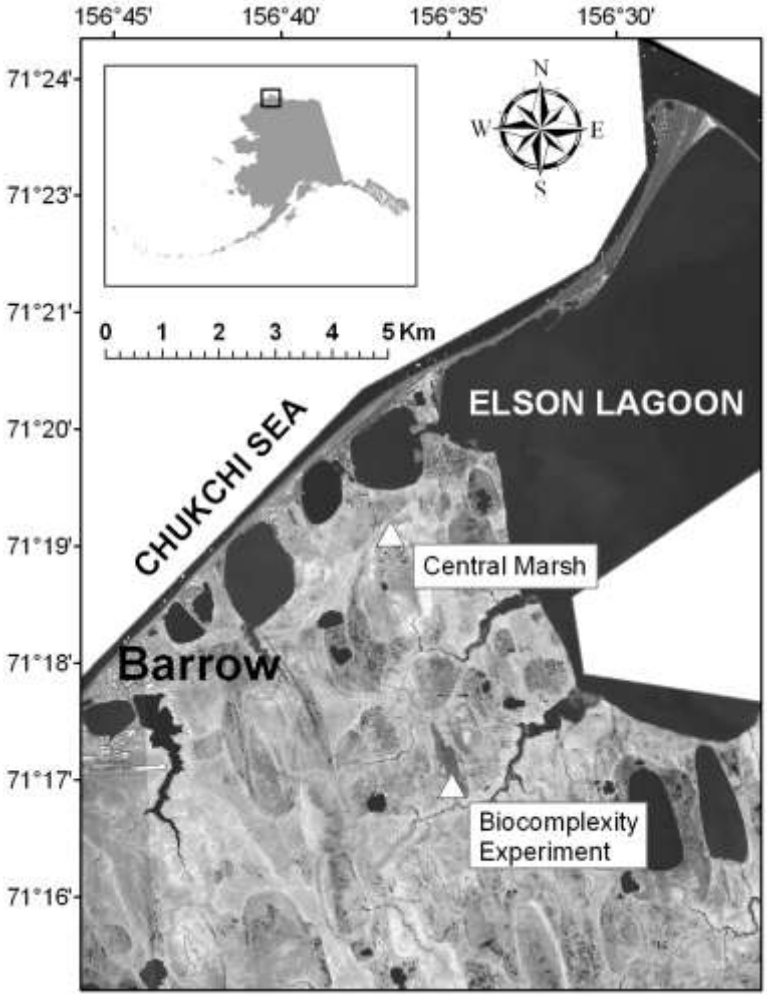

Figure 3.1 The Central Marsh (CM) and the Biocomplexity Experiment (BE) sites are located at separate vegetated drained thaw lake basins within 3 kilometers from the ocean outside the town of Barrow, Northern Alaska.

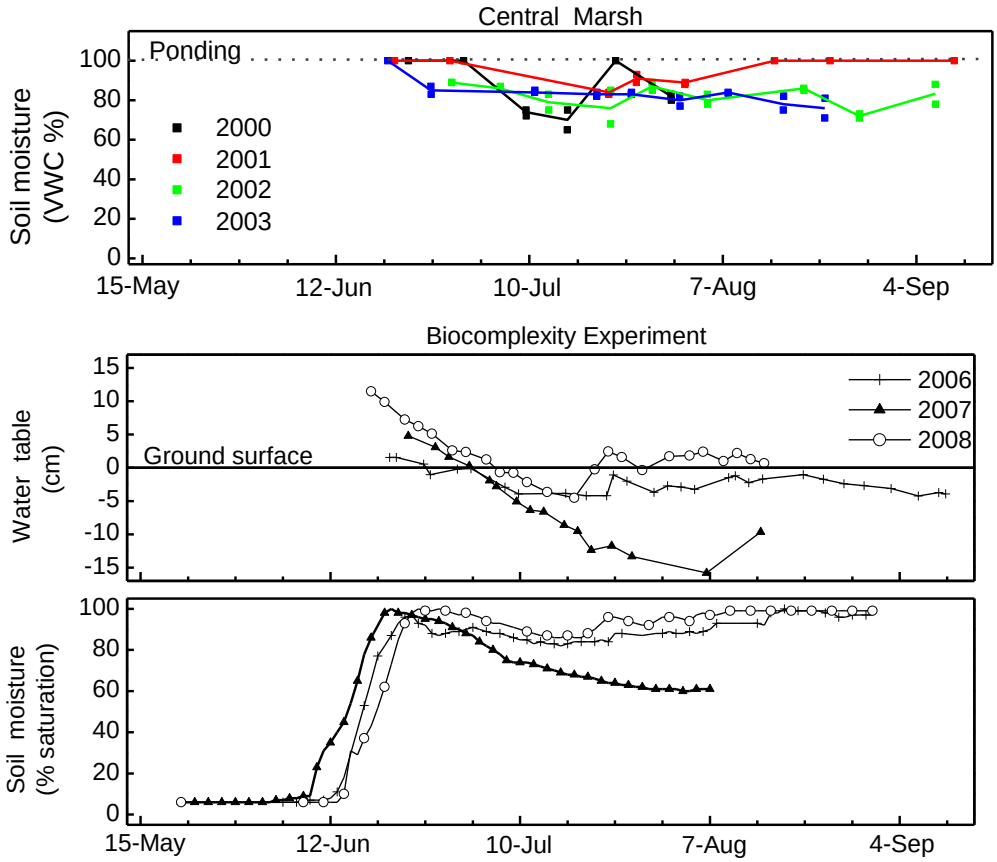

Figure 3.2 The soil water status during the study period (no measurements from 1999) at the CM site (2a) and the BE site (2b and c). Figure 2a and 2b represents multiple locations across the vegetated drained lake basins. Figure 2c is a continuous record soil moisture measurements at 10 cm depth (organic soil) near the BE eddy covariance tower presented as % saturation where the spring peak in soil moisture was assumed to represent saturated conditions (i.e. 100% since all micro and macro pore spaces are filled with liquid water) and frozen soil was assumed to have 6 % saturation with unfrozen water content [*Hinzman et al.*, 1991].

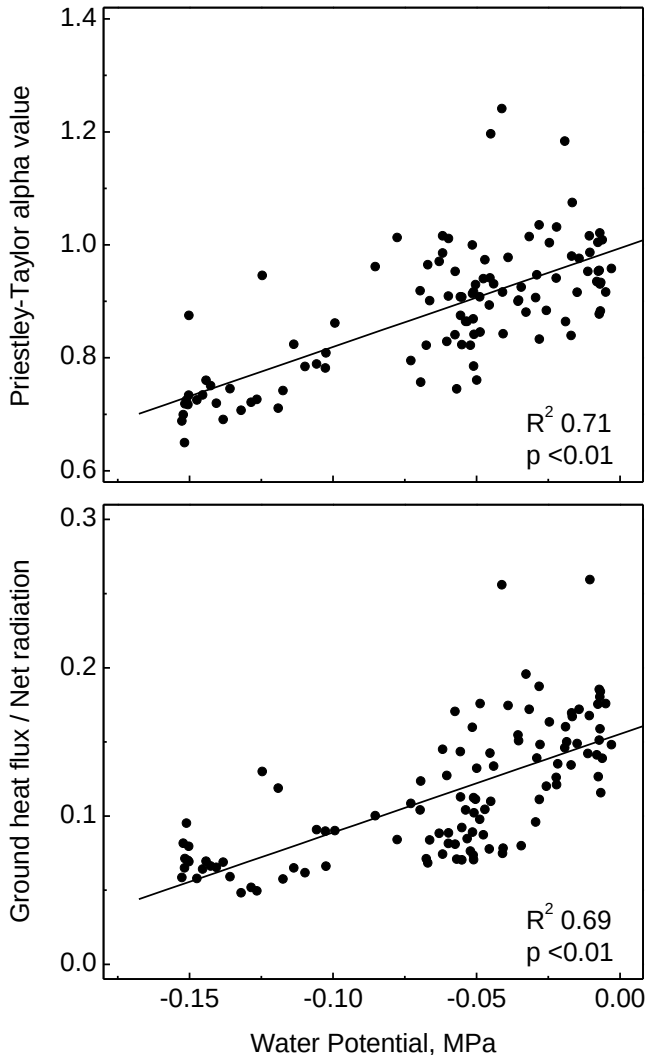

Figure 3.3 The measured rate of evapotranspiration in relation to the calculated equilibrium rate (Priestley-Taylor α) and near-surface soil moisture at the BE site (3a). The partitioning of net radiation into ground heat flux is linearly correlated to near-surface (10 cm depth) soil moisture (3b). The results represents mean midday values at the BE site.

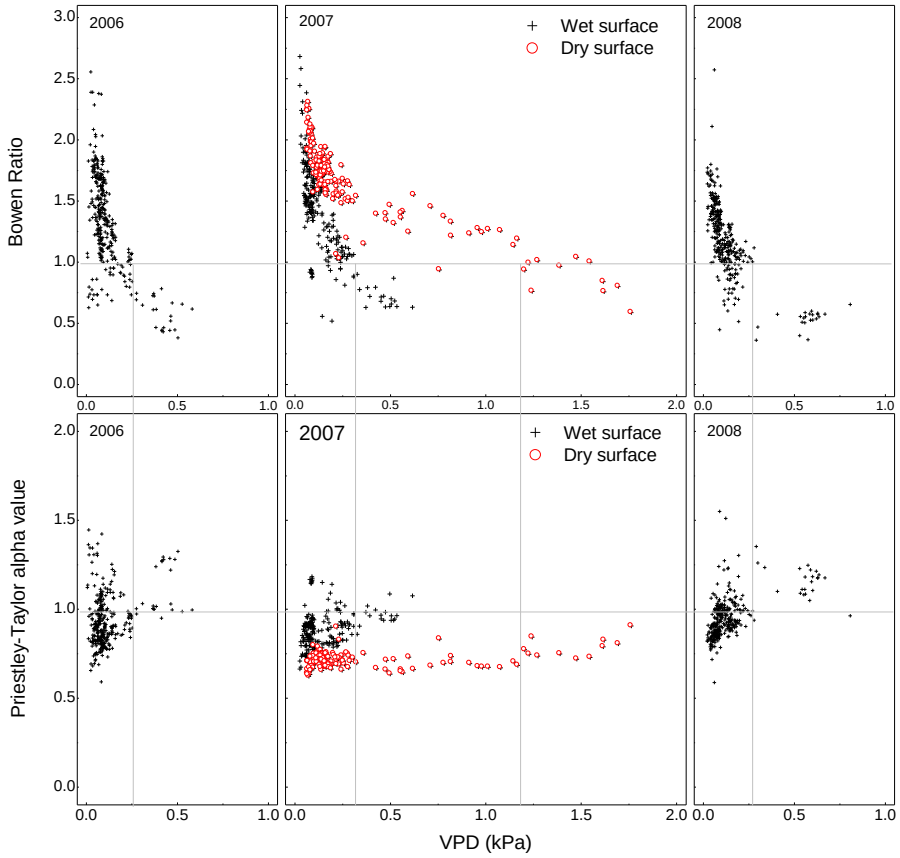

Figure 3.4 The relationship of hourly vapor pressure deficit (VPD) to Bowen ratio (β) (5a) and Priestley-Taylor α (5b) during differing soil moisture conditions at the BE site 2006-2008. Dry soils represent a soil water potential below – 0.12 MPa. The vertical dashed lines represent a VPD-threshold higher VPD's resulted in a β below 1 and the subsequent response in the Priestley-Taylor α with an α near or above 1. The identified VPD-thresholds were 0.25 (2006), 0.31 (2007), and 0.28 kPa (2008) for wet soils and 1.19 kPa for dry soils (2007).

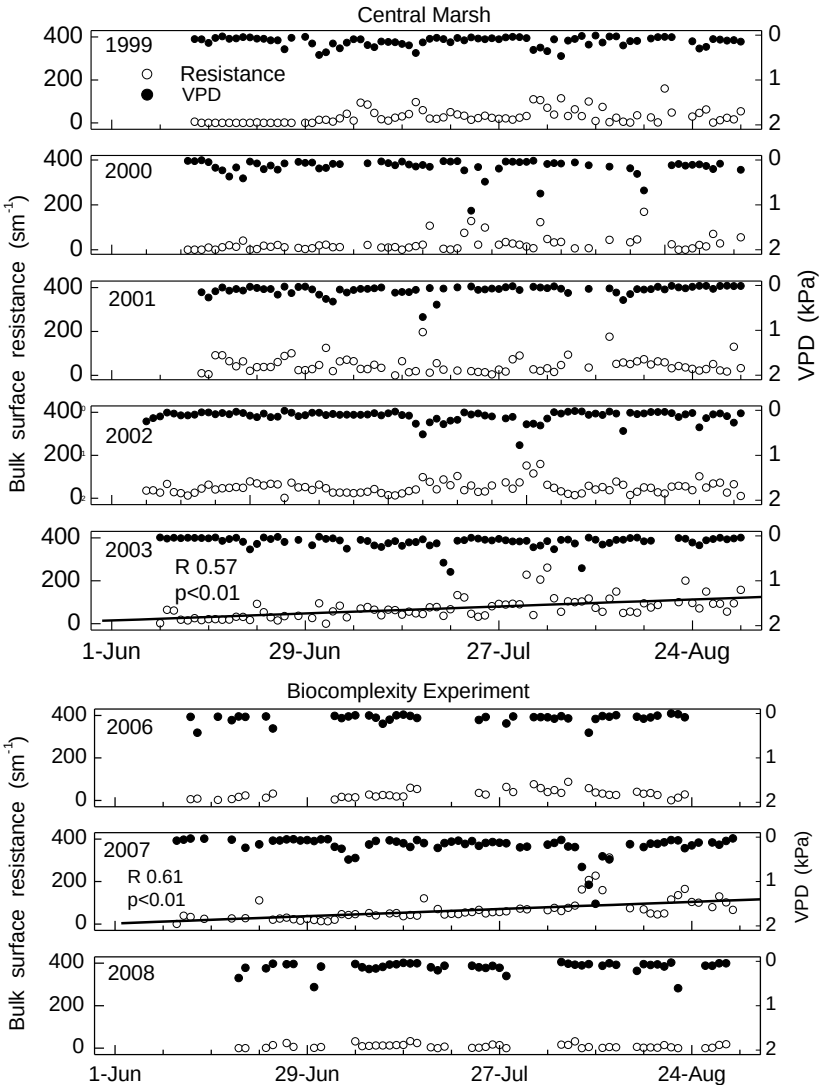

Figure 3.5 Mean midday values of bulk surface resistance (r_c) and vapor pressure deficit (VPD) at the CM and BE sites.

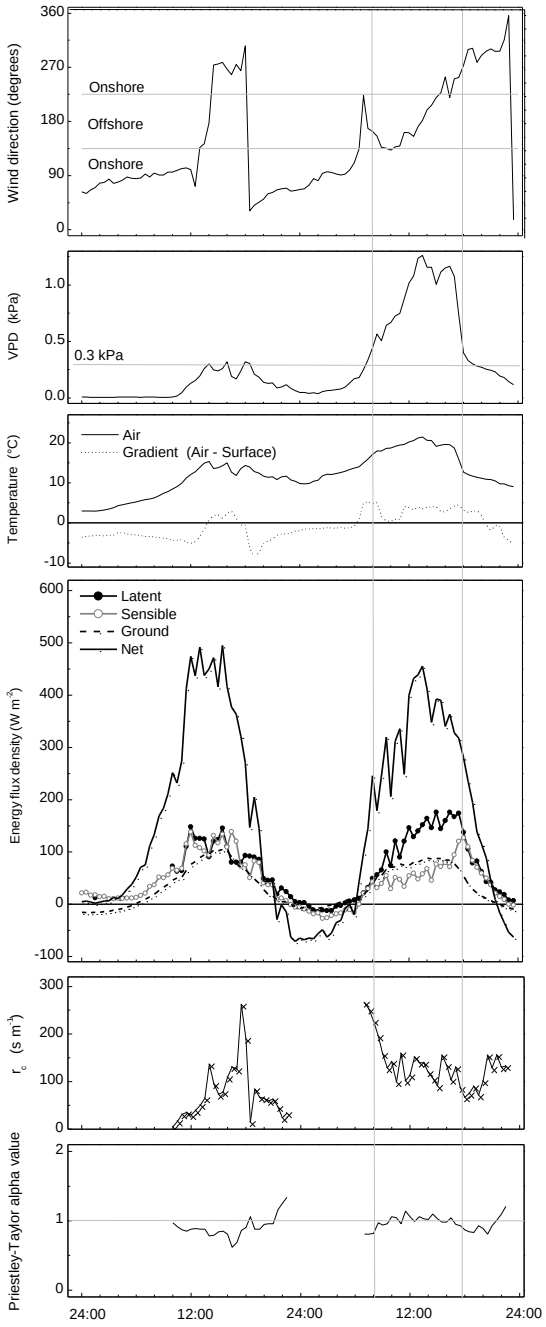

Figure 3.6 Meteorological conditions, energy balance, and bulk parameters during a two-day time period (July 22nd and 23rd, 2000) when the wind shifted from onshore to offshore. The high VPD on July 23rd coincides with offshore winds. Latent heat became the dominant heat sink when air vapor pressure deficit reached above 0.3 kPa.

3.11 Tables

Table 3.1 Meteorological conditions during the study period (1999-2008) such as Snow Water Equivalent (SWE) prior to snowmelt, total precipitation from June through September, mean air temperature June through August, mean midday air vapor pressure deficit (VPD), and the number of days that experienced a VPD above 0.3 kPa. Mean precipitation and air temperature 1999-2008 (86 mm and 3.2°C, respectively) were near the long-term (1979-2008) conditions of 99 mm and 3.4 °C, respectively.

	1999	**2000**	**2001**	**2002**	**2003**	**2006**	**2007**	**2008**	**Mean**
SWE (mm)	122	113	123	93	95	137	98	158	117
Precipitation, Jun.-Sep. (mm)	82	128	124	114	72	72	24	68	86
Mean air temperature, Jun.-Aug. (°C)	4.2	3.1	2.1	2.3	2.5	2.9	5.4	3.3	3.2
Mean midday VPD, Jun.-Aug. (kPa)	0.12	0.13	0.1	0.12	0.12	0.11	0.17	0.12	0.12
VPD > 0.3 kPa, Jun.-Aug. (days)	12	10	14	9	8	10	13	10	11

Table 3.2 Differences in energy balance partitioning, bulk parameters and air conditions during offshore (from land to ocean) and onshore (from ocean to land) winds at the CM site. The temperature gradient (ΔT) represents the air minus the ground surface temperature.

	Offshore	**Onshore**
LE/Q	0.41	0.29
H/Q	0.22	0.35
G/Q	0.22	0.15
β	0.87	1.37
α	1.08	0.95
ΔT (°C)	2.33	-1.30
VPD (kPa)	0.21	0.12

Table 3.3 Average midday energy partitioning and bulk parameters at the CM (1999-2003) and BE (2006-2008) sites.

	Central Marsh	**Biocomplexity Experiment**
LE/Q	0.29	0.36
H/Q	0.35	0.46
G/Q	0.16	0.12
Closure	0.80	0.97
β	1.40	1.38
Ω	0.74	0.79
α	0.94	0.88
r_c (s m^{-1})	46	40
r_a (s m^{-1})	62	62
r_i (s m^{-1})	14	6

Closure = $(LE+H+G)/Q$

Table 3.4 Average midday energy partitioning and bulk parameters at the BE site between July 20 and August 12 during wet and dry near-surface conditions. Only days with VPD below 0.3 kPa are included.

	Wet	**Dry**
LE/Q	0.35	0.38
H/Q	0.43	0.65
G/Q	0.14	0.06
Closure	0.92	1.10
β	1.30	1.75
Ω	0.84	0.61
α	0.90	0.73
r_c (s m^{-1})	29	63
r_a (s m^{-1})	62	48
r_i (s m^{-1})	6	10

Closure = $(LE+H+G)/Q$
Dry = $\Psi < -0.13$ MPa

3.12 References

Barnett, T. P., J. C. Adam, and D. P. Lettenmaier (2005), Potential impacts of a warming climate on water availability in snow-dominated regions, *Nature, 438*, 303–309, doi:10.1038/nature04141.

Bockheim, J. G., L. R. Everett, K. M. Hinkel, F. E. Nelson, and J. Brown (1999), Soil organic carbon storage and distribution in arctic tundra, Barrow, Alaska, *Soil Sci. Soc. Am. J., 63*, 934–940.

Boike, J., C. Wile, and A. Abniozva (2008), Climatology and summer energy and water balance of polygonal tundra in the Lena River Delta, Siberia, *J. Geophys. Res., 113*, G03025, doi:10.1029/2007JG000450.

Bowling, L. C., D. L. Kane, R. E. Gieck, L. D. Hinzman, and D. P. Lettenmaier (2003), The role of surface storage in a low-gradient Arctic watershed, *Water Resour. Res., 39*(4), 1087, doi:10.1029/2002WR001466.

Bowling, L. C. and D. P. Lettenmaier (2010), Modeling the effects of lakes and wetlands on the water balance of arctic environments, *J. Hydrometeorol., 11*(2), 276–295.

Brown, J., and P. L. Johnson (1965), Pedo-ecological investigations at Barrow, Alaska, *Tech. Rep.*, 159:32, 32 pp., US Army CRREL, Hanover, USA.

Brown, J. R., S. L. Dingman, and R. I. Lewellen (1968), Hydrology of a drainage basin on the Alaskan Coastal Plain, *Res. Rep. 240*, 18 pp., US Army CRREL, Hanover, USA.

Brutsaert, W. (1982), *Evaporation into the atmosphere*, reprinted 1991, 299 pp., Kluwer Academic Publishers, Dordrecht, The Netherlands.

Cava, D., D. Contini, A. Donateo, and P. Martano (2008), Analysis of short-term closure of the surface energy balance above short vegetation, *Agric. Forest Meteorol., 148,* 82–93.

DeBruin, H. A. R. (1983), A model for the Priestley-Taylor parameter α, *J. Climate and Appl. Meteorol., 22*, 572–578.

Dennis, J. G., and P. L. Johnson (1970), Shoot and rhizome-root standing crops of tundra vegetation at Barrow, Alaska, *Arctic Alp. Res., 2*(4), 253–266.

Dennis, J. G., L. L. Tieszen, and M. A. Vetter (1978), Seasonal dynamics of above- and below-ground production of vacular plants at Barrow, Alaska, in *Vegetation and production ecology of an Alaska Arctic tundra*, edited by L. L. Tieszen, pp. 113–140, Springer-Verlag, New York.

Engstrom, R., A. Hope, D. A. Stow, G. L. Vourlitis, and W. C. Oechel (2002), Priestley-Taylor coefficient: Variability and relationship to NDVI in arctic tundra landscapes, *J. Am. Water Resour. Ass., 38*(6), 1647–1659.

Engstrom, R., A. Hope, H. Kwon, D. Stow, and D. Zamolodchikov (2005), Spatial distribution of near surface soil moisture and its relationship to microtopography in the Alaskan Arctic coastal plain, *Nordic Hydrol., 36*(3), 219–234.

Engstrom, R., A. Hope, H. Kwon, Y. Harazono, M. Mano, and W. C. Oechel (2006), Modeling evapotranspiration in Arctic coastal plain ecosystems using a modified BIOME-BGC model, *J. Geophys. Res*., 111, G02021, doi:10.1029/2005JG000102

Eugster, W., W. Rouse, R. A. Pielke, J. P. McFadden, D. D. Baldocchi, T. G. F. Kittel, F. S. Chapin III, G. E. Liston, P. L. Vidale, E. Vaganov, and S. Chambers (2000), Land-atmosphere energy exchange in Arctic tundra and boreal forest: Available data and feedbacks to climate, *Global Change Biol., 6*, 84–115.

Farouki, O. T. (1981), Thermal properties of soil, *Report* 81-1, U.S. Army Cold Regions Research and Engineering Lab., Hanover, N.H.

Harazono, Y., M. Yoshimoto, M. Mano, G. L. Vourlitis, and W. C. Oechel (1998), Characteristics of energy and water budgets over wet sedge and tussock tundra ecosystems at North Slope Alaska, *Hydrol. Process., 12*, 2163–2183.

Harazono, Y., M. Mano, A. Miyata, R. C. Zulueta, and W. C. Oechel (2003), Inter-annual carbon dioxide uptake of a wet sedge tundra ecosystem in the Arctic, *Tellus, 55B*, 215–231.

Hayward, P. M., and R. S. Clymo (1982), Profiles of water-content and pore-size in Sphagnum and peat, and their relation to peat bog ecology, *Royal Soc. London Series B – Biol. Sci. Conf. Proceed., 215*(1200), 299–325.

Hinkel, K. M., W. R. Eisner, J. G. Bockheim, F. E. Nelson, K. M. Peterson, and X. Dai (2003), Spatial extent, age, and carbon stocks in drained thaw lake basins on the Barrow Peninsula, Alaska, *Arctic, Antarctic, and Alpine Res. 35*, 291–300.

Hinkel, K. M., R. C. Frohn, F. E. Nelson, W. R. Eisner, and R. A. Beck (2005), Morphometric and spatial analysis of thaw lakes and drained lake basins in the western Arctic Coastal Plain, Alaska, *Permafrost Periglacial. Proc., 16*, 327–341.

Hinzman, L. D., D. L. Kane, R. E. Gieck, and K. R. Everett (1991), Hydrological and thermal properties of the active layer in the Alaskan Arctic, *Cold Regions Sci. Technol., 19*, 95–110.

Hollister, R. D., and K. J. Flaherty (2010), Above- and below-ground plant biomass response to experimental warming in northern Alaska, *Appl. Veg. Sci.*, 1–10, DOI: 10.1111/j.1654-109X.2010.01079.x.

Johnson, D. A., and M. M. Caldwell (1975), Gas exchange of four Arctic and Alpine tundra plant species in relation to atmospheric and soil moisture stress, *Oecologia, 21*, 93–108.

Kaimal, J. C., and J. E. Gaynor (1991), Another look at sonic thermometry, *Boundary Layer Meteorol*., *56,* 401–410.

Kane, D. L., L. D. Hinzman, C. S. Benson, and K. R. Everett (1989), Hydrology of Imnavait Creek, an arctic watershed, *Holarctic Ecol.*, *12*, 262–269.

Kane, D. L., L. D. Hinzman, M-K. Woo, and K. R. Everett (1992), Arctic hydrology and climate change, in *Arctic Ecosystem in a Changing Climate*, edited by F. S. Chapin III, R. L. Jeffries, J. E. Reynolds, G. R. Shaver, and J. Svoboda, pp. 35–57, Academic, San Diego, CA.

Kane, D. L., and D. Yang (2004), Overview of water balance determinations for high latitude watersheds, in *Northern Research Basins Water Balance*, edited by D. L. Kane and D. Yang, pp. 1–12, IAHS, Oxfordshire, UK.

Kane, D. L., R. E. Gieck, and L. D. Hinzman (2008), Water balance for a low-gradient watershed in Northern Alaska, in *Proceedings of the Ninth International Conference on Permafrost*, edited by D. L. Kane and K. M. Hinkel, pp. 883–888, University of Alaska Fairbanks, AK.

Kozo, T. L. (1979), Evidence for sea breezes on the Alaskan Beaufort Sea coast, *Geophys Res. Lett., 6,* 849–852.

Kozo, T. L. (1982), An observational study of sea breezes along the Alaskan Beaufort Sea coast: Part 1, *J. Appl. Meteorol., 21*(7), 891–905.

Lafleur, P. M. (1993), Potential water balance response to climatic warming: The case of a coastal wetland ecosystem of the James Bay lowland, *Wetlands, 13*(4), 270–276.

Lafleur, P. M., and W. R. Rouse (1988), The influence of surface cover and climate on energy partitioning and evaporation in a subarctic wetland, *Boundary Layer Meteorol., 44*, 327–347.

Lafleur, P. M., and W. R. Rouse (1995), Energy partitioning at treeline forest and tundra sites and its sensitivity to climate change, *Atmos.-Ocean, 33*, 121–133.

Leuning, R., E. Ohtaki, O. T. Denmead, and A. R. G. Lang (1982), Effects of heat and water vapor transport on eddy covariance measurement of CO2 fluxes, *Boundary Layer Meteorol., 23,* 209–222.

Mackay, J. R. (1963), The Mackenzie Delta area, N. W. T., 202 pp., *Geographical Branch Memoir 8*, Department of Mines and Technical Surveys, Ottawa, Canada.

Mano, M. (2003), Study on the budget of carbon dioxide and methane at an arctic coastal wet sedge tundra (in Japanese), Ph.D. thesis, Chiba Univ., Chiba, Japan.

McNaughton, K., and P. G. Jarvis (1983), Predicting effects of vegetation changes on transpiration and evaporation, in *Water deficits and plant growth, Vol. VII*, , edited by T. T. Koslowski, pp. 1–47, Academic Press, NY.

Mendez, J., L. D. Hinzman, and D. L. Kane (1998), Evapotranspiration from a wetland complex on the Arctic Coastal Plain of Alaska, *Nordic Hydrol., 29*(4/5), 303–330.

Miller, P. C., and L. Tieszen (1972), A preliminary model of processes affecting primary production in the Arctic tundra, *Arctic and Alpine Res., 4*(1), 1–18.

Minke, M., N. Donner, N. Karpov, P. De Klerk, and H. Joosten (2007), Distribution, diversity, development and dynamics of polygons mires: Examples from Northeast Yakutia (Siberia), *Peatlands Int., 1*, 36–40.

Monteith, J. L. (1965), Evaporation and the environment, *Symp. Soc. Exp. Biol., 19*, 205–234.

Monteith, J. L. (1973), *Principles of Environmental Physics,* Edward Arnold, London.

Moore, C. J. (1986), Frequency response corrections for eddy correlation system, *Boundary Layer Meteorol., 37*, 17–35.

Moritz, R. E. (1977), On a possible sea-breeze circulation near Barrow, Alaska, *Arctic and Alpine Res., 9*(4), 427–431.

Myers, J. P., and F. A. Pitelka (1979), Variations in summer temperature patterns near Barrow, Alaska: Analysis and ecological interpretation, *Arct. Alp. Res., 11*, 131–144.

Oechel, W. C., and B. Sveinbjörnsson, (1978), Photosynthesis of Arctic Bryophytes, in *Vegetation and Production Ecology of an Alaskan Arctic Tundra*, edited by L.L. Tieszen, Springer-Verlag, NY.

Oechel, W. C., and K. van Cleve (1986), The role of bryophytes in nutrient cycling in the taiga, in *Forest Ecosystems in the Alaskan Taiga: A Synthesis of Structure and Function,* edited by K. van Cleve, F. S. Chapin III, P. W. Flanagan, L. A. Viereck, and C. T. Dyrness, pp. 121–137, Springer-Verlag, NY.

Oechel, W. C., G. L. Vourlitis, S. J. Hastings, R. P. Ault, and P. Bryant (1998), The effects of water table manipulation and elevated temperature on the net CO_2 flux of wet sedge tundra ecosystems, *Clim. Ch. Biol., 4*, 77–90.

Olivas, P. C., S. F. Oberbauer, C. E. Tweedie, W. C. Oechel, and A. Kuchy (2010), Responses of CO2 flux components of Alaskan Coastal Plain tundra to shifts in water table, *J. Geophys. Res.,* 115, G00I05, doi:10.1029/2009JG001254

Ostendorf, B., and J. E. Reynolds (1993), Relationships between a terrain-based hydrologic model and patch-scale vegetation patterns in an arctic tundra landscape, *Landscape Ecol., 8*(4), 229−237.

Price, J. (1991), Evaporation from a blanket bog in a foggy coastal environment, *Boundary Layer Meteorol., 57*, 391–406.

Price, J., T. W. D. Edwards, Y. Yi, and P. N. Whittington (2009), Physical and isotopic characterization of evaporation from Sphagnum moss, *J. Hydrol., 369,* 175–182.

Priestley, C. H. B., and R. J. Taylor (1972), On the assessment of surface heat flux and evaporation using large-scale parameters, *Mon. Weather Rev., 100*(2), 81–92.

Rastorfer, J. R. (1978), Composition and bryomass of the moss layers of two wet-tundra-meadow communities near Barrow, Alaska, in *Vegetation and Production Ecology of an Alaskan Arctic Tundra*, edited by L.L. Tieszen, pp. 169–184, Springer-Verlag, NY.

Rouse, W. R., S. G. Hardill, and P. Lafleur (1987), The energy balance in the coastal environment of James and Hudson Bay during the growing season, *J. Climatol., 7,* 165–179.

Rouse, W. R., D. W. Carlson, and E. J. Wieck (1992), Impacts of summer warming on the energy and water balance of wetland tundra, *Climatic Ch., 22,* 305–326.

Rovansek, R. J., L. D. Hinzman, and D. L. Kane (1996), Hydrology of a tundra wetland complex on the Alaskan Arctic Coastal Plain, U.S.A., *Arctic, Alp Res., 28*(3), 311–317.

Ryu, Y., D. D. Baldocchi, S. Ma, and T. Hehn (2008), Interannual variability of evapotranspiration and energy exchange over an annual grassland in California, *J. Geophys. Res., 113*, D09104, doi:10.1029/2007JD009263.

Shiklomanov, N. I., D. A. Streletskiy, F. E. Nelson, R. D. Hollister, V. E. Romanovsky, C. E. Tweedie, J. Brown (2010), Decadal variations of active-layer thickness in moisture-controlled landscapes, Barrow, Alaska, *J. Geophys. Res.*, 115, G00I04, doi:10.1029/2009JG001248.

Shulski, M., and G. Wendler (2007), *Climate of Alaska*, 216 pp., University of Alaska Press, Fairbanks, AK.

Stewart, J. B., and A. S. Thom (1973), Energy budget in pine forest, *Q. J. R. Meteorol. Soc., 99,* 154–170.

Stoner, W. A., and P. C. Miller (1975), Water relations of plant species in the wet coastal tundra at Barrow, Alaska, *Arctic and Alpine Res., 7*(2), 109–124.

Tanner, C. B., and G. W. Thurtell (1969), Anemoclinometer measurements of Reynolds stress and heat transport in the atmospheric surface layer, *Tech Rep*. *ECOM-66-G22-F*, 82 pp., University of Wisconsin, USA. [Available from US Army Electronic Command, Atmospheric Sciences Laboratory, Ft. Huachuca, AZ 85613.]

Thom, A. S. (1975), Momentum, mass, and heat exchange of plant communities, in *Vegetation and the Atmosphere Vol. 1,* edited by J. L. Monteith, pp. 57–110, Academic Press, NY.

Tieszen, L. L. (1978), *Vegetation and production ecology of an Alaskan Arctic tundra*, Ecological Studies, Springer-Verlag, New York, NY.

van Genuchten, M. T. (1980), A closed-form equation for predicting the hydraulic conductivity of unsaturated soils, *Soil Sci. Soc. Am. J., 44*(5), 892–898.

Vörösmarty, C. J., L. D. Hinzman, B. J. Peterson, D. H. Bromwich, L. C. Hamilton, J. Morison, V. E. Romanovsky, M. Sturm, and R. S. Webb (2001), The hydrologic cycle and its role in Arctic and global environmental change: A rational and strategy for synthesis study, *Report*, 84 pp., Arct. Res. Consortium of the U. S., Fairbanks, AK.

Vourlitis, G. L., and W. C. Oechel (1997), Landscape scale CO_2, H_2O vapor and energy flux of moist-wet coastal tundra ecosystem over two growing seasons, *J. Ecol., 85*, 575–590.

Walker, D. A., M. K. Raynolds, F. J. A. Daniels, E. Einarsson, A. Elvebakk, W. A. Gould, A. E. Katenin, S. S. Skholod, C. J. Markon, S. Evgeny, N. G. Moskalenko, S. S. Talbot, B. A. Yurtsev et al. (2005), The circumpolar arctic vegetation map, *J. Vegetation Sci., 16,* 267–282.

Walsh, J. E. (1977), Measurement of the temperature, wind, and moisture distribution across the northern coast of Alaska, *Arctic and Alpine Res., 9,* 175–182.

Walsh, J. E. (2008), Climate of the Arctic Marine Environment, *Ecol. App., 18(2)*, 3–22.

Webb, E. K., G. I. Pearman, and R. Leuning (1980), Correction of flux measurements for density effects due to heat and water vapor transfer. *Q. J. R. Meteorol. Soc. 106*, 85–100.

Webber, P. J. (1974), Tundra primary productivity, in *Arctic and Alpine Environments*, edited by J. D. Ives and R. G. Barry, pp. 445–473, Methuen, London, UK.

Webber, P. J. (1978), Spatial and temporal variation of the vegetation and its productivity, in V*egetation and Production Ecology of an Alaskan Arctic Tundra*, edited by L.L. Tieszen, pp. 37–112, Springer-Verlag, NY.

Wilson, K., A. Goldstein, E. Falge, M. Aubinet, D. Baldocchi, P. Berbigier, C. Berndorfer, R. Ceulemans, H. Dolman, C. Field, A. Grelle, A. Ibrom, B. E. Law, A. Kowalski, T. Meyers, J. Moncrieff, R. Monson, W. Oechel, J. Tenhunen, R. Valentini, and S. Verma (2002), Energy balance closure at FLUXNET sites, *Agri. Forest Meteorol., 113*, 223–243.

Woo, M.-K., K. L. Young, and L. Brown (2006), High-Arctic patchy wetlands: Hydrologic variability and their sustainability, *Phys. Geogr.*, 2006, **27**, 4, 297–307.

Woo, M. K., D. L. Kane, S. K., Carey, and D. Yang (2008), Progress in permafrost hydrology in the new millennium, *Permafrost and Periglacial Proc., 19*, 237–254.

Yang, D., B. E. Goodison, S. Ishida, and C. Benson (1998), Adjustment of daily precipitation data of 10 climate stations in Alaska: Applications of world meteorological organization intercomparison results, *Water Resour. Res., 34*(2), 241–256.

Zona, D., W. C. Oechel, J. Kochendorfer, K. T. Paw U, A. N. Salyuk, P. C. Olivas, S. F. Oberbauer, and D. Lipson (2009a), Methane fluxes during the initiation of a large-scale water able manipulation experiment in the Alaskan Arctic tundra, *Global Biogeochem. Cycles*, *23*, GB2013, doi:10.1029/2009GB003487.

Zona, D., W. C. Oechel, K. M. Peterson, R. J. Clements, K. T. Paw, and S. L. Ustin (2009b), Characterization of the carbon fluxes of a vegetated drained lake basin chronosequence on the Alaskan Arctic Coastal Plain, *Global Change Biol*., doi:10:1111/j.1365-2486.2009.02107.x.

Zona, D., W. C. Oechel, J. H. Richards, S. Hastings, I. Kopetz, H. Ikawa, and S. Oberbauer (in press), Light stress avoidance mechanisms in *Sphagnum* dominated wet coastal Arctic tundra ecosystem in Alaska, *Ecology*, 9(93), 633–644.

CHAPTER 4
THE ROLE OF LOW- AND HIGH-CENTERED POLYGONS IN ARCTIC WETLAND WATER BALANCE

Abstract

Polygonal ground and related microtopographic features are ubiquitous to landscapes underlain by permafrost. Polygonal ground can be divided into two main classes dominated by either high- or low-centered polygons. Surprisingly, their different role on hydrologic fluxes and stocks is not well quantified. We performed hydrologic modeling analyses using the physically-based model WaSiM-ETH thaw was forced and validated by data from the Biocomplexity Experiment, Barrow, Alaska, (1999 to 2009) to investigate the effect of these microtopographical features on the overall basin water balance. During the 2-3 weeks directly following snowmelt, the measured water levels in the vegetated drained thaw lake basin measured up to 15 cm above the ground surface. Measured water levels in four neighboring low-centered polygons and site photographs showed a period of brief surface connectivity during snowmelt followed by a nearly two-month lateral disconnection. A relatively large rain event (6 mm) in combination with thicker active layer depths established a sub-surface connection in early August. The timing of rain events in relation to the thaw depth of the active layer accounted for the sub-surface connectivity. The presence of elevated rims in model simulations, aimed to represent low-centered polygon tundra, reduced runoff while increasing evapotranspiration and surface water storage. The absence of rims resulted in increased runoff, and reduced storage, with evapotranspiration similar to that of low-centered polygon tundra. The high-centered polygon landscape produced more than twice the runoff than the low-centered polygon scenario, while storage and runoff drastically decreased. The observed extensive inundation period at the Barrow study site was only replicated by WaSiM-ETH when low-centered

polygon rims were represented. It is evident that microtopography plays an important role on the hydrologic fluxes and stocks of low-gradient arctic wetlands. Moderate climate warming can transform low-centered polygons into high-centered polygons when permafrost degrades and rims subside, allowing the formation of small drainage channels. Differential ground subsidence could potentially dominate the direct effects of climate change on arctic wetland hydrology.

4.1 Introduction

Wetlands are common across the pan-arctic landscape [*Tarnocai and Zoltai*, 1988; *Hall et al.*, 1994; *Minke et al.*, 2007] and their unique geomorphological and hydrologic features are important components of the tundra ecosystem [*Walker et al*., 2004] but also of the global climate system [*Chapin et al*., 2005]. For example, inundated areas offer breeding grounds for migrating birds [*Hansen and McKnight,* 1964], and the extensive soil reservoir of carbon [*Post et al.,* 1982] combined with saturated soils that results in the release of the powerful greenhouse gas methane [*Christensen et al*., 2004]. Landforms associated with arctic wetlands, such as vegetated drained thaw lakes and patterned ground [*Britton*, 1957; *Black*, 1969; *Hinkel et al*., 2005] may play an important role in basin hydrology [*Kane et al., 2003*]. It has been proposed that not accounting for the role of tundra micro-scale heterogeneity could lead to large uncertainty in regional estimates of carbon and energy exchange [*Sellers et al*., 1997; *Ostendorf et al*. 2001].

Polygon mires are a common classification of Arctic wetlands (Fig. 4.1). In the field of geochryology, the term polygon refers to closed, multisided, roughly equidimensional patterned ground features, bounded by more or less straight sides [*van Everdingen*, 1998]. The two major types of ice wedge polygons are low-centered and high-centered polygons. Both these features result in meter-scale variations in near-surface soil moisture [*Engstrom et al*., 2005], plant distribution [*Webber*, 1978], snow accumulation [*Webber et al.,* 1980], active layer depth

[*Minke et al*., 2009], soil biological activity [*Mueller et al.*, 1999], and the export of natural chlorine and bromine to the stratosphere [*Teh et al*., 2009]. Even though the tundra wetlands may seem like a featureless plain, its typical polygonal landforms result in a highly variable and dynamic environment.

Low-centered and high-centered polygons form much of the hydrologic, pedological, and biological variations in low-land tundra [*Brown et al*., 1980]. The amount of soil organic matter over lateral distances less than 1 m can differ up to a factor of 2 [*Gersper et al*., 1980] due to the mosaic of hydrologic regimes. Basins of low-centered polygons are either temporary or continuously flooded during the summer. High-centered polygons are well drained with the troughs often serving as effective pathways for the movement of water and nutrients, especially during snowmelt. Rims of the low-centered polygons and centers of the high-centered polygons are both exposed to summer and winter climate extremes. Accordingly, the microtopographical patterns results in extensive spatial variations in soil respiration [*Sommerkorn,* 2008] and net ecosystem carbon fluxes [*Olivas et al*., submitted]. A topographic reversal of a low-centered polygon into the formation of troughs and thus, eventually a well-drained high-centered polygon, can therefore have major implications for ecosystem structure and functioning.

Changes to the surface topography of Arctic wetlands can be abrupt and easily initiated. Despite the cold and continuous permafrost in Northern Alaska, *Jorgenson et al*. [2006] documented a wide-spread degradation of ice wedges occurring over a decadal time scale of moderate climate warming (2 to 5 ºC). Further, *Fortier et al.* [2007] demonstrated that in just four summers, infiltration of snowmelt runoff into ice wedge cracks can result in a continuous system of gullies through thermo-erosion. Thus, in a relatively short time period, a low-centered polygon landscape can turn into a high-centered polygon landscape due to melting of ice wedges.

Projected effects on the tundra ecosystem might not have properly accounted for the dynamic control of geomorphology under a changed climate [*Ellis and Rocherfort*, 2004]. Considering that a) a substantial portion of the Pan-Arctic landscape is represented by polygon mires (250 000 km^2) [*Minke et al*., 2007] with b) dynamic low- and high-centered polygons, and c) that the air temperature and precipitation is projected to increase [*Walsh,* 2008], more research is needed to examine the effect of patterned ground on hydrology. This paper assesses the hydrologic impact as a low-centered polygon landscape is transformed into high-centered polygonal tundra. We evaluate the change in individual basin water balance components through modeling experiments and field measurements by using data collected at a vegetated drained thaw lake basin in Barrow, Northern Alaska. The model experiments represent a first approximation in assessing the effects of polygonal features on watershed hydrology as frozen ground was not represented in the model simulations.

4.2 Background

Unique landscape features are associated with permafrost. The development of patterned ground, which includes a variety of periglacial landforms, is driven by several interconnected processes that are linked to numerous freeze/thaw cycles. Differential frost heaving, cracking (thermal or desiccation induced), clast heaving, and changes in the water table and hydrostatic pressure [*Washburn*, 1956; *Ballantyne and Matthews*, 1983; *van Vliet-Lanoe*, 1991; *Hallet and Prestrud*, 1986; *Overduin and Kane, 2006*; *Peterson and Krantz*, 2008] establish these geometric surface structures over century timescales. The associated changes in vegetation properties and peat accumulation further shape the development [*Ellis and Rochefort*, 2004; *Shur and Jorgenson*, 2007] by affecting the ground heat transfer. Variations in freezing depth, depth of the water table, textural properties of the soil, and local relief [*van Vliet-Lanoe*, 1998; *Kling*, 1998; *Francou et al*., 2001; *Peterson*

and Krantz, 2008] affect patterned ground morphology, resulting in sorted and non-sorted polygons, circles, nets, stripes or steps [*Washburn*, 1979; *van Everdingen*, 1998].

Sorted ice wedge polygons are one form of patterned ground that is common across the pan-Arctic wetlands. The cold climatic conditions and large fluctuations in winter temperature results in thermal contraction cracking of frozen soils [*Leffingwell*, 1919; *Lachenbruch*, 1962; *Mackay*, 1990], which allow the formation of ice wedges when snowmelt water infiltrates into the 3 to 10 m deep polygonal array of cracks (Fig. 4.2) [*French*, 1996]. Seen from the air, the 10 to 30 m wide polygons are bounded by 0.5 to 3 m wide ice wedges. Low-centered polygons have bounding ridges (i.e. rims) formed by soil warped upward by active ice wedges, while the centers of high-centered polygons are elevated above the boundaries (i.e. troughs) where (often inactive or decaying) ice wedges occur [*Davis,* 2001]. As the ice wedges are composed by pure ice, any melting of the ice wedges can cause dramatic changes to the microtopography of arctic wetlands [*Jorgenson et al*., 2006; *Fortier et al*., 2007].

On a seasonal scale, ice wedge polygons, snow distribution, and the seasonal development of the active layer can result in complex lateral flow patterns in Arctic wetlands [*Boike et al.,* 2008]. However, widespread flooding [*Rovansek et al*., 1996; *Bowling et al*., 2003] allows effective surface flow connectivity during freshets [*Woo and Guan*, 2006]. In summer, the shallower thaw in combination with a higher ground surface of low-centered polygon rims form ridges of frozen ground [*Minke et al*., 2007], which can serve as hydrologic barriers [*Donner*, 2007]. Accordingly, the threshold water level that allows for a subsurface lateral connection varies in time due to the seasonal development of the active layer. Adding to the complexity is the advective heat transfer, where lateral flow can produce ―hydrologic windows" within these barriers [*Donner*, 2007]. Such thermal erosion is an effective positive feedback mechanism that results in further lowering

of the threshold water levels. Thus, hydrologic fluxes and stores are intrinsically and dynamically linked to the unique tundra microtopographic units. Still, the role of low- and high-centered polygonal ground on basin water balance is poorly constrained and rarely, if ever, represented in hydrologic models.

4.3 Site Description

The site, here referred to as the Biocomplexity Experiment, (71°16'51"N 156°35'47"W, elevation 4.5 m) is located a few kilometers from the Beaufort Sea near Barrow on the Arctic Coastal Plain, Northern Alaska. Mean annual air temperature at Barrow Airport is –12.0 °C (1977-2009) where summer (June through August) averages 3.3 °C. About 55 % of the annual precipitation (173 mm, 1977-2009) falls during June through September (99 mm) (adjusted following the WMO method described by *Yang et al.* [1998]).

The Biocomplexity Experiment site is representative of vegetated drained thaw lake basins, which occupy approximately 26 % of the western Arctic Coastal Plain [*Hinkel et al.,* 2005] and 50 % of the Barrow Peninsula north of ~71° latitude [*Hinkel et al*., 2003]. The lake drained between 50 and 300 years ago [*Hinkel et al.,* 2003] leaving a poorly drained wet tundra meadow with Typic Aquiturbels soils [*Bockheim et al.*, 1999] underlain by 600 m of ice-rich permafrost [*Brown and Johnson,* 1965]. Low-centered polygons are common within the lake bed, while high-centered polygons dominate the upland tundra. Interannual variation of the mean active layer depth at nearby locations varied from 29 to 35 cm (1995-2009) [*Brown et al.,* 2000; *Shiklomanov et al.*, 2010].

Non-vascular vegetation contributes significantly to biomass and cover in these ecosystems [*Oechel and Sveinbjornsson,* 1978; *Rastorfer,* 1978]. Moss may reach depths of 20 cm at wet sites, but the bulk of their living biomass is usually within ~1 cm of the soil surface [*Engstrom et al.,* 2005]. Mosses represent most of the live above ground biomass at the site [*Zona et al*., 2009]. Vascular plant

composition is represented by sedges (*Carex aquatilis*) and grasses (*Eriophorum* and *Dupontia*) with an average LAI in mid-August 2006 of 0.43, 0.13 and 0.02, respectively [*Zona et al*., 2011]. In comparison, standing dead leaf biomass in the Barrow area reaches LAI‘s of 1.23 [*Dennis et al.,* 1978]. Senescence in the region begins in August [*Myers and Pitelka,* 1979].

4.4 Methods

4.4.1 Schematic DEMs

The effect of polygon rims on the water balance was quantified using three artificially produced DEMs (Fig. 4.3). The artificial DEM represent a simplistic vegetated drained thaw lake basin (DTLB) by having the same slope (0.03 %) as the DTLB at the Biocomplexity Experiment, Barrow, Alaska [*Liljedahl, 2011*]. Airborne Lidar and field surveys of the Barrow DTLB show low-centered polygon rims up to about 10 cm height. Accordingly, low-centered polygon rims were represented by a network of elevated pixels (+ 8 cm) within the schematic DTLB. A second schematic DEM represents the DTLB as a flat surface, while the third presents a DTLB having high-centered polygons and a connected network of 30 cm deep troughs.

4.4.2 Hydrologic Model

We chose the physically-based hydrologic model Water Balance Simulation Model (WaSiM-ETH) [*Schulla*, 1997; *Schulla and Jasper*, 2007]. WaSiM-ETH is a well established tool for modeling the spatial and temporal variability of hydrologic processes in complex basins ranging from less than 1 km^2 to more than 500,000 km^2. Its application has ranged from water management in arid and semi-arid regions [*Bharati et al*., 2008], flood forecasting [*Jasper et al*., 2002; *Cullmann et al*., 2008], water balance analyses of wetlands within lowland floodplains [*Krause and Bronstert*, 2005; *Krause et al*., 2007], to the distribution of water and

phosphorus yield-producing areas [*Lindenschmidt et al*., 2004] and many other hydrologic studies.

Different lateral routing modules were applied to the schematic DEMs. We utilized the surface routing module in the low-centered polygon and flat ground scenarios, while the troughs represented a channel network in the high-centered polygon landscape. The channel routing is based on a hydraulic calculation of the flow velocities (Manning-Strickler approach) through a kinematic wave approach by using different flow velocities for different water levels in the channel. The effects of diffusion and retardation are included by applying a linear storage to the routed discharge.

In addition to representing lateral flow through channel routing, base flow, and interflow, WaSiM-ET includes a surface routing module designed for small-scale applications. Infiltration excess and direct runoff from snow melt is used as input for the surface routing model. The surface runoff flow from cell-to-cell until a river cell is reached. In diverging areas, up to three flow paths are possible, while only one flow direction is allowed in converging areas (the steepest slope). A concentration factor may be used to take into account small-scale variations of the surface leading to preferred flow paths in small channels. The flow velocity depends on slope, roughness and water film depth (Manning Strickler approach) where the slope depends upon the elevation model plus the water storage. The dynamic generation of ponds occurs when elevation and local storage leads to a zero or inverted gradient. However, it is still not a hydrodynamic wave approach but rather a kinematic wave approach with stepwise constant parameters. The time step of surface routing is dynamically decreased, but if necessary, it can also be parameterized.

The WaSiM-ETH uses the Richards-equation for modeling the fluxes within the unsaturated soil zone. It is a one-dimensional finite difference scheme with multiple user-defined discrete soil layers. The upper boundary condition to the

unsaturated zone is the infiltration, which is estimated after *Green and Ampt* [1911] using the extended approach after *Peschke* [1977, 1987]. The lower boundary condition is the groundwater layer (i.e. saturated zone), which is constant for a specific time step but variable in time. The extraction of water from the different soil layers is done separately for soil evaporation and for transpiration before calculating the soil water fluxes. The first extraction step is the extraction through transpiration (Penman-Monteith), which includes stress induced by soil moisture. The second step is the extraction of soil evaporation from bare soil (or moss), which is also linked to soil moisture status. The modeling of the groundwater and lateral flow is two dimensional where the flux is estimated from the continuity and Darcy equations through an implicit finite difference approach (Gauss-Seidel-Algorithm with automatic estimation of successive over relaxation factors).

WaSiM-ETH was forced with 11 summers of hourly meteorological data collected near Barrow, Alaska, by the Center for Climate Change at San Diego State University, Circumpolar Active Layer Monitoring program, NOAA, ARM, and the National Weather Service. The model simulations were started just prior to each year‘s snow ablation and stopped during the onset of winter. The latter was defined as being the first day of ten consecutive days experiencing mean daily air temperatures below 0 ºC. In this particular application we did not represent the seasonal changes in the active layer nor the presence of permafrost. Instead, the model sensitivity analysis is solely based upon the change in one parameter such as the addition/removal of polygon rims. Model parameters were given the same values as those presented by *Liljedahl* [2011].

4.4.3 Field Measurements

Water levels were recorded in four neighboring low-centered polygons during summer 2009 at the edge of the DTLB in Barrow (Fig. 4.4). Non-vented pressure transducers (HOBO U20-001-04-Ti) were suspended in metal wire in white 5 cm

diameter PVC tubes at the center of each polygon during the snowmelt. The PVC tubes were installed in fall 2008 with the lower 30 cm of PVC tubes placed in the permafrost using a jack-hammer. During the summer, regular site visits (three in total) ensured that the 15 cm long transducers were continuously immersed in the water column as the frost and water tables receded. The recorded data was processed with the HOBOware-Pro software to account for the water temperature affect on fluid density and the variations in atmospheric pressure.

Another set of water level measurements were monitored at 30 m intervals along a 300 m long transect across the DTLB in 2006-2009 (Fig. 4.4). The water level was recorded in relation to the local ground surface. Each location was identified by 2.5 cm diameter PVC pipe anchored into the permafrost along the boardwalk. These sites were unavailable during peak flooding due to extensive snow drifting caused by the elevated boardwalk. Therefore, the water levels in the DTLB transect does not represent a) the maximum water levels and b) the entire inundation period.

Near-surface soil moisture was monitored at a low-centered polygon with wide rims separated by meter-wide troughs (Fig 4.4). Nine CS616 volumetric water content sensors were buried horizontally at about 7 to 10 cm depth to record the variability within the organic layer across a transect that included a trough, rim, and a low center. The data were recorded as 5 min intervals and stored as 30 minute average values on a CR10X data logger. Unfrozen soil moisture was estimated from volumetric water content (VWC) observations. Spring peak in VWC was assumed to represent saturated conditions (all micro and macro pore spaces filled with liquid water) and in the winter-low of 6% saturation [*Hinzman et al*., 1991].

4.5 Results

4.5.1 Field Measurements

The Barrow DTLB experienced extensive snowmelt flooding during all four years (Fig. 4.4). The duration of the snowmelt flooding varied from year to year. The inundation in 2006 lasted for at least one week, while in 2008 observations show a three week long event with water depths reaching 12 cm. Surface water covered the entire DTLB on June 8 2009, which is nearly a week prior to the initiation of the 2009 water level measurements. Even though not entirely represented in our record due to a late-lying snowdrift, 2009 had at least a three week long flooding of the DTLB.

All four individual low-centered polygons were completely flooded and therefore laterally connected through surface water on June 5th 2009 (Fig 4.5). Two days later, the rims separating the polygons were visible. When the recording of the water levels started on June 9th, the water level in east and south polygon had receded about 7 cm more than the north and west polygons. Although the absolute magnitude varied, all of the polygons were laterally disconnected from each other until a rain event (6 mm) on August 8th. After August 8th, all four polygons show a similar water level although at a markedly lower elevation than during the snowmelt flooding in early June.

The 9 sites representing the top 10 cm soil moisture at the trough-rim-center transect all showed an increase from 6 % to 12 % in the liquid water content on May 25th 2008 (Fig. 4.6). All sites experienced a drying following the snowmelt until summer rainfall in late July. The rapid decrease in autumn soil liquid water content was due to the freezing of the soils. The lower sites, particularly the trough and the polygon center, showed later freeze-up due to latent heat storage. Liquid water contents below 25 % were reached earlier at the rim (October 9th) than at the trough (November 15th). The average time required to increase from 25 to 85 %

was 8 days in spring (2 to 20 days), while the reverse required on average 27 days in autumn (9 to 48 days).

4.5.2 Modeling Analysis

The polygon rims affect several components of the water balance.

First, the multi-week long ponding (hydroperiod) of the DTLB was only replicated when low-centered polygons were represented (Table 4.1, Fig. 4.7). When no elevated rims were present, the hydroperiod was limited to 5.2 (flat) and 0 days (high-centered) compared to 36 days in the low-centered polygon scenario. The mean inundated depth at low-centered polygons was 40 mm compared to 11 mm at the flat scenario. Water levels were higher throughout the summer in the low-centered polygon DTLB, where the absence of rims resulted in larger soil water storage deficits prior to freeze-up. In five of the 11 years, the ground surface was inundated prior to freeze-up in the low-centered polygon scenario, while the fall water table was always below the ground surface in late summer during the flat and high-centered polygon ground. The change in soil water storage, ΔS, was negligible on a decadal time scale but year to year variations were found in all three scenarios.

Secondly, despite the larger soil water storage deficit, total runoff was higher in the high-centered polygon DTLB (96 mm) than the flat (53 mm) and low-centered polygon (49 mm). No summer runoff was produced in either scenario. The runoff ratio (runoff/SWE) was nearly doubled from the high-centered polygons (0.83) compared to the low-centered and flat basins (0.44 and 0.47, respectively).

Thirdly, total evapotranspiration was reduced when troughs are present and also less variable amongst years (Table 4.1). The flat and the low-centered polygon scenario had nearly identical evapotranspiration losses (156 and 160 mm, respectively), while the high-centered polygon area lost on average 116 mm. Total transpiration was the same amongst the scenarios (mean 55 mm). Accordingly, the

role of transpiration on total evapotranspiration was enhanced during the high-centered polygon scenario (47 % of total evapotranspiration) compared to the low-centered (34 %).

4.6 Discussion

Micro-scale variations in surface topography, induced by polygon features, control the water balance in these extremely low-gradient arctic watersheds. A transition from low- to high-centered polygon landscape results in an altered partitioning of the water balance. Losses from the low-centered polygon scenario were dominated by evapotranspiration but total evapotranspiration and runoff were similar at the high-centered polygon landscape. Although the modeling analysis highlights the role of low- and high-centered polygons on hydrologic fluxes and stores, our field measurements acknowledge that the reality is more complex. Nonetheless, it is evident that short- and long term structural changes in the upper portion of the Arctic soils have dramatic effects on the hydrology.

4.6.1 Surface and Soil Water Storage

Although a brief ponding was simulated at the flat wetland (5 days), the modeling sensitivity analysis showed that the observed multi-week ponding was only achieved when low-centered polygons were represented. Accordingly, rims are encountered in the Barrow DTLB (Fig 4.4). Evidently, the presence of these natural barriers supports a wet environment including the temporary existence of shallow ponds.

Low-centered polygon rims served as a hydrologic barrier in several aspects. The near-surface was typically saturated when rims were present (Table 4.1). Autumn water table fluctuated above and below the ground surface amongst the years in the low-centered polygon scenario, while the fall water table of high-centered polygons always remains at depths where one would expect the permafrost table [see *Shiklomanov et al*., 2010]. In that sense, the water table of

high-centered polygons was less variable by supporting a consistently deep water table.

The 11 years of simulations suggest that it is typical for these systems, whether they are dominated by low or high-centered polygons, to experience interannual variations in the soil water storage change, ΔS (Table 4.1). Annual water balance calculations based on assumptions of no change in ΔS would, according to the simulations, result in errors of up to 90 mm, which is half of the long-term mean annual precipitation in the Barrow area. Our simulations suggest that such methods should only be applied to datasets representing approximately a decade.

4.6.2 Lateral Flow

The type of polygon ground feature affects the total discharge as well as the timing of the runoff. About half of the SWE did not contribute to streamflow from the low-centered polygon (56 %) and flat wetland (53 %). Their limited difference was due to the larger soil water storage deficit (fall water table depth) at the flat wetland, which equals to the surface storage capacity of the low-centered polygons. The high-centered polygon scenario resulted in 27 % of the SWE recharging the soils. In comparison, field studies performed by *Kane et al*. [2008] showed that on average 22 % (1999-2007) of the SWE did not contribute to runoff in the Putuligayuk River watershed (471 km^2), Arctic Coastal Plain, Alaska. In addition, the simulated runoff exits the basin earlier from the high-centered polygon scenario due to an effective network of channels and steeper micro-topographical gradients when compared to other surface conditions. Runoff is therefore not only drastically reduced due to the presence of lakes and wetlands [*Bowling and Lettenmaier*, 2010] but also due to micro-scale features within the wetlands such as the absence of a connected network of troughs and short, relatively steep slopes typical of high-centered polygons.

Field measurements of inter-polygonal lateral connectivity show a more complex hydrologic setting of the low-centered polygon landscape than what the modeling analysis can provide. The watershed acted as one unit during springmelt when the entire drained thaw lake basin was connected through the inundation of snowmelt water. During this brief time period, the troughs in the high-centered polygon areas acts as efficient drainage networks by routing the water towards the low-centered polygons that are located within the DTLB. About two days after the peak runoff, the water levels in the four monitored low-centered polygons suggest a separation of the basin into sub-units, which lasts most of the summer. The water level measurements indicate that individual low-centered polygons can represent separate hydrologic units. Most likely, the number of individual polygons representing one unit varies across the summer depending on the precipitation regime and thaw depths.

The complex lateral connection can be related to the spatially and temporally variable elevation of the frozen table. The combination of relatively deep thaw in late summer (i.e. lower barriers) and the infiltration of rainwater allowed the re-connection of the four polygons on August 8th. Although the water table was higher during the rain event on July 9th, no lateral connection was initiated in the former despite the identical precipitation amounts (6 mm). Unlike the spring when plenty of snowmelt water allowed a surface water connection, the late summer lateral linkage was through sub-surface hydrology. Further, the larger response of polygon water levels to the rain event on August 8th compared to July 9th indicates lateral input from upstream areas on August 8th.

The measured water levels present a complex hydrologic problem that is unique to low-centered polygon environments, where the watershed is alternating between acting as one connected unit and multiple separate sub-units across the season. As the warmer climate is projected to increase the active layer depths [*Kane et al.,* 1991; *Hinzman et al.*, 1992] and the summer precipitation [*Walsh*, 2008], we

may anticipate a lengthening of the time period where the watershed acts as one unit in late summer. However, morphological changes linked to permafrost degradation through a transition from a low-centered polygon landscape into high-centered polygons would further enhance the lateral connectivity.

4.6.3 Vertical Fluxes

Total evapotranspiration from high-centered polygons scenario was similar to the total amount of runoff. This is partly due to a larger runoff compared to flat and low-centered scenarios but also due to reduced evaporation. Open water/moss evaporation was lower from the high-centered polygons as the surface was water-limited due to the deeper water tables (~ 30 cm). The simulated water table in the flat wetland rarely dropped below 10 cm depth, which was within the parameterized zone of water accessible for evaporation. *Sphagnum* moss has shown to effectively transport water from 10-15 cm deep water table through capillary flow [*Price et al*., 2009]. Hence, the position of the water table resulted in similar total evapotranspiration amongst the flat and low-centered polygon scenario, while reduced at the high-centered polygons.

The receding rate of the monitored water levels was at first similar among the four polygons, while mid-summer rates vary. Evapotranspiration rates are most likely similar in the four polygons in early summer due to the wet near-surface conditions. However, we cannot discern whether the varying recession rates in later summer are due to differing evapotranspiration rates amongst the four polygons and/or due to lateral hydrologic connections with other neighboring units.

The simulated infiltration of water into the soils during snowmelt was supported by field measurements. All seven sites showed an increase in the liquid water content on May 25th 2008, which coincided with an early isolated melt event (air temperatures above 0°C). Water generated by melting snow can percolate into the unsaturated frozen active layer and into ice wedge cracks [*Kane and Stein*,

1983], which can have a major impact on the thermal evolution of soils [*Hinkel and Outcalt*, 1994; *Hinkel et al*., 1997; *Kane et al*., 2001]. Accordingly, the time period required to increase the percent saturation from 25 to 85 % (thawing) was much shorter than the time period required decreasing from 85 to 25 % (freezing). Further, the longer freeze-up period in the concave areas such as the trough and low-center is indicative of higher absolute water content of the near surface soils, which is a soil moisture distribution pattern that the model replicated.

4.6.4 Future Directions

The modeling analysis presented a first-order approach in simulating the role of low- and high-centered polygons on arctic wetland hydrology. Neither the freeze-thaw dynamics within the active layer nor the permafrost were represented, both of which have shown to be important in wetland hydrology. Consequently, the modeling did not include the presence of lateral and vertical hydrologic barriers due to the presence of frozen ground. The time period and geographical extent of lateral sub-surface connectivity within the watershed is therefore likely overestimated. Further, the high-centered polygon scenario also presented an extreme scenario of the basin scale lateral connectivity through the unified drainage network. Field observations have shown that the ground subsidence in low-centered polygonal landscapes may not necessarily form a continuous network but rather disconnected channels and therefore small water bodies [*Jorgenson et al*., 2006]. A future analysis that includes permafrost, the seasonal dynamics of the active layer, and the continuously evolving geomorphology is a desired future direction in assessing Arctic wetland hydrology.

4.7 Conclusion

A shift from low-centered to high-centered polygon dominated landscape results in drastic changes to watershed-scale soil water storage, runoff, and evapotranspiration. Low-centered polygons promote extensive ponding, while

high-centered polygons enhance drainage and runoff. Evapotranspiration is suppressed at high-centered polygon landscapes as the near-surface soil moisture is reduced. Therefore, not accounting for the role of microtopographical variability on hydrology can have dramatic consequences when estimating regional scale water and energy exchange. Large interannual changes in the storage component limit the application of annual water balance methods that are based upon assumptions of no change in ΔS. The model experiments presented a first order approach in evaluating the role of microtopography on hydrology, while field measurements revealed a more complex hydrologic system. The watershed acted as one unit during springmelt when the entire drained thaw lake basin was connected through the inundation of snowmelt water. Individual low-centered polygons were later laterally disconnected until late summer rain and deep thaw allowed a sub-surface connection. It is necessary to account for the microtopography and the dynamic role of geomorphology in regulating tundra microclimate in order to reduce the uncertainty in present and future pan-Arctic hydrologic fluxes and stores.

4.8 Acknowledgements

The contributing authors were L. D. Hinzman and J. Schulla. The Atmospheric Radiation Measurement Program sponsored by the U.S. Department of Energy, Environmental Sciences Division, provided radiation measurements. B. Cable and J. Long provided technical assistance. Financial support for this research was provided through the National Science Foundation (grants 0652838, 0632263, and 0421588), and student grants from the Swedish-America Foundation, Gemzeus Foundation, American Water Resources Association-Alaska Section, and the Center for Global Change and Arctic System Research. Any opinions, findings, conclusions, or recommendations expressed are those of the author and do not necessarily reflect the views of sponsoring organizations. Mention of specific product names does not constitute endorsement by sponsoring organizations.

4.9 Figures

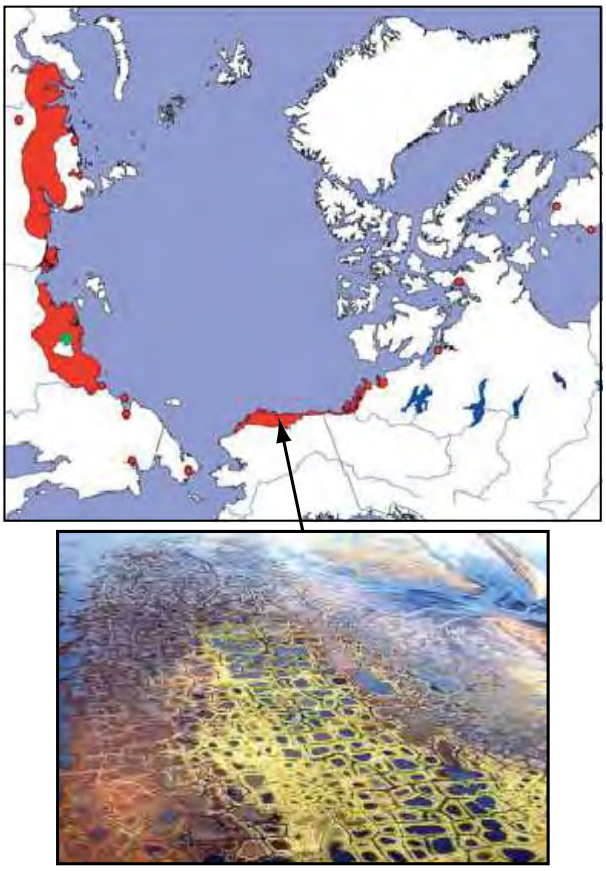

Figure 4.1 Distribution of polygon mires (red) (250 000 km^2) across the pan-Arctic region based upon analyses of satellite imagery by *Minke et al*. [2007]. The photo show inundated low-centered polygons at the Arctic Coastal Plain, Alaska [photo by M. Druckenmiller].

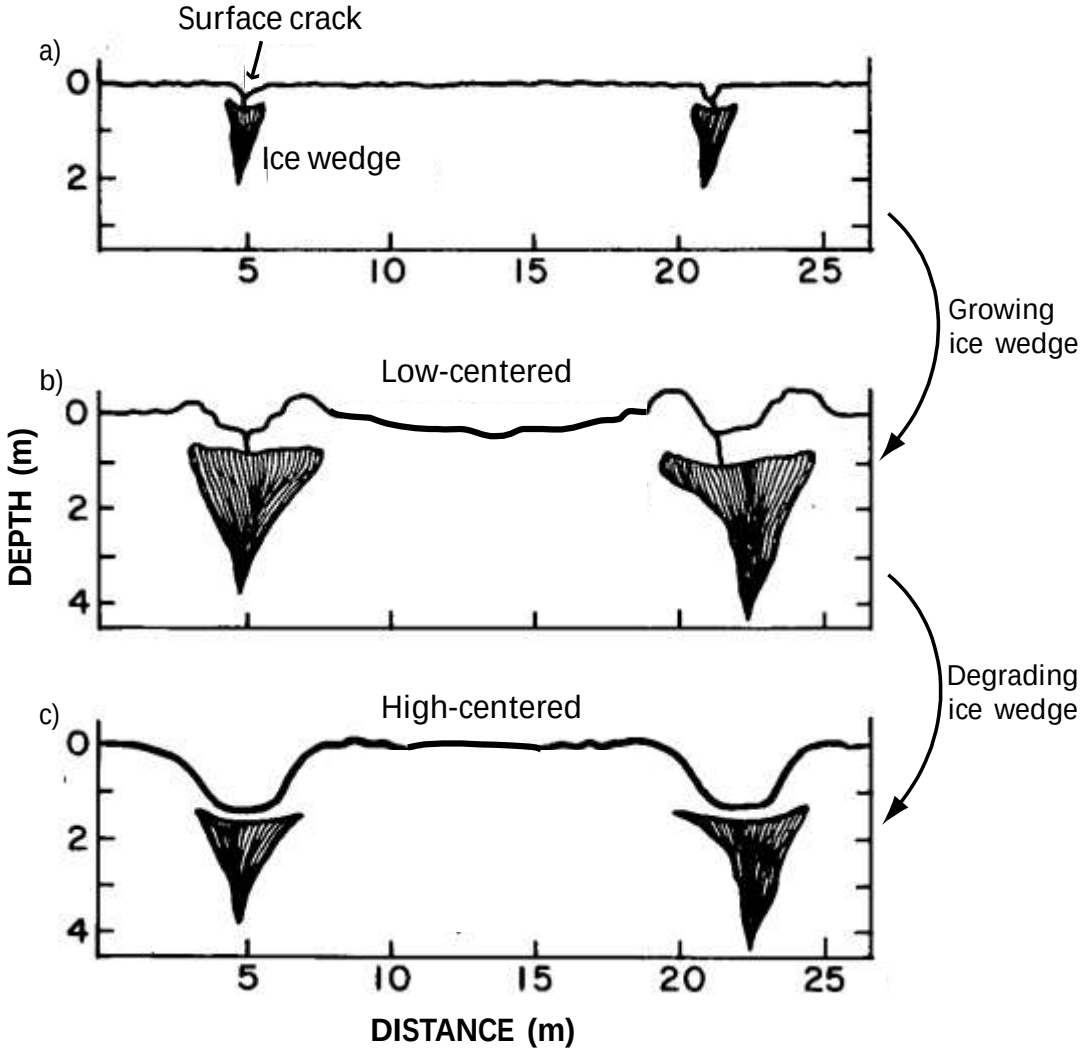

Figure 4.2 Schematic representation of the development of ice wedges as water infiltrates into the deep thermal contraction cracks and freezes (a). The ice wedge becomes several meter wide at the top due to the repetition of the process; b) The growing ice wedge pushes the soil upwards, which allows the formation of elevated rims and hence, a low-centered polygon; c) A degradation of the near-surface permafrost and therefore the melting of ice wedges results in differential ground subsidence and the formation of high-centered polygons, which are surrounded by troughs. It may require thousands of years to go from a) to b) but only tens of year to go from b) to c). The figure was modified after the description presented by *Brown et al.* [1980].

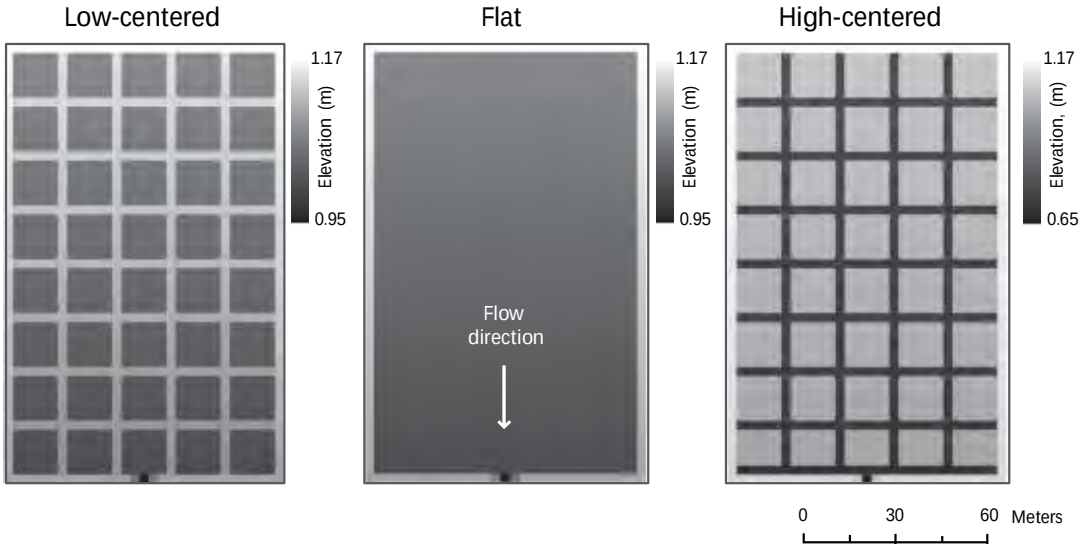

Figure 4.3 The schematic digital elevation models used in the modeling analysis representing low-centered polygons with 8 cm high rims, a flat surface, and high-centered polygons with 30 cm deep troughs. The surface has a general slope of 0.03 % as determined by airborne Lidar surveys of a vegetated drained lake basin near Barrow, Alaska.

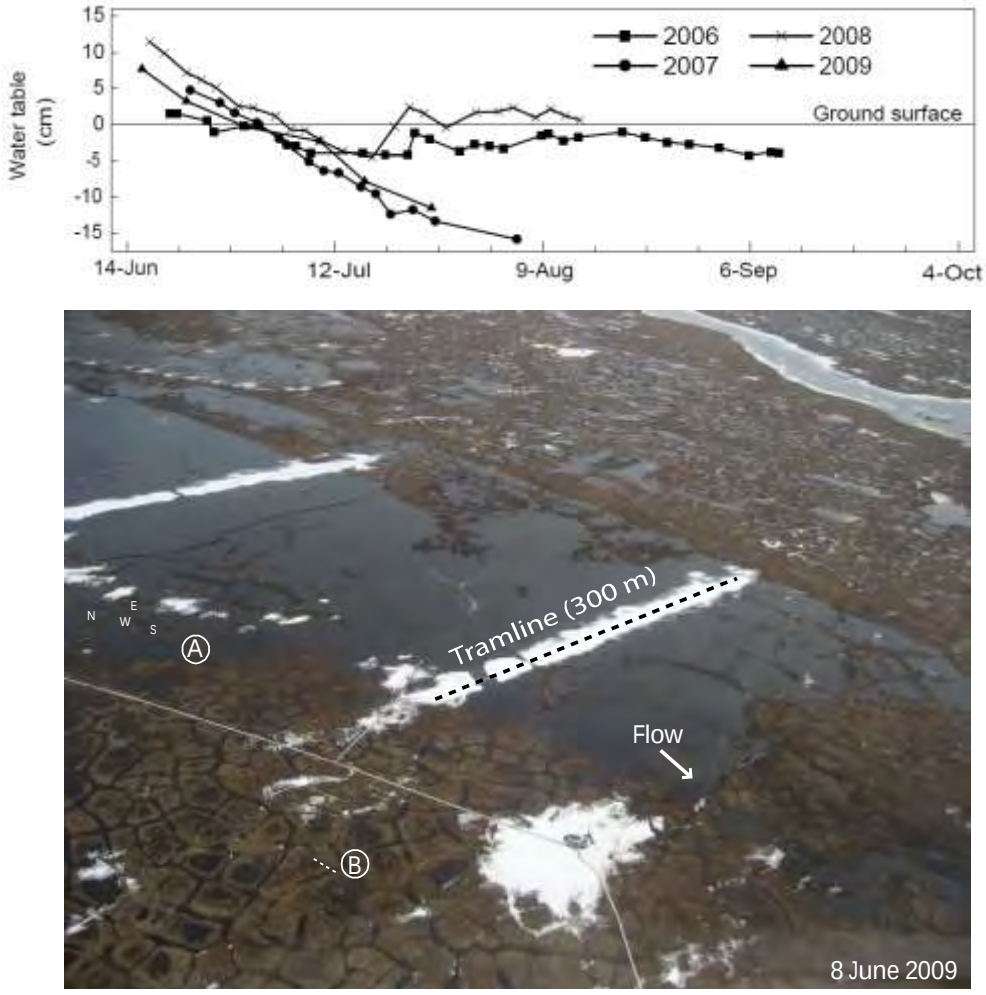

Figure 4.4 Aerial photo of the vegetated drained thaw lake basin (DTLB) in Barrow, Alaska, taken two days after peak spring runoff in spring 2009 (photo by H. Eicken). The flow is directed towards the lower right corner of the photo. The entire DTLB is inundated with snowmelt water apart from the rims, while the surrounding tundra has a reduced extent of open water. Water levels were measured at 11 locations spaced 30 m apart along the 300 m long tramline. As can be seen in the photo, the tramline has caused increased snow accumulation, which prevented early season water table measurements along the tramline. Although water tables varied from 15 cm below to 5 cm above in late summer in 2006-2009, the DTLB experienced an early summer inundation lasting for several weeks in all years. Also marked is the location of the two other field studies: A) The continuous water level measurements at the four neighboring low-centered polygons, which results are presented in Figure 4.5; and B) the continuous near-surface soil moisture measurements across the polygon rim, which results are presented in Figure 4.6.

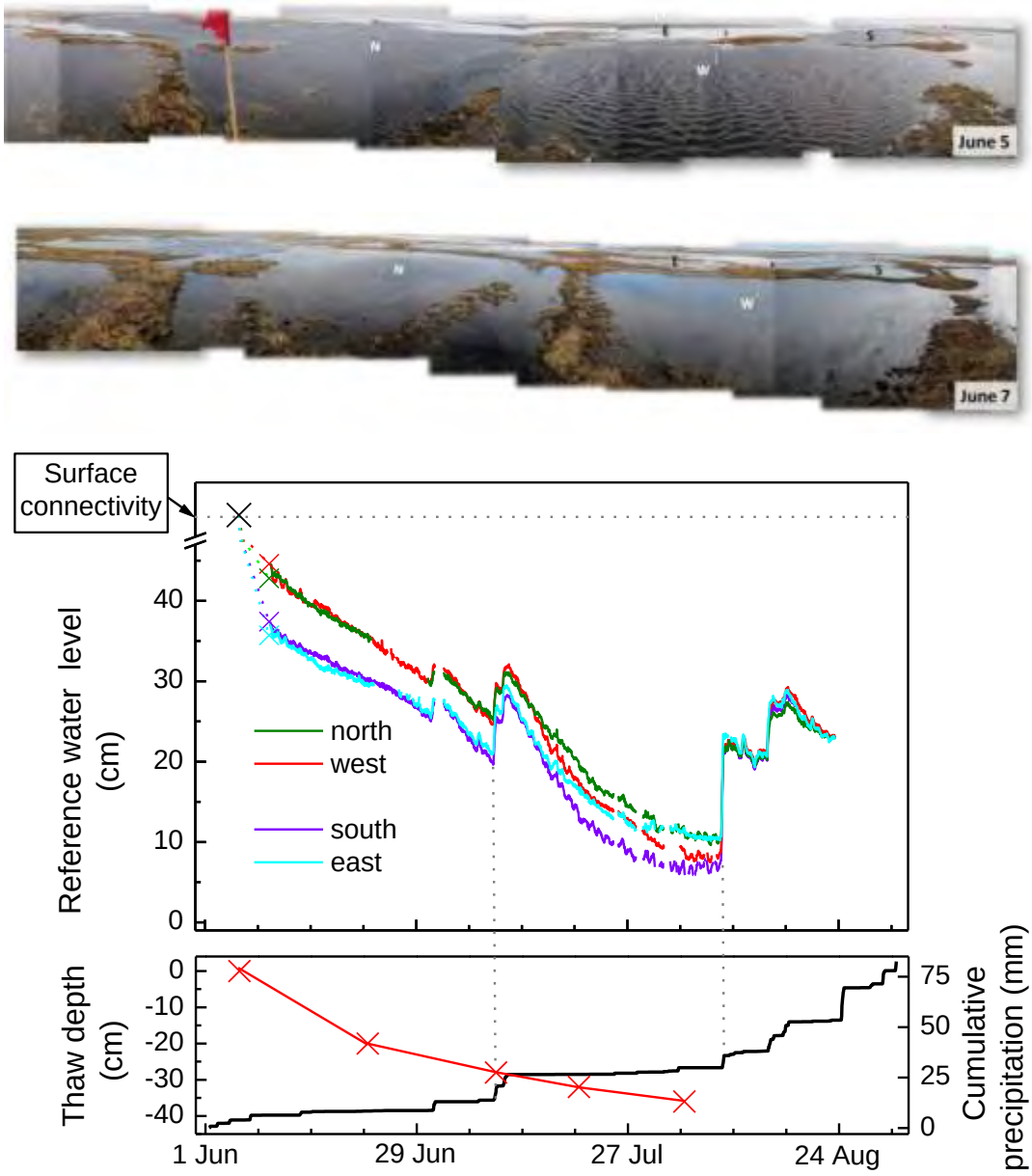

Figure 4.5 Measured water levels at the four neighboring low-centered polygons in 2009. All four polygons were laterally connected through surface water on the day of peak runoff (June 5th). Two days later, the water level had receded leaving the rims exposed. The water levels varied between the polygons until the early August rain event when all four polygons became connected through sub-surface water.

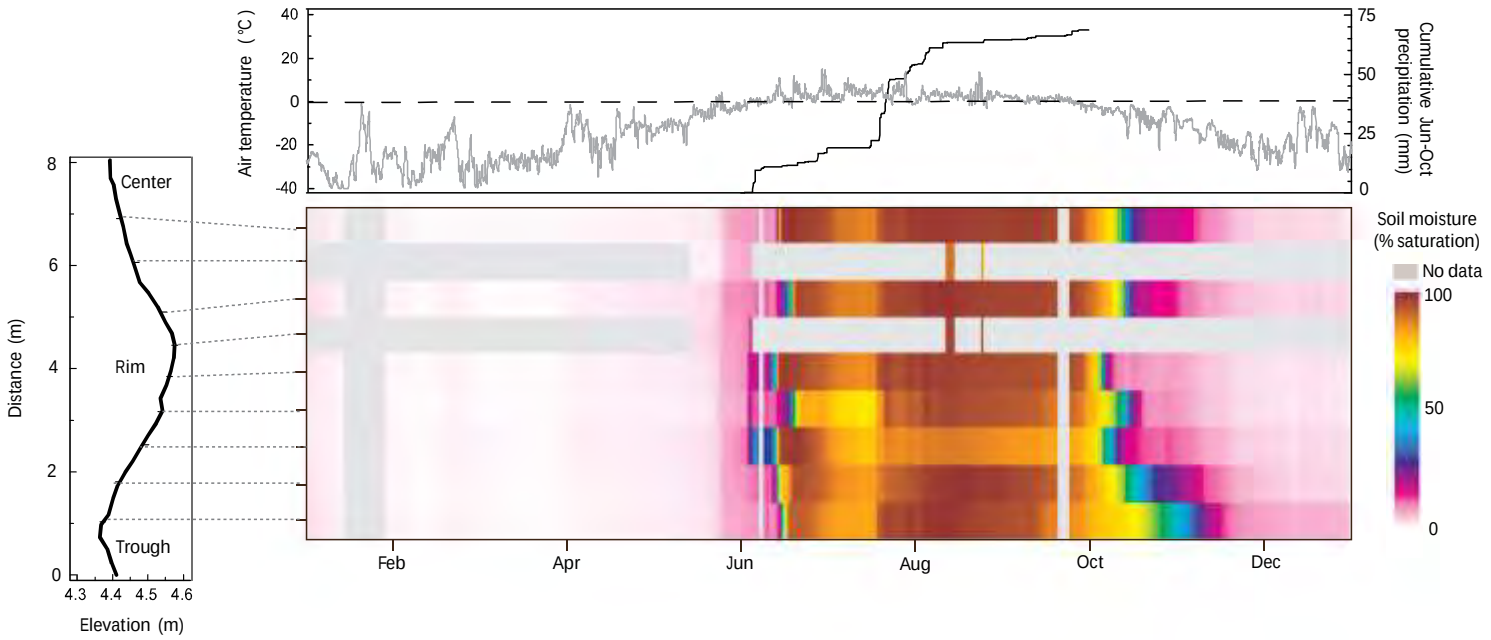

Figure 4.6 Measured near-surface (10 cm depth) liquid soil water content at 0.62 m intervals along a 6 m long transect representing the 2008 calendar year. The organic soil holds 6 % liquid water when frozen [*Hinzman et al.*, 1991]. A longer freeze-up period is encountered in the concave areas (low center and trough).

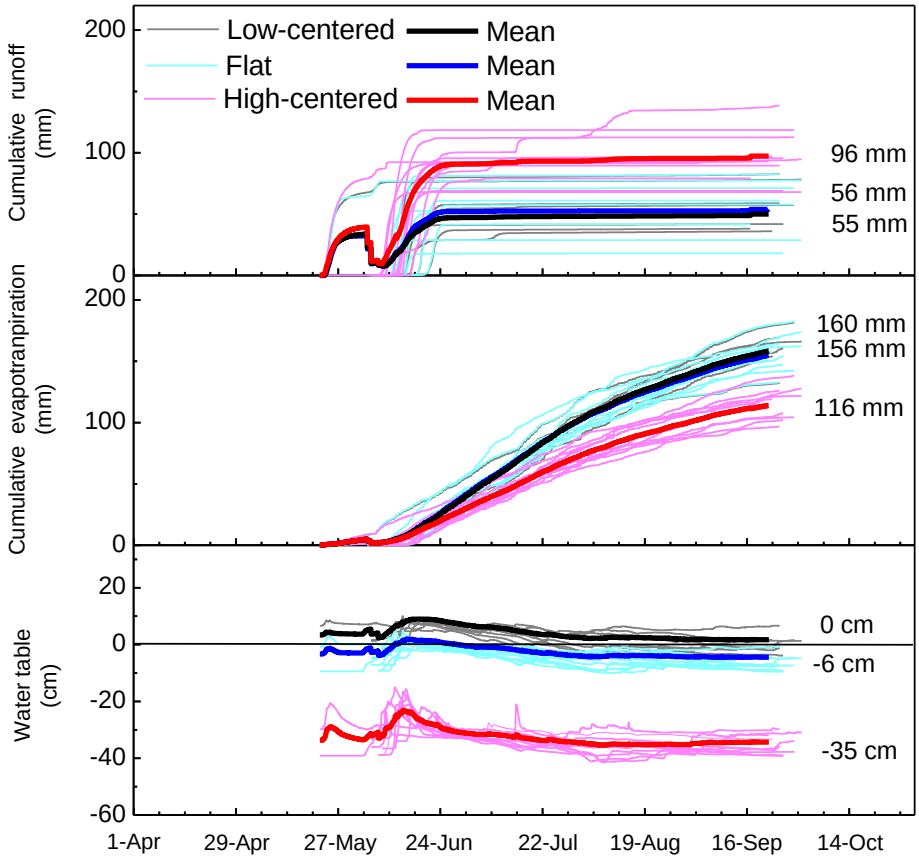

Figure 4.7 Simulated water table and cumulative runoff and evapotranspiration from the three schematic DEM's. Thin lines represent individual years, while thick lines are the long-term average. The mean runoff was about twice as high from the high-centered polygons compared to the low-centered polygons and the flat wetland. Evapotranspiration and soil water storage was reduced at the high-centered polygon. The multi-week long ponding was only produced by the low-centered DEM.

4.10 Tables

	1999	2000	2001	2002	2003	2004	2005	2006	2007	2008	2009	*Mean*	*Stdev*
End ablation	15-Jun	16-Jun	13-Jun	6-Jun	22-Jun	13-Jun	20-Jun	11-Jun	9-Jun	14-Jun	10-June	***13-Jun***	***4.8***
End summer	26-Sep	23-Sep	25-Sep	1-Oct	17-Sep	27-Sep	25-Sep	29-Sep	1-Oct	27-Sep	22-Sep	***26-Sep***	***4.1***
Snow Water Equivalent, mm	122	113	123	93	95	119	106	137	98	158	123	***117***	***19.3***
Summer precipitation, mm	75	120	118	114	78	155	97	71	24	59	105	***92***	***35.7***
Low-centered polygons													
Specific runoff, mm	42	36	83	78	38	57	59	68	24	4	51	***49***	***23.5***
Evapotranspiration, mm	161	154	132	166	155	182	170	145	190	151	155	***160***	***16.4***
Transpiration, mm	51	48	38	50	53	68	66	49	81	46	56	***55***	***12.1***
Evaporation, mm	110	106	94	116	102	114	104	96	109	105	99	***105***	***7.0***
Water table depth, mm	-39	16	66	13	-13	16	-14	-17	-397	-38	6	***-36***	***123.2***
P-ET summer, mm	-86	-34	-14	-52	-77	-27	-73	-74	-166	-92	-50	***-68***	***41.2***
ΔS, mm	-6	43	26	-37	-20	35	-26	-5	-92	62	22	***0***	***43.6***
Runoff ratio (Q/SWE)	0.34	0.32	0.67	0.84	0.40	0.48	0.56	0.50	0.24	0.03	0.41	***0.44***	***0.22***
% Evaporation	0.68	0.69	0.71	0.70	0.66	0.63	0.61	0.66	0.57	0.70	0.64	***0.66***	***0.04***
Mean daily evapotranspiration, mm	1.56	1.56	1.27	1.42	1.78	1.72	1.75	1.32	1.67	1.44	1.49	***1.5***	***0.17***
Hydroperiod, days	31.2	38.1	41.5	41.5	41.5	37.8	41.5	38.0	25.9	31.6	27.0	***36.0***	***6.0***
Mean water depth hydroperiod, mm	43	46	48	40	46	43	46	26	41	28	32	***40***	***7.7***
Flat													
Specific runoff, mm	47	42	82	77	42	58	61	71	29	18	53	***53***	***19.8***
Evapotranspiration, mm	154	158	133	162	152	183	165	142	174	147	151	***156***	***14.2***
Transpiration, mm	51	48	38	50	53	68	66	49	81	46	56	***55***	***12.1***
Evaporation, mm	103	110	95	112	99	115	99	93	93	101	95	***101***	***7.8***
Water table, mm	-91	-45	-7	-48	-72	-47	-72	-73	-547	-94	-50	***-104***	***148.9***
P-ET summer, mm	-79	-38	-15	-48	-74	-28	-68	-71	-150	-88	-46	***-64***	***36.5***
ΔS, mm	-4	33	26	-32	-21	33	-23	-5	-81	52	24	***0***	***38.4***
Runoff ratio (Q/SWE)	0.39	0.37	0.67	0.83	0.44	0.49	0.58	0.52	0.30	0.11	0.43	***0.47***	***0.19***
% Evaporation	0.67	0.70	0.71	0.69	0.65	0.63	0.60	0.65	0.53	0.69	0.63	***0.65***	***0.05***
Mean daily evapotranspiration, mm	1.50	1.60	1.28	1.38	1.75	1.73	1.70	1.29	1.53	1.40	1.45	***1.5***	***0.17***
Hydroperiod, days	4.9	4.0	4.9	14.9	3.5	6.8	4.9	4.1	2.8	2.0	4.7	***5.2***	***3.4***
Mean water depth hydroperiod, mm	8	8	20	5	9	8	12	21	8	6	11	***11***	***5.2***
High-centered polygons													
Specific runoff, mm	96	97	139	95	79	113	90	119	68	69	93	***96***	***21.3***
Evapotranspiration, mm	107	119	97	122	117	139	126	104	128	102	112	***116***	***12.7***
Transpiration, mm	51	48	38	50	53	68	66	49	81	46	56	***55***	***12.1***
Evaporation, mm	56	71	59	72	64	71	60	55	47	56	56	***61***	***8.0***
Water table depth, mm	-390	-333	-298	-310	-365	-340	-361	-377	-993	-391	-319	***-407***	***196.9***
P-ET summer, mm	-32	1	21	-8	-39	16	-29	-33	-104	-43	-7	***-23***	***34.6***
ΔS, mm	-6	17	5	-10	-23	22	-13	-15	-74	46	23	***-3***	***31.5***
Runoff ratio (Q/SWE)	0.79	0.86	1.13	1.02	0.83	0.95	0.85	0.87	0.69	0.44	0.76	***0.83***	***0.18***
% Evaporation	0.52	0.60	0.61	0.59	0.55	0.51	0.48	0.53	0.37	0.55	0.50	***0.53***	***0.07***
Mean daily evapotranspiration, mm	1.04	1.20	0.93	1.04	1.34	1.31	1.30	0.95	1.12	0.97	1.08	***1.1***	***0.15***
Hydroperiod, days	0	0	0	0	0	0	0	0	0	0	0	***0.0***	***0.0***
Mean water depth hydroperiod, mm	0	0	0	0	0	0	0	0	0	0	0	***0***	***0.0***

Table 4.1 The simulated water balance components and bulk factors for the 11 years at each of the three topographical scenarios. *P-ET* represents summer precipitation minus evapotranspiration, *Q/SWE* is the runoff divided by the snow water equivalent, and ΔS represent the change in storage during each hydrological year ($P+SWE-E-Q$). The water table depth represents the value prior to freeze-up.

4.11 References

Ballantyne, C. K., and J. A. Matthews (1983), Desiccation cracking and sorted polygon development, Jotunheimen, Norway, *Arctic and Alpine Res., 15*, 339–349.

Bharati, L., C. Rodgers, T. Erdenberger, M. Plotnikova, S. Shumilov, P. Vlek, and N. Martin (2008), Integration of economic and hydrologic models: Exploring conjuctive irrigation water use strategies in the Volta Basin, *Agr. Water Manag., 95*, 925–936.

Billings, W. D. (1987), Carbon balance of Alaskan tundra and taiga ecosystems: past, present and future*, Quaternary Sci. Rev., 6*(2), 165–177.

Billings, W. D., and K. M. Peterson (1980), Vegetational change and ice wedge polygons through the thaw-lake cycle in Arctic Alaska, *Arctic Alp. Res., 12*(4), 413-432.

Black, R. F. (1969), Thaw depressions and thaw lakes—a review, *Biuletyn Peryglacjalny, 19*, 131–150.

Black, R. F. (1970), Thermokarsts in Siberia and its impact on the development of lowland relief, *Quaternary Res., 1*, 103–120.

Bockheim, J. G., L. R. Everett, K. M. Hinkel, F. E. Nelson, and J. Brown (1999), Soil organic carbon storage and distribution in arctic tundra, Barrow, Alaska, *Soil Sci. Soc. Am. J., 63*, 934–940.

Boike, J., C. Wile, and A. Abniozva (2008), Climatology and summer energy and water balance of polygonal tundra in the Lena River Delta, Siberia, *J. Geophys. Res., 113*, G03025, doi:10.1029/2007JG000450.

Bowling, L. C., D. L. Kane, R. E. Gieck, L. D. Hinzman, and D. P. Lettenmaier (2003), The role of surface storage in a low-gradient Arctic watershed, *Water Resour. Res., 39*(4), 1087, doi:10.1029/2002WR001466.

Bowling L. C., and D. P. Lettenmaier (2010), Modeling the Effects of Lakes and Wetlands on the Water Balance of Arctic Environments, *J. Hydrometeorol., 11*(2), 276–295. doi: 10.1175/2009JHM1084.1

Britton, M. E. (1957), Vegetation in the arctic tundra, in *Arctic Biology*, 2nd edition, edited by H. P. Hansen, pp. 26–72, Oregon State University Press, Corvallis, OR.

Bronstert, A., A. Bardossy, C. Bisnuth, H. Buiteveld, M. Disse, H. Engel., U. Fritsch, Y. Hundecha, R. Lammersen, D. Niehoff, and N. Ritter (2007), *River Res. Appl., 23*, 1102–1125.

Brown, J., and P. L. Johnson (1965), Pedo-ecological investigations at Barrow, Alaska, *Tech. Rep.*, 159:32, 32 pp., US Army CRREL, Hanover, USA.

Brown, J. K. R., Everett, P. J. Webber, S. F. MacLean, and D. F. Murray (1980), The coastal tundra at Barrow, in *An arctic ecosystem: the coastal tundra at Barrow, Alaska*, editors J. Brown, P. C. Tieszen, and F. L. Bunnell, pp. 1–29, Dowden, Hutchinson and Ross Inc., Stroudsburg, PA.

Brown, J., K. M. Hinkel, and F. E. Nelson (2000), The circumpolar active layer monitoring (CALM) program: Research designs and initial results, *Polar Geogr., 24*(3), 165–258.

Chapin III, F. S., M. Sturm, M. C. Serreze, J. P. McFadden, J. R. Key, A. H. Llpyd, A. D. McGuire, T. S. Rupp, A. H. Lynch, J. P. Schimel, J. Beringer, W. L. Chapman, H. E. Epstein, E. S. Euskirchen, L. D. Hinzman, G. Jia, C.-L. Ping, K. D. Tape, C. D. C. Thompson, D. A. Walker, and J. M. Welker (2005), Role of land-surface changes in arctic summer warming, *Science, 310*, 657–660.

Christensen, T. R., T. Johansson, H. J. Åkerman, M. Mastepanov, N. Malmer, T. Friborg, P. Crill, and B. H. Svensson (2004), Thawing sub-arctic permafrost: Effects on vegetation and methane emissions, *J. Geophys. Res. Lett., 31*, L04501, doi:10.1029/2003GL018680.

Cullmann, J., T. Krause, and A. Philipp (2008), Enhancing flood forecasting with the help of a process based calibration, *Phys. Chem. Earth, 33*, 1111–1116.

Czudek, T., and J. Demek, (1970), Thermokarst in Siberia and its influence on the development of lowland relief, *Quaternary Res., 1*, 103–120.

Davis, N. (2001), *Permafrost: A guide to frozen ground in transition*, University of Alaska Press, Fairbanks, AK.

Dennis, J. G., L. L. Tieszen, and M. A. Vetter (1978), Seasonal dynamics of above- and below-ground production of vacular plants at Barrow, Alaska, in *Vegetation and production ecology of an Alaska Arctic tundra,* edited by L. L. Tieszen, pp. 113-140, Springer-Verlag, NY.

Donner, N. (2007), Hydrological windows in low-centered arctic polygons: A landscape ecological perspective on polygon mires, M.S. thesis, Greifswald University, Germany.

Ellis, C. J., and L. Rochefort (2004), Century-scale development of polygon-patterned tundra wetland, Bylot Island (73° N, 80° W), *Ecol., 85(4)*, 963–978.

Engstrom, R., A. Hope, H. Kwon, D. Stow, and D. Zamolodchikov (2005), Spatial distribution of near surface soil moisture and its relationship to microtopography in the Alaskan Arctic coastal plain, *Nordic Hydrol., 36(3)*, 219–234.

Fortier, D., M. Allard, and Y. Shur (2007), Observation of rapid drainage system development by thermal erosion of ice wedges on Bylot Island, Canadian Arctic Archipelago, *Permafrost and Periglac. Process., 18*, 229–243

Francou, B, N. Le Mehaute, and V. Jomelli (2001), Factors controlling spacing distances of sorted stripes in a low-latitude, alpine environment (Cordillera Real, 168S, Bolivia), *Permafrost and Periglac. Process., 12*, 367–377.

French, H. M. (1996), *The periglacial environment*, Addison Wesley Longman, Edinburgh Gate, England.

Gersper, P. L., V. Alexander, S. A. Barkley, R. J. Barsdate, and P. S. Flint (1980), The soils and the nutrients, in *An arctic ecosystem: the coastal tundra at Barrow, Alaska*, editors J. Brown, P. C. Tieszen, and F. L. Bunnell, pp. 219–254, Dowden, Hutchinson and Ross Inc., Stroudsburg, PA.

Green, W. H. and G. A. Ampt (1911), Studies on Soil Physics: I. The flow of air and water trough soils, *J. Agric. Sci.*, 4, 1–24.

Hall, J. V., W. E. Frayer, and B. O. Wilen (1994), Status of Alaska wetlands, U.S. Fish and Wildlife Service, Alaska Region, Anchorage, AK.

Hallet, B., and S. Prestrud (1986), Dynamics of periglacial sorted circles in western Spitsbergen, *Quaternary Res., 26*, 81–99.

Hansen, H. A., and D. E. McKnight (1964), Emigration of drought-displaced ducks to the Arctic, in *Transactions of the North American Wildlife and Natural Resource Conference, 29*, 119–127.

Hinkel, K. M., and S. I. Outcalt (1994), Identification of heat transfer processes during soil cooling, freezing, and thaw in central Alaska, *Perm. Periglac. Process., 5 (4)*, 217–235.

Hinkel, K. M., S. I. Outcalt, and A. E. Taylor (1997), Seasonal patterns of coupled flow in the active layer at three sites in northwest north America, *Can. J. Earth Sci., 34*, 667– 678.

Hinkel K. M., W. R. Eisner, J. G. Bockheim, F. E. Nelson, K. M.Peterson, and X. Dai (2003), Spatial extent, age, and carbon stocks in drained thaw lake basins on the Barrow Peninsula, Alaska, *Arctic, Antarctic, and Alpine Res. 35*, 291–300.

Hinkel, K. M., R. C. Frohn, F. E. Nelson, W. R. Eisner, and R. A Beck (2005), Morphometric and spatial analysis of thaw lakes and drained lake basins in the western Arctic Coastal Plain, Alaska, *Permafrost Periglacial. Proc., 16*, 327–341.

Hinzman, L. D., D. L. Kane, R. E. Gieck, and K. R. Everett (1991), Hydrologic and thermal properties of the active layer in the Alaskan Arctic, *Cold Regions Sci. Technol., 19*, 95–110.

Hinzman, L. D., and D. L., Kane (1992), Potential response of an Arctic watershed during a period of global warming, *J. Geophys. Res., 97*(D3), 2811–2820.

Jasper, K., J. Gurtz, and H. Lang (2002), Advanced flood forecasting in Alpine watershed by coupling meteorological observations and forecasts with a distributed hydrological model, *J. Hydrol*., 327, 40–52.

Jorgenson, M. T., Y. L. Shur, and E. R. Pullman (2006), Abrupt increase in permafrost degradation in Arctic Alaska, *Geophys. Res. Lett., 33*, L02503, doi:10.1029/2005GL024960.

Kane, D. L., and J. Stein (1983), Water movement into seasonally frozen soils, *Water Resources Res. 19(6)*, 1547–1557.

Kane, D. L., L. D. Hinzman, and J. P. Zarling (1991), Thermal response of the active layer to climatic warming in a permafrost environment, *Cold Regions Sci. Technol., 19*, 111–122.

Kane, D. L., K. M. Hinkel, D. J. Goering, L. D. Hinzman, and S. I. Outcalt (2001), Non-conductive heat transfer associated with frozen soils, *Global and Planetary Ch., 29*, 275–292.

Kane D. L., R. E. Gieck, L. C. Bowling (2003), Impacts of surficial permafrost landforms on surface hydrology, in *Proceedings of the Eight International Conference on Permafrost*, edited by Phillips, Springman and Anderson, pp. 507–511, Balkema Publishers, Zurich, Switzerland.

Kane, D. L., R. E. Gieck, and L. D. Hinzman (2008), Water balance for a low-gradient watershed in Northern Alaska, In *Proceedings Ninth International Conference on Permafrost*, edited by D. L. Kane and K. M. Hinkel, University of Alaska Press, Fairbanks, AK.

Kling, J. (1998), The difference between sorted circle and polygon morphology and their distribution in two alpine areas, northern Sweden, *Zeitschrift fur Geomorphologie, N.F., 42*, 439–452.

Krause, S., and A. Bronstert (2005), An advanced approach for catchment delineation and water balance modeling within wetlands and floodplains, *Adv. Geosci., 5*, 1–5.

Krause, S., J. Jacobs, and A. Bronstert (2007), Modelling the impacts of land-use and drainage density on the water balance of a lowland-floodplain landscape in northeast Germany, *Ecol. Modell., 200*, 475–492.

Lachenbruch, A. H. (1962), Mechanics of thermal contraction cracks and ice wedge polygons in permafrost, Spec. Pap. Geol. Soc. Am. 70.

Leffingwell, E. de K. (1919), The Canning River region of northern Alaska, U.S. Geol. Surv. Prof. Pap. 109.

Levy, J. S., J. W. Head, and D. R. Marchant (2008), The role of thermal contraction polygons in cold-desert fluvial systems, *Ant. Sci., 20(6)*, 565–579.

Liljedahl, A. K. (2011), *The hydrologic regime at sub-arctic and arctic watersheds: present and projected,* PhD Dissertation, University of Alaska, Fairbanks, AK.

Liljedahl, A. K., L. D. Hinzman, R. C. Busey, and K. Yoshikawa (2007), Physical short-term changes after a tussock tundra fire, Seward Peninsula, Alaska, *J. Geophys. Res*., F02S07, doi:10.1029/2006JF000554.

Lindenschmidt, K.-E., G. Ollesch, and M. Rode (2004), Physically-based hydrological modeling for non-point dissolved phosphorous transport in small and medium sized river basins, *Hydrol. Sci. J., 49(3)*, 495–510.

Mackay, J. R. (1990), Some observation on the growth and deformation of epigenetic, syngenetic and anti-syngenetic ice wedges, *Perm. Periglac. Process., 1*, 15–29.

Minke, M., N. Donner, N. Karpov, P. De Klerk, and H. Joosten (2007), Distribution, diversity, development and dynamics of polygons mires: Examples from Northeast Yakutia (Siberia), *Peatlands Int., 1*, 36–40.

Minke, M., N. Donner, N. Karpov, P. De Klerk, and H. Joosten (2009), Patterns in vegetation composition, surface height and thaw depth in polygon mires in the Yakutian Arctic (NE Siberia): A microtopographical characterization of the active layer, *Perm. Perigl. Process., 20*, 357–368.

Mueller, G., G. Broll, and C. Tarnocai (1999), Biological activity as influenced by microtopography in a cryosolic soils, Baffin Island, Canada, *Perm. Periglac. Process., 10*, 279–288.

Myers, J. P., and F. A. Pitelka (1979), Variations in summer temperature patterns near Barrow, Alaska: Analysis and ecological interpretation, *Arct. Alp. Res., 11*, 131–144.

Oechel, W. C. and B. Sveinbjornsson, (1978), Photosynthesis of Arctic Bryophytes, in *Vegetation and production ecology of an Alaskan arctic tundra*, edited by L.L. Tieszen, Springer-Verlag, NY.

Olivas, P. C., S. Oberbauer, and A Kuchy (submitted), Effects of fine-scale topography on CO2 flux components of Alaskan Coastal Plain Tundra: Response to contrasting growing seasons, submitted to *Arctic, Antarctic, and Alpine Research*.

Ostendorf, B., D. W. Hilbert, B. Kostner, U. Tappeiner, and E. Tasser, (2001), The importance of understanding spatial pattern for scaling up plot-level matter and energy fluxes to regional scales, *Syst. Analys. Model. Sim., 41(3)*, 391–408.

Overduin, P. P., and D. L. Kane (2006), Frost boils and soil ice content: field observations, *Permafrost and Periglacial Process., 17*, 291–307.

Peterson, R. A., and W. B. Krantz (2008), Differential frost heave model for patterned ground formation: Corroboration with observations along a North American Arctic Transect, J. *Geophys. Res., 113*: DOI: 10.1029/2007JG000559.

Peschke, G. (1977), Ein zweistufiges Modell der Infiltration von Regen in geschichtete Böden, *Acta hydrophysica*, *22 (1)*, 39–48.

Peschke, G. (1987), Soil Moisture and Runoff Components from a Physically Founded Approach, *Acta hydrophysica*, *31 (3/4)*, 191–205.

Ping, C.-L., G. J. Michaelson, M. T. Jorgenson, J. M. Kimble, H. Epstein, V. E. Romanovsky, and D. A. Walker (2008), High stocks of soil organic carbon in the North American Arctic Region, *Nature Geosci.*, doi:10.1038/ngeo284.

Post, W. M., W. R. Emanuel, P. J. Zinke, A. G. Stangenberger (1982), Soil carbon pools and world life zones, *Nature, 298*, 156–159, doi:10.1038/298156a0

Price, J., T. W. D. Edwards, Y. Yi, and P. N. Whittington (2009), Physical and isotopic characterization of evaporation from Sphagnum moss, *J. Hydrol., 369,* 175-182.

Rastorfer, J. R. (1978), Composition and bryomass of the moss layers of two wet-tundra-meadow communities near Barrow, Alaska, in *Vegetation and production ecology of an Alaskan arctic tundra*, edited by L. L. Tieszen, pp. 169–184, Springer-Verlag, NY.

Rovansek, R. J., L. D. Hinzman, and D. L. Kane (1996), Hydrology of a tundra wetland complex on the Alaskan Arctic Coastal Plain, U.S.A., *Arctic, Alp Res., 28*(3), 311–317.

Schulla, J. (1997), Hydrologische Modellierung von Flussgebieten zur Abschatzung der Folgen von Klimaanderungen (Hydrological modelling of river basins for estimating the effects of climate change), *Zurcher Geographische Schriften 69*, ETH Zurich, Switzerland.

Schulla, J., and K. Jasper (2007), Model description WaSiM-ETH, *Internal Report*, Institute for Atmospheric and Climate Science, ETH Zurich, Switzerland.

Sellers, P. J., M. D. Heiser, F. G. Hall, S. B. Verma, R. L. Desjardins, P. M. Schuepp, and J. I. MacPherson (1997), The impact of using area-averaged land surface properties - topography, vegetation condition, soil wetness - in calculations of intermediate scale (approximately 10 km^2) surface-atmosphere heat and moisture fluxes, *J. Hydrol*., *190*, 269–301.

Shiklomanov, N. I., D. A. Streletskiy, F. E. Nelson, R. D. Hollister, V. E. Romanovsky, C. E. Tweedie, and J. Brown. (2010), Decadal variations of active-layer thickness in moisture-controlled landscapes, Barrow, Alaska, *J. of Geophys. Res.* doi:10.1029/2009JG001248.

Shur, Y. L., and M. T. Jorgenson (2007), Patterns of permafrost formation and degradation in relation to climate and ecosystems, *Perm. Periglac. Process. 18*, 7–19.

Sommerkorn, M. (2008), Micro-topographic patterns unravel controls of soil water and temperature on soil respiration in three Siberian tundra systems, *Soil Biol. Biochem., 40*, 1792–1802, doi:10.1016/j.soilbio. 2008.03.002.

Tarnocai, C. (2006), The effects of climate change on carbon in Canadian peatlands, *Global Plan. Ch., 53*, 222–232.

Tarnocai, C., and S. C. Zoltai, (1988), Wetlands of Arctic Canada, in *Wetlands of Canada*. *Ecological Land Classification Series No. 24*., pp. 29–53, Environment Canada and Polysciences Publications Inc., Montreal, Canada.

Teh, Y. A., O. Mazeas, A. R. Artwood, T. Abel, and R. C. Rhew (2009), Hydrologic regulation of gross methyl chloride and methyl bromide uptake from Alaskan Arctic tundra, *Glob. Ch. Biol., 15,* 330–345, doi: 10.1111/j.1365-2486.2008.01749.x.

van Everdingen, R. O. (1998), *Multilanguage glossary of permafrost and related ground-ice terms*, International Permafrost Association, The Arctic Institute of North America, Calgary, Canada.

van Vliet-Lanoe, B. (1991), Differential frost heave, load casting and convection: converging mechanisms; a discussion of the origin of cryoturbation, *Permafrost and Periglacial Proc., 2*, 123–139.

van Vliet-Lanoe, B. (1998), Frost and soils: implications for paleosols, paleoclimates and stratigraphy, *Catena, 34*, 157–183.

Walker, D. A., H. E. Epstein, W. A. Gould, A. M. Kelley, A. N. Kade, J. A. Knudson, W. B. Krantz, G. Michaelson, R. A. Peterson, C.-L. Ping, M. K. Raynolds, V. E. Romanovsky and Y. Shur (2004), Frost-boil ecosystems: Complex interactions between landforms, soils, vegetation and climate, *Perm. Periglac. Process. 15,* 171–188.

Walsh, J. E. (2008), Climate of the Arctic Marine Environment, *Ecol. App., 18(2)*, 3–22.

Washburn, A. L. (1956), Classification of patterned ground and review of suggested origins, *Bull. Geol. Soc. Am., 67*, 823–865.

Washburn, A. L. (1979), *Geocryology*, Edward Arnold, London, 406 pp.

Webber, P. J. (1978), Spatial and temporal variation of the vegetation and its productivity, in *Vegetation and Production Ecology of an Alaskan Arctic Tundra*, edited by L.L. Tieszen, pp. 37–112, Springer-Verlag, New York, NY.

Webber, P. J., P. C. Miller, F. S. Chapin III, and B. H. McCown (1980), The vegetation: Pattern and succession, in *An arctic ecosystem: the coastal tundra at Barrow, Alaska*, edited by J. Brown *et al*., pp. 30-56, Dowden, Hutchinson and Ross Inc., Stroudsburg, PA.

Wiggins, I. L. (1951), The distribution of vascular plants on polygonal ground near Point Barrow, Alaska, *Contributions of Dudley Herbarium, 4*, 41–56.

Woo, M.-K., and X. J. Guan (2006), Hydrological Connectivity and Seasonal Storage Change of Tundra Ponds in a Polar Oasis Environment, Canadian High Arctic, *Perm. Perigl. Process., 17*, 309–323.

Yang, D., B. E. Goodison, S. Ishida, and C. Benson (1998), Adjustment of daily precipitation data of 10 climate stations in Alaska: Applications of world meteorological organization intercomparison results, *Water Resour. Res., 34*(2), 241–256.

Zona, D., W. C. Oechel, K. M. Peterson, R. J. Clements, K. T. Paw, and S. L. Ustin (2009), Characterization of the carbon fluxes of a vegetated drained lake basin chronosequence on the Alaskan Arctic Coastal Plain, *Global. Ch. Biol.*, doi: 10:1111/j.1365-2486.2009.02107.x

Zona, D., W. C. Oechel, J. H. Richards, S. Hastings, I. Kopetz, H. Ikawa, and S. Oberbauer (2011), Light stress avoidance mechanisms in *Sphagnum* dominated wet coastal Arctic tundra ecosystem in Alaska, *Ecology*, 92(3), 633–644.

CHAPTER 5
WATER BALANCE OF AN ARCTIC COASTAL WETLAND, BARROW, ALASKA

Abstract

There is a lack of multi-year field studies in tundra landscapes that include measurements of all components of the water balance. This data gap complicates efforts aimed at increasing understanding of hydrologic processes in the arctic ecosystem and hence increases uncertainty in model projections. We assessed recent (1999-2009) water balance of a wetland near Barrow, Alaska, to gain knowledge of interannual variations and controls by combining an extensive hydrologic field campaign with the physically-based hydrologic model WaSiM-ETH. Arctic Coastal Plain wetlands exhibit an interannual hydrologic connectivity through changes in soil water storage that controls the partitioning of the melting snowpack in spring. Evapotranspiration was the major pathway of water loss, but it was the interannual variations in total summer precipitation that primarily defined the differences in autumn soil water storage status. Large interannual changes in soil water storage restrict applications of the water balance method when assumptions of negligible soil water storage change are made. Modeled evapotranspiration and near-surface soil moisture agreed well with measurements within the drained thaw lake basins. The multi-week long ponding was only replicated by WaSiM-ETH when rims of low-centered polygons were included. We believe that the model performance was limited by the resolution of the digital elevation model as the 5 m DEM did not resolve the high-centered polygons. The integration of a physically-based model, extensive field campaign, and micro-scale digital elevation models (<1 m) serve as a promising approach in exploring hydrologic processes in arctic wetlands.

5.1 Introduction

Arctic wetland hydrology plays a major role in energy, carbon, and nutrient exchange at various scales [*Gorham,* 1991; *Gutowski et al.,* 2007]. Arctic hydrologic monitoring networks are spatially sparse and in decline [*Shiklomanov et al*., 2002; *Bring and Destouni*, 2009]. Rarely are all individual components of the Arctic water balance measured simultaneously with runoff observations being the most common (and reliable) measurement available [*Kane and Yang,* 2004]. The lack of the ability to validate models and the limited input parameters increases the uncertainty in hydrologic assessments of arctic wetlands.

Most arctic water balance studies are based upon measurements of precipitation (including snow accumulation) and runoff [*Kane and Yang,* 2004], while evapotranspiration and storage terms are commonly derived from indirect estimates [*Shutov et al*., 2006]. While integrated into runoff measurements, variations across space and time further complicates estimates of the individual components of the water balance equation. Errors in one or more components of the water balance are difficult to constrain when measurements are lacking.

This research watershed at Barrow, Arctic Coastal Plain, Northern Alaska, is one of the few arctic wetland basins where all components of the water balance were directly measured during a multi-year time period. Due to the extensive monitoring, which included physical and biological parameters, this watershed is an appropriate location to test and apply a physically-based water balance model. In this paper we use the hydrologic model WaSiM-ETH, which is an established tool at lower latitudes. This research is the first application of WaSiM-ETH to a basin underlain by permafrost. The validation includes comparisons of measured evapotranspiration, water tables, snow water equivalent, and runoff. Finally, we assess recent (1999-2009) water balance to gain an understanding of the interannual variations and controls on arctic wetland hydrology. For clarity, we refer to evapotranspiration as measured, estimated, and simulated. Measured is aimed to

represent observations from an eddy covariance system, simulated to our model analyses, and estimated to other methods.

5.2 Background

5.2.1 Wetlands

A large region of the terrestrial arctic domain is represented by extremely low-gradient tundra (> 400,000 km^2) [*Walker et al*., 2005; *Minke et al.*, 2009]. The area is classified as a wetland with abundant lakes and seasonal ponds, despite a near-desert annual precipitation and negative summer net P-ET [*Mendez et al*., 1998]. What may be seen as a paradox can be explained by low hydraulic gradients, short summers, abundance of snowmelt water, and the presence of impermeable permafrost [*Bowling et al*., 2003; *Woo and Young*, 2003]. The coastal wetlands are further supported by the maritime air due to the persistent onshore winds that results in reduced vapor pressure deficits (VPD) [*Rouse et al.,* 1987] and non-linear soil moisture and VPD controls on evapotranspiration [*Liljedahl,* 2011].

5.2.2 Landscape Features

Permafrost is associated with terrain units of various scales that may play an important role in arctic wetland hydrology. Shallow thaw lakes, many of which freeze completely in the winter, are formed by surface depressions that accompany degraded permafrost. *Hussey and Michaelson* [1966] estimated that 50–75 % of the Arctic Coastal Plain is covered either by lakes or former thaw lake basins. Drained thaw lakes, which have a vegetated, nearly leveled surface [*Mackay*, 1990], occupy approximately 26 % of the western Arctic Coastal Plain, Northern Alaska, [*Hinkel et al.,* 2005] and 50 % of the Barrow Peninsula north of ~71° latitude [*Hinkel et al*., 2003]. In addition to these larger landforms of 100‘s of meters are a patch-work of high- and low-centered polygons with diameters ranging from 10 to 30 m. Thermal contraction cracking of permafrost over century time scales [*Leffingwell*, 1919; *Lachenbruch*, 1962; *Mackay*, 1990] allow the formation of ice wedges when

snowmelt water infiltrates into the polygonal array of cracks [*French*, 1996]. Both drained thaw lakes and patterned ground are suggested to play an important role in arctic wetland hydrology [*Kane et al., 2003*].

Vegetation distribution is strongly correlated with subtle landscape features. Poorly drained wet tundra meadow communities are found within the vegetated drained thaw lake basins, within troughs of high-centered polygon landscapes [*Brown et al*., 1980], and low-center polygon depressions [*Minke et al.,* 2009]. Mosses are abundant, representing the majority of the live biomass and carbon uptake [*Zona et al*., 2009a]. Accordingly, a majority of the evapotranspiration within vegetated drained thaw lake basins is estimated as evaporation from moss or ponding water (55 to 85%) [*see Engstrom et al*., 2006]. On the other extreme are the well-drained domes of high-centered polygons and elevated rims of low-centered polygons where mesic moss carpets, graminoids, and lichens prevail [see *Minke et al*., 2009].

5.2.3 Hydrology

While assessments of the Arctic hydrologic cycle face similar obstacles as those at lower latitudes, such as difficulty in accurate precipitation estimates [*Black*, 1954; *Benson,* 1969*; Groisman and Legates*, 1994], unique challenges are encountered in an environment underlain by permafrost. Continuous permafrost acts as an impermeable hydrologic barrier reducing soil water storage capacity and limiting subsurface flow [*Hinzman et al*., 1991a; 1998; *Kane et al*., 1991; *Woo et al.,* 2000]. Although the absence of deeper groundwater flow simplifies the hydrologic system, there are several physical processes unique to the cryosphere that complicate modeling efforts. For example, the seasonal development of the active layer (the soil layer above the permafrost that experiences seasonal freeze and thaw) results in a varying soil water storage capacity that affects runoff [*Sand and Kane*, 1986]. Further, the elevation of the frozen table is not uniform [*Minke et al*., 2009], which

can result in effective blockage of subsurface lateral flow in extremely low-gradient terrain [*Donner*, 2007; *Boike et al*., 2008]. The seasonally frozen soils are not necessarily impermeable to infiltration of water. Snowmelt water can enter, percolate, and laterally drain through unsaturated frozen soils [*Kane et al*., 1978]. Plot-scale studies have shown that pre-freeze soil moisture levels are an important regulator of spring runoff in northern regions with substantial amounts of the meltwater percolating into the frozen soils [*Kane and Stein*, 1984]. Such interannual hydrologic connectivity has also been found in modeling studies with surface water storage changes in lakes affecting the proceeding spring runoff [*Bowling and Lettenmaier*, 2010].

Hydrologic modeling efforts of extremely-low gradient arctic wetlands have been limited to large scale models that neglect the subsurface transfer of moisture between grid cells [*Wei et al*., 2002; *Bowling and Lettenmaier*, 2010], and modeling of individual fluxes [*Wessel and Rouse*, 1994; *Mendez et al.,* 1998, *Engstrom et al*., 2006] to provide information of one or more components in water balance analyses [*Rovansek et al*., 1996]. Integrative assessments of wetland hydrologic processes at fine spatial scales and its role on large-scale fluxes are limited. By combining an extensive multi-year Arctic wetland monitoring program with a physically-based hydrology model, we are able to validate individual hydrologic components near the scale of the measurement footprint and then define important factors that affect the hydrologic cycle.

5.3 Site Description

The site, here referred to as the Biocomplexity Experiment (BE), (71°16'51"N 156°35'47"W, elevation 4.5 m) is located a few kilometers from the Beaufort and Chukchi Seas near Barrow on the Arctic Coastal Plain, Northern Alaska (Fig. 5.1). Mean annual air temperature at Barrow Airport is –12 °C (1977-2009) where summer air temperature (June through August) averages 3.3 °C. A substantial

amount of the annual precipitation (173 mm, 1977-2009) falls during June through September (99 mm) (adjusted following the method by *Yang et al.*, [1998]). Fog and drizzle are common during the summer because the sites receive a steady cool and moist wind (mean 5 m s^{-1}) from the ocean (east to northeast) [*Shulski and Wendler*, 2007].

The BE is representative of vegetated drained thaw lake basin (DTLB) that drained between 50 and 300 years ago [*Hinkel et al.,* 2003]. The old lake basin is now a poorly drained wet tundra meadow with Typic Aquiturbels soils [*Bockheim et al.*, 1999] underlain by ~600 m thick permafrost [*Brown and Johnson,* 1965]. Low-centered polygons are found within the DTLB, while it is surrounded by high-centered polygons. The active layer depth at a nearby drained lake basin varied from 19 to 62 cm (mean 36 cm) in 1995-2009, while mean active layer depth at the BE site was 30 cm (2006), 26 cm (2007 and 2008), and 27 cm (2009) [*Shiklomanov et al*., 2010].

Non-vascular vegetation contributes significantly to biomass and cover in these ecosystems [*Webber* 1978; *Oechel and Sveinbjornsson,* 1978; *Rastorfer* 1978]. Across the BE lake bed, mosses represent most of the live above ground biomass [*Zona et al*., 2009a]. Moss may reach depths of 20 cm at wet sites, but the bulk of their living biomass is usually within ~1 cm of the soil surface [*Engstrom et al.,* 2005]. Vascular plant composition is represented by *Carex aquatilis*, *Eriophorum* and *Dupontia* with an average LAI in mid-August 2006 of 0.43, 0.13 and 0.02, respectively [*Zona et al*., 2011]. In comparison, standing dead leaf biomass in the Barrow area reaches LAI‘s of 1.23 [*Dennis et al.,* 1978]. Underlying bryophytes typically receive only 10-20 % of direct solar radiation during a clear day (modeled) and averages 11 % throughout the summer (measured) due to the low solar altitude [*Miller and Tieszen*, 1972]. Senescence in the region occurs at the end of August to late September [*Myers and Pitelka, 1979*].

5.4 Methods

5.4.1 Measurements

All components of the summer water balance were measured simultaneously during a two year period (2007-2008) while 11 yr of meteorological data forced the model simulations (Table 5.1). Meteorological and energy flux information was obtained from an eddy covariance tower located within the basin in 2005-2009 (Fig. 5.2). Latent heat fluxes were measured at 1.6 m height with an open path infrared gas analyzer (Li-7500, Li-COR) and a sonic anemometer (WindMasterPro, Gill Instruments Ltd.). Horizontal sensor separation of the Li-7500 and WindMasterPro was 10 cm. The Li-7500 was calibrated every two to four weeks using ultra high purity nitrogen as zero and a dew point generator (Li-610, Li-COR) that produced an air stream with a known water vapor dew point (typically 7 °C lower than the air temperature in the laboratory).

The following supporting micrometeorological data was measured at the BE site: air temperature and relative humidity at several heights (Vaisala HMP45C, 0.46 m, 1.6 m and 2.95 m), atmospheric pressure (BE: Li-COR 7500, 1.6 m), net radiation (REBS Q7, 0.25-0.6 μm, 1.35 m), wind speed (RM Young Wind Sentry 1.6 m), wind direction (RM Young Wind Sentry, 3 m), soil temperatures (T-thermocouples), surface temperature (thermocouples at 1 cm depth) and soil moisture (CS616, 10 cm depth). Meteorological data for 1999-2004 was obtained from another DTLB ~ 2 km away [*Harazono et al*., 2003]. Micrometeorological variables were sampled on a data logger every 10 s and then averaged every 30 minutes.

Runoff measurements were made with a flow meter (Flo-Mate^{TM} Model 2000, Marsh-McBirney) in early morning (low-flow) and early evening (high-flow) throughout the spring runoff period with simultaneous readings of water levels to obtain a stage-discharge relationship. Daily site visits and a mounted camera with a timed photographic interval provided water levels observations at the weir

throughout the summer after the spring runoff event in 2007 and 2008. In 2009, the water level at the weir was recorded using a non-vented pressure transducer (HOBO U20-001-04-Ti), which was suspended inside 5 cm diameter PVC tube. The white PVC tube was attached to the weir. During the summer, regular site visits (three in total) ensured that the 15 cm long transducer was continuously immersed in the water column as the water table receded. The recorded data was processed with the HOBOware-Pro software to account for the water temperature affect on fluid density and the variations in atmospheric pressure.

Water table depths were monitored manually along an east-west transect across the vegetated drained thaw lake basin at 11 fixed locations in 2007-2009. Each site was marked with a 2.5 cm diameter PVC tube. The water levels were measured in reference to the local ground surface. An extensive snowdrift developed each spring along the water table transect due to permanently installed boardwalks. This prevented measurement of water levels until ~1 week after peak runoff. The measured inundation period was defined as the day of peak runoff until at least five of the 11 measurement sites had water tables below the ground surface. In 2006, the water table measurements represent the conditions only at the flux tower.

Two of the years (2008 and 2009) include snow ablation measurements, which were based upon five locations in an east-west transect about 100 m south of the water table transect. Two of the ablation sites were located within the high-centered polygonal tundra and three within the vegetated drained lake basin (low-centered polygons). Daily snow water equivalents were calculated from five snow density measurements and 50 snow depth measurements at each of the five sites following the method outlined by *Rovansek et al*. [1994].

Hourly precipitation was obtained from the National Climatic Data Center (NCDC) web archive (http://cdo.ncdc.noaa.gov/cgi-bin/cdo/cdostnsearch.pl). Long-term records of daily precipitation and air temperature were retrieved from the

NCDC web archive of Barrow Airport (STN 700260, WBAN 27502, www.7.ncdc.noaa.gov/CDO/cdoselect.cmd?datasetabbv=GSOD). Trace recordings from hourly NCDC precipitation data were given a precipitation amount of 0.01 mm according to *Woo and Steer* [1979]. Daily precipitation was adjusted according to *Yang et al.* [1998]. Hourly precipitation observations were manually fitted to the adjusted daily dataset by increasing observed events. The resultant precipitation is referred to as adjusted precipitation. Incoming solar radiation (direct and diffuse) was downloaded from the Atmospheric Radiation Measurement (ARM) program (http://ncvweb.archive.arm.gov/). The 20 second interval of solar radiation was averaged into hourly values.

5.4.2 Data Quality Control and Analysis

We calculated fluxes of heat and momentum in 30 min intervals according to typical covariance calculation procedures. The following corrections were applied (see *Zona et al*. [2009a, b]): the humidity effect on the sonic thermometry [*Kaimal and Gaynor,* 1991], effects of path length and sensor separation on the spectrum on high-frequency flux ranges [*Moore,* 1986], air density effects [*Webb et al*., 1980; *Leuning et al*., 1982], and coordinate rotation [*Tanner and Thurtell,* 1969]. We removed calculated fluxes during rain, fog, and low wind, which may have caused a bias (i.e. reduced representation of low evapotranspiration rates). Extreme amplitudes in the flux data (greater than three times the average) were removed. Fluxes of latent heat were calculated using the EdiRe program and software (version 1.4.3.1169, Robert Clement, University of Edinburgh). No gap filling was performed. Measured latent heat fluxes were presented as a daily mean midday (defined as ± 2 hours from local solar noon ~ 14:00 Alaska Standard Time), morning (7:00 – 11:00), and afternoon (17:00-21:00) or as a daily total. Gap filling was only performed for the daily total evapotranspiration by linearly interpolating

up to 2 hours of missing data. Negative latent heat values (downward fluxes) were given a zero flux.

5.4.3 Hydrologic Modeling

5.4.3.1 Model Description

We chose the physically-based hydrologic model *Water Balance Simulation Model – Swiss Federal Institute of Technology* (WaSiM-ETH) [*Schulla*, 1997; *Schulla and Jasper*, 2007] to analyze the present and future hydrologic fluxes and stores. WaSiM-ETH is a well established tool for modeling the spatial and temporal variability of hydrologic processes in complex basins ranging from less than 1 km^2 to more than 500,000 km^2 [*Kleinn et al.,* 2005]. Its applications have ranged from water management in arid and semi-arid regions [*Bharati et al*., 2008], flood forecasting [*Cullmann et al*., 2008], water balance analyses of wetlands within lowland floodplains [*Krause et al*., 2007], to the role of polygon patterned ground on arctic wetland hydrology [*Liljedahl,* 2011] and many other hydrologic studies.

Four modules in WaSiM-ETH are of special interest to this particular application: 1) The extraction of water from the different soil layers is done separately for evapotranspiration and bare soil (moss) evaporation. WaSiM-ETH represents evapotranspiration through the Penman-Monteith equation coupled to the unsaturated zone‘s soil moisture condition (Richard‘s equation) suppressing evapotranspiration rates during large negative soil water potentials. The second step is the extraction of bare soil (or moss)evaporation from the top soil layer, which is also linked to soil moisture status; 2) In addition to representing lateral flow through channel routing, base flow, and interflow, WaSiM-ET includes a surface routing module designed for small scale applications. Infiltration excess and direct runoff is used as input for the surface routing model. The surface runoff, assumed to flow as a consistent layer, will follow the flow paths from cell to cell until a river cell is reached. In diverging areas, multiple flow paths (up to three) are possible,

while only one flow direction is allowed in converging areas (the steepest slope). The flow velocity depends on slope, roughness and water film depth (Manning Strickler approach) where the slope includes the elevation model plus the water storage. The dynamic generation of ponds occurs when elevation and local storage leads to a zero or inverted gradient. However, it is still not a hydrodynamic wave approach but rather a kinematic wave approach with stepwise constant parameters. The time step of surface routing is dynamically decreased to maintain the CFL (Courant–Friedrichs–Lewy) condition, but if necessary, it can also be parameterized; 3) Due to the uniqueness of the seasonally changing soil water storage capacity of soils underlain by the relatively impermeable permafrost, WaSiM-ETH simulates the seasonal development of the active layer through a simple static approach:

$$d_{thaw} = \propto \sqrt{n_{sf}} \qquad (1)$$

where d_{thaw} is thaw depth in m (obtained from measurements), α is an empirical coefficient, and n_{sf} is the number of snow free days (or more precisely; days with a snow water equivalent below a certain threshold [*Hinzman et al.*, 1991]). The thaw (and hence the count of snow free days) is initiated when the SWE falls below the pre-defined SWE threshold value. Although not used here, the simple re-freezing algorithm can be represented by a pre-defined accumulated count of snow covered days where the soil refreezes instantly and the n_{sf} is reset to 0. Frozen soils are given a hydraulic conductivity of 10^{-12} m s^{-1}. In this application, the α-value is calibrated to measured thaw depths; 4) The module which calculates snowmelt is based upon a temperature-wind-index approach:

$$M = [c_1 + (c_2 \times u)] \times (T - T_{0,m}) \times \frac{\Delta t}{24} \qquad (2)$$

where M is the melt rate (mm h^{-1}), c_1 is the temperature dependent melt factor (mm C^{-1} d^{-1}), c_2 the wind dependent melt factor (mm C^{-1} d^{-1} · m s^{-1}), u wind speed (m s^{-1}), T air temperature (ºC), $T_{0,m}$ the temperature for beginning of snow melt (ºC) and Δt the time step (h).

The model was forced by measured snow accumulation in late April (snow water equivalent) and precipitation adjusted for wind-undercatch after the method by *Yang et al.* [1998] from May through September. The simulations were initiated a few days prior to the onset of the ablation period and stopped during the start of winter, which was defined as the first of 10 consecutive days that experienced mean daily air temperature below 0 °C. Soil and surface water distribution at the end of each simulation was used as initialization conditions for the following year. The initial condition of the first year in the simulation (1999) was established by running the model into an equilibrium state with the forcing data from summer 2006. Only two simulations that used the same forcing variables were required to reach an equilibrium state where the end-of-summer water table was unchanged from one year to the other. The model simulations represent an 11 year time period (1999-2009).

5.4.3.2 Digital Elevation Model

The original DEM (0.25 m horizontal resolution) was derived from airborne LIDAR measurements, 4th October 2005, at an altitude of approximately 600 meters using an Optech 70 kHz Airborne Laser Terrain Mapper (ALTM 30/70). The processed and quality checked LIDAR data had a mean difference to ground based surveys of 0.003 meters (median = 0.004, RMSE = 0.043 meters, n=286 points). A 5 m DEM (Fig. 5.1, Fig. 5.2) was produced from the original 0.25 m

DEM by arithmetic averaging using the pre-processing tools available with WaSiM-ETH. Since the 5 m DEM was not able to resolve the polygonal ground features, the hydrology model was also forced with a modified DEM. The modification included an addition of an artificial elevated rim within the lower portion of the vegetated drained thaw lake. The elongated rim was intended to substitute for a patchwork of low-centered polygons that are found within the vegetated drained lake. Aerial photos served to define its horizontal location, which included a 0.08 m increase of the local ground surface. The height was defined by a) evaluating the micro-topographical variations along the east-west transect across the drained lake basin from the original 0.25 m DEM and b) assessing the threshold rim-elevation which resulted in an altered watershed delineation using the WaSiM-ETH pre-processing tool TANALYS.

5.4.3.3 Variables and Parameter Settings

In addition to the DEM, model input data included vegetation and soil data as well as meteorological data from the eddy covariance tower (hourly air temperature, wind speed, vapor pressure), the National Climatic Data Center (hourly precipitation), and the Atmospheric Radiation Measurement program (hourly shortwave incoming radiation). The watershed was parameterized with one type of vegetation cover but with two classes in the soil map (drained thaw lake basin and upland tundra) (Table 5.2). Parameters used in the separate modules are presented in Table 5.3.

Leaf area index (LAI) was described through a polynomial function developed from LAI measurements in 2007 (Fig. 5.3). In the evapotranspiration module, LAI information was linearly interpolated between time steps of 10 days. The senescence period was set to be initiated on Julian day 224, while the start of the LAI curve was adjusted to the timing of the end of ablation period for each

individual year. As a result, the length of the peak LAI period (LAI 0.53) varied amongst years.

5.4.3.4 Calibration and Validation

The model was calibrated to and validated on evapotranspiration, runoff, water tables, and snow ablation. Evapotranspiration rates were compared to those evaluated by the eddy covariance method during easterly winds in the summer of 2006, 2007, and 2008. We extracted and averaged the simulated evapotranspiration across a 150x150 m square of the vegetated drained lake basin similar to the typical footprint of the eddy covariance tower (Fig. 5.1). The calibration of evapotranspiration rates was a two step process due to the non-linear controls by VPD on evapotranspiration rates [*Liljedahl*, 2011]. Firstly, days with VPD > 0.3 kPa were calibrated by tuning the minimum bulk surface resistance (referred to as *rs_evaporation* in the model), which controls evaporation from the top soil layer. All remaining days were calibrated last and given the same *rs_evaporation* value.

The model validation of evapotranspiration rates includes three statistical methods; the relative index of agreement (I_a) [*Willmott and Wicks*, 1980], the root mean square error (*RMSE*) [*Willmott*, 1982], and the mean bias error (*MBE*). The I_a is defined as

$$I_a = 1 - \left[\frac{\sum_{i=1}^{N} (P_i - O_i)^2}{\sum_{i=1}^{N} \left(|P_i - O_m| + |O_i - O_m| \right)^2} \right] \qquad (3)$$

where P and O are predicted and observed values, respectively, and O_m is the mean observed value and N is the number of data points used. An I_a-value close to zero represents a poor model performance, while a value of one represents the best

possible performance. The *RMSE* provides a measure of the total systematic error (mm h^{-1}), therefore a value near zero suggests an effective model simulation.

$$RMSE = \sqrt{\frac{\sum_{i=1}^{N} (P_i - O_i)^2}{N}} \qquad (4)$$

The mean bias error, *MBE*, provides a measure of the systematic error (mm h^{-1}) and indicates whether a model under- or overpredicts (negative and positive *MBE*) a variable throughout a given period of time. If the error is completely random, the *MBE* value will be zero.

$$MBE = \frac{\sum_{i=1}^{N} (P_i - O_i)}{N} \qquad (5)$$

Comparisons to measured water tables during summer 2006 to 2009 were based upon the 11 DEM pixels that represent the same locations as water table measurements (Fig. 5.1). We averaged the 11 locations instead of evaluating each location separately due to the known difficulty of the 5 m DEM in resolving the variations in the true ground surface. We calibrated the degree-day melting factor and the threshold temperature for snowmelt based upon a) the sudden increase in net-radiation that occurs when the ground surface becomes snow-free (yr 1999-2003 and 2005-2006), b) the runoff measurements in 2007, and c) the ablation measurements in 2008 and 2009.

5.5 Results

5.5.1 Measurements 2006-2009

No summer runoff occurred in 2007-2009. The partitioning of SWE into runoff showed large interannual variations while the overall mean was 60 % (Table 5.4). In comparison, on average 39 % of the annual precipitation went to runoff. During the peak flow period (~3 days), networks of troughs within the high-centered polygon tundra served as channels that effectively transported the meltwater into the DTLB. The DTLB became a temporary shallow lake flooded with up to 20 cm of melt water near the day of peak runoff (June 9th in both 2007 and 2008 and June 5th in 2009).

Following the peak runoff, the hydroperiod (defined as ≥ 6 sites having water tables above the ground surface) lasted for more than 3 weeks. The water table within the DTLB remained close to the surface throughout summers with near-normal precipitation (2006, 2008 and 2009), temporarily receding to only about 5 cm below the ground surface near mid-July (Fig. 5.4a-d). In comparison, the unusually low-precipitation summer of 2007 (24 mm) resulted in a water table 20 cm below the surface by early August. The timing of water table recession below the ground surface was similar in all summers occurring in the last week in June and the first week in July (average of all 11 sites).

Measured evapotranspiration from the DTLB (June through August) ranged between 1.3 and 7.2 mm day^{-1}. Although the higher rates were concentrated to the weeks near the solstice, a large day-to-day variation occurred. For example, the evapotranspiration on July 11 2006 measured 5.4 mm while it reached 1.9 mm three days later. Daily evapotranspiration was measured on 24 % (58 days) of all summer days (242 days) 2006-2008 (start of thaw through August), with most of the measurements in summer 2007 (30 days). Days with measured daily evapotranspiration had slightly larger mean daily air vapor pressure deficits (0.09

kPa) than the overall mean (0.06 kPa). The evapotranspiration rates were representative of the DTLB and therefore NE, E, and SE winds.

The area experienced some spatial variation in the timing of the snowmelt completion amongst the two landscape types within the watershed. The two sites located within the drained thaw lake basin (site 2 and 3) became snowfree 1 to 3 days earlier than the upland sites in 2008 (Fig. 5.5). The ablation in 2009 on the other hand resulted in a simultaneous exposure of all four sites (June 6th). Bare ground was exposed at the top of some high-centered polygons on May 25 indicating melting prior to the onset of the 2009 survey. The fifth site was not included in the analysis as it was affected by a snowdrift in 2009 due to a structure onsite.

5.5.2 Validation of Hydrology Simulations 2006-2009

The original 5 m DEM was not able to reproduce the observed multi-week ponding or the depth of the inundation (Fig. 5.6). However, the modified 5 m DEM, which included an 8 cm high rim, produced a multi-week long ponding in all four years. Therefore, the modified DEM was used in the water balance analysis 1999-2009. Simulated water tables were in general within 5 cm of the measured values (Fig. 5.4a-d). However, the error is up to ~ 10 cm in early summer 2008 (underestimated) and late summer 2009 (overestimated).

The identified parameters for the snowmelt module closely resembled those of *Hinzman and Kane* [1991]. The calibrated threshold temperature for snowmelt ranged from 0 to –2ºC (Table 5.5), while *Hinzman and Kane* [1991] determined a range of 0 to –1.9 ºC at Imnavait watershed near the foothills of the Brooks Range, North Slope, Alaska. The sum of the temperature and wind dependent melt factors (mean 3.6 mm $^{o}C^{-1}$ d^{-1}) (Table 5.5) compared well to the Imnavait study (3.5 mm $^{o}C^{-1}$ d^{-1}).

As observed, the runoff was only simulated in early summer in connection to the snowmelt 2007-2009. Total simulated runoff was underestimated in all three years due to overestimated infiltration rates. The simulated runoff represented 53, 65, and 38 % of the measured runoff quantities in 2007, 2008, and 2009, respectively, which correspond to errors of 25, 18, and 70 mm, respectively.

Simulated ET rates closely followed those measured by the eddy covariance system (Fig. 5.4a-c) with most *I*-values near 0.9 and *RMSE* values ≤ 0.002 (Table 5.6). The sum of the total bias (*MBE*) was 6.5 (2006), 16.2 (2007), and 9.8 mm (2008), which show a general, but small, overestimation of simulated evapotranspiration rates. The evapotranspiration errors were in general largest in the morning and decreased later in the day. Simulated afternoon evapotranspiration was slightly underestimated in 2006 (a total of –4.3 mm).

5.5.3 Simulated Water Balance 1999-2009

The water exchange was dominated by the vertical fluxes of water. Evapotranspiration represented the major pathway of water loss, accounting for 77 % of the mean annual precipitation 1999-2009 (Table 5.7). The simulated mean summer evapotranspiration ranged from 1.3 to 1.7 mm day^{-1} (mean 1.5 mm day^{-1}) across the watershed resulting in a total evapotranspiration of 134 to 186 mm (mean 160 mm). Total evapotranspiration was significantly correlated to the mean daily evapotranspiration rates (R^2 0.88, $P < 0.01$) while no significant correlation was found to the length of the summer (R^2 0.08, $P > 0.1$). Simulated mean daily evapotranspiration from the DTLB in 2006-2008 (1.6 mm) was in the lower range of the measured daily evapotranspiration rates (1.3 and 7.2 mm day^{-1}). Note that the measured daily evapotranspiration represented only a portion (24%) of the entire summer in 2006-2008.

The majority of the cumulative evapotranspiration was evaporation from moss and ponded water. Evaporation represents 60-73 % (mean 68 %) of the

cumulative evapotranspiration from the footprint of the BE tower (Table 5.8), while its basin wide portion was slightly lower (mean 66 %) due to the lateral redistribution of water (Table 5.2). In comparison, an individual day in late summer 2007 had only 32 % of the total evapotranspiration as evaporation. The role of evaporation decreased during the 2007 season (55 %), which was a summer with extremely low precipitation (24 mm).

The large evapotranspiration, which experienced modest interannual variability (stdev 14 mm) compared to the summer precipitation (stdev 36 mm), resulted in a negative net summer water balance (P-ET) in all years. Although not statistically significant, an increasingly negative P-ET trend was found in 1999-2009 (Fig. 5.7). The variation in P-ET during the 11 yr time period was strongly correlated (R^2 0.92, $p < 0.01$) to summer precipitation (Fig. 5.8). Further, the normalized spring runoff (runoff/SWE) was statistically correlated (R^2 0.90, $p < 0.01$) to the previous summer‘s P-ET (Fig. 5.9).

Simulated runoff was concentrated in the snowmelt event, which usually occurred during the first three weeks in June. On average, about half (46 %) of the accumulated SWE (mean 115 mm) contributed to streamflow. However, there was considerable year to year variation (22 to 72 %). Of the total annual precipitation (mean 208 mm), only 26 % left the basin as runoff with an interannual variation ranging from 16 to 35 %. Apart from summer 2001, which had 12 mm of simulated runoff in late summer, no runoff was modeled in response to summer precipitation events even though 45 % of the annual precipitation occurred during the summer months.

The DTLB was flooded for a long period every spring and early summer but the surface was usually exposed by the end of growing season. Springtime expressed a consistent deep ponding with up to ~15 cm of meltwater inundation. The DTLB was on average flooded 40 days per summer (mean length of summer was 108 days). Fall water tables within the drained thaw lake basin were in all but

one yr (2001) below the ground surface (mean depth 43 mm). The autumn water table represented the seasonal low in 6 of the 11 yrs. Late summer precipitation reduced soil water deficits in other years or, although rare, resulted in flooding prior the onset of winter such as in 2001.

The annual change in the annual soil water storage was up to 78 mm, which is comparable to nearly half of the mean annual precipitation. Time series of simulated storage and cumulative fluxes 1999-2009 are presented in Appendix 1a-c.

5.6 Discussion

5.6.1 Measurements

In agreement with *Brown et al.* [1968] and *Kane et al.* [2000, 2008a], we found the runoff regime at Arctic Coastal Plain watersheds being dominated by snowmelt floods. Snowfall represented 55 % of the annual precipitation (208 mm), which is a slightly higher ratio than that of Putuligayuk River watershed, eastern Arctic Coastal Plain (40 %) [*Kane et al.,* 2000]. No summer runoff was observed in 2007-2009. The lack of measured summer runoff may be an artifact of the short measurement period. *Brown et al*. [1968] measured summer runoff from a nearby Barrow watershed (1.6 km^2), which also includes a drained lake, in 1963 (19 mm) and in 1966 (2 mm). Both were summers that they described as cool and wet to extremely wet compared to mean summer precipitation. Small peaks in response to summer precipitation has also been observed at the Putuligayuk River [*Kane et al*., 2008b], which has a similar mean summer precipitation (85 mm) as Barrow (93 mm). Further, the USGS monitored watershed located a few kilometers to the southwest of Barrow, Nunavak Cr. (8 km^2) has several years with major summer runoff (< 120 mm) in 1973-2004. The Nunavak Cr. contains steeper slopes than any of the other two Barrow basins and also a large lake, which probably explain the differing summer runoff regimes across such short distances.

Large soil water storage deficits, relative to annual precipitation, suppress the ratio of runoff/SWE, which reduces the lateral export (Fig. 5.8). The runoff/SWE ratio in 2008 was reduced compared to 2007 and 2009. Simultaneously, the summers net water balance (P-ET) was extremely negative in 2007 (Table 5.7). Even though the P-ET in summer 2008 (–93 mm) was similar to 2006 (–73 mm), the Q/SWE in 2009 (0.91) was drastically higher than 2007 (0.54). The rainfall event (2.4 mm) during the end of the snowmelt in 2009 likely elevated the partitioning into runoff. The range of end-of-winter accumulated SWE (mean 115 mm) that left the basin as runoff in spring 2007, 2008, and 2009 (34 to 91 %) is comparable to that observed at the Putuligayuk River watershed, Arctic Coastal Plain, in 1999-2007 (49-98 %, mean SWE 95 mm) [*Kane et al*., 2008b]. However, the mean partitioning of SWE into runoff at our study site in 2007-2009 (60 %) is lower than that of the Putuligayuk River watershed (78 %) [*Kane et al.,* 2008b]. The difference in the mean partitioning of SWE into runoff between the two Arctic Coastal Plain watersheds are likely caused by the short record in combination with spring 2008 at the Barrow site, which followed the extremely dry summer of 2007. We concur with previous research [*Rovansek et al*., 1996; *Bowling et al.,* 2003; *Kane et al.,* 2008b] that the hydrology of the extremely-low gradient watersheds at the Arctic Coastal Plain, Alaska, exhibit an interannual connectivity through changes in the subsurface and surface soil water storage.

The DTLB experienced higher maximum evapotranspiration rates (< 7.2 mm day^{-1}) than other reported eddy covariance measurements of tundra wetlands at the Arctic Coastal Plain (< 4.7 mm day^{-1}) [see *McFadden et al*., 1998, *Vourlitis and Oechel*, 1997, 1999; *Engstrom et al.*, 2006]. Unusually high air vapor pressure deficits (~ 1kPa) occurred in 2007 [*Liljedahl*, 2011], which was when the high evapotranspiration rates were observed. The apparent variation supports the need for longer-term direct measurements of evapotranspiration in order to more accurately define the water vapor loss to the atmosphere.

The extensive ponding produced by the snowmelt freshet appears to be a typical phenomenon of extremely low-relief arctic watersheds. The freshet pulse from surrounding areas served to inundate the drained lake for several weeks. Similarly, spring overland flow has been observed to recharge pond storage [*Rovansek et al*., 1996; *Woo and Guan*, 2006] and temporarily inundate large sections of low-gradient watersheds [*Bowling et al*., 2003]. The surface flow hydraulic connectivity between the surrounding high-centered polygon landscape and the DTLB was only observed during the days surrounding the peak runoff, which is a shorter time period than observed by *Woo and Guan* [2006] in Canadian High Arctic between ponds and their surrounding areas (~2 weeks). As up to 75 % of the Arctic Coastal Plain is covered by either lakes or DTLB [*Hussey and Michaelson*, 1966] a significant portion of the region is inundated in early summer for several weeks every year. The water table receded as summer progressed but late summer precipitation reduced the storage deficit during a time period with low ET, which is an observation in agreement with *Kane et al*. [2008b].

5.6.2 Modeling

The range of simulated total evapotranspiration from the DTLB footprint (140-202 mm) agrees well with what *Harazono et al*. [1998] measured in 1995 from wet sedge tundra near Prudhoe Bay (197 mm). In comparison, previous estimates of mean coastal pond evaporation (1.8-2 mm day^{-1}) [*Kane and Carlson*, 1973; *Rovansek et al*., 1996; *Bowling et al*., 2003] are slightly higher than the mean daily rate from the DTLB in 1999-2009 (mean 1.6 mm day^{-1}). Both the simulated DTLB (170 mm) and overall watershed (158 mm) mean total evapotranspiration are within the wide range of previous estimates (50 to 210 mm) from coastal arctic wetlands (see *Kane et al*., [2008b], *Kane et al.* [1990], *Vourlitis and Oechel* [1997], and *Mendez et al.* [1998]). They are also similar to Barrow pan-evaporation estimates (160 mm) by *Brown et al*. [1968]. The total evapotranspiration from our

study watershed is on the higher end than to most previous estimates from Arctic Coastal Plain wetlands. This is intriguing as a) the landscape features within the study watershed (drained lake, low-and high-centered polygon, pond) are representative of the Arctic Coastal Plain in general; and b) most of the previous estimates at the Arctic Coastal Plain represent a similar time period (1990‘s through 2000‘s). It is apparent that past total evapotranspiration estimates from arctic coastal wetlands are distributed across an extremely large range of values, while our results do not support the existence of such large variability. Therefore, we recommend continued efforts in directly measuring total seasonal evapotranspiration to determine if the variations in past estimates are real or an artifact due to differing methods.

The uncertainty in simulated evapotranspiration rates from the DTLB was well defined and low (< 16.2 mm per summer) (Table 5.6). On the other hand, we were not able to validate the model on the high-centered polygon dominated landscape due to the absence of direct measurements. If there were errors in the evapotranspiration from the high-centered polygon landscape, this might affect the overall watershed hydrology as the high-centered polygon landscape represents a major portion of the study area. High-centered polygons exhibit large micro-scale variability in soil moisture, while DTLB wetness is more spatially continuous [*Engstrom et al*., 2005]. Therefore, the modeling analysis would have benefitted from eddy covariance measurements from the high-center polygon area.

The rims of low-centered polygons play a major role in the hydrology of tundra wetlands. The observed multi-week ponding of the vegetated drained lake basin was impossible to simulate using the original 5 m DEM. The long ponding period was not replicated until we added an 8 cm high barrier, which was intended to represent the low-center polygon rims found near the outlet of the watershed. As suggested by *Kane et al*. [2003], we showed that low-center polygons promoted

increased storage of snowmelt water that buffered against near-surface soil drying in summer.

The modeling results, which highlight the role of the antecedent soil moisture conditions on spring runoff, complement the model simulations by *Bowling and Lettenmaier* [2010] who emphasized the importance of fall lake storage status on the follow spring runoff. Although summer precipitation rarely produced runoff by itself, it had a major control on the following spring runoff. This because variations in net summer water balance (P-ET) was mainly determined by changes in the summer precipitation.

Simulated runoff was about half of the measured quantities. It is unlikely that our underprojected runoff was mainly caused by errors in snow accumulation as snow measurements were made within each landscape feature. Although we did not account for the snow stored in the snowdrift along the boardwalk, the drift cannot possibly account for up to 70 mm of specific runoff by itself. *Sand and Kane* [1986] showed that good simulations of snowmelt runoff were not achievable until the effects of frozen ground on soil hydrologic parameters were included into the HBV hydrologic model. Here, the lower infiltration capacity of frozen soils was not accounted for (the reduced hydraulic conductivity of frozen soils was only applied to lateral flows). The underestimated runoff was therefore most likely caused by overestimated infiltration of snowmelt water. Further, the 5 m DEM failed to represent the extensive microtopographical variations within the high-centered polygon landscape such as the troughs and elevated domes. Field observations showed that troughs acted as temporary channels during snowmelt, effectively transmitting the water from the upland tundra into the DTLB. *Woo and Guan* [2006] also observed troughs acting as drainage networks in Canadian arctic wetlands. Model experiments by *Liljedahl* [2011] examining the role of high- and low-centered polygons on watershed hydrology found that the lateral export was

twice as high from the high- as from the low-centered polygons or a surface with no features.

We established good simulations of the water table elevations and evapotranspiration rates within the DTLB but the model performance of the high-centered polygon landscape is unclear. The lack of the DEM to resolve the high-centered polygon features may have a) reduced runoff and b) overestimated near-surface soil moisture. The latter could have resulted in overestimated evapotranspiration rates. However, challenges in modeling the hydrology at high-centered polygon landscape may not be the sole cause. Another possible explanation includes the unmeasured trace precipitation and condensation [*Dingman et al*., 1980; *Benson*, 1982], which would buffer the system against an increasing moisture deficit. For example, *Dingman et al.* (1980) commented that condensation of fog and dew on vegetation may equal 23 to 50 % of summer precipitation [*Hobbie*, 1980]. The addition of small but frequent trace precipitation events and evapotranspiration may produce a recycling of water vapor while the change in longer-term net vertical exchange is reduced. As the answer is likely to be complex and our information is limited (despite the extensive field data collection), we encourage future studies to refine the understanding of the hydrologic pathways and storage within high-centered polygon landscapes.

The interannual variability limits the use of traditional hydrologic techniques. Water balance methods, which are often used by assuming a negligible change in the soil water storage, can result in major errors when applied in individual years. This is notable as hydrologic field studies in the Arctic are often of short duration and rarely includes direct measurements of all components of the water balance.

Continuous permafrost is often described as a key factor in the existence of wetlands under a near-desert precipitation regime by limiting the soil water storage capacity that results in a perched water table [*Woo and Young*, 2003; 2006]. Our

results present another important role of permafrost on wetland hydrology through its unique landforms (i.e. low-centered polygons), which control the lateral fluxes. We highlight the need to further explore the role of high-centered polygons on arctic wetland hydrology as they may offset the impact of low-centered polygons on watershed-scale fluxes and stocks. We recommend further experimental model analyses coupled with field studies to explore the role of permafrost in arctic wetland hydrology.

5.7 Conclusions

The application of a physically-based model at an extensively monitored site allowed for an assessment of important hydrologic controls and model performance on evapotranspiration, runoff, and water storage. Permafrost terrain features such as rims of low-centered polygons were critical in promoting the early season surface water inundation within the vegetated drained lake. However, by the end of the summer, the negative P-ET resulted in soil water storage deficits prior to freeze-up. Total summer precipitation controlled the net summer water balance (P-ET). Drained thaw lake basins appear to rarely produce summer runoff. The melting of the snowpack in spring produced the only runoff event of the year, while simultaneously recharging the antecedent soil moisture deficit. Simulations suggest that the previous summer‘s P-ET controlled the amount of the snowpack that was partitioned into runoff, while measured runoff indicates additional controls. Rain during the snowmelt and a melt event about a month before the major ablation period seemed to favor an increased partitioning of snow into runoff. The model provided good estimates of evapotranspiration, while the overestimated infiltration capacity and the coarse DEM likely prevented increased runoff simulations. Large interannual variations in all components of the water balance equation raise the importance for multi-year applications when the change in soil water storage is assumed to be negligible.

5.8 Acknowledgements

The contributing authors were L. D. Hinzman, C. E. Tweedie, J. Schulla, W. C. Oechel, and D. Zona. Thanks to Barrow Arctic Science Consortium for logistical assistance and Ukpeagvik Iñupiat Corporation for land access to the Barrow Environmental Observatory. C. L. Ping and G. Michaelson provided soil classification data from the vegetated drained thaw lake basin. R. Busey, B. Cable, and J. Long provided technical assistance. The Arctic Region Supercomputing Center offered computational support. Meteorological data and flux measurements were obtained from the Center for Global Change, San Diego State University, and radiation measurements by the Atmospheric Radiation Measurement Program, U.S. Department of Energy, Environmental Sciences Division. Financial support for this research was provided through the National Science Foundation (grants 0652838, 0632263, and 0421588), and student grants from the Swedish-America Foundation, Gemzeus Foundation, American Water Resources Association-Alaska Section, and the Center for Global Change and Arctic System Research. Any opinions, findings, conclusions, or recommendations expressed are those of the author and do not necessarily reflect the views of sponsoring organizations. Mention of specific product names does not constitute endorsement by sponsoring organizations.

5.9 Figures

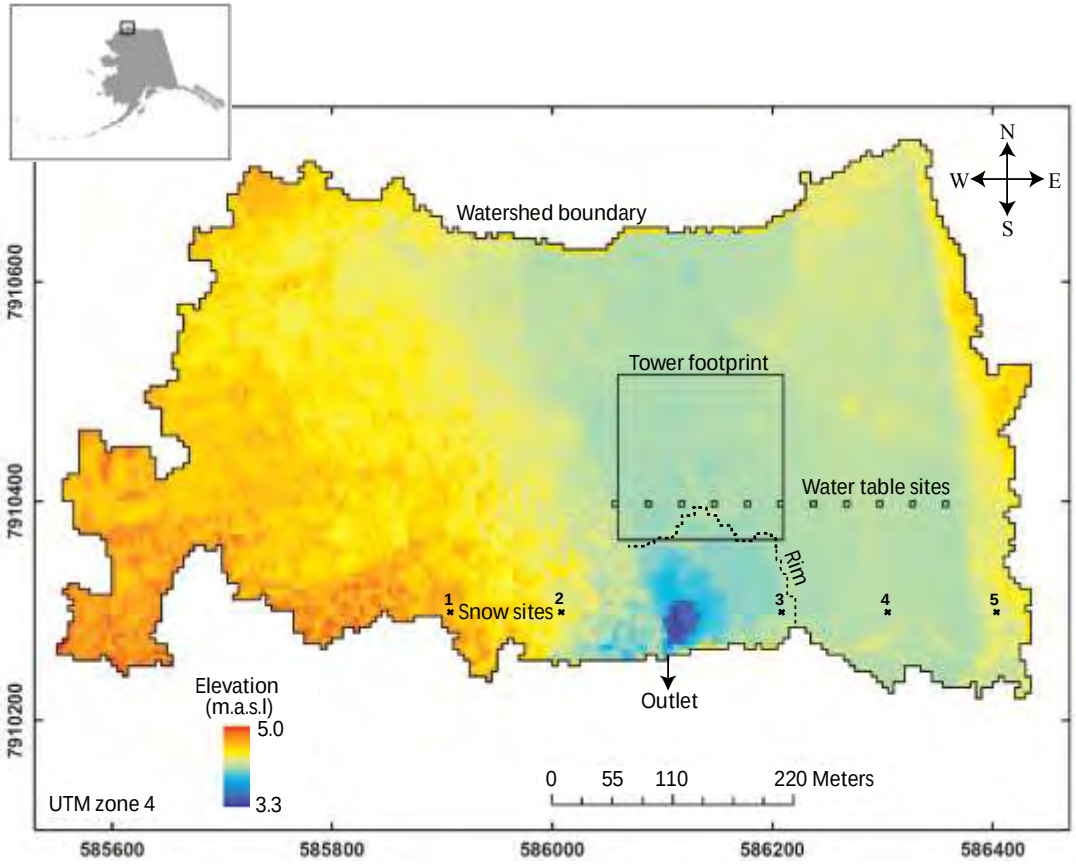

Figure 5.1 The extremely low-gradient watershed (0.31 km^2) represented by the original 5 m resolution digital elevation model (DEM), near Barrow, Northern Alaska. The slope within the vegetated drained lake basin is about 0.1 m per 1000 m (0.0001). The modified DEM was elevated (+0.08 m) at the pixels marked by a dashed black line. Also marked (black squares) are the west-east transect of water table observations (11 individual pixels), snow depth monitoring sites, the basin outlet, and the approximate footprint of the eddy covariance tower.

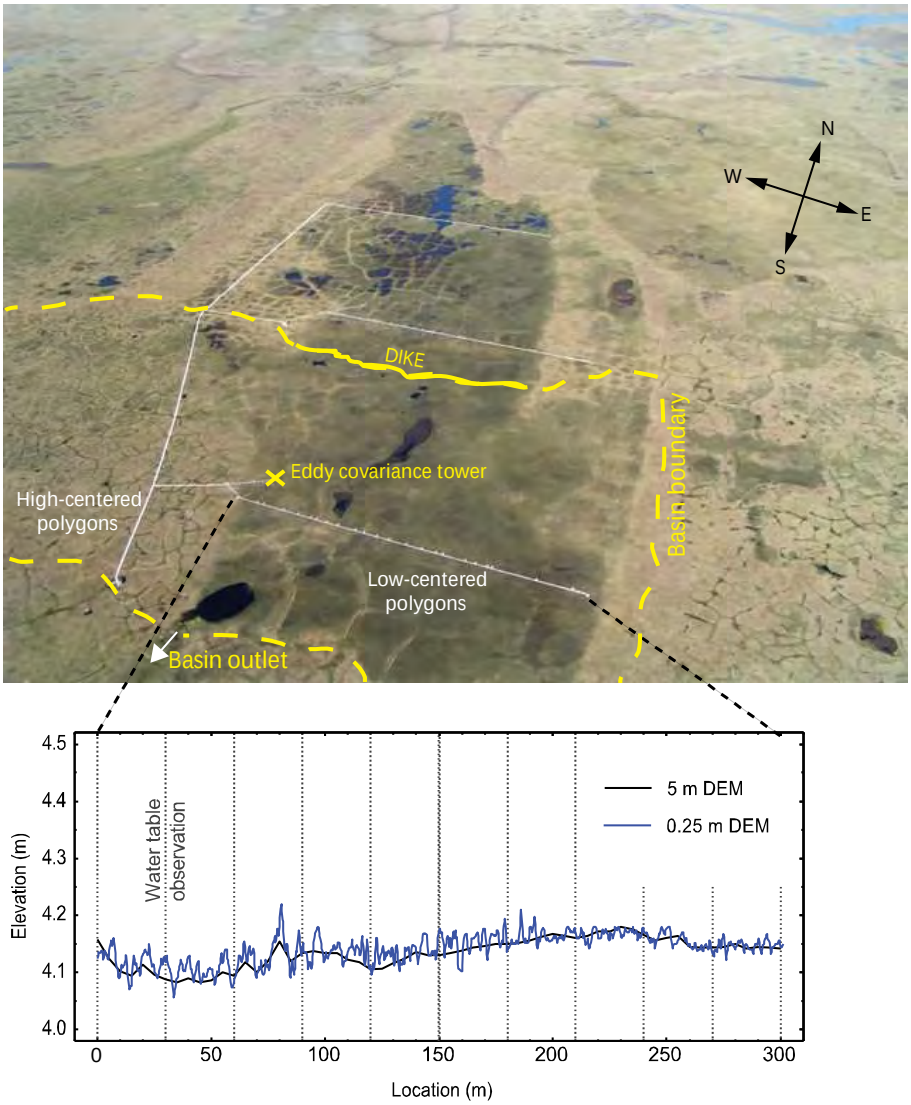

Figure 5.2 Photo including ~90% of the entire watershed was taken in August 2006. The approximate watershed boundary is marked in yellow. Solid yellow line represents the installed dike [*Zona et al.*, 2009b]. White lines represent wooden boardwalks. High-centered polygons are scattered throughout the higher elevation zones, while the vegetated drained thaw lake basin has large diameter (>15 m) low-centered polygons. Flow measurements were made approximately 20 m south of the lake (at white arrow). Bottom: The west-east transect where the water table was measured (vertical lines). Plotted is the elevation along the transect extracted from the 0.25 m DEM and the 5 m DEM.

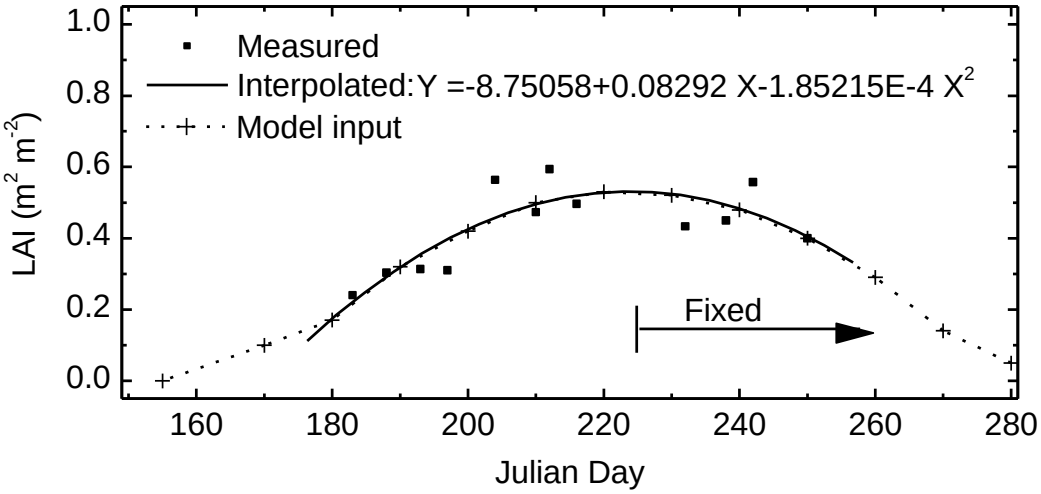

Figure 5.3 Measured (yr 2007) and modeled leaf area index (LAI) within the vegetated drained thaw lake basin. LAI for model input was obtained from every 10^{th} day LAI from the fitted equation (R^2 0.6, $P<0.01$). The senescence period was set to be initiated on Julian day 224 (start of arrow), while the start of the LAI curve was adjusted to the timing of the end of ablation period for each individual year. As a result, the length of the peak LAI period (LAI 0.53) varied amongst years.

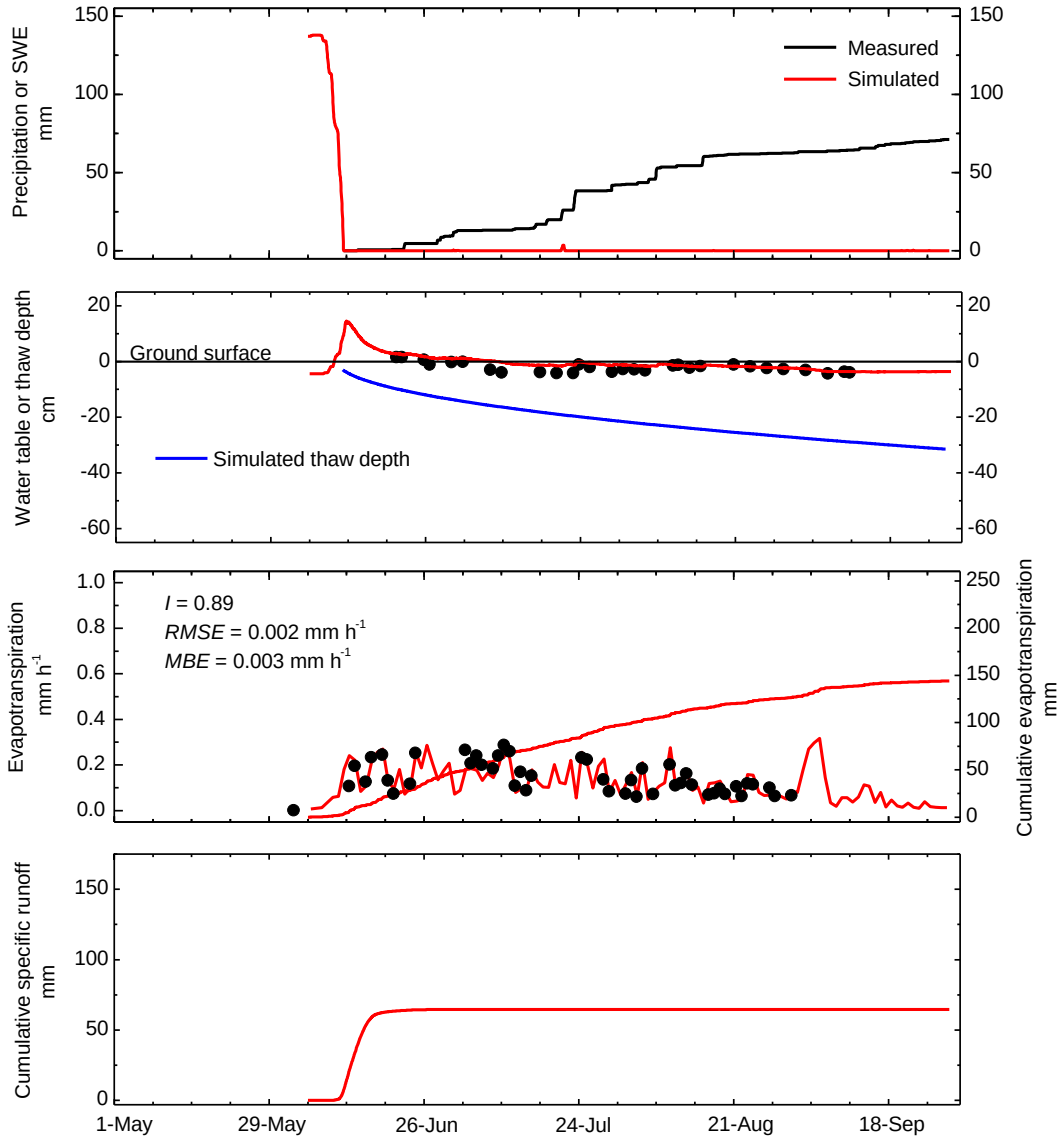

Figure 5.4a Hydrological model simulations (red) and measurements (black) of yr 2006. Only water table and evapotranspiration measurements were made in 2006.

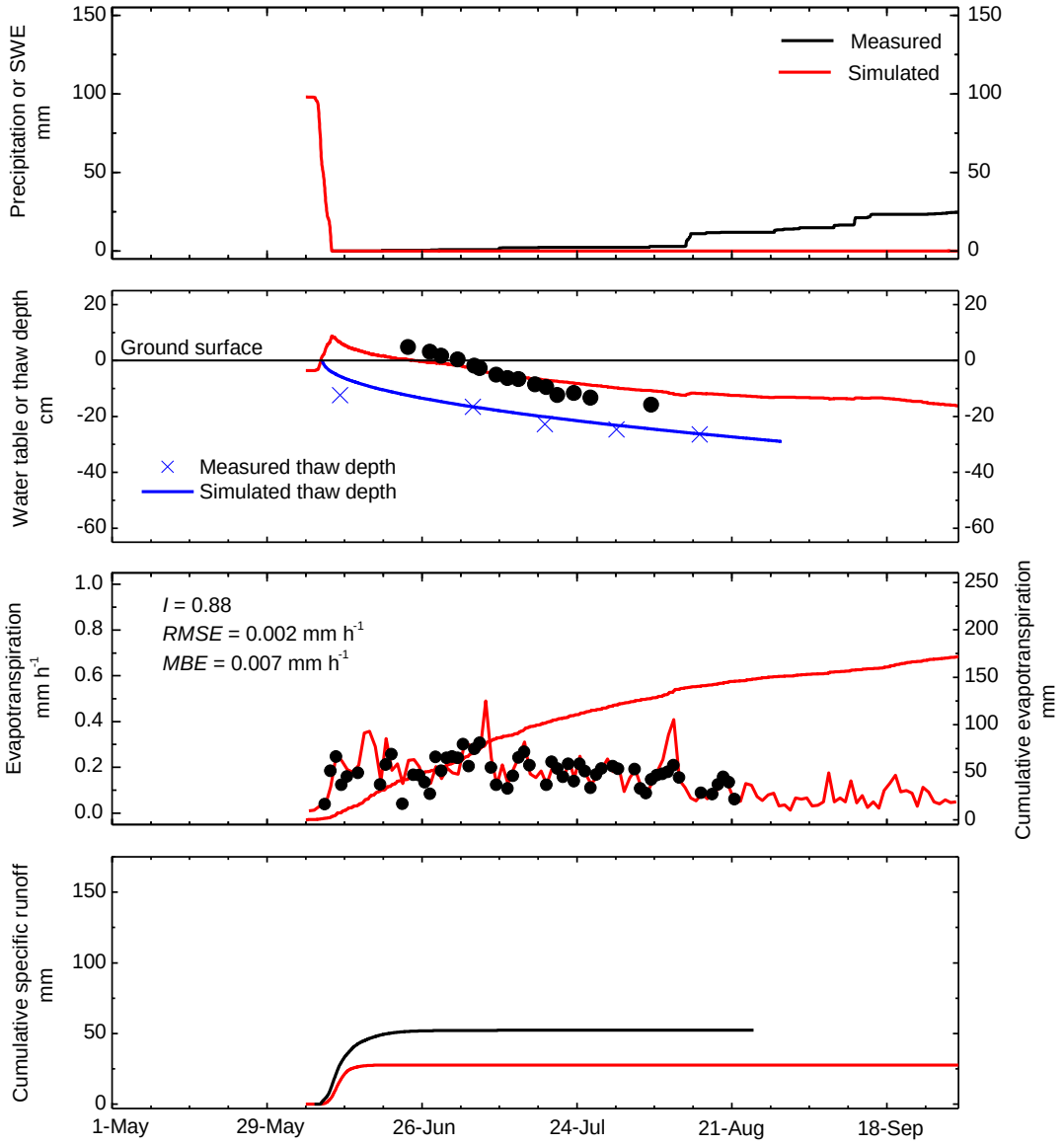

Figure 5.4b Hydrological model simulations (red) and measurements (black) of yr 2007.

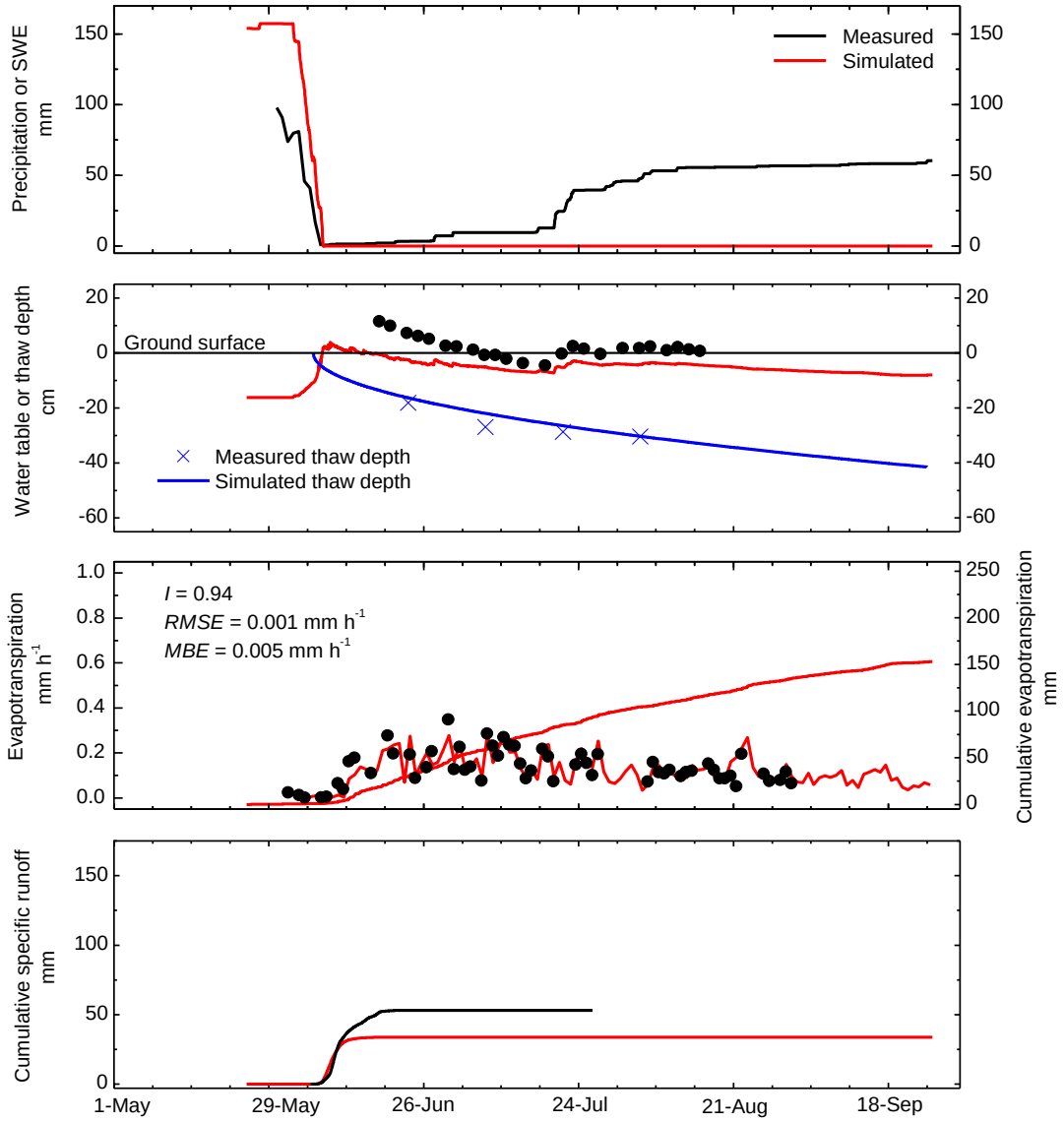

Figure 5.4c Hydrological model simulations (red) and measurements (black) of yr 2008.

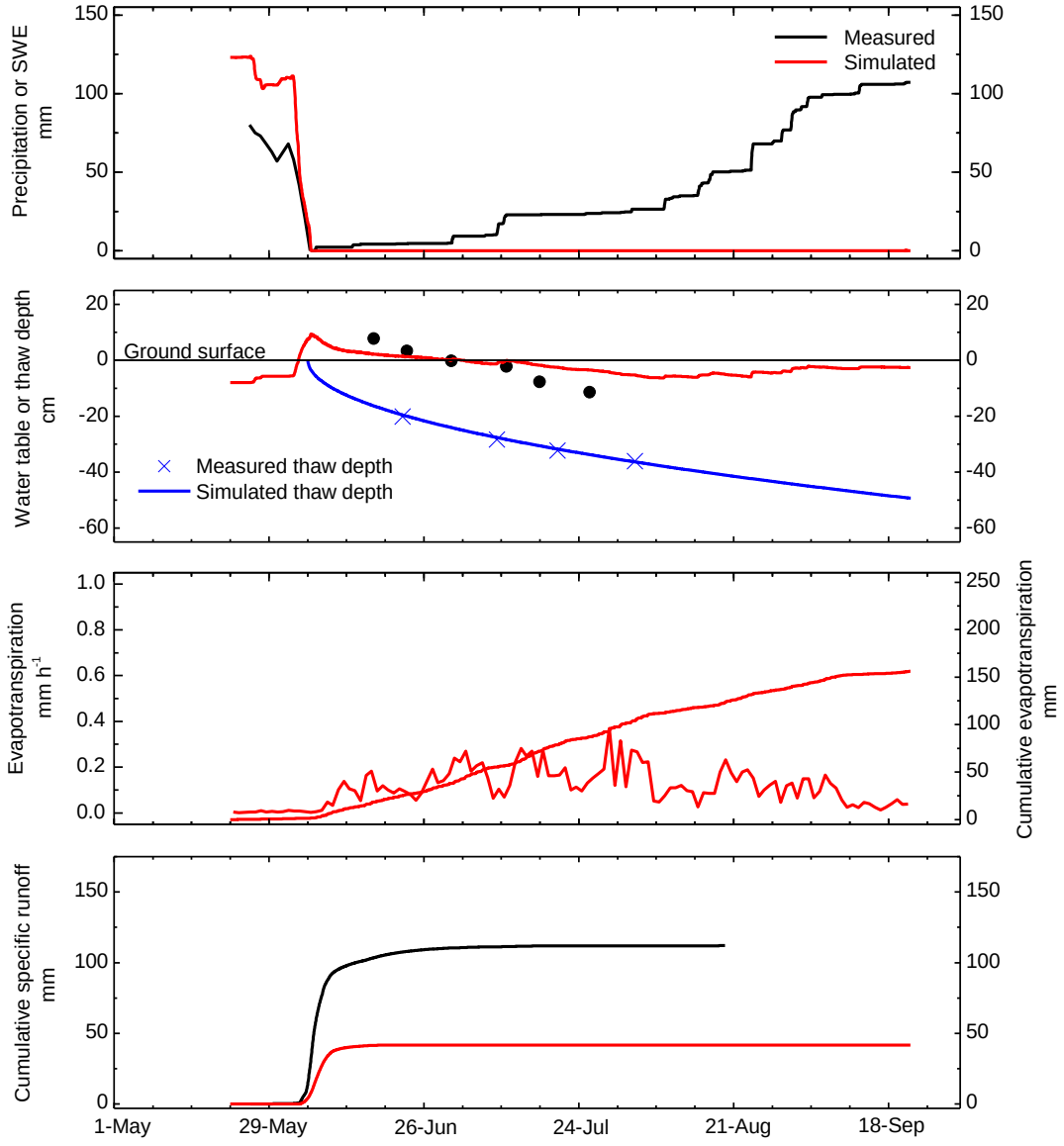

Figure 5.4d Hydrological model simulations (red) and measurements (black) of yr 2009.

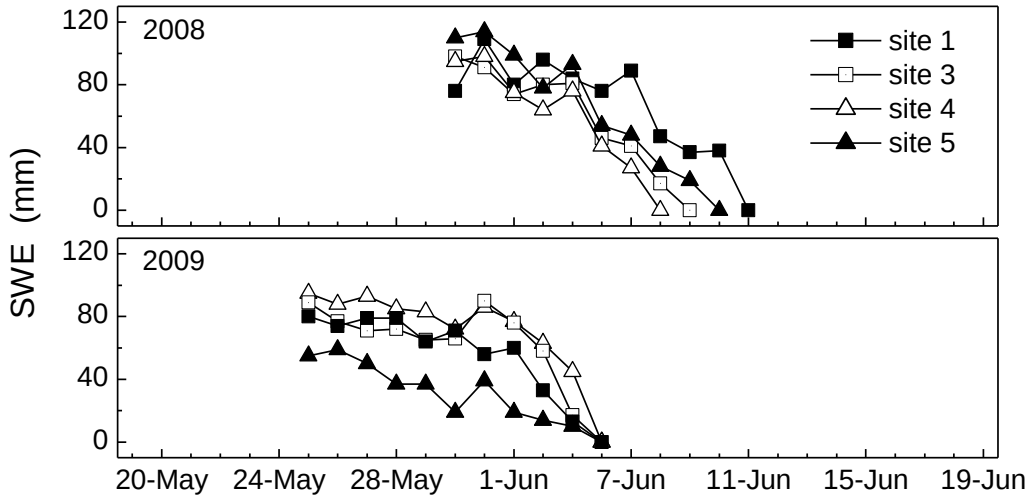

Figure 5.5 Measured ablation curve along the west-east transect, which was located ~100 m south of the water table transect, during the snowmelt period in 2008 and 2009.

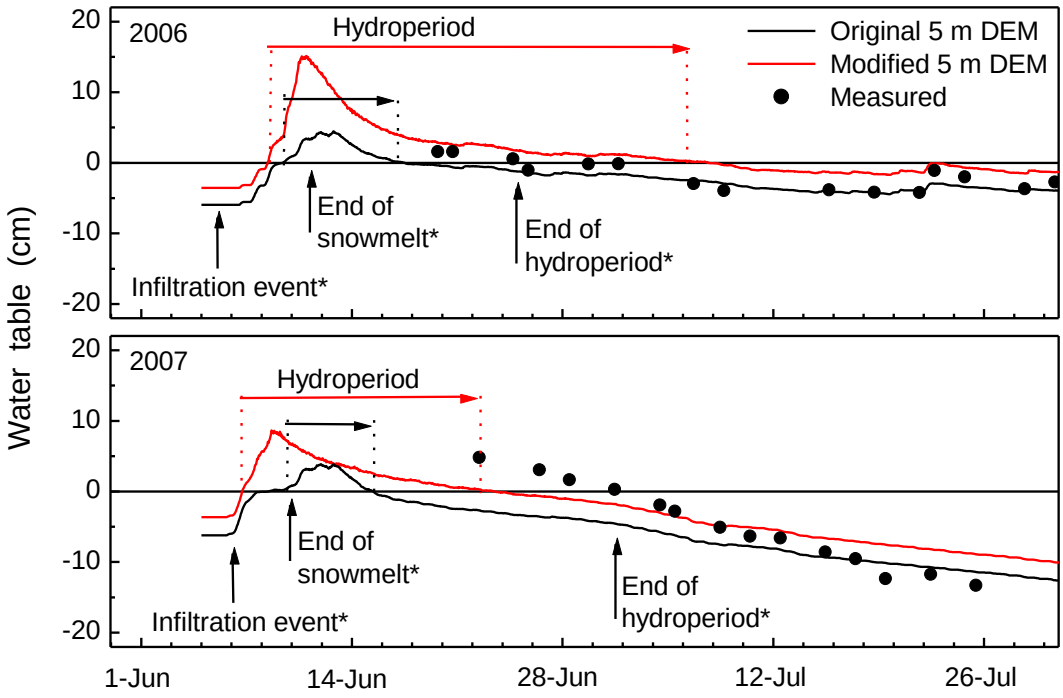

Figure 5.6 Simulations of water tables 2006 and 2007 based upon the original 5 m DEM (i.e. no modification to account for low-centered polygon rims in the lower portion of the vegetated drained thaw lake basin) in (black lines) and simulations using modified DEM (red lines). The measured (black dots) and simulated water table using modified DEM remains above the ground surface for several weeks, while the simulations using the original DEM show a brief (< 1 week) hydroperiod. Also marked are measurements (*) of infiltration events as detected by volumetric water content sensors (CS616) at 10 cm depth and the day where midday net radiation increased rapidly due to the disappearance of snow; end of ablation curve; and water table below the ground surface in the drained lake basin. The initiation of the hydroperiod was later in the original DEM due to a larger soil water storage deficit.

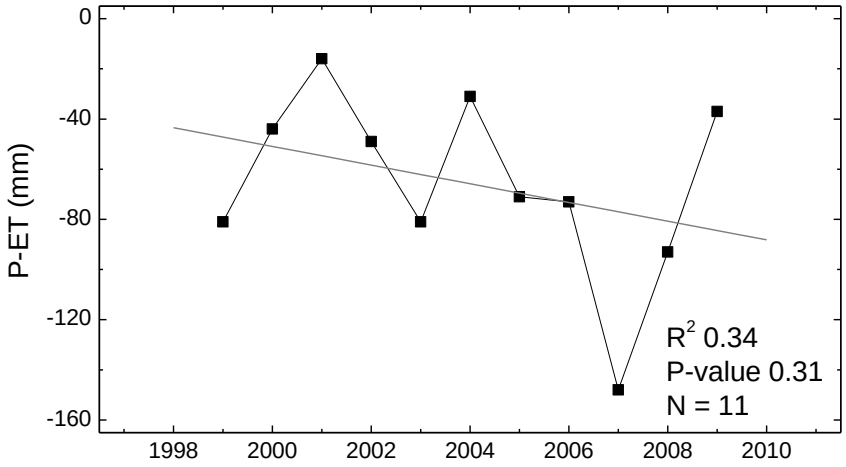

Figure 5.7 Interannual variation of net summer water balance (P-ET) 1999-2009 based upon adjusted summer precipitation and simulated evapotranspiration.

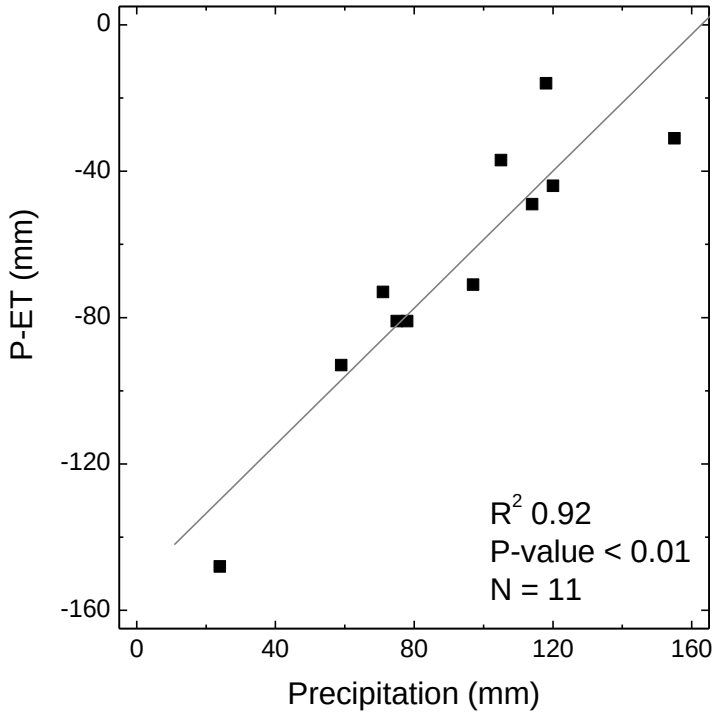

Figure 5.8 Summer net P-ET plotted against adjusted summer precipitation. The two are highly correlated (R^2 0.92, $P < 0.01$) suggesting that variations in summer precipitation was the major controller of changes in soil water storage deficit.

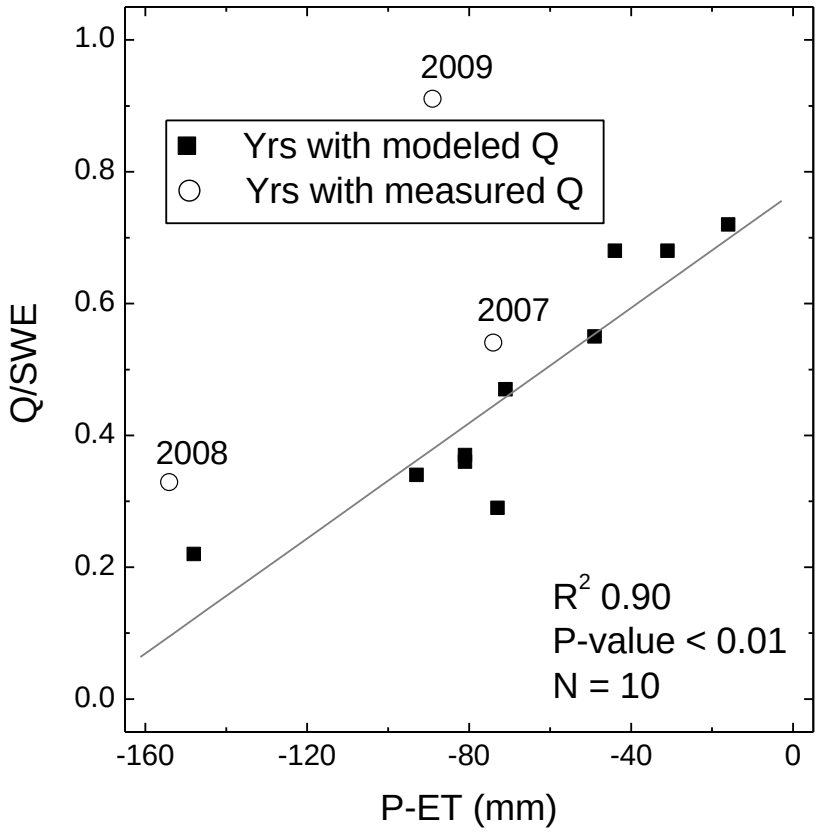

Figure 5.9 The partitioning of the accumulated snow (SWE) into runoff (Q) compared to the previous summer's net water balance (P-ET). The simulated (black) partitioning was statistically correlated to P-ET (R^2 0.90, P <0.01), while the 3 yrs or measured runoff (open circles) show larger interannual variation. The measured Q/SWE of 0.91 represented year 2009 that experienced a rainfall event (2.4 mm) during the snowmelt period.

5.10 Tables

Table 5.1 Measurements (x) of meteorology represents 1999-2009, while the hydrological field measurements of runoff, water table within the DTLB, evapotranspiration from the DTLB, and daily snow ablation was limited to the later section of the measurement period (2006-2009).

Yr	Meteorological	Snow accumulation	Runoff	Water table	Evapo-transpiration	Snow melt
1999	x	x				[1)]
2000	x	x				[1)]
2001	x	x				[1)]
2002	x	x				[1)]
2003	x	x				[1)]
2004	x	x				
2005	x	x				[1)]
2006	x	x		x	x	[1)]
2007	x	x	x	x	x	[1)]
2008	x	x	x	x	x	x
2009	x	x	x	x		x

Table 5.2 Soil parameters used in the hydrological simulations. Soil parent material was characterized by C.-L. Ping and G. Michaelson during the LAII-ATLAS study resulting in parent material clay, silt, and sand content ranging between 13-28%, 19-29%, and 46-57%, respectively.

Parameter	Horizon 1	Horizon 2	Units
Vegetated drained lake basin			
Soil type	Organic	Sandy-clay-loam	-
k_{sat}	1.00E-04 [3)]	1.00E-06 [2)]	m s^{-1}
k_recession	0.0001	1	-
theta_sat	0.8	0.4	m^3 m^{-3}
alpha	10.47 [1)]	2.34 [2)]	m^{-1}
Par_n	2.53 [1)]	1.23 [2)]	-
thickness	0.15	0.15	m
layers	1	10	-
High-centered polygon area			
Soil type	Organic	Sandy-clay-loam	-
k_{sat}	1.00E-04 [3)]	1.00E-06 [2)]	m s^{-1}
k_recession	0.0001	1	-
theta_sat	0.6	0.4	m^3 m^{-3}
alpha	10.47 [1)]	2.34 [2)]	m^{-1}
Par_n	2.53 [1)]	1.23 [2)]	-
thickness	0.1	0.15	m
layers	1	10	-

[1)] [*Price et al.*, 2008]
[2)] [*Parker et al.*, 1985]
[3)] [*Hinzman et al.*, 1991]

Table 5.3 Model parameters used in the hydrological simulations. The soil water potential for beginning of water stress (HReduDry) was based upon the most common vascular plant species *C. aquatilis*.

[*Module*] & parameter	**Value**	**Unit**
[*soil_table*]		
PMacroThresh	1000	mm h^{-1}
[*multilayer_landuse*]		
k_extinct	0.25 [1)]	-
LAI_scale	1	-
[*landuse_table*]		
SoilTillage	9_10	Julian day
RootDistr	1	-
TReuWet	1.1	-
HreduDry	10 [3,4)]	m
IntercepCap	0.16 [2)]	mm
Albedo	0.15	-
rs_interception	1	s m^{-1}
rsc	1 [3)]	s m^{-1}
rs_evaporation*	40	s m^{-1}
[*snow_model*]		
Transient zone	0.6	°C
Albedo	0.85	-
[*SurfaceRoutingModel*]		
Shortest sub-time step	1	sec.
Longest sub-time step	400	sec.
ConentrationFactor	2	-
[*permafrost*]		
SWE threshold	50	mm
Alpha	0.03	-

* rs_evaporation was calibrated to 62, 36, and 18 s m^{-1} in 2006, 2007, and 2008, respectively. Year 1999-2005, and 2009 were parameterized with the 2006-2008 average (40 s m^{-1}).

[1)] *Miller and Tieszen* [1972]

[2)] *Herwitz* [1985]

[3)] *Stoner and Miller* [1975]

[4)] *Johnson and Caldwell* [1975]

Table 5.4 Measured quantities of precipitation, accumulated snow, runoff, and length of the inundation period (hydroperiod) in 2007-2009.

	2007	2008	2009	Mean
Total annual precipitation (mm)	122	217	228	189
SWE (mm)	98	154	123	125
Runoff, Q (mm)	53	52	112	72
Hydroperiod (days)[1)]	24	28	27	26
Q/SWE	0.54	0.34	0.91	0.60
Q/P_{tot}	0.43	0.24	0.49	0.39

[1)] Defined from the end-of-snowmelt until ≥ 5 sites having water tables below the ground surface.

Table 5.5 Calibrated model parameters in the snowmelt module and their interannual variation.

	T0	**C1**	**C2**
	(°C)	(mm d^{-1} $°C^{-1}$)	(mm d^{-1} $°C^{-1}$)
1999	0	1	2.2
2000	0	1.5	2.5
2001	0	1	1.8
2002	0	1	1.8
2003	-0.5	1	3
2005	-0.3	1.5	2.5
2006	0	1	1.8
2007	0	1	1.8
2008	-2	1.5	3.5
2009	-0.9	1.5	2.6
Mean	-0.4	1.2	2.4
Min	-2	1	1.8
Max	0	1.5	3.5

T0 = Threshold air temperature for snowmelt

C1 = Temperature dependent melt factor

C2 = Wind dependent melt factor

Table 5.6 Statistical evaluation of the simulated evapotranspiration rates during morning (7 AM to 11 AM AKST), midday (12 PM to 4 PM) and evening (5 PM to 9 PM). Total mean bias error represents the total over/underestimated evapotranspiration from end of snowmelt to August 31st.

	2006			**2007**			**2008**		
	AM	Midday	PM	AM	Midday	PM	AM	Midday	PM
I	0.901	0.892	0.852	0.685	0.880	0.887	0.919	0.936	0.913
RMSE, mm	0.001	0.002	0.001	0.006	0.002	0.001	0.001	0.001	0.001
MBE, mm	0.022	0.003	-0.010	0.024	0.007	0.006	0.013	0.005	0.004
Total MBE, mm	9.6	1.2	-4.3	10.6	3.0	2.6	5.9	2.2	1.7

Table 5.7 Simulated water balance for calendar years 1999 to 2009. The snow water equivalent (SWE) is representative of the total amount of accumulated water in the snow pack prior to melt. Values in parenthesis are based upon measured runoff. The water table at the end-of-summer and the hydroperiod information represents the 11 water table measurement sites within the DTLB. All other values are representative of the entire watershed.

	1999	**2000**	**2001**	**2002**	**2003**	**2004**	**2005**	**2006**	**2007**	**2008**	**2009**	***Min***	***Max***	***Mean***	***Stdev***
End ablation	12-Jun	11-Jun	13-Jun	6-Jun	7-Jun	12-Jun	15-Jun	11-Jun	9-Jun	9-Jun	5-Jun	***5-Jun***	***15-Jun***	***10-Jun***	***3***
End summer	26-Sep	23-Sep	25-Sep	1-Oct	17-Sep	27-Sep	25-Sep	29-Sep	1-Oct	27-Sep	22-Sep	***17-Sep***	***1-Oct***	***25-Sep***	***4***
Summer length, days	106	104	104	117	102	107	102	110	114	110	109	***102***	***117***	***108***	***5***
Snow Water Equivalent, mm	119	106	123	93	95	119	95	137	98	154	123	***93***	***154***	***115***	***20***
Summer precipitation, mm	78	121	118	114	79	155	98	71	24	60	107	***24***	***155***	***93***	***36***
Specific runoff (Q), mm	59	39	84	67	52	43	65	65	28	34	42	***28***	***84***	***53***	***20***
Evapotranspiration (ET), mm	159	165	134	163	160	186	169	144	172	153	156	***134***	***186***	***160***	***14***
Transpiration, mm	51	48	38	49	58	70	67	48	77	46	55	***38***	***77***	***55***	***12***
Evaporation, mm	108	117	96	114	102	116	102	96	95	107	101	***95***	***117***	***105***	***8***
Water table end-of-summer, mm	-63	-14	26	-8	-61	-1	-44	-36	-162	-80	-26	***-162***	***26***	***-43***	***50***
Runoff ratio (Q/P_{tot})	0.30	0.17	0.35	0.32	0.30	0.16	0.34	0.31	0.23	0.16	0.18	***0.16***	***0.35***	***0.26***	***0.08***
Runoff ratio (Q/SWE)[1)]	0.50	0.37	0.59	0.72	0.55	0.36	0.68	0.47	0.29	0.22	0.34	***0.22***	***0.72***	***0.46***	***0.16***
SWE into S, %	50	63	41	28	45	64	32	53	71	78	66	***28***	***78***	***54***	***16***
Change in storage (ΔS) mm	-21	23	23	-23	-38	45	-41	-1	-78	27	32	***-78***	***45***	***-5***	***38***
Hydroperiod (HP), days	25	66	76	42	26	60	28	43	13	24	34	***13***	***76***	***40***	***20***
HP mean water depth, mm	37	35	33	13	35	24	36	34	22	24	28	***13***	***37***	***29***	***8***
HP, % of summer	24	63	73	36	25	56	27	39	11	22	31	***11***	***73***	***37***	***19***
P-ET, mm	-81	-44	-16	-49	-81	-31	-71	-73	-148	-93	-49	***-148***	***-16***	***-67***	***36***
Evaporation, % of ET	68	71	72	70	64	62	60	67	55	70	65	***55***	***72***	***66***	***5***
Mean total daily ET, mm	1.50	1.59	1.29	1.39	1.57	1.74	1.66	1.31	1.51	1.39	1.43	***1.29***	***1.74***	***1.49***	***0.14***

Table 5.8 Simulated evapotranspiration within the vegetated drained thaw lake basin 1999-2009.

	1999	**2000**	**2001**	**2002**	**2003**	**2004**	**2005**	**2006**	**2007**	**2008**	**2009**	***Min***	***Max***	***Mean***	***Stdev***
Evapotranspiration (ET), mm	174	168	140	175	175	195	184	153	202	166	167	140	202	***173***	***17***
Evaporation, mm	122	120	102	125	116	125	116	104	122	118	111	102	125	***116***	***8***
Transpiration, mm	52	48	38	50	58	70	68	49	80	48	57	38	80	***56***	***12***
% Evaporation	0.70	0.71	0.73	0.71	0.66	0.64	0.63	0.68	0.60	0.71	0.66	0.60	0.73	***0.68***	***0.04***
Mean daily ET, mm	1.64	1.62	1.35	1.50	1.72	1.82	1.80	1.39	1.77	1.51	1.53	1.35	1.82	***1.60***	***0.16***

5.12 Appendix

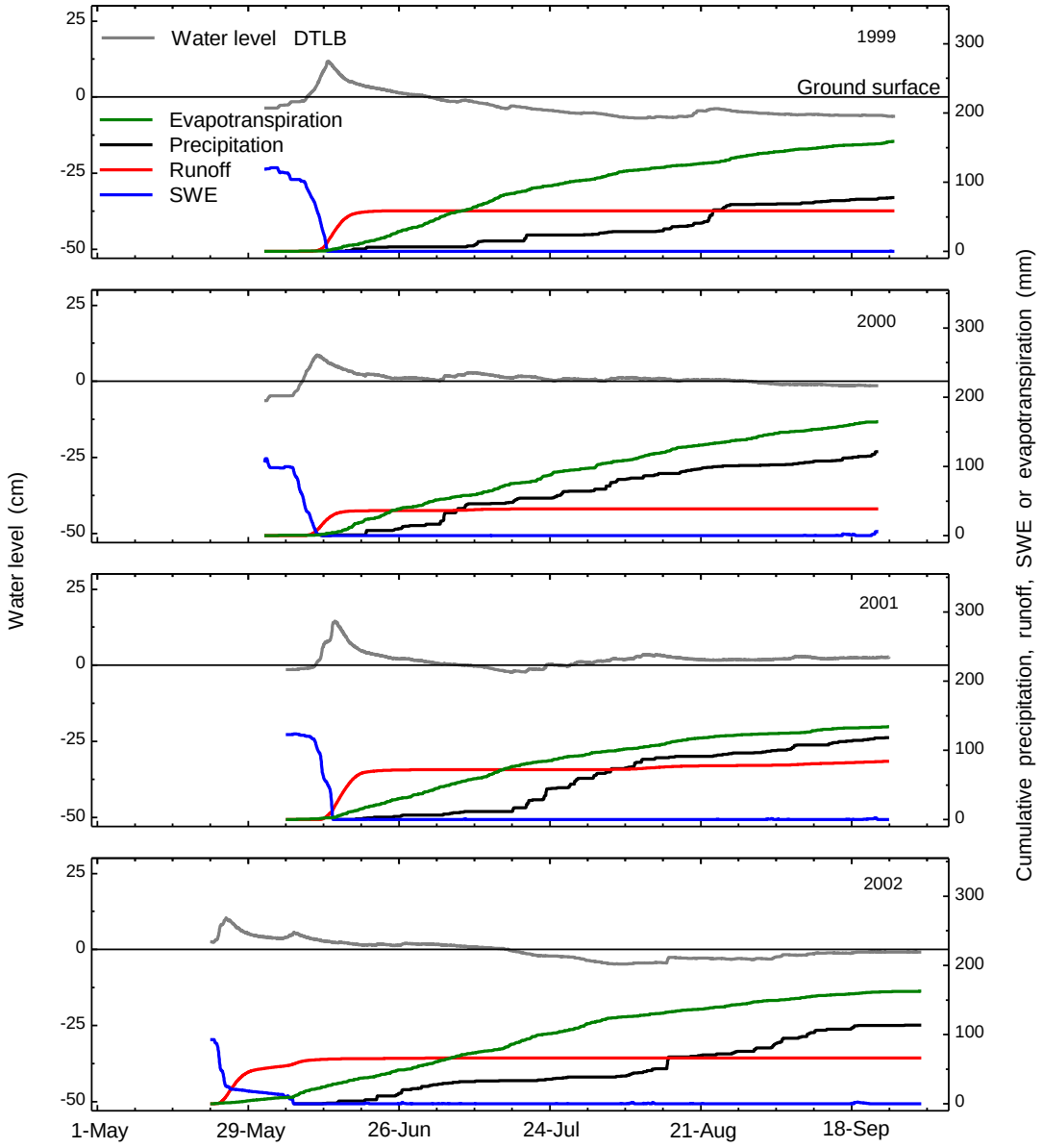

Appendix 5.1a Simulated water table, specific runoff, snow water equivalent (SWE), and evapotranspiration 1999-2002.

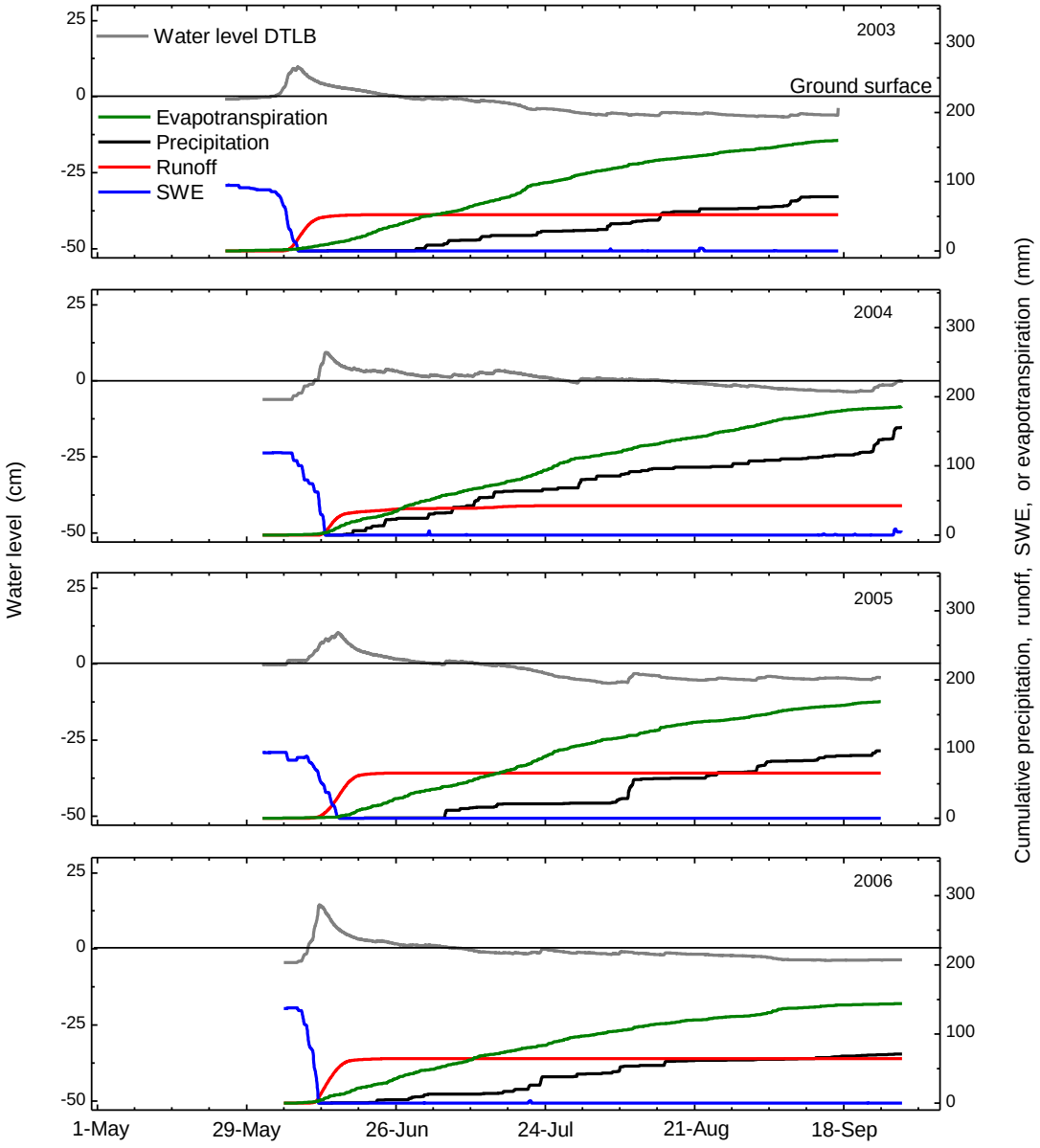

Appendix 5.1b Simulated water table, specific runoff, snow water equivalent (SWE), and evapotranspiration 2003-2006.

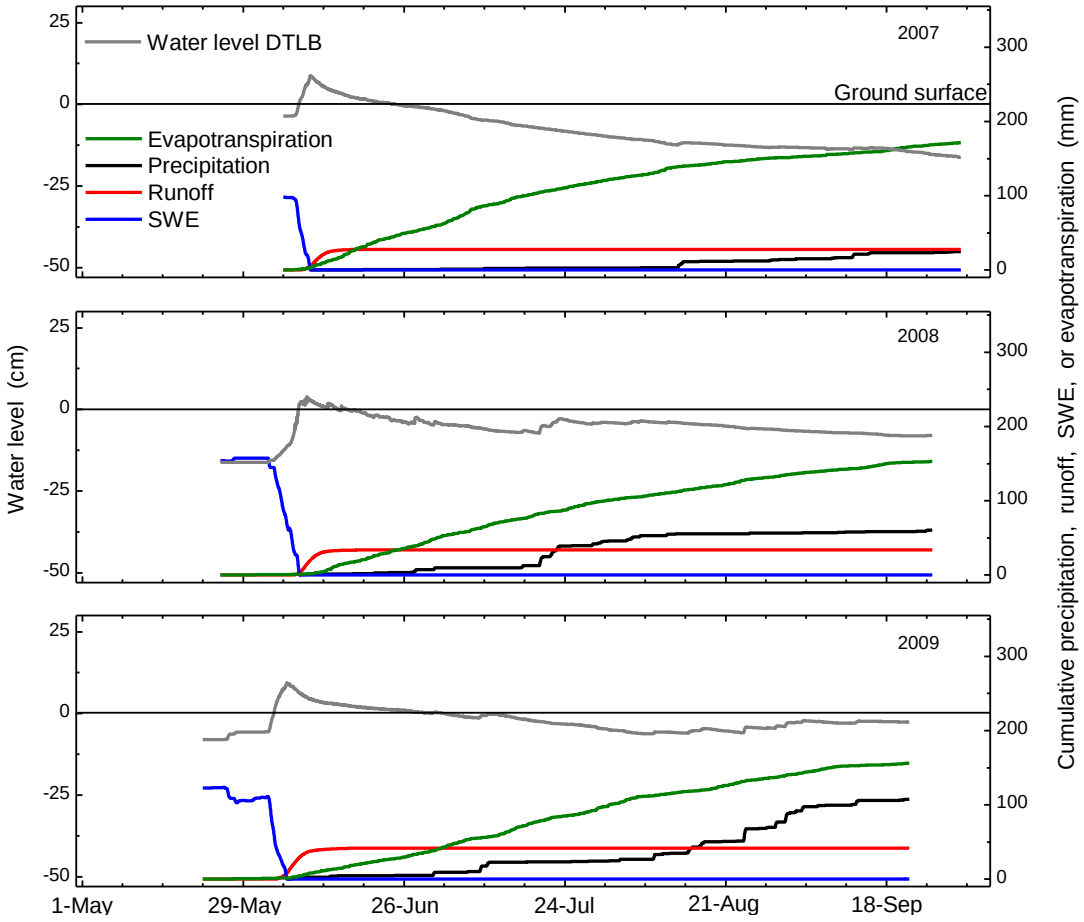

Appendix 5.1c Simulated water table, specific runoff, snow water equivalent (SWE), and evapotranspiration 2007-2009.

5.11 References

Benson, C. S. (1969), The seasonal snow cover of arctic Alaska, *Arctic Institute of North America Research Paper 51*, 47.

Benson, C. S. (1982), Reassessment of winter precipitation of Alaska's arctic slope and measurements on the flux of windblown snow, *Research Report UAG R-288*, Geophysical Institute, University of Alaska Fairbanks, Fairbanks, AK.

Bharati, L., C. Rodgers, T. Erdenberger, M. Plotnikova, S. Shumilov, P. Vlek, and N. Martin (2008), Integration of economic and hydrologic models: Exploring conjuctive irrigation water use strategies in the Volta Basin, *Agr. Water Manag., 95*, 925–936.

Black, R. F. (1954), Precipitation at Barrow, Alaska, greater than recorded, *Trans. Am. Geophys. Union, 35*, 203–206.

Bockheim, J. G., L. R. Everett, K. M. Hinkel, F. E. Nelson, and J. Brown (1999), Soil organic carbon storage and distribution in arctic tundra, Barrow, Alaska, *Soil Sci. Soc. Am. J., 63*, 934–940.

Boike, J., C. Wile, and A. Abniozva (2008), Climatology and summer energy and water balance of polygonal tundra in the Lena River Delta, Siberia, *J. Geophys. Res., 113*, G03025, doi:10.1029/2007JG000450.

Bowling, L. C., D. L. Kane, R. E. Gieck, L. D. Hinzman, and D. P. Lettenmaier (2003), The role of surface storage in a low-gradient Arctic watershed, *Water Resour. Res., 39*(4), 1087, doi:10.1029/2002WR001466.

Bowling, L. C., and D. P. Lettenmaier (2010), Modeling the Effects of Lakes and Wetlands on the Water Balance of Arctic Environments, *J. of Hydrometeorol., 11*(2), 276–295. doi: 10.1175/2009JHM1084.1

Bring, A., and G. Destouni (2009), Hydrological and hydrochemical observation status in the pan-Arctic drainage basin, *Polar Res., 28*(3), 327–338.

Brown, J., and P. L. Johnson (1965), Pedo-ecological investigations at Barrow, Alaska, *Tech. Rep. 159:32*, 32 pp., U.S. Army CRREL, Hanover, NH.

Brown, J., S. L. Dingman, and R. I. Lewellen (1968), Hydrology of a drainage basin on the Alaskan Coastal Plain, *Report 240*, Cold Regions Research and Engineering Laboratory, U.S. Army, Hanover, NH.

Brown, J., P. C. Miller, L. L. Tieszen, and F. L. Bunell (1980), An Arctic Ecosystem: The coastal tundra at Barrow, US/ISP synthesis series 12, Dowden, Hutchingson and Ross, Inc., Stroudsburg, PA.

Cullmann, J., T. Krause, and A. Philipp (2008), Enhancing flood forecasting with the help of a process based calibration, *Phys. Chem. Earth, 33*, 1111–1116.

Dennis, J. G., L. L. Tieszen, and M. A. Vetter (1978), Seasonal dynamics of above- and below-ground production of vascular plants at Barrow, Alaska, in *Vegetation and production ecology of an Alaska Arctic tundra*, edited by L. L. Tieszen, pp. 113–140, Springer-Verlag, New York, NY.

Dingman, S. L., R.G. Barry, G. Weller, C. Benson, E.F. LeDrew, and C.W. Goodwin, (1980), Climate, snow cover, microclimate, and hydrology, in *An Arctic Eco- system: the Coastal Tundra at Barrow, Alaska*, edited by J. Brown *et al*., pp. 30-56. Dowden, Hutchinson and Ross Inc., Stroudsburg, PA.

Donner, N. (2007), Hydrological windows in low-centered arctic polygons: A landscape ecological perspective on polygon mires, M.S. thesis, Greifswald University, Germany.

Engstrom, R., A. Hope, H. Kwon, D. Stow, and D. Zamolodchikov (2005), Spatial distribution of near surface soil moisture and its relationship to microtopography in the Alaskan Arctic coastal plain, *Nordic Hydrol., 36(3)*, 219–234.

Engstrom, R., A. Hope, H. Kwon, Y. Harazono, M. Mano, and W. C. Oechel (2006), Modeling evapotranspiration in Arctic coastal plain ecosystems using a modified BIOME-BGC model, *J. Geophys. Res*., *111*, G02021, doi:10.1029/2005JG000102

French, H. M. (1996), *The periglacial environment*, Addison Wesley Longman, Edinburgh Gate, England.

Gorham, E., (1991), Northern peatlands -Role in the carbon-cycle and probable responses to climatic warming. *Ecol. Appl., 1*, 182–195.

Groisman, P. Y., and D. R. Legates (1994), The accuracy of United States precipitation, *Bulletin Am. Meteorol. Soc., 75*(2), 215–227.

Gutowski, W. J., H. Wei, C. J. Vörösmarty, and B. M. Fekete (2007), Influence of Arctic wetlands on Arctic atmospheric circulation, *J. Climate, 20*, 4243–4254.

Harazono, Y., M. Yoshimoto, M. Mano, G. L. Vourlitis, and W. C. Oechel (1998), Characteristics of energy and water budgets over wet sedge and tussock tundra ecosystems at North Slope Alaska, *Hydrol. Process., 12*, 2163–2183.

Harazono, Y., M. Mano, A. Miyata, R. C. Zulueta, and W. C. Oechel (2003), Inter-annual carbon dioxide uptake of a wet sedge tundra ecosystems in the Arctic, *Tellus*, B(55), 215–231.

Herwitz, S. R. (1985), Interception storage capacities of tropical rainforest canopy trees, *J. Hydrol*., 77(1-4), 237–252.

Hinkel, K. M., W. R. Eisner, J. G. Bockheim, F. E. Nelson, K. M. Peterson, and X. Dai (2003), Spatial extent, age, and carbon stocks in drained thaw lake basins on the Barrow Peninsula, Alaska, *Arctic, Antarctic, and Alpine Res. 35*, 291–300.

Hinkel, K. M., R. C. Frohn, F. E. Nelson, W. R. Eisner, and R. A. Beck (2005), Morphometric and spatial analysis of thaw lakes and drained lake basins in the western Arctic Coastal Plain, Alaska, *Permafrost Periglacial. Proc., 16*, 327–341.

Hinzman, L. D., D. L. Kane, R. E. Gieck, and K. R. Everett (1991), Hydrological and thermal properties of the active layer in the Alaskan Arctic, *Cold Regions Sci. Technol., 19*, 95–110.

Hinzman, L. D., and D. L. Kane (1991), Snow hydrology of a headwater arctic basin: 2 Conceptual analysis and computer modeling, *Water Resources Res., 27*(6), 1111–1121.

Hinzman, L. D., D. J. Goering, and D. L. Kane (1998), A distributed thermal model for calculating soil temperature profiles and depth of thaw in permafrost regions, *J. Geophys. Res., 103*(22). 28, 975–28,991.

Hobbie, J. E. (1980), Introduction and site description, In Hobbie, J. E. (ed.), Limnology of Tundra Ponds, Stroudsburg, PA, Dowden, Hutchinson, and Ross, 19–50.

Hussey, K. M., and R. W. Michelson (1966), Tundra relief features near Point Barrow, Alaska, *Arctic, 19*, 162–184.

Johnson, D. A., and M. M. Caldwell (1975), Gas exchange of four arctic and alpine tundra plant species in relation to atmospheric and soil moisture stress, *Oecologia, 21*(2), 93–108.

Kaimal, J. C. and J. E. Gaynor (1991), Another look at sonic thermometry, *Boundary Layer Meteorol*. *56,* 401–410.

Kane, D. L., and R. E. Carlson (1973), Hydrology of the central arctic river basins of Alaska, Report, IWR-41, University of Alaska Institute of Water Resources, 51 pp.

Kane, D. L., J. D. Fox, R. D. Seifert, and G. S. Taylor (1978), Snowmelt infiltration and movement in frozen soils, in *Proceedings of the Third International Permafrost Conference*, pp. 201-206, National Research Council of Canada, Edmonton, Alberta, Canada.

Kane, D. L., and J. Stein (1984), Plot measurements of snowmelt runoff for varying soil conditions, *Geophysica, 20*(2), 123–135.

Kane, D. L., R. E. Gieck, and L. D. Hinzman (1990), Evapotranspiration from a small Alaskan watershed, *Nordic Hydrol., 21*, 253–272.

Kane, D. L., L. D. Hinzman, C. S. Benson, and G. E. Liston, (1991), Snow hydrology of a headwater Arctic basin 1. Physical measurements and process studies, *Water Resources Res., 27*(6), 1099–1109.

Kane, D. L., L. D. Hinzman, J. P. McNamara, Z. Zhang, and C. S. Benson (2000), An overview of a nested watershed study in Arctic Alaska, *Nordic Hydrol., 31*(4/5), 245–266.

Kane, D. L., R. E. Gieck, L. C. Bowling (2003), Impacts of surficial permafrost landforms on surface hydrology, in *Proceedings of the Eight International Conference on Permafrost*, edited by Phillips, Springman and Anderson, pp. 507-511, Balkema Publishers, Zurich, Switzerland.

Kane, D. L., and D. Yang (2004), Overview of water balance determinations for high latitude watersheds, in *Northern Research Basins Water Balance*, edited by D. L. Kane and D. Yang, pp. 1-12, IAHS, Oxfordshire, UK.

Kane, D. L., L. D. Hinzman, R. E. Gieck, J. P. McNamara, E. K. Youcha, and J. A. Oatley (2008a), Contrasting extreme runoff events in areas of continuous permafrost, Arctic Alaska, *Hydrol. Res., 39*(4), 287-298.

Kane, D. L., R. E. Gieck, and L. D. Hinzman (2008b), Water balance for a low-gradient watershed in Northern Alaska, in *Proceedings Ninth International Conference on Permafrost*, edited by Kane and Hinkel, University of Alaska Press, Fairbanks, AK.

Kleinn, J., C. Frei, J. Gurtz, D. Luthi, P. L. Vidale, and C. Schar (2005), Hydrologic simulations in the Rhine basin driven by a regional climate model, *J. Geophys. Res., 110* (D0), 4102.doi:10.1029/2004JD005143.

Krause, S., J. Jacobs, and A. Bronstert (2007), Modelling the impacts of land-use and drainage density on the water balance of a lowland-floodplain landscape in northeast Germany, *Ecol. Modell., 200*, 475–492.

Lachenbruch, A. H. (1962), Mechanics of thermal contraction cracks and ice wedge polygons in permafrost, Spec. Pap. Geol. Soc. Am. 70.

Leffingwell, E. de K. (1919), The Canning River region of northern Alaska, U.S. Geol. Surv. Prof. Pap. 109.

Leuning, R., E. Ohtaki, O. T. Denmead, and A. R. G. Lang (1982), Effects of heat and water vapor transport on eddy covariance measurement of CO2 fluxes, *Boundary Layer Meteorol., 23,* 209–222.

Liljedahl, A. K. (2011), *The hydrologic regime at sub-arctic and arctic watersheds: Present and projected,* PhD Dissertation, University of Alaska, Fairbanks, AK.

Mackay, J. R. (1990), Some observations on the growth and deformation of epigenic, syngenic, and anti-syngenic ice wedges, *Perm. Periglac. Process., 1*, 15–29.

McFadden, J. P., F. S. Chapin III, and D. Y. Hollinger (1998), Subgrid-scale variability in the surface energy balance of arctic tundra, *J. Geophys. Res., 103*, D22, 28,947-28,961.

Mendez, J., L. D. Hinzman, and D. L. Kane (1998), Evapotranspiration from a wetland complex on the Arctic Coastal Plain of Alaska, *Nordic Hydrol., 29* (4/5), 303–330.

Miller, P. C., and L. Tieszen (1972), A preliminary model of processes affecting primary production in the Arctic tundra, *Arctic and Alpine Res., 4*(1), 1–18.

Minke, M., N. Donner, N. Karpov, P. De Klerk, and H. Joosten (2009), Patterns in vegetation composition, surface height and thaw depth in polygon mires in the Yakutian Arctic (NE Siberia): A microtopographical characterization of the active layer, *Permafrost and Periglac. Process., 20*, 357–368.

Moore, C. J. (1986), Frequency response corrections for eddy correlation system, *Boundary Layer Meteorol., 37*, 17–35.

Myers, J. P., and F. A. Pitelka (1979), Variations in summer temperature patterns near Barrow, Alaska: Analysis and ecological interpretation, *Arct. Alp. Res., 11*, 131–144.

Oechel, W. C. and B. Sveinbjornsson, (1978), Primary production processes in Arctic Bryophytes at Barrow, Alaska, in *Vegetation and Production of an Alaskan Arctic Tundra*, edited by L.L. Tieszen, pp. 269–298, Springer-Verlag, New York, NY.

Parker, J. C., J. B. Kool, and T. van Genuchten (1985), Determining soil hydraulic properties from one-step outflow experiments by parameter estimation: II Experimental studies, *Soil Sci. Soc. Am. J., 49*, 1354–1359.

Price, J. S., P. N. Whittington, D. E. Elrick, M. Strack, N. Brunet, and E. Faux (2008), A method to determine unsaturated hydraulic conductivity in living and undecomposed *Sphagnum* moss, *Soil Sci. Soc. Am. J., 72*, 487–491.

Rastorfer, J. R. (1978), Composition and bryomass of the moss layers of two wet-tundra-meadow communities near Barrow, Alaska, in *Vegetation and Production Ecology of an Alaskan Arctic Tundra*, edited by L.L. Tieszen, pp. 169–184, Springer-Verlag, New York, NY.

Rouse, W. R., S. G. Hardill, and P. Lafleur (1987), The energy balance in the coastal environment of James and Hudson Bay during the growing season, *J. Climatol., 7,* 165–179.

Rovansek, R. J., D. L. Kane, and L. D. Hinzman (1994), Improving estimates of snowpack water equivalent using double sampling. In: Proceedings: The 50th Anniversary Eastern Snow Conference, Quebec City, Quebec, Canada, 157-163.

Rovansek, R. J., L. D. Hinzman, and D. L. Kane, (1996) Hydrology of a tundra wetland complex on the Alaskan Arctic Coastal Plain, U.S.A., *Arctic Alpine Res., 28* (3), 311–317.

Sand, K. and D. L. Kane (1986), Effects of seasonally frozen ground in snowmelt modeling, in Proceedings of the Symposium: Cold Regions Hydrology. University of Alaska-Fairbanks, Fairbanks, Alaska, American Water Resources Association, Bethesda Maryland, 321–327.

Schulla, J. (1997), Hydrologische Modellierung von Flussgebieten zur Abschatzung der Folgen von Klimaanderungen (Hydrological modelling of river basins for estimating the effects of climate change), *Zurcher Geographische Schriften 69*, ETH Zurich, Switzerland.

Schulla, J., and K. Jasper (2007), Model description WaSiM-ETH, *Internal Report*, Institute for Atmospheric and Climate Science, ETH Zurich, Switzerland.

Shiklomanov, A. I., R. B. Lammers, and C. Vörösmarty (2002), Widespread decline in hydrological monitoring threatens Pan-Arctic research, *Eos, Transactions Am. Geophys. Union, 83*(2), 13–0.

Shiklomanov, N. I., D. A. Streletskiy, F. E. Nelson, R. D. Hollister, V. E. Romanovsky, C. E. Tweedie, and J. Brown (2010), Decadal variations of active-layer thickness in moisture-controlled landscapes, Barrow, Alaska, *J. of Geophys. Res.* doi:10.1029/2009JG001248.

Shulski, M., and G. Wendler (2007), *Climate of Alaska*, 216 pp., University of Alaska Press, Fairbanks, AK.

Shutov, V., R. E. Gieck, and L. D. Hinzman, D. L. Kane (2006), Evaporation from land surface in high latitude areas: a review of methods and study results, *Nordic Hydrol,*. ***37,*** 393–411.

Stoner, W. A, and P. C. Miller (1975), Water relations of plant species in the wet coastal tundra at Barrow, *Alaska, Arctic Alpine Res., 7*(2), 109–124.

Tanner, C. B., and G. W. Thurtell (1969), Anemoclinometer measurements of Reynolds stress and heat transport in the atmospheric surface layer, *Tech Rep*. *ECOM-66-G22-F*, 82 pp., University of Wisconsin, USA.

Vourlitis, G. L., and W. C. Oechel (1997), Landscape-scale CO2, H2O vapor and energy flux of moist-wet coastal tundra ecosystems over two growing seasons, *J. Ecol., 85*, 5, 575–590.

Vourlitis, G. L., and W. C. Oechel (1999), Eddy covariance measurement of CO_2 and energy fluxes of Alaskan tussock tundra ecosystem, *Ecol., 80*(2), 686–701.

Walker, D. A., H. E. Epstein, W. A. Gould, A. M. Kelley, A. N. Kade, J. A. Knudson, W. B. Krantz, G. Michaelson, R. A. Peterson, C.-L. Ping, M. K. Raynolds, V. E. Romanovsky and Y. Shur (2004), Frost-boil ecosystems: Complex interactions between landforms, soils, vegetation and climate, *Perm. Periglac. Process. 15,* 171–188.

Walker, D. A., M. K. Reynolds, F. J. A., C. Daniels, E. Einarsson, A. Elvebakk, W. A. Gould, A. E. Katenin, S. S. Kholod, C. J. Markon, E. S. Melnikov, N. G. Moskalenko, S. S. Talbot, and B. A. Yurtsev (2005), The circumpolar arctic vegetation map*, J. Veg. Sci., 16*, 267–282.

Webb, E. K., G. I. Pearman, and R. Leuning (1980), Correction of flux measurements for density effects due to heat and water vapor transfer. *Q. J. R. Meteorol. Soc. 106*, 85–100.

Webber, P. J. (1978), Spatial and temporal variation of the vegetation and its productivity, in *Vegetation and Production Ecology of an Alaskan Arctic Tundra*, edited by L.L. Tieszen, pp. 37–112, Springer-Verlag, New York, NY.

Wei, H., W. J. Gutowski Jr., C. J. Vörösmarty, and B. M. Fekete (2002), Calibration and validation of a regional climate model for pan-Arctic hydrologic simulation, *J. Climate*, 15, 3222–3236.

Wessel, D. A., and W. R. Rouse (1994), Modelling evaporation from wetland tundra, *Boundary-Layer Meteorol., 68,* 109-130.

Willmott, C. J. (1982), Some comments on the evaluation of model performance, *Bull. of Am. Meteorol. Soc., 63*, 1309–1313.

Willmott, C. J., and D. E. Wicks (1980), An empirical method for the spatial interpolation of monthly precipitation within California, *Phys. Geogr., 1*, 59–73.

Woo, M. K., and P. Steer (1979), Measurement of trace rainfall at a high arctic site, *Arctic*, *32*(1), 80–84.

Woo, M. K., P. Marsh, and J. Pomeroy (2000), Snow, frozen soils and permafrost hydrology in Canada, 1995–1998, *Hydrol. Process., 14*, 1591–1611.

Woo, M. K., and K. L. Young (2003), Hydrogeomorphology of patchy wetlands in the High Arctic, polar desert environment, *Wetlands, 23*, 291–309.

Woo, M. K., and K. L. Young (2006), High Arctic wetlands: their occurrence, hydrological characteristics, and sustainability, *J. Hydrology*, *320*, 432–450.

Woo, M. K., and X. J. Guan (2006), Hydrological connectivity and seasonal storage change of ponds in a polar oasis environment, Canadian High Arctic, Permafrost Periglac. Process., 17, 309–323.

Yang, D., B. E. Goodison, S. Ishida, and C. Benson (1998), Adjustment of daily precipitation data of 10 climate stations in Alaska: Applications of world meteorological organization intercomparison results, *Water Resour. Res., 34*(2), 241–256.

Zona, D., W. C. Oechel, K. M. Peterson, R. J. Clements, K. T. Paw, and S. L. Ustin (2009a), Characterization of the carbon fluxes of a vegetated drained lake basin chronosequence on the Alaskan Arctic Coastal Plain, *Global. Ch. Biol*., doi: 10:1111/j.1365-2486.2009.02107.x

Zona, D., W. C. Oechel, J. Kochendorfer, K. T. Paw U., A. N. Salyuk, P. C. Olivas, S. F. Oberbauer, and D. A. Lipson (2009b), Methane fluxes during the initiation of a large-scale water table manipulation experiment in the Alaskan Arctic tundra, Global Biogeochem. Cycles, 23, GB2013, doi: 10.1029/2009GB003487.

Zona, D., W. C. Oechel, J. H. Richards, S. Hastings, I. Kopetz, H. Ikawa, and S. Oberbauer (2011), Light stress avoidance mechanisms in *Sphagnum* dominated wet coastal Arctic tundra ecosystem in Alaska, *Ecology*, 9(93), 633–644.

CHAPTER 6
WATER BALANCE OF AN ARCTIC COASTAL WETLAND, BARROW, ALASKA: END-OF-21ST CENTURY PROJECTIONS

Abstract

General Circulation Model simulations were dynamically downscaled and combined with high-resolution, physically-based hydrologic modeling to project future water balance at an Arctic Coastal Plain wetland, Alaska. End-of 21st century hydrologic projections results in an intensified hydrologic cycle, with twice the annual precipitation, and increased evapotranspiration, and runoff compared to present (1999-2009). Lateral export increased four-fold from this extremely-low gradient watershed, although summer runoff remained rare. The increased evapotranspiration offset the increased summer precipitation resulting in a nearly absent change in autumn water tables within the drained lake basin (+1 cm). The reduced soil water storage deficit prior to the onset of winter and the increased accumulation of snow enhanced the spring freshet export and the partitioning of snow into runoff. The interannual variability increased in total runoff and evapotranspiration. An early snowmelt (long warm-season and higher total evapotranspiration) combined with normal summer precipitation caused one dry soil year in the future projection. This low water table was comparable to that of summer 2007 although an unusually low summer precipitation combined with near-normal evapotranspiration produced the present soil moisture anomaly. The simulations suggest limited changes to the overall surface and soil water regime under a scenario where permafrost distribution and vegetation types were held similar to present day. Given the low sensitivity of near-surface soil moisture to projected climate, changes in the surface structure and morphology could potentially dominate any direct effects by climate on the hydrologic regime.

6.1 Introduction

The Arctic is projected to receive increased air temperatures and precipitation [*Walsh*, 2008; *ACIA* 2005], while the hydrologic response is less defined [*Allen and Ingram*, 2002], particularly at scales of importance to society [*White et al.*, 2007]. General Circulation Model (GCM) simulations allow for global scale projections under a range of scenarios, but coarse spatial and temporal resolution makes it hard to assess local impacts. This is particularly true for areas such as Alaska due to complex micro-scale topography [*Kane et al*., 2003] and contrasting regional-scale orography [*Leung et al.*, 2003]. Thus, there is a need to combine downscaled climate simulations with high-resolution hydrologic modeling to produce future scenarios at scales of importance to communities.

6.2 Background

GCMs are the most widely used tools for projections of global climate change and have been heavily used in pan-Arctic scale hydrologic assessments [*McClelland et al*., 2006; *Holland et al*., 2007; *Kattsov et al*., 2007; *Rawlins et al*., 2010]. Periodic assessments by the Intergovernmental Panel on Climate Change (IPCC) have relied heavily on global model simulations of future climate. However, the enormous mathematical complexity of GCMs limits the geographical resolution that they can provide (1°-5° latitude and longitude) and hence, reduces their suitability for local-scale hydrologic predictions. The coarse resolution of GCMs further limits their capability to capture detailed synoptic and meso-scale weather systems and associated heterogeneous distribution of precipitation [*Zhang et al*., 2007a]. Regional climate downscaling techniques are therefore commonly applied to better represent and understand local weather systems and associated precipitation [*Bengtsson et al.*, 1996; *Lynch et al.*, 1998; *Wilby et al.*, 2000]. However, efforts to use downscaled climate as forcing to local scale hydrologic modeling are still limited.

Efforts in projecting the effect of a warmer climate on local-scale arctic hydrology have included various methods: hydrologic modeling forced by a specified and constant decrease/increases in air temperature and precipitation on measured time series [*Hinzman and Kane*, 1992], hydrologic modeling efforts forced by GCM [*Marsh and Lesack*, 1996], hydrologic assessments under measured specific weather conditions [*Rouse et al*., 1992; *Lafleur*, 1993], discussions of coarse GCM results on various tundra landscapes [*Woo*, 1990; *Rouse et al*., 1997] and paleoclimate analyses [*Gorham and Janssens*, 1992].

Literature suggests that warmer climate is expected to increase precipitation [*Walsh*, 2008], evapotranspiration [*Woo,* 1990; *Hinzman and Kane*, 1992; *Rouse et al*., 1992; *Lafleur,* 1993], and runoff [*Rawlins et al*., 2010]. As evapotranspiration is currently a major pathway of water loss and summer precipitation is less than evapotranspiration [*Rovansek et al*., 1996; *Mendez et al*., 1998; *Bowling et al*., 2003; *Liljedahl*, 2011], a lengthening of the thawed season may result in a drying of the Arctic wetlands [*Woo*, 1990; *Lafleur*, 1993; *Rouse et al*., 1992, 1997; *Barnett et al*., 2005]. Drier soils would not only have major local effects on vegetation [*Waltzin et al.,* 2000], but also on the regional carbon and energy exchange by becoming significant sources of CO_2 to the atmosphere [*Oechel et al.,* 1998; *Oberbauer et al*., 2007]. On the other hand, increases in soil moisture will likely result in greater carbon accumulation [*Oechel et al*., 1998].

The expectation that both precipitation and evapotranspiration will increase in a warmer climate has lead to the hypothesis of an intensified (accelerated) water cycle [*Loaciaga et al*., 1996; *Trenberth,* 1999; *Huntington*, 2006], which has been supported by Arctic observations and modeling analyses [*Rawlins et al*., 2010]. But despite the observed warming [*Houghton et al., 2001; ACIA 2005*], pan-evaporation has decreased in the Northern Hemisphere in the last 50 yrs [*Peterson et al*., 1995]. The cause of the ―pan-evaporation paradox" has been widely debated [*Brutsaert and Parlange*, 1998; *Roderick and Farquhar*, 2002; *Ohmura and Wild*,

2002; *Hobbins and Ramirez*, 2004] and is by some suggested to be consistent with an intensified water cycle [*Brutsaert and Parlange*, 1998; *Golubev et al.*, 2001; *Roderick and Farquhar*, 2002, 2004]. With a projected increase in both precipitation and evapotranspiration, the change in near-surface soil moisture may therefore be less straight-forward to determine than previously thought.

Soil moisture exerts a strong influence upon the amount of heat transferred into soils and thus the depth of the active layer [*Chahine*, 1992, *Harvey*, 1988]. For the cold, continuous permafrost zone in Northern Alaska, soil temperatures are projected to increase by the end of the century, although not enough to pass the critical hydrologic threshold of permafrost degradation [*Marchenko et al.,* 2008]. However, these simulations are based upon the assumption that present and future soil moisture variation in space and time is similar. Any deviations in the projected surface water and near-surface soil moisture compared to present conditions can therefore provide information of potential changes in ground heat transfer, and hence, shed light on future permafrost conditions.

Conversely, permafrost plays an important role on sub-arctic and arctic hydrology. In continuous permafrost landscapes, the soil water storage capacity is limited to the top soil layer that seasonally freezes and thaws (the active layer) above the permafrost [*Slaughter and Kane*, 1979]. The surface water storage capacity in seasonally inundated wetlands depends upon the unique land features that are associated with permafrost [*Liljedahl*, 2011]. Degradation of permafrost can result in major geomorphological changes [*Jorgenson et al*., 2006] due to the extensive variability in near-surface (top 10 m) ice-content. Modest climate changes [*Jorgenson et al*., 2006] and surface disturbances such as vehicle traffic and fire [*Billings and Peterson*, 1980; *Liljedahl et al*., 2007] can degrade the near-surface permafrost resulting in clearly visible surface depressions on decadal or shorter time scales. The change from a low- to a high-centered polygon landscape

associated with permafrost degradation can have major implications on overall watershed hydrology [*Liljedahl*, 2011].

This paper was formulated with one objective: to project end-of 21st century hydrologic conditions at an extremely low-gradient Arctic wetland by forcing a hydrologic model with downscaled GCM simulations. In order to gain a perspective on the degree of change from current to future hydrologic conditions, we compared our end-of-the 21st century projections to the modeling results (yr 1999-2009) presented by *Liljedahl* [2011]. Assuming that the surface topography and vegetation type stays unchanged with a limited change in active layer depth, we hypothesize that despite the projected increase in air temperatures and longer thaw season, an increase in summer precipitation will offset any increase in evapotranspiration. Our selection of GCM for downscaling was limited as we chose to run the hydrologic model in sub-diurnal time steps. Accordingly, our hydrologic projections were forced with downscaled climate from one GCM.

6.3 Site Description

The site, here referred to as the Biocomplexity Experiment (BE), (71°16'51"N 156°35'47"W, elevation 4.5 m) [*Zona et al*., 2009] is located a few kilometers from the ocean near Barrow on the Arctic Coastal Plain, Northern Alaska (Fig. 6.1). Mean annual air temperature at Barrow Airport is –12.0 °C (1977-2009) where summer (June through August) averages 3.3 °C. A substantial amount of the annual precipitation (173 mm, 1977-2009) falls during June through September (99 mm) (adjusted following the method by *Yang et al.*, [1998]). Fog and drizzle are common during the summer because the sites receive a steady cool and moist wind (mean 5 m s^{-1}) from the ocean (ENE) [*Shulski and Wendler*, 2007].

The BE is representative of vegetated drained thaw lake basins [*Mackay,* 1963], which occupy approximately 26 % of the western Arctic Coastal Plain [*Hinkel et al.,* 2005] and 50 % of the Barrow Peninsula north of ~71° latitude

[*Hinkel et al*., 2003]. The poorly drained wet tundra meadow of Typic Aquiturbels soils [*Bockheim et al.*, 1999] is underlain by 600 m thick permafrost [*Brown and Johnson,* 1965]. High- and low-centered polygons are common ground features. Interannual variation of the mean active layer depth at nearby locations varies from 29 to 35 cm (1995-2009) [*Brown et al.,* 2000; *Shiklomanov et al.*, 2010].

Non-vascular vegetation contributes significantly to biomass and cover in these ecosystems [*Webber* 1974, 1978; *Oechel and Sveinbjornsson,* 1978; *Rastorfer* 1978]. Across the BE lakebed, mosses represent most of the live above ground biomass [*Zona et al*., 2009]. Vascular plant composition is represented by sedges and grasses *(Carex aquatilis*, *Eriophorum* and *Dupontia*) with an average LAI in mid-August 2006 of 0.43, 0.13 and 0.02, respectively [*Zona et al*., 2011]. In comparison, standing dead leaf biomass in the Barrow area reaches LAI‘s of 1.23 [*Dennis et al.,* 1978] resulting in only 10-20 % of direct solar radiation reaching the underlying bryophytes due to the low solar altitude [*Miller and Tieszen*, 1972]. Senescence in the region occurs at the end of August to late September [*Myers and Pitelka, 1979*].

6.4 Methods

6.4.1 Regional Climate Downscaling

The high-resolution regional model, MM5, was used to dynamically downscale global climate simulations (CCSM3) for the Alaska region in a 30 km grid resolution. Generally, there are three downscaling approaches: regional climate modeling [e.g., *Lynch et al.*, 1998], time-slice simulations with a higher resolution model driven by a GCM [e.g., *Bengstsson et al.*, 1996], and statistical downscaling [e.g., *Wilby et al.*, 2000]. Regional models are computationally prohibitive to integrate for periods on the order of a century. Further, the sparseness of meteorological data over Alaska along with its complex geographical features makes statistical downscaling problematic. Thus, we applied the time-slice

approach, which has worked successfully in a study of Alaskan glaciers‘ response to climate change [*Zhang et al.*, 2007a, b].

We employed the National Center for Atmospheric Research (NCAR) Community Climate System Model Version 3 (CCSM3) [*Collins et al*., 2006] to provide global scale perspective and a sophisticated Arctic regional modeling system, Arctic MM5 [*Zhang and Zhang*, 2004], based on the Fifth-Generation PSU/NCAR Mesoscale Model (MM5) [*Grell et al*., 1994] with the addition of coupled thermodynamic sea ice [*Zhang and Zhang*, 2001] and mixed layer ocean models [*Kantha and Clayson*, 1994], for the high-resolution regional climate downscaling. The downscaling domain employed by the Arctic MM5 has a grid spacing of 30 km, covering Alaska along with parts of northwestern Canada and northeastern Russia. The model‘s physical schemes include: Reisner mixed-phase microphysics [*Reisner et al.,* 1998]; Grell cumulus [*Grell*, 1993]; Rapid Radiative Transfer Model (RRTM) longwave radiation [*Mlawer et al*., 1997]; MRF (Medium Range Forecast) planetary boundary layer [*Hong and Pan*, 1996]; and the NOAH land surface model [*Chen and Dudhia*, 2001] where the thermodynamic sea ice model and mixed layer ocean model referenced above are coupled.

Long-term simulations with the Arctic MM5 often include nudging techniques to ensure that the model does not deviate significantly from reality [*Zhang et al*., 2007a]. We applied nudging to the region above the model-defined boundary layer, which is beneficial in maintaining an accurate synoptic environment over the course of a long-term simulation while still allowing the high-resolution model to develop the boundary layer according to its own physics. Further, we determined an systematic underestimation of simulated incoming solar radiation during spring and summer, which we corrected by applying a mean bias removal technique [*Zhang et al*., 2007a] and measurements from the ARM site in Barrow. One future time-slice projection (Sep 2090 – Nov. 2097) was used to provide changes for the 21st century based on the middle-of-the-road A1B scenario,

which represents balanced fossil and non-fossil fuel use. The climate forcing results (air temperature, wind speed, relative humidity, precipitation, and incoming solar radiation) were obtained in 2-hourly intervals.

6.4.2 Hydrologic Modeling

We chose the physically-based hydrologic model *Water Balance Simulation Model* (WaSiM-ETH) [*Schulla*, 1997; *Schulla and Jasper*, 2007] to analyze the present and future hydrologic fluxes and stores. WaSiM-ETH is a well established tool for modeling the spatial and temporal variability of hydrologic processes in complex basins ranging from less than 1 km^2 to more than 500,000 km^2. Its application has ranged from water management [*Verbunt et al.,* 2005; *Kunstmann et al*., 2008], hydrologic impacts of land use change [*Niehoff et al*., 2002; *Krause et al*., 2007], simulation of high alpine [*Klok et al.,* 2001] and arctic catchments [*Liljedahl*, 2011], to the effect of climate change on the hydrologic regime in temperate regions [*Jasper et al.,* 2006; *Middelkoop et al.*, 2001; *Kunstmann et al.,* 2004] and many others.

Four modules in WaSiM-ETH are of special interest to this particular application: 1) The extraction of water from the different soil layers is done separately for evapotranspiration and bare soil (moss) evaporation; 2) In addition to representing lateral flow through channel routing, base flow, and interflow, WaSiM-ET includes a surface routing module designed for small scale applications.; 3) Due to the uniqueness of the seasonally changing soil water storage capacity of soils underlain by impermeable permafrost, WaSiM-ETH simulates the seasonal development of the active layer through a simple static approach:

$$d_{thaw} = \propto \sqrt{n_{sf}} \qquad (1)$$

where d_{thaw} is thaw depth in m (obtained from measurements), α is an empirical coefficient, and n_{sf} is the number of snow free days (or more precisely; days with a snow water equivalent below a certain threshold [*Hinzman et al.*, 1991]). The coefficient was determined from active layer depths measurements presented by *Shiklomanov et al*. [2010]. The thaw (and hence the count of snow free days) is initiated when the SWE falls below the pre-defined SWE threshold value. Frozen soils are given a lateral hydraulic conductivity of 10^{-12} m s^{-1} while the infiltration (vertical hydraulic conductivity) is described as if the soils were unfrozen. In this application, the α-value is calibrated to measured thaw depths; 4) The module which calculates snowmelt is based upon a temperature-wind-index approach:

$$M = [c_1 + (c_2 \times u)] \times \left(T - T_{0,m}\right) \times \frac{\Delta t}{24} \qquad (2)$$

where M is the melt rate (mm h^{-1}), c_1 is the temperature dependent melt factor (mm C^{-1} d^{-1}), c_2 the wind dependent melt factor (mm C^{-1} d^{-1} · m s^{-1}), u wind speed (m s^{-1}), T air temperature (ºC), $T_{0,m}$ the temperature for beginning of snow melt (ºC) and Δt the time step (h). The temperature-wind-index parameters were determined through calibration [see *Liljedahl*, 2011].

The simulations were initiated a few days prior to the onset of the ablation period and stopped during the start of winter, which was defined as the first of 10 consecutive days that experienced mean daily air temperature below 0°C. All winter precipitation was assumed to contribute to the accumulated SWE. Leaf area index (LAI) was described through a polynomial function developed from LAI measurements in 2007 [*Liljedahl*, 2011]. The LAI was linearly interpolated between time steps of 10 days beginning from the start of thaw. The senescence was set to start on julian day 231 (August 18). Hence, the length of the maximum LAI period varied between years. Soil and surface water distribution at the end of

each simulation was used as initialization conditions for the following year. The initial condition for the first year was established by running the model into an equilibrium state with the forcing data from yr 2091. Only two simulations that used the same forcing variables were required to reach an equilibrium state where the end-of-summer water table was unchanged from one year to the other. The model has been calibrated to and validated on runoff (measured), evapotranspiration (eddy covariance method), and water table (measured) from the study basin [*Liljedahl*, 2011].

The original DEM (0.25 m horizontal resolution) was derived from airborne LIDAR. A 5 m DEM was produced from the original 0.25 m DEM by arithmetic averaging. However, the 5 m DEM was not able to resolve the polygon patterned ground features, which are important in controlling the water balance. We therefore modified the DEM to include an artificial elevated rim within the lower portion of the vegetated drained thaw lake aimed to substitute the patchwork of low-centered polygons [*Liljedahl, 2011*] (Fig. 6.1).

6.5 Results

6.5.1 Climate

The regional climate downscaling resulted in warmer conditions by the end of the century (Table 6.1). In general, the start of the summer (end of snowmelt ablation) occurred two weeks earlier (May 26). The onset of winter on the other hand remained at a similar time (late September). Mean air temperatures in June through August (JJA) increased to 4.5 ºC, which included a 1 ºC shift in both minimum and maximum mean annual JJA air temperature. The mean JJA air vapor pressure deficit (VPD) increased slightly but remained overall low (0.15 kPa). Still, the number of days in JJA that experienced a maximum VPD above 0.3 kPa more than doubled from 13 to 31 days. In fact, the minimum number of days >0.3 kPa in 2091-2097 (19 days) was higher than the mean in 1999-2009 (13 days).

Both the summer and winter precipitation doubled compared to measurements in 1999-2009. The accumulated snow by the end of the winter was on average 229 mm (2091-2097) compared to 115 mm in 1999-2009. Summer precipitation, which was in general evenly distributed across the summer (Fig. 6.2a-b), averaged 189 mm from the downscaled climate results. Interestingly, the cumulative incoming solar radiation remained nearly identical to present conditions despite the longer summers, due to more frequent clouds.

6.5.2 Hydrology

In five of the seven years, evapotranspiration represented the major pathway of water loss from the system (Table 6.2). Half of the evapotranspiration was from vascular transpiration, while moss/soil/open water evaporation represented up to 57 % in an individual year. Mean daily evapotranspiration ranged from 1.8 to 2.2 mm (mean of 1.9 mm day^{-1}). Overall, the mean total evapotranspiration (238 mm) was barely higher than the total lateral export (211 mm).

Simulated runoff occurred in connection to the snowmelt. Nearly all of the accumulated SWE was partitioned into runoff (88 %). The snow ablation was in some years interrupted by cold weather, resulting in two separate spring runoff peaks (yr 2091, 2092, and 2096). The lateral export represented on average 49 % of the annual precipitation. Only one out of the seven years showed a runoff event during the late thawed season (yr 2095). Projected summer precipitation was also the highest in 2095 (241 mm), which resulted in a water table ~5 cm above the ground surface prior to freeze-up.

Deep surface inundation in connection to the snowmelt appeared in all years at the drained thaw lake basin. The ponding was temporarily ~25 cm in depth. The hydroperiod within the drained lake lasted on average 22 days each summer, which equals 18 % of the entire mean summer length. In addition to the snowmelt inundation, two of the seven years also experienced shallow ponding prior to

freeze-up. The water table often receded to 5-10 cm depth below the ground surface in mid-summer, but late summer rainfall in combination with lower evapotranspiration rates commonly reduced the moisture deficit. The ground water table at the drained thaw lake prior to the onset of winter was on average near the surface (–2 cm).

Summer net water balance (P-ET) showed large interannual variability (-109 to 5 mm). Nonetheless, summer precipitation was on average 49 mm lower than the evapotranspiration.

6.6 Discussion

Our results are in agreement with previous global [*Huntington*, 2006] and regional scale studies [*Dery et al*., 2009], which suggested an intensification of the arctic hydrologic cycle in a warming climate [*Rawlins et al*., 2010]. All components of the water cycle increased (Table 6.3), including the soil water storage within the drained thaw lake basin. However, model projections of individual components exhibit non-linear responses to the increased precipitation and air temperatures.

Runoff drastically increased in the future projections. Even though the precipitation doubled, the overall lateral export was four times larger than the simulated present runoff (1999-2009) (Table 6.3). Although the relative change is unmatched, a projected increase in runoff is in agreement with regional-scale modeling efforts of mountainous sub-Arctic and Arctic regions [*Nohara et al*., 2006; *Kattsov et al*., 2007; *Woo et al.,* 2008]. Here, the reduced soil moisture deficits prior to freeze-up and the doubled SWE favored the large increase in spring runoff. Soil and surface water status prior to the onset of winter has shown to be a major controller on the partitioning of SWE into runoff from Arctic Coastal Plain watersheds [*Rovansek et al*., 1996; *Bowling et al*., 2003, 2010; *Liljedahl*, 2011] as snowmelt recharges any soil and surface water deficit from the previous summer. All of the accumulated snow was exported as runoff in four of the simulated years,

all which were preceded by saturated soils within the drained lake basin. It should be noted that we did not account for sublimation, which is estimated to range from 11 to 67 % of the total annual precipitation in tundra landscapes [*Hirashima et al*., 2004; *Zhang et al*., 2004] although slightly lower values have been estimated for Barrow (0 to 30 %) [*Wagner et al*., 2008]. Despite a doubled summer precipitation, summer runoff was still rare (if not absent) as is currently typical for many of the extremely low-gradient watershed at the Arctic Coastal Plain (see [*Brown et al*., 1968; *Kane et al*., 2008; *Liljedahl*, 2011].

Evapotranspiration was projected as 1.5 times that of the present summer totals, which equals an additional 78 mm yr^{-1}. The increase in evapotranspiration was favored by the increased VPD and the lengthening of the summer through an earlier onset of the thawed season. *Liljedahl* [2011] identified a threshold VPD of 0.3 kPa where the surface energy balance partitioning was no longer dominated by the sensible heat fluxes, but rather by latent heat fluxes. Therefore, the downscaled climate results, which showed an increase in the number of days experiencing a VPD > 0.3 kPa (13 to 31 days yr^{-1}), favored an increased evapotranspiration even though the net radiation remained unchanged. A slight reduction in the total incoming solar radiation during the summer prevented any additional increases in evapotranspiration. Any increased evapotranspiration caused by a longer summer, and especially an earlier thaw, was partially offset by an increased cloudiness, which resulted in almost no net change in accumulated solar radiation.

The role of vascular plants on total evapotranspiration increased during the future climate scenario. Transpiration has previously been estimated to represent between 15 and 45 % of the total evapotranspiration near Barrow [see *Engstrom et al*., 2006] and the companion study of the same watershed estimated 33 % [*Liljedahl*, 2011]. The shift in the snowmelt, which resulted in a smaller portion of the watershed experiencing saturated near-surface soils during solstice, and the extended period of peak LAI favored the increased role of vascular plants on

evapotranspiration (50 % of total evapotranspiration). It should be noted the biomass in Alaskan sedge-dominated tundra is projected to increase [*Euskirchen et al*., 2009], a potential effect on the hydrology that was not fully developed here. Accordingly, our future projections of evapotranspiration partitioning should be viewed as a first approximation.

Despite increased evapotranspiration, the altered climate forcing resulted in limited changes to the soil and surface water regime. The extensive surface inundation, which is a typical occurrence at the Arctic Coastal Plain following snowmelt [*Bowling et al*., 2003; *Liljedahl*, 2011], was also projected during the end-of-the century. Both the length of the hydroperiod and the mean inundation depth slightly increased (40 to 43 days and 29 to 65 mm, respectively). Even though the evapotranspiration increased, the water table at the vegetated drained lake was projected to be somewhat elevated (from –43 to –21 mm) prior to the onset of the winter. The limited future changes in soil water status differs from previous projections [*Woo*, 1990; *Lafleur*, 1993; *Rouse et al*., 1992, 1997; *Barnett et al*., 2005] which suggest a drying of the near-surface soils due to projected evapotranspiration drastically exceeding summer rainfall.

Nonetheless, interannual variability in our future projection resulted in individual summers experiencing dry soils (yr 2093) not unlike what *Liljedahl* [2011] documented from Barrow in summer 2007. However, important differences exist between the cause of future and present soil drying events. The dry soil of 2007 was mainly a result of an extremely low summer precipitation (24 mm), while the projected event experienced precipitation that is typical of future conditions (197 mm). Instead, the soil water deficit was promoted by the unusually long and early summer of yr 2093, which increased the total evapotranspiration (306 mm) to such an extent that it drastically exceeded the (for the future) normal summer precipitation. The role of meteorological factors in controlling the soil water status is therefore likely to shift in the future. Presently, dry wetlands soils are connected

to summers with unusually low precipitation, while future dry events are linked to an unusually early snowmelt. In other words, a normal summer precipitation in combined with an early May snowmelt can result in unusually dry soils by the end of the century.

Geomorphological changes induced by permafrost degradation could override our projections of a continued wet landscape. Micro-topographical features such as low- and high centered polygons play a major role on hydrology [*Kane et al*., 2003; *Donner*, 2007; *Liljedahl*, 2011]. Low-centered polygons retard runoff and promote surface and subsurface storage, while high-centered polygons increase runoff and reduce storage if troughs form a connected drainage network [*Liljedahl*, 2011]. In the projections presented here, we assumed no changes in the surface topography and limited change to the active layer depths. We know that rims of low-centered polygons are affecting the hydrology of the studied watershed [*Liljedahl*, 2011]. Hence, any degradation of ice-rich near-surface permafrost (i.e. the disappearance of rims and the sequential formation of troughs) could drastically affect the hydrologic fluxes and stocks and potentially dominate any direct climate forcing effects on the local hydrology. *Jorgenson et al.* [2006] documented wide-spread increase in thermokarst features at the Arctic Coastal Plain during moderate climate warming in the late 1980‘s to late 1990‘s. Accordingly, we may expect degradation of ice wedges to occur under the projected climate regime. Future efforts are therefore encouraged to merge hydrology, permafrost, vegetation, and geomorphology models and field measurements in order to further reduce the uncertainties in hydrologic projections.

6.7 Conclusion

Despite a warmer climate, the near-surface soils are projected to remain wet and temporarily inundated by the end-of-the 21st century as the projected increase in evapotranspiration is offset by an increased summer precipitation. Interannual

variability in the timing of the snowmelt, rather than the present control of below-normal summer precipitation, is projected to cause fall soil water storage deficits comparable to yr 2007. Overall, the high water table prior to freeze-up in combination with increased winter precipitation resulted in an enhanced partitioning of the accumulated snow into spring runoff. The nival-dominated runoff regime is projected to continue, although smaller late-summer lateral flow could be anticipated. Year-to-year differences in both runoff and evapotranspiration increased in the future scenarios. The intensified hydrologic regime was particularly evident in regards to runoff, which increased four-fold even though the winter precipitation doubled.

6.8 Acknowledgements

The contributing authors were L. D. Hinzman, J. Schulla, and J. Zhang. C.-L. Ping and G. Michaelson provided soil classification data from the vegetated drained thaw lake basin. U. Bhatt, J. Walsh, and X. Zhang offered thoughtful comments at the early stages of the manuscript. The Arctic Region Supercomputing Center offered computational support. Financial support for this research was provided through the National Science Foundation (grants 0652838, 0632263, and 0421588), and student grants from the Swedish-America Foundation, Gemzeus Foundation, American Water Resources Association-Alaska Section, and the Center for Global Change and Arctic System Research. Any opinions, findings, conclusions, or recommendations expressed are those of the author and do not necessarily reflect the views of sponsoring organizations. Mention of specific product names does not constitute endorsement by sponsoring organizations.

6.9 Figures

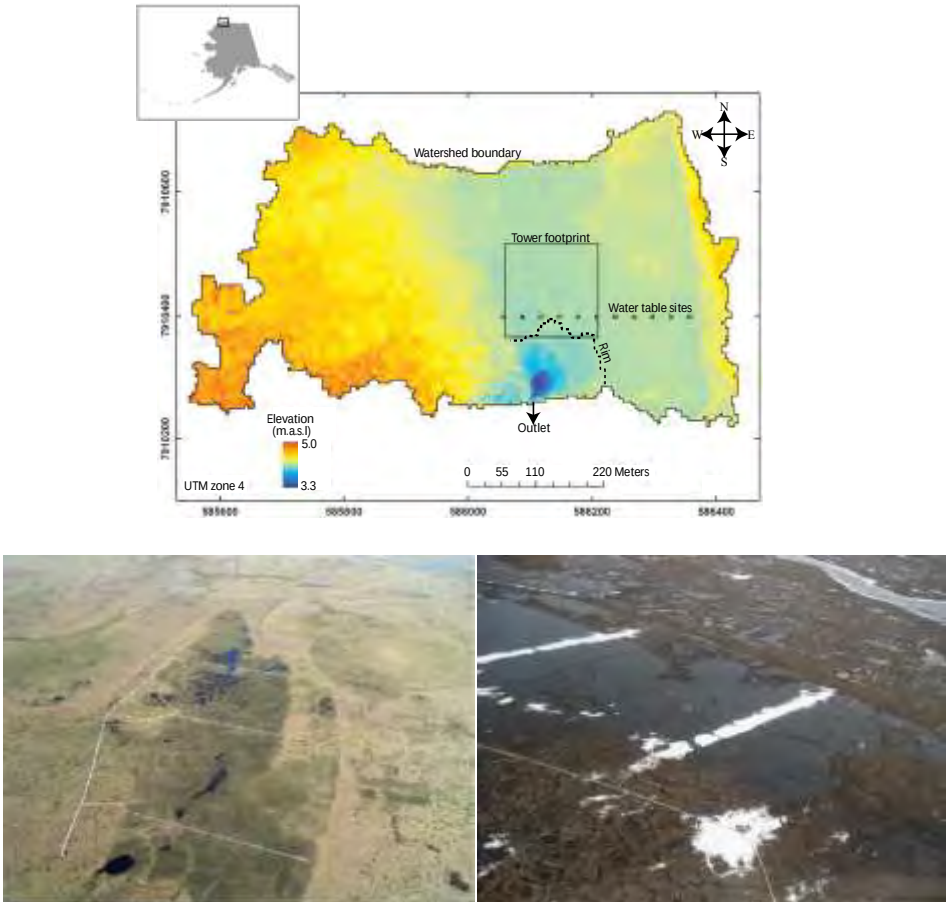

Figure 6.1 The extremely low-gradient watershed (0.31 km^2) represented by the original 5 m resolution digital elevation model (DEM), near Barrow, Northern Alaska. The slope within the vegetated drained lake basin is about 0.1 m per 1000 m (<0.1 %). The modified DEM was elevated (+0.08 m) at the pixels marked by a dashed black line. Also marked are the west-east transect of water table sites (11 individual pixels), and the basin outlet. The square represents the approximate footprint of the eddy covariance tower measurements that were used to validate simulated evapotranspiration in *Liljedahl* [2011]. The estimated model error in total seasonal evapotranspiration was defined as < 16 mm/yr. At the bottom are aerial photos of the basin in August 2006 (left) and June 2009 (right) (photo credit R. Perales and H. Eicken). The drained thaw lake basin experiences extensive surface water inundation during the weeks following snowmelt, which is seen in the photo from June 2009. Also seen are late lying snowdrifts caused by elevated boardwalks and a small building.

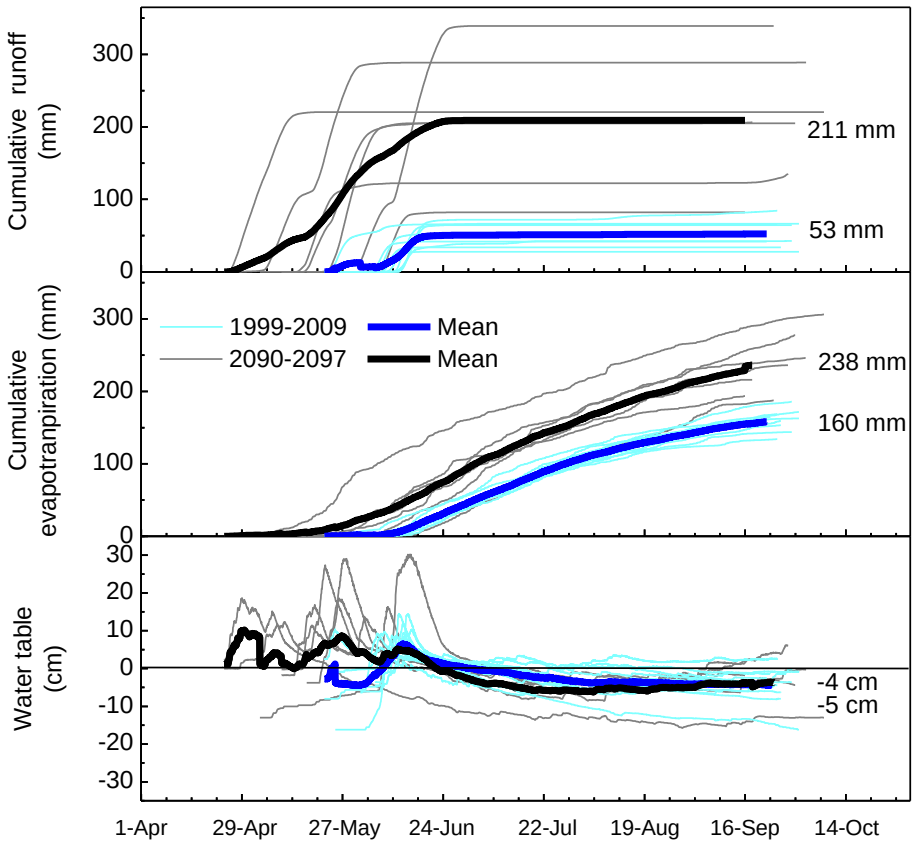

Figure 6.2 Hydrological simulations yr 2091-2097 and 1999-2009 [*Liljedahl*, 2011] of snowmelt, water table, and cumulative runoff, evapotranspiration, and summer precipitation. The water table represents the drained thaw lake basin (DTLB) and is presented in relation to the ground surface. Thin lines represent individual years while bold lines represent average conditions.

6.10 Tables

Table 6.1 A comparison between present and projected future climate variables at Barrow. The start of the summer was defined by the characteristical increase in net radiation or through ablation measurements (1999-2009) and by the simulated completion of snowmelt (2091-2097). The end of the summer was defined as the last of 10 consecutive days experiencing mean air temperatures below 0ºC. The count of days with vapor pressure deficits (VPD) exceeding 0.3 kPa were based upon daily maximum VPD (30 minute averaging intervals).

	Present (1999-2009)			Future (2091-2097)			
	Mean	**Min**	**Max**	**Mean**	**Min**	**Max**	**Change**
Start-of-summer	10-Jun	5-Jun	15-Jun	26-May	7-May	15-Jun	-14
End-of-summer	25-Sep	17-Sep	1-Oct	25-Sep	15-Sep	7-Oct	0
Length of summer, days	108	102	117	122	100	153	14
Cumulative solar radiation, MJ	1393	1170	1660	1272	846	1851	-121
SWE, mm	115	93	154	229	155	332	114
P_{summer}, mm	93	24	155	189	111	241	96
Mean JJA air temperature, ºC	3.7	2.1	5.3	4.5	3.0	6.3	1
Mean JJA VPD, kPa	0.09	0.07	0.11	0.15	0.10	0.18	0.06
VPD > 0.3 kPa, days	13	8	26	31	19	46	19

Table 3.2 Hydrological simulations yr 2091-2097. The change in storage (ΔS) across the hydrological year (onset of winter to the next onset of winter) was calculated as $P - Q - ET = \Delta S$ where P is precipitation (accumulated SWE and summer precipitation), Q runoff, and ET evapotranspiration. The hydroperiod represents the length of the inundation period, which is here defined from the average water levels at the 11 sites within the drained thaw lake basin (see Fig. 6.1).

	2091	**2092**	**2093**	**2094**	**2095**	**2096**	**2097**	***Mean***	***Min***	***Max***	***Stdev***
End ablation	21-May	27-May	7-May	7-Jun	19-May	15-Jun	27-May	***26-May***	***7-May***	***15-Jun***	***13***
End summer	2-Oct	17-Sep	7-Oct	15-Sep	27-Sep	23-Sep	29-Sep	***25-Sep***	***15-Sep***	***7-Oct***	***8***
Snow Water Equivalent, mm	289	200	225	173	155	332	266	***234***	***155***	***332***	***64***
Summer precipitation, mm	214	206	197	138	241	111	213	***189***	***111***	***241***	***46***
Specific runoff (Q), mm	289	206	220	82	135	339	205	***211***	***82***	***339***	***87***
Evapotranspiration (ET), mm	246	216	306	194	236	188	278	***238***	***188***	***306***	***43***
Transpiration, mm	118	92	193	87	114	88	153	***121***	***87***	***193***	***39***
Evaporation, mm	128	124	113	107	122	100	125	***117***	***100***	***128***	***11***
Water table end-of-summer, mm	-3	24	-130	-18	60	-37	-44	***-21***	***-130***	***60***	***60***
Runoff ratio (Q/P_{tot})	0.57	0.51	0.52	0.26	0.34	0.77	0.43	***0.49***	***0.26***	***0.77***	***0.16***
Runoff ratio (Q/SWE)	1.00	1.03	0.98	0.47	0.87	1.02	0.77	***0.88***	***0.47***	***1.03***	***0.20***
SWE into S, %	0	-3	2	53	13	-2	23	***12***	***-3***	***53***	***20***
Change in storage (ΔS) mm	-32	-16	-104	35	25	-84	-4	***-26***	***-104***	***35***	***52***
Hydroperiod (HP), days	54	54	30	28	59	48	30	***43***	***28***	***58***	***13***
HP mean water depth, mm	68	47	81	45	40	89	88	***65***	***40***	***89***	***21***
HP, % of summer	40	48	20	28	44	48	24	***36***	***20***	***48***	***12***
P-ET, mm	-32	-10	-109	-56	5	-77	-65	***-49***	***-109***	***5***	***40***
Evaporation, % of ET	52	57	37	55	52	53	45	***50***	***37***	***57***	***7***
Mean total daily ET, mm	1.84	1.91	2.00	1.94	1.80	1.88	2.22	***1.94***	***1.80***	***2.22***	***0.14***

Table 6.3 A comparison between simulated mean hydrological fluxes and stocks of 1999-2009 [*Liljedahl*, 2011] and 2091-2097.

	1999-2009	2091-2097	Diff.
End ablation	10-Jun	26-May	-15
End summer	25-Sep	25-Sep	0
Snow Water Equivalent, mm	115	234	120
Summer precipitation, mm	93	189	95
Specific runoff (Q), mm	53	211	158
Evapotranspiration (ET), mm	160	238	78
Transpiration, mm	55	121	66
Evaporation, mm	105	117	12
Water table end-of-summer, mm	-43	-21	21
Runoff ratio (Q/P_{tot})	0.26	0.49	0
Runoff ratio (Q/SWE)	0.46	0.88	0
SWE into S, %	54	12	-42
Change in storage (ΔS) mm	-5	-26	-21
Hydroperiod (HP), days	40	43	3
HP mean water depth, mm	29	65	36
HP, % of summer	37	36	-1
P-ET, mm	-67	-49	18
Evaporation, % of ET	66	50	-16
Mean total daily ET, mm	1.49	1.94	0

6.11 References

Allen, R. M, and W. J. Ingram (2002), Constraints on future changes in climate and the hydrological cycle, *Nature, 419*, 224–232.

Arctic Climate Impact Assessment (2005), *Impacts of a Warming Arctic: Arctic Climate Impact Assessment,* 144 pp., Cambridge Univ. Press, New York, NY.

Barnett, T. P., J. C. Adam, and D. P. Lettenmaier (2005), Potential impacts of a warming climate on water availability in snow dominated regions, *Nature, 438*, 303–309.

Bengtsson, L., M. Botzett, and M. Esch (1996), Will greenhouse gas-induced warming over the next 50 years lead to higher frequency and greater intensity of hurricanes? *Tellus, 48*A, 57–73.

Billings, W. D., and K. M. Peterson (1980), Vegetational change and ice-wedge polygons through the thaw-lake cycle in Arctic Alaska, *Arctic Alp. Res., 12*(4), 413-432.

Bockheim, J. G., L. R. Everett, K. M. Hinkel, F. E. Nelson, and J. Brown (1999), Soil organic carbon storage and distribution in arctic tundra, Barrow, Alaska, *Soil Sci. Soc. Am. J., 63*, 934–940.

Bowling, L. C., D. L. Kane, R. E. Gieck, L. D. Hinzman, and D. P. Lettenmaier (2003), The role of surface storage in a low-gradient Arctic watershed, *Water Resour. Res., 39*(4), 1087, doi:10.1029/2002WR001466.

Bowling, L. C., and D. P. Lettenmaier (2010), Modeling the Effects of Lakes and Wetlands on the Water Balance of Arctic Environments, *J. of Hydrometeorol., 11*(2), 276–295. doi: 10.1175/2009JHM1084.1

Brown, J., and P. L. Johnson (1965), Pedo-ecological investigations at Barrow, Alaska, *Tech. Rep. 159:32*, 32 pp., U.S. Army CRREL, Hanover, NH.

Brown, J., S. L. Dingman, and R. I. Lewellen (1968), Hydrology of a drainage basin on the Alaskan Coastal Plain, *Report 240*, Cold Regions Research and Engineering Laboratory, U.S. Army, Hanover, NH.

Brown, J., K. M. Hinkel, and F. E. Nelson (2000), The circumpolar active layer monitoring (CALM) program: Research designs and initial results, *Polar Geogr., 24*(3), 165–258.

Brutsaert, W., and M. Parlange (1998), Hydrologic cycle explains the evaporation paradox, *Nature 396*, 30.

Chahine, M. T. (1992), The hydrologic cycle and its influence on climate, *Nature 359*, 373–380.

Chen, F., and J. Dudhia (2001), Coupling an advanced land-surface hydrology model with the PSU/NCAR MM5 modeling system. Part I: Model description and implementation, *Mon. Wea. Rev., 129*, 569–585.

Collins, W. D., C. M. Bitz, M. L. Blackmon, G. B. Bonan, C. S. Bretherton, J. A. Carton, P. Chang, S. C. Doney, J. J. Hack, T. B. Henderson, J. T. Kiehl, W. G. Large, D. S. McKenna, B. D. Santer, and R. D. Smith (2006), The Community Climate System Model Version 3 (CCSM3), *J. Climate, 19*, 2122–2143.

Dennis, J. G., L. L. Tieszen, and M. A. Vetter (1978), Seasonal dynamics of above- and below-ground production of vascular plants at Barrow, Alaska, in *Vegetation and production ecology of an Alaska Arctic tundra*, edited by L. L. Tieszen, pp. 113–140, Springer-Verlag, New York, NY.

Dery, S. J., M. A. Hernandez-Henriquez, J. E. Burford, and E. F. Wood (2009), Observational evidence of an increasing hydrological cycle in northern Canada, *Geophys. Res. Lett., 36*, L13402, doi:10.1029/2009GL038852.

Donner, N. (2007), *Hydrological windows in low-centered arctic polygons: A landscape ecological perspective on polygon mires*, M.S. thesis, Greifswald University, Germany.

Engstrom, R., A. Hope, H. Kwon, Y. Harazono, M. Mano, and W. C. Oechel (2006), Modeling evapotranspiration in Arctic coastal plain ecosystems using a modified BIOME-BGC model, *J. Geophys. Res*., *111*, G02021, doi:10.1029/2005JG000102

Euskirchen, E. S., A. D. McGuire, F. S. Chapin III, S. Yi, and C. C. Thompson (2009), Changes in vegetation in northern Alaska under scenarios of climate change, 2003-2100: implications for climate feedbacks, *Ecol. Appl., 19*(4), 1022–1043.

Farouki, O. T. (1981), Thermal properties of soil, *Report* 81-1, U.S. Army Cold Regions Research and Engineering Lab., Hanover, N.H.

Golubev, V. S., J. H. Lawrimore, P. Y. Groisman, N. A. Speranskaya, S. A. Zhuravin, M. J. Menne, T. C. Peterson, and R. W. Malone, (2001), Evaporation changes over the contiguous United States and the former USSR: a reassessment, *Geophys. Res. Lett.* 28, 2665–2668.

Gorham, E., and J. Janssens (1992), The paleorecord of geochemist and hydrology in northern peatlands and its relation to global change, *Suo, 43*, 117–126.

Grell, G. (1993), Prognostic evaluation of assumptions used by cumulus parameterizations, *Mon. Wea. Rev., 121*, 764–787.

Grell, G., J. Dudhia, and D. Stauffer (1994), A description of the Fifth-Generation Penn State/NCAR Mesoscale Model (MM5), *Tech. Note NCAR/TN-398+STR,* National Center for Atmospheric Res., Boulder, CO.

Harvey, L. D. D. (1988), On the role of high latitude ice, snow, and vegetative feedbacks in the climatic response to external forcing changes, *Climate Change, 13*,191–224.

Hinkel, K. M., W. R. Eisner, J. G. Bockheim, F. E. Nelson, K. M. Peterson, and X. Dai (2003), Spatial extent, age, and carbon stocks in drained thaw lake basins on the Barrow Peninsula, Alaska, *Arctic, Antarctic, and Alpine Res. 35*, 291–300.

Hinkel, K. M., R. C. Frohn, F. E. Nelson, W. R. Eisner, and R. A. Beck (2005), Morphometric and spatial analysis of thaw lakes and drained lake basins in the western Arctic Coastal Plain, Alaska, *Permafrost Periglacial. Proc., 16*, 327–341.

Hinzman, L. D., D. L. Kane, R. E. Gieck, and K. R. Everett (1991), Hydrological and thermal properties of the active layer in the Alaskan Arctic, *Cold Regions Sci. Technol., 19*, 95–110.

Hinzman, L. D., and D. L. Kane (1992), Potential response of an Arctic watershed during a period of global warming, *J. Geophys. Res., 97*(D3), 2811–2820.

Hirashima, H., T. Ohata, Y. Kodama, H. Yabuki, N. Sato, and A. Georgadi (2004), Nonuniform distribution of tundra snow cover in Eastern Siberia, *J. Hydrometeorol.*, 5, 373–389.

Hobbins, M. T., and J. A. Ramirez (2004), Trends in pan evaporation and actual evapotranspiration across the conterminous U.S.: paradoxical or complementary? *Geophys. Res. Lett. 31*, doi: 10.1029/2004GL019846.

Holland, M. M., J. Finnis, A. P. Barrett, and M. C. Serreze, (2007), Projected changes in Arctic Ocean freshwater budgets. *J. Geophys. Res., 112*, G04S55, doi:10.1029/2006JG000354.

Hong, S. Y., and H.-L. Pan (1996), Nonlocal boundary layer vertical diffusion in a medium-range forecast model, *Mon. Wea. Rev., 124*, 2322–2339.

Houghton, J. T., Y. Ding, D. C. Griggs, M. Noguer, P. J. van Der Linden, X. Dai, K. Maskell, C. A. Johnson (2001), Climate Change 2001: The Scientific Basis. Cambridge University Press, Cambridge, UK.

Huntington, T. G. (2006), Evidence for intensification of the global water cycle: Review and synthesis, *J. Hydrol., 319*, 86–95.

Jasper, K., P. Calanca, and J. Fuhrer (2006), Changes in summertime soil water patterns in complex terrain due to climatic changes, *J. Hydrol*., 327, 550–563.

Jorgenson, M. T., Y. L. Shur, and E. R. Pullman (2006), Abrupt increase in permafrost degradation in Arctic Alaska, *Geophys. Res. Lett., 33*, L02503, doi:10.1029/2005GL024960.

Kane, D. L., R. E. Gieck, L. C. Bowling (2003), Impacts of surficial permafrost landforms on surface hydrology, In *Proceedings of the Eight International Conference on Permafrost*, edited by Phillips, Springman and Anderson, pp. 507-511, Balkema Publishers, Zurich, Switzerland.

Kane, D. L., R. E. Gieck, and L. D. Hinzman (2008), Water balance for a low-gradient watershed in Northern Alaska, In *Proceedings Ninth International Conference on Permafrost*, edited by D. L. Kane and K. M. Hinkel, University of Alaska Press, Fairbanks, AK.

Kantha, L. H. and C. A. Clayson (1994), An improved mixed layer model for geophysical applications, *J. Geophys. Res., 99*, 25,235–25,266.

Kattsov, V. M., J. E. Walsh, W. L. Chapman, V. A. Govorkova, T. V. Pavlova, and X. Zhang (2007), Simulation and projection of Arctic freshwater budget components by the IPCC AR4 global climate models, *J. Hydrometeorol., 8*(3), 571–589.

Klok, E. J., K. Jasper, K. P. Roelofsma, A. Badoux, J. Gurtz (2001), Distributed hydrological modelling of a glaciated alpine river basin. *J. Hydrol., 46(4)*, 553–570.

Krause, S., J. Jacobs, and A. Bronstert (2007), Modelling the impacts of land-use and drainage density on the water balance of a lowland–floodplain landscape in northeast Germany, *Ecol. Model., 200,* 475–492.

Kunstmann, H., K. Schneider, R. Forkel, and R. Knoche (2004), Impact analysis of climate change for an Alpine catchment using high resolution dynamic downscaling of ECHAM4 time slices, *Hydrol. Earth Syst. Sci., 8(6)*, 1030–1044.

Kunstmann, H., G. Jung, S. Wagner, and H. Clottey (2008), Integration of atmospheric sciences and hydrology for the development of decision support systems in sustainable water management, *Phys. Chem. Earth, 33*, 165–174.

Lafleur, P. M. (1993), Potential water balance response to climatic warming: The case of a coastal wetland ecosystem of the James Bay lowland, *Wetlands, 13*(4), 270–276.

Leung, L. R., L. O. Mearns, F. Giorgi, and R. Wilby (2003), Workshop on regional climate research: Needs and opportunities, *Bull. Amer. Met. Soc., 84, 89–95*.

Liljedahl, A. K. (2011), *The hydrologic regime at sub-arctic and arctic watersheds: Present and projected,* PhD Dissertation, University of Alaska, Fairbanks, AK.

Liljedahl, A. K., L. D. Hinzman, R. C. Busey, and K. Yoshikawa (2007), Physical short-term changes after a tussock tundra fire, Seward Peninsula, Alaska, *J. Geophys. Res*., F02S07, doi:10.1029/2006JF000554.

Loaciga, H. A., J. B. Valdes, R. Vogel , J. Garvey, and H. Schwarz, (1996), Global warming and the hydrologic cycle, *J. Hydrol., 174*, 83–127.

Lynch, A. H., D. L. McGinnis, and D. A. Bailey (1998), Snow-albedo feedback and the spring transition in a regional climate system model: Influence of land surface model, *J. Geophys. Res. 103*, 29037–29049.

Mackay, J. R. (1963), The Mackenzie Delta area, N. W. T., *Geographical Branch Memoir 8*, Department of Mines and Technical Surveys, Ottawa, Canada.

Marchenko, S., V. Romanovsky, and G. Tipenko (2008), Numerical Modeling of Spatial Permafrost Dynamics in Alaska, in *Proceedings of the Ninth International Conference on Permafrost*, pp. 1125–1130, University of Alaska, Fairbanks, AK.

Marsh, P., and L. F. W. Lesack (1996), Climate change and the hydrologic regime of the lakes in the Mackenzie Delta, *Limnol. Oceanogr. Spec. Iss., 41*, 849–856.

McClelland, J. W., S. J. Dery, B. J. Peterson, R. M. Holmes, and E. F. Wood (2006), A pan-arctic evaluation of changes in river discharge during the latter half of the 20th century, *Geophys. Res. Lett., 33*, L06715, doi:10.1029/2006GL025753.

Mendez, J., L. D. Hinzman, and D. L. Kane (1998), Evapotranspiration from a wetland complex on the Arctic Coastal Plain of Alaska, *Nordic Hydrol., 29* (4/5), 303–330.

Middelkoop, H., K. Daamen, D. Gellens, W. Grabs, J. C. J., Kwadjik, H. Lang, B. W. A. H. Parmet, B. Schödler, J. Schulla, and K. Wilke (2001), Impact of climate change on hydrological regimes and water resources management in the Rhine basin, *Climatic Ch., 49*, 105–128.

Miller, P. C., and L. Tieszen (1972), A preliminary model of processes affecting primary production in the Arctic tundra, *Arctic and Alpine Res., 4*(1), 1–18.

Mlawer, E. J., S. J. Taubman, P. D. Brown, and M. J. Iacono (1997), Radiative transfer for inhomogeneous atmospheres: RRTM, a validated correlated-k model for the longwave, *J. Geophys. Res., 102*, 16,663–16,682.

Myers, J. P., and F. A. Pitelka (1979), Variations in summer temperature patterns near Barrow, Alaska: Analysis and ecological interpretation, *Arct. Alp. Res., 11*, 131–144.

Niehoff, D., U. Fritsch, and A. Bronstert (2002), Land-use impacts on storm-runoff generation: scenarios of land-use change and simulation of hydrological response in a meso-scale catchment in SW-Germany, *J. Hydrol., 267*, 80–93.

Nohara, D., A. Kitoh M. Hosaka, and T. Oki (2006), Impact on climate change on river discharge projected by multimodel ensemble, *J. Hydrometeorol., 7*(5), 1076–1089.

Oberbauer, S. F., C. E. Tweedie, J. M. Welker, J. T. Fahnestock, G. H. R. Henry, P. J. Webber, R. D. Hollister, M. D. Walker, A. Kuchy, E. Elmore, and G. Starr (2007), Tundra CO2 fluxes in response to experimental warming across latitudinal and moisture gradients, *Ecol. Mono., 77*(2), 221–238.

Oechel, W. C., and B. Sveinbjornsson (1978), Primary production processes in Arctic Bryophytes at Barrow, Alaska, in *Vegetation and Production of an Alaskan Arctic Tundra*, edited by L.L. Tieszen, pp. 269–298, Springer-Verlag, New York, NY.

Oechel, W. C., G. L. Vourlitis, S. J., Hastings, R. P. Ault, and P. Bryant (1998), The effects of water table manipulation and elevated temperature on the net CO2 flux of wet sedge tundra ecosystems, *Global Change Biol., 4*, 77–90.

Ohmura, A., and W. Wild (2002), Is the hydrological cycle accelerating? *Science 29*8, 1345–1346.

Peterson, T. C., V. S. Golubev, and P. Y. Groisman (1995), Evaporation losing its Strength, *Nature, 377*, 687–688.

Rastorfer, J. R. (1978), Composition and bryomass of the moss layers of two wet-tundra-meadow communities near Barrow, Alaska, in *Vegetation and Production Ecology of an Alaskan Arctic Tundra*, edited by L.L. Tieszen, pp. 169–184, Springer-Verlag, New York, NY.

Rawlins, M. R., M. Steele, M. M. Holland, J. C. Adam, J. E. Cherry, J. A. Francis, P. Y. Groisman, L. D. Hinzman, T. G. Huntington, D. L. Kane, J. S. Kimball, R. Kwok, R. B. Lammers, C. M. Lee, D. P. Lettenmaier, K. C. McDonald, E. Podest, J. W. Pundsack, B. Ridels, M. C. Serreze, A. Shiklomanov, Ø. Skagseth, T. J. Troy, C. J. Vörösmarty, M. Wensnahan, E. F. Wood, R. Woodgate, D. Yang, K. Zhang, and T. Zhang (2010), Analysis of the arctic system for freshwater cycle intensification: Observations and expectations, *Am. Meteorol. Soc., 23*, 5715–5737.

Reisner, J., R. M. Rasmussen, and R. T. Bruintjes (1998), Explicit forecasting of supercooled liquid water in winter storms using the MM5 mesoscale model. *Quart. J. Roy. Meteor. Soc*., *124,* 1071–1107.

Roderick, M. L., and G. D. Farquhar (2002) The cause of decreased pan evaporation over the past 50 years, *Science 298*, 1410–1411.

Roderick, M. L., and G. D. Farquhar (2004), Changes in Australian pan evaporation from 1970 to 2002, *Int. J. Climatol., 24*, 1077–1090.

Rouse, W. R., D. W. Carlson, and E. J. Wieck (1992), Impacts of summer warming on the energy and water balance of wetland tundra, *Climatic Change, 22,* 305–326.

Rouse, W. R., M. S. V. Douglas, R. E. Hecky, A. E. Hershey, G. W. Kling, L. Lesack, P. Marsh, M. McDonald, B. J. Nicholson, N. T. Roulet, and J. P. Smol (1997). Effects of climate change on the freshwaters of Arctic and Subarctic North America, *Hydrol. Process., 11*, 873–902.

Rovansek, R. J., L. D. Hinzman, and D. L. Kane (1996), Hydrology of a tundra wetland complex on the Alaskan Arctic Coastal Plain, U.S.A., *Arctic Alpine Res., 28* (3), 311–317.

Schulla, J. (1997), Hydrologische Modellierung von Flussgebieten zur Abschatzung der Folgen von Klimaanderungen (Hydrological modelling of river basins for estimating the effects of climate change), *Zurcher Geographische Schriften 69*, ETH Zurich, Switzerland.

Schulla, J., and K. Jasper (2007), Model description WaSiM-ETH, *Internal Report*, Institute for Atmospheric and Climate Science, ETH Zurich, Switzerland.

Shiklomanov, N. I., D. A. Streletskiy, F. E. Nelson, R. D. Hollister, V. E. Romanovsky, C. E. Tweedie, and J. Brown. (2010), Decadal variations of active-layer thickness in moisture-controlled landscapes, Barrow, Alaska, *J. of Geophys. Res.* doi:10.1029/2009JG001248.

Shulski, M., and G. Wendler (2007), *Climate of Alaska*, 216 pp., University of Alaska Press, Fairbanks, AK.

Slaughter, C. W., and D. L. Kane (1979), Hydrologic role of shallow organic soils, In *Canadian Hydrology Symposium: 79*, Nat. Res. Council Can., 380–389.

Trenberth, K. E. (1999), Conceptual framework for changes of extremes of the hydrological cycle with climate change, *Climatic Ch., 42*, 327–339.

Verbunt, M., J. M. G. Zwaaftink, and J. Gurtz (2005), The hydrologic impact of land cover changes and hydropower stations in the Alpine Rhine basin,

Wagner, A. M., M. Sturm, G. E. Liston, L. Mahrt, and D. Vickers (2008), Five snow sublimation estimates from Barrow, Alaska, using eddy correlation and one- and two-level profile methods, Am. Geophys. Union, Fall Meeting 2008, abstract C21A-0511.

Walsh, J. E. (2008), Climate of the Arctic Marine Environment, *Ecol. App., 18(2)*, 3–22.

Waltzin, J. F., J. Pastor, C. Harth, S. D. Bridgham, K. Updegraff, and C. T. Chapin (2000), Response of bog and fen plant communities to warming and water table manipulations, *Ecol., 81*(12), 3464–3478.

Webber, P. J. (1974), Tundra primary productivity, in *Arctic and Alpine Environments*, edited by J.D. Ives and R.G. Barry, pp. 445–473, Methuen, London.

Webber, P. J. (1978), Spatial and temporal variation of the vegetation and its productivity, in *Vegetation and Production Ecology of an Alaskan Arctic Tundra*, edited by L.L. Tieszen, pp. 37–112, Springer-Verlag, New York, NY.

White, D., L. Hinzman, L. Alessa, J. Cassano, M. Chambers, K. Falkner, J. Francis, W. J. Gutowski Jr., M. Holland, R. M. Holmes, H. Huntington, D. Kane, A. Kliskey, C. Lee, J. McClelland, B. Peterson, T. S. Rupp, F. Straneo, M. Steele, R. Woodgate, D. Yang, K. Yoshikawa, and T. Zhang (2007), The arctic freshwater system: Changes and impacts, *J. Geophys. Res., 112*, G04S54, doi:10.1029/2006JG000353.

Wilby, R. L., L. E. Hay, W. J. Gutowski, R. W. Arritt, E. S. Tackle, Z. Pan, G. H. Leavesley, and M. P. Clark (2000), Hydrological responses to dynamically and statistically downscaled climate model output, *Geophys. Res. Lett., 27*, 1199–1202.

Woo, M. K. (1990), Consequences for climatic change for hydrology in permafrost zones, *J. Cold Reg. Engrg., (4)1*, 15–20.

Woo, M. K., R. Thorne, K. Szeto, and D. Yang (2008), Streamflow hydrology in the boreal region under the influences of climate and human interference, *Phil. Trans. R. Soc. B, 363*(1501), 2249–2258, doi:10.1098/rstv.2007.2197.

Yang, D., B. E. Goodison, S. Ishida, and C. Benson (1998), Adjustment of daily precipitation data of 10 climate stations in Alaska: Applications of world meteorological organization intercomparison results, *Water Resour. Res., 34*(2), 241–256.

Zhang, X. and J. Zhang (2001), Heat and freshwater budgets and pathways in the Arctic Mediterranean in a coupled ocean/sea-ice model, *J. Oceanography, 57*, 207–237.

Zhang, J., U. S. Bhatt, W. V. Tangborn, and C. S. Lingle (2007a), Climate downscaling for estimating glacier mass balances in Northwestern North America: Validation with a USGS benchmark glacier, *Geophys. Res. Lett*., doi:10.1029/2007GL031139.

Zhang J., U. S. Bhatt, W. V. Tangborn, and C. S. Lingle (2007b), Response of glaciers in northwestern North America to future climate change: An atmosphere/glacier hierarchical modeling approach, *Ann. Glaciol., 46*, 283–290.

Zhang, J., and X. Zhang (2004), Modeling study of the Arctic storm with the coupled MM5-sea ice-ocean model, In *The 5th WRF and 14th MM5 Users' Workshop*, Boulder, CO.

Zhang, Y., M. Ishikawa, T. Ohata, and D. Oyunbaatar (2004), Role of snow playing in semi-arid region of Mongolia – sublimation (evaporation) of snow cover, In *Proceedings of the 3rd International Workshop on Terrestrial change in Mongolia*, Tsukuba, Japan, p. 23–24.

Zona, D., W. C. Oechel, K. M. Peterson, R. J. Clements, K. T. Paw U, and S. L. Ustin (2009b), Characterization of the carbon fluxes of a vegetated drained lake basin chronosequence on the Alaskan Arctic Coastal Plain, *Global. Ch. Biol*., doi: 10:1111/j.1365-2486.2009.02107.x

Zona, D., W. C. Oechel, J. H. Richards, S. Hastings, I. Kopetz, H. Ikawa, and S. Oberbauer (in press), Light stress avoidance mechanisms in *Sphagnum* dominated wet coastal Arctic tundra ecosystem in Alaska, *Ecology*, 9(93), 633–644.

CHAPTER 7

7.1 General Discussion

Barrow, on the northern coast of Alaska, and Kougarok, on the central Seward Peninsula, are located hundreds of miles apart. Nonetheless, the current hydrology share common controls such as permafrost, while the present differences in fire regimes may become more similar in the future. Apart from applying site-specific physically-based models when developing future scenarios, one can substitute modern geographic proxies for time. Climatic gradients such as those between the Seward Peninsula and the Arctic Coastal Plain result in differing permafrost conditions and hydrology. The permafrost is not projected to degrade in the Northern part of Alaska by the end-of-the 21st century [*Marchenko et al.*, 2008], but field observations show that modest climate warming in recent decades has caused ground subsidence in an area of the Arctic Coastal Plain [*Jorgenson et al*., 2006]. Further, the postfire effects on the surface energy balance can be enough to cause permafrost degradation in both regions [*Racine et al.*, 2004; *Liljedahl et al*., 2007; *Shur and Jorgenson*, 2007; *Shaver*, 2010]. Thermokarst development, whether initiated by warmer air temperatures, increased snow depth, fire, water flow, or other disturbance, has drastic effects on the hydrology by the altering of vegetation, increasing the spatial variability of near-surface soil moisture and developing drainage systems [*Jorgenson et al.*, 2006; *Fortier et al*., 2007]. In the extremely low-gradient watersheds of the Arctic Coastal Plain, melting of ice wedges can change the hydraulic gradients resulting in cascading effects on the water and energy balance.

Fires are relatively common on the Seward Peninsula, which typically has more well drained near-surface soils than the Arctic Coastal Plain. The Anaktuvuk River fire was promoted by the unusual and strongly negative P-ET during summer 2007 that resulted in dry near-surface soils. Although the general condition of the projected near-surface soil moisture at Barrow suggests continued wet conditions,

individual dry summers are still likely. One dry summer is enough to allow ignition and initiate a wildfire, which may have long-term consequences for the ecosystem by introducing high-centered polygons on an otherwise low-relief landscape.

Our future model simulations assumed no changes in the topography. However, it is evident that modest climate warming can degrade the ice-rich near-surface permafrost within a decadal time frame in the continuous cold permafrost region of the Arctic Coastal Plain [*Jorgenson et al*., 2006]. The model experiment in chapter four presented a first-order analysis for the consequences for watershed hydrology when low-centered polygons are transformed into high-centered polygons. Micro-topography evidently plays an important role on the wetland water balance, with high-centered polygons resulting in a drier surface. Accordingly, thermokarst and associated erosion processes may have as large an impact, if not larger, than any direct climate forcing.

Both permafrost conditions and vegetation composition remained static in the presented simulations, which limits our ability to predict the future of the Arctic wetlands. Any literature that modeled a coupled thermal, hydrologic, and biological regime in 3-D with the scale and processes of importance to Arctic wetland watershed hydrology represented is unknown to me. The computational resources are now less restricting, and multiple models (which describe at least a part of the system in detail) exist and have begun to merge. So the largest challenges lie in a) quantifying and defining the environmental parameters such as ground ice distribution, soil properties, and surface topography for use in models and b) garnering more field measurements (quantity and quality) of all individual water balance components – particularly simultaneously within the same watershed – to use in model validation. The lack of accurate measurements limits the capacity to validate models. For example, the apparent difficulty in producing the observed water table levels initiated an analysis that emphasized the importance of low-centered polygon rims. Combining field and modeling studies of the same system is

a ―win-win" situation that can advance the science further than any individual modeling or field assessment may have done by itself. Projections of value to the local arctic and sub-arctic communities, such as future water availability and quality, require effective models. Field measurements in combination with careful model development and evaluation can reduce the uncertainty in projections by identifying thresholds and feedback mechanisms and, at the same time, contribute to the advancement of the basic science.

The multimillion-dollar NSF funded Biocomplexity Experiment project at the Barrow Environmental Observatory accommodated extensive logistics and data collection. Apart from providing the rare opportunity to measure all components of water balance, several scientists from multiple disciplines participated in the project. Hydrology was a vital component of the study as it included a large-scale water table manipulation experiment of a drained thaw lake basin. Chapter 3-6 focused on the experiment's ―control area", while many opportunities still exists in exploring the wealth of data collected in the other water table treatment areas. As most field experiments have been on the plot scale with a biological focus, the Biocomplexity Experiment serves as an excellent opportunity to not only integrate processes at differing scales but also among the disciplines themselves.

The role of vegetation on arctic and subarctic water and energy fluxes is only briefly discussed in the individual articles. Chapter two, for example, which described the postfire changes in soil temperature and moisture regimes, used a shrub site as a ―control site" in order to differentiate between fire and weather induced impacts at a tussock tundra site. The analysis was likely complicated by the differing vegetation cover. In fact, the prefire comparison between the two sites could represent a paper in itself due to the measured differences in near-surface soil moisture regime and in temperatures throughout the soil profile. With the observed increase in shrubs on the tundra [*Silapaswan et al*., 2001; *Sturm et al*., 2001; *Tape et al*., 2006], plant-water studies are desired. As the mechanisms controlling the

processes of transpiration and evaporation differ between the two biomes, so do the mechanisms controlling the hydrology. *Beringer et al*. [2005] hypothesized that transpiration and evaporation dominate the latent heat loss from the shrub and tussock tundra, respectively. Research in the lower latitudes have acknowledged the role of shrub encroachment on hydrology [*Huxman et al*., 2005], while ecohydrology is still a young promising field in the sub-Arctic and Arctic environments.

7.2 General Conclusions

The individual manuscripts addressed four hypotheses with respective findings summarized as follows:

H1: A severe fire on tussock tundra results in a post-fire warming and wetting of the near-surface soil.

Not rejected. Active layer depth doubled at the tussock site after the fire and mean September soil temperature increased 2.5 °C at 50 cm depth at the tussock site from 2000 to 2006. However, the soil warming was partly caused by favorable weather conditions after the burn as the control (shrub) site also experienced a warming of mean September soil temperatures at 50 cm depth (1.5 °C). Further, mean annual temperature in year 2000 compared to 2006 increased with a similar magnitude at both sites (1.1 °C and 0.8 °C at 0.3 m depth at the tussock and at 0.4 m depth at the shrub site, respectively). Prefire near-surface soils (top 10 cm) at the tussock site rapidly dried following snowmelt, while postfire near-surface soils remained moist throughout the summer (note that the surface soil type changed from pre- to postfire). The burn site experienced warmer soil conditions caused by the fire surface disturbance, but the warming was also caused by favorable meteorological conditions.

H2: Midday evapotranspiration rates from a vegetated drained thaw lake basin are only energy limited.

Rejected. The evapotranspiration rates from the vegetated drained lake basin experience multiple limitations. Near-surface soil moisture and air vapor pressure deficits (VPD) express non-linear effects on midday evapotranspiration rates. VPD appear to play an important hydrologic threshold near 0.3 kPa, allowing latent heat fluxes to exceed sensible heat fluxes. Although increased atmospheric demand (high VPD) initially favors latent heat fluxes, an increased bulk surface resistance prevents evapotranspiration from reaching its potential rate (Priestley-Taylor α ~1.26) despite wet soils. Further, the evapotranspiration is suppressed during both dry and wet soil conditions through differing mechanisms. Dry soils results in an increased bulk surface resistance (water-limited) while the altered surface energy partitioning during wet soils favors ground heat flux and therefore reduces the energy available to midday sensible and latent heat fluxes (energy-limited). The study analyzed midday (solar noon ± 3 h) evapotranspiration. Accordingly, wet and inundated soils may have a different effect on daily total evapotranspiration.

H3: A change from a low- to a high-centered polygon-dominated landscape affects overall watershed hydrology by increasing runoff, reducing evapotranspiration and near-surface soil moisture.

Not rejected. The presence of elevated rims in model experiments, intended to represent low-centered polygon tundra, reduced runoff while increasing evapotranspiration and surface and soil water storage. The near-surface was typically saturated when rims were present and also allowed temporary ponds to form. The high-centered polygon landscape produced more than twice the runoff compared to the low-centered polygon scenario, while storage and runoff drastically decreased. About half of the SWE did not contribute to streamflow from the low-centered polygon (56 %), while the high-centered polygon scenario

resulted in 27 % of the SWE recharging the soils. Total evapotranspiration from high-centered polygons scenario was comparable to the total runoff while evapotranspiration drastically exceeded the runoff from the low-centered polygons. This first-order approach suggests that excluding the role of microtopographical variability on hydrology severely limits the ability to estimate regional scale water and energy exchange.

H4: The projected increase in end-of-the 21st century air temperature and precipitation will lead to a drying of Arctic Coastal Plain wetlands.

Rejected. Despite a warmer climate, the near-surface soils are projected to remain wet by the end of the 21st century as the projected increase in evapotranspiration was offset by an increased summer precipitation. However, interannual variability through the timing of the snowmelt, rather than the present control of below-normal summer precipitation, was projected to cause large soil water storage deficits. Overall, the water table prior to freeze-up was projected to increase, resulting in an enhanced partitioning of the accumulated snow into spring runoff. The nival-dominated runoff regime is projected to continue, although small late-summer lateral flow could be anticipated. The intensified hydrologic regime was particularly evident in regards to runoff, which increased four-fold even though the winter precipitation doubled. The simulations presented limited changes to the overall surface and soil water regime under a scenario where permafrost distribution and vegetation types were held similar to present day.

7.3 References

Beringer J., F. S. Chapin III, C. C. Thompson, and A. D. McGuire (2005), Surface energy exchanges along a tundra-forest transition and feedbacks to climate, *Agr. Forest Meteorol., 131*, 143–161.

Fortier, D., M. Allard, and Y. Shur (2007), Observation of rapid drainage system development by thermal erosion of ice wedges on Bylot Island, Canadian Arctic Archipelago, *Permafrost, and Periglac. Process., 18*, 229–243.

Huxman, T. E., B. P. Wilcox, D. D. Breshears, R. L. Scott, K. A. Snyder, E. E. Small, K. Hultine, W. T. Pockman, R. B. Jackson (2005), Ecohydrological implications of woody plant encroachment, *Ecology, 86*(2), 308–319.

Jorgenson, M. T., Y. L. Shur, and E. R, Pullman (2006), Abrupt increase in permafrost degradation in Arctic Alaska, *Geophys. Res. Lett., 33*, L02503, doi:10.1029/2005GL024960.

Liljedahl, A. K., L. D. Hinzman, R. C. Busey, and K. Yoshikawa (2007), Physical short-term changes after a tussock tundra fire, Seward Peninsula, Alaska, *J. Geophys. Res*., F02S07, doi:10.1029/2006JF000554.

Marchenko, S., Romanovsky, V., Tipenko, G. (2008) Numerical modeling of spatial permafrost dynamics in Alaska, in *Proceedings of the Ninth International Conference on Permafrost*, edited by D. L. Kane and K. M. Hinkel, pp. 1125-1130, Univ. of Alaska Fairbanks, Fairbanks, AK.

Racine, C. H., R. R. Jandt, C. R. Meyers, and J. Dennis (2004), Tundra fire and vegetation change along a hillslope on the Seward Peninsula, Alaska, U.S.A. *Arctic, Antarctic, and Alpine Res., 36*(1), 1–10.

Shaver, G. R. (2010), Fire and ice: Surprised in a warming Arctic land surface, abstract presented at State of the Arctic Conference, Miami, FL.

Shur, Y. L., and M. T. Jorgenson (2007), Patterns of permafrost formation and degradation in relation to climate and ecosystems, *Permafrost and Periglac. Process., 18*(1), 7–19.

Silapaswan, C. S., D. L. Verbyla, A. D. McGuire (2001), Land cover change on the Seward Peninsula: The use of remote sensing to evaluate the potential influences of climate warming on historical vegetation dynamics, *Can. J. Remote Sens. 27*, 542–554

Sturm, M., C. Racine, and K. Tape (2001), Climate change - Increasing shrub abundance in the Arctic, *Nature, 411*, 546–547.

Tape K., M. Sturm, and C. Racine (2006), The evidence for shrub expansion in Northern Alaska and the Pan-Arctic, *Global Change Biol., 12*, 686–702.